Self adhesion of semi-crystalline polymers between their glass transition temperature and their melting temperature

Gauthier Jarrousse

THÈSE DE DOCTORAT DE L'UNIVERSITÉ PARIS VI

Ecole Doctorale de Chimie Physique et Chimie Analytique

Spécialité :

Matière condensée : chimie et organisation

Présentée par :

Gauthier Jarrousse

pour obtenir le titre de :

DOCTEUR DE L'UNIVERSITÉ PARIS VI

Sujet de la thèse :

Adhésion des polymères semi-cristallins entre leur température de transition vitreuse et leur température de fusion

Self adhesion of semi-crystalline polymers between their glass transition temperature and their melting temperature

Soutenue le 13 Décembre 2004

devant le jury composé de :

Mme Liliane LEGER, Professeur, Collège de France	Co-directrice de thèse
M. Costantino CRETON, Directeur de recherche, ESPCI	Directeur de thèse
M. Jean-Claude WITTMANN, Directeur de recherche, Institut Charles Sadron	Rapporteur
M. Jean-Yves CAVAILLE, Professeur, INSA de Lyon	Rapporteur
M. Alain FRADET, Professeur, Université Paris VI	Président
M. John Christopher PLUMMER, Professeur, EPFL	Invité

Table of contents

Introduction

Introduction

Adhesion is an immensely complicated subject concerned with the strength of the coupling that can occur between any pair of materials. It is also a subject of wide ranging usefulness with a steadily increasing importance in many technologies. The reason of the complexity of the science of adhesion lays in the fact that adhesion is at the cross section of many fundamental sciences, since in order to understand how two materials can be associated one should be aware of the different chemical or physical coupling that can occur at the interface.

In the present study, we consider only the adhesion between pairs of polymeric materials, and more specifically between semicrystalline polymers. This field has been widely but quite recently studied, since most of the polymers used in the industry are semicrystalline polymers. For example, the association of two or more polymers in alloys or in blends, to obtain optimized products by combining their properties, is of great industrial importance. Some of the industrial processes require a good and rapid adhesion such as the over molding process, where a polymer melt is injected on top of another polymer which is solid. In this type of process, the crystallinity at the very surface of the solid polymer is certainly playing a significant role and a better understanding of the way this crystallinity acts upon the adhesion is needed.

Although both the mechanisms of reinforcement of an interface between amorphous polymers and the fracture mechanisms of such interfaces are now relatively well established, their extension to semicrystalline interfaces is not straightforward. Several ideas have emerged from the studies of adhesion between semicrystalline polymers, but still a clear vision of the different mechanisms active for the reinforcement of the interfaces at the molecular level and the fractures mechanisms of such interfaces, is still far beyond reach.

The present investigation is a contribution aimed at elucidating the role of crystallinity upon adhesion and fracture mechanisms between semicrystalline polymers. Since the adhesion between amorphous polymers has been well described, the natural attempt in previous studies was to try to apply the mechanisms found in the case of amorphous polymers to the case of semicrystalline polymers. Although some similarities have been established, differences have been underlined such as the critical role played by the crystallinity.

Typically, it is well established that when co-crystallization occurs at the interface, the fracture toughness of such interfaces is largely increased. However, the conditions which will allow a co-crystallization are unclear. It has been shown also that the crystalline orientation at the interface had a great influence on the adhesion. However the reasons of this influence remain unknown.

Thus, several questions were at the onset of this work. What was the influence on the level of adhesion of the amorphous part of a semicrystalline polymer welded above T_g but

below T_m. Was there a degree of crystallinity below which the amorphous part is the principal actor of the adhesion?
Other questions emerged quite rapidly after starting this work. What could be the preponderant mechanism of interface reinforcement (co-crystallization, interdiffusion, crystalline reorganization at the interface)? Was it possible to enhance the adhesion by cold crystallizing samples in contact? What was the influence of the crystalline structure at the interface on adhesion?

In order to try to answer these questions, we coupled several experimental techniques providing information on the crystallinity in the bulk (Temperature Modulated Differential Scanning Calorimetry), and at the interface (optical and TEM observations), as well as on the degree of adhesion (double cantilever beam test).

We decided to work with a model system of copolymers, all synthesized by step-growth polymerization with nearly identical average molecular weights and molecular weight distributions, and with nearly identical T_g, but with an overall crystallinity which could be varied (by using copolymers with different overall degrees of crystallinity and different crystallization kinetics). This system was much more complicated than initially thought, since the overall degree of crystallinity was indeed not the only parameter which varied between the different copolymers. However, by a detailed characterization of this complex system, it was possible to investigate the different effects of the crystallization behavior on adhesion.

A key experimental aspect of our work was the careful control of temperatures and temperature gradients. All of our copolymers are very sensitive to thermal history because of the inherently slow nature of the crystallization process in polymers. In turn the crystallization process affected both adhesive and mechanical properties of the polymer, which is a fact reflected in the values of fracture toughness that we measured by DCB. We specially built a mold to realize bilayers with a precise control of the temperature of each surface and of the interface. Cooling conditions were well controlled to be reproducible and to span a wide range of cooling rates.

With these tools in hand, our goal was to realize a comprehensive and thorough investigation of adhesive mechanisms potentially active below the melting point of the crystalline phase of semi-crystalline polymers. After a chapter introducing the main concepts used in the analysis of the experimental work and a review of the state of the art, chapter 2 is dedicated to the characterization of the materials and the bulk of the results are presented in chapter 3. Chapter 4 summarizes the main results and discusses them in a more general view also in relation with previous work on the topic and finally the conclusion summarizes the main results.

Chapter 1

Introduction to the adhesion of semicrystalline polymers and state of the art

Table of contents

This chapter has the dual purpose to briefly present the basic concepts of polymer science and fracture mechanics needed to understand my experimental work as well as to review the state of the art in the adhesion between two identical semicrystalline polymers.

We will start with some basic concepts of polymer science which are meant to be a short introduction to the semicrystalline polymers section, in which more details will be given.

Knowing those basic notions on amorphous and semicrystalline polymers, we will introduce some well known concepts in the fracture behavior of polymers, concepts that will be applied in polymer adhesion problems.

Finally, a comprehensive state of art of the field of adhesion between polymers will then be presented, first with examples of adhesion between amorphous polymers and then between semicrystalline polymers.

1.1 Basic concepts

In this section, we will present basic notions on polymers. We will focus on the notions required for the characterization of the materials used in this study and for the interpretation of our adhesion results.

1.1.1 Brief introduction to polymers

A very brief introduction will be given in this section. A more detailed introduction to polymer science can be found in the textbooks of Young and Lovell[1] and Strobl[2].

1.1.1.1 Introduction

The notion of *macromolecule* appears in 1922 in the studies of Staudinger, and can be defined as follows : a macromolecule is a long molecule containing atoms held together by primary covalent bonds along the molecule.

Macromolecules are made by a process called *polymerization* whereby *monomer* molecules react together chemically to form linear or branched chains or three-dimensional networks.

[1]Young, R. J. and Lovell, P. A. Introduction to polymers. (Chapman & Hall, London, 1991

[2]Strobl, G. The Physics of Polymers. (Springer-Verlag, Berlin, 1996)

A macromolecule is characterized by its molar mass M related to the degree of polymerization x, which is the number of repeat units in the macromolecule, by the simple relation :

$$M = xM_0 \qquad \textit{Eq. 1.1-1}$$

where M_0 is the molar mass of the repeat unit.

The term *polymer* is applied when the number of repeat units is typically above one hundred. Experimentally, for such a number of repeat units, properties such as the melting temperature, become x-independent.

Experimentally the synthesis of macromolecules leads to polymers which consist of chains with a range of molar masses, which changes discontinuously in intervals of M_0. It is convenient to characterize the distribution in terms of mass averages. Considering N_i macromolecules of mass M_i, the number-average mass, M_n and the weight-average mass, M_w are defined as follows (equation 1.1-2 and 1.1-3) :

$$\overline{M}_n = \frac{\sum_i N_i M_i}{\sum_i N_i} \qquad \textit{Eq. 1.1-2}$$

$$\overline{M}_w = \frac{\sum_i N_i M_i^2}{\sum_i N_i M_i} \qquad \textit{Eq. 1.1-3}$$

The ratio $I = M_w/M_n$ represents the polydispersity of the material and is an indication of the breadth of the molecular weight distribution.

1.1.1.2 Types of polymers and classification

We can classify the different polymers as follow : *Thermoplastics*, which can melt upon the application of heat, *elastomers* which are crosslinked rubbery polymers that can be stretched easily to high extensions and which rapidly recover their original dimensions and *thermosets* which normally are rigid materials and are network polymers in which chain motion is greatly restricted. Elastomers and thermosets are intractable once formed and degrade rather than melt upon the application of heat.

Thermoplastics are widely used in industry because they can be molded into virtually any shape using processing techniques. Generally, thermoplastics do not crystallize easily upon cooling to the solid state because crystallization requires considerable ordering of the highly coiled and entangled macromolecules. Those which do crystallize are rather semi-crystalline with both crystalline and amorphous regions. Amorphous polymers are

characterized by their glass transition temperature T_g while semi-crystalline polymers are characterized by both the glass transition and the melting temperature T_m.

If only one type of monomer is used the resulting polymer is called a *homopolymer* whereas if more than one type of monomer is used the polymer is termed a *copolymer*.

There are several categories of copolymers, each being characterized by a particular form of arrangement of the repeat units along the polymer chain. If two types of monomer are used, we can classify the copolymers as follows :
- *Statistical copolymers* are copolymers in which the sequential distribution of the repeat units obeys known statistical laws. Random copolymers are statistical copolymers in which the distribution is truly random.
- *Alternating copolymers* are arranged in a strictly alternating way along the polymer chain.
Block copolymers are linear copolymers in which the repeat units exist only in long sequences, or blocks, of the same type.
- *Graft copolymers* are branched polymers in which the branches have a chemical structure different from that of the main chain

Statistical copolymers -A-A-B-A-B-B-B-A-A-B-B-A-A-A-A-B-A-A-B-B-B-A-
Alternating copolymers -A-B-A-B-A-B-A-B-A-B-A-B-A-B-A-B-A-B-A-B-A-B-
Block copolymers -A-A-A-A-A-A-A-A-A-A-A-B-B-B-B-B-B-B-B-B-B-

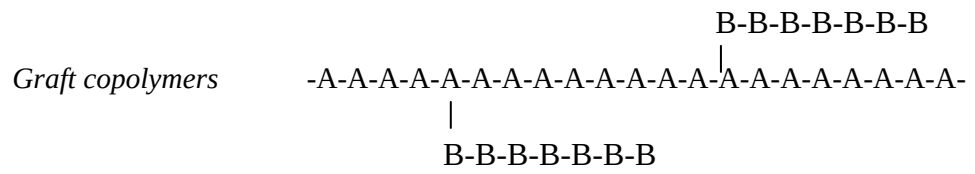

1.1.1.3 A few words on polymerization

The synthesis of polymers is a very large and extensive topic. It is covered in details in several textbooks (Rempp and Merrill[1], Champetier and Monnerie[2] and Odian[3]). Synthesis of polymers can be divided into two main categories, namely step-growth polymerizations, where the polymer chains grow step-wise by reactions that can occur between any two molecular species, and chain growth polymerization, where a polymer chain grows only by reaction of individual monomers with a reactive end-group on the growing chain.

We will focus here on polycondensations, which are step polymerizations that involve reactions in which small molecules are eliminated.

[1]Rempp, P. and Merrill, E. W. Polymer Synthesis. (Hüthig & Wepf Verlag Basel, New York, 1991)
[2] Champetier, G. and Monnerie, L. Introduction à la chimie macromoléculaire. (Masson, Paris, 1969)
[3] Odian, G. *Principles of Polymerization*. (Wiley, New York, 1981)

The formation of polyesters is typical of these reactions and may be represented more generally by :

n HOOC-R_1-COOH + nHO-R_2-OH $\rightarrow$H-[-OOC-R_1-COO-R_2-]$_n$-OH + (2n-1)H_2O

1.1.1.4 Basic considerations of polymer physics

From section 1.1.1.1, we saw that the polymer was constituted of macromolecules made of hundreds of repeat units. In order to understand the basic properties of polymers, it is useful to consider its constituent, the chain, from a physical point of view (de Gennes[1]).

1.1.1.4.1 A single chain

One of the simplest idealizations of a flexible polymer chain consists in replacing it by a random walk on a periodic lattice. The succession of *N* steps will lead to the following mean square end to end distance

$$\left\langle r^2 \right\rangle = Na^2 \qquad \textit{Eq. 1.1-4}$$

It has been also demonstrated that the radius of gyration of a *Gaussian chain* has the same dependence with *N*, i.e. :

$$R \sim N^{1/2}a \qquad \textit{Eq. 1.1-5}$$

1.1.1.4.2 Dense system of chains

From a static point of view, the chains in a polymer melt can be considered as Gaussian and ideal (Flory[2]).

The dynamics of a chain among others has been well described by the so-called *reptation* model proposed by de Gennes[3] and Doi and Edwards[4].

In a melt, the chains can move by Brownian motion, but they cannot intersect each other. A useful picture is to consider the chain trapped in a network. The chain is not allowed to cross any obstacle but can move in between in a wormlike fashion, called *reptation*. Edwards introduced the notion of tube, which contains the chain as represented in Figure 1.1-1.

[1]de Gennes, P. G. Scaling concepts in Polymer Physics (Cornell university press, London, 1979)
[2]Flory, P. J. Journal of Chemical Physics, 17: 303, (1949).
[3]de Gennes, P. G. Journal of Chemical Physics, 55: 572-579, (1971).
[4]Doi, M. and Edwards, S. J. Journal of the Chemical Society; Faraday Transactions 2, 74: 1789-1801, 1802-1818, 1818-1832, (1978).

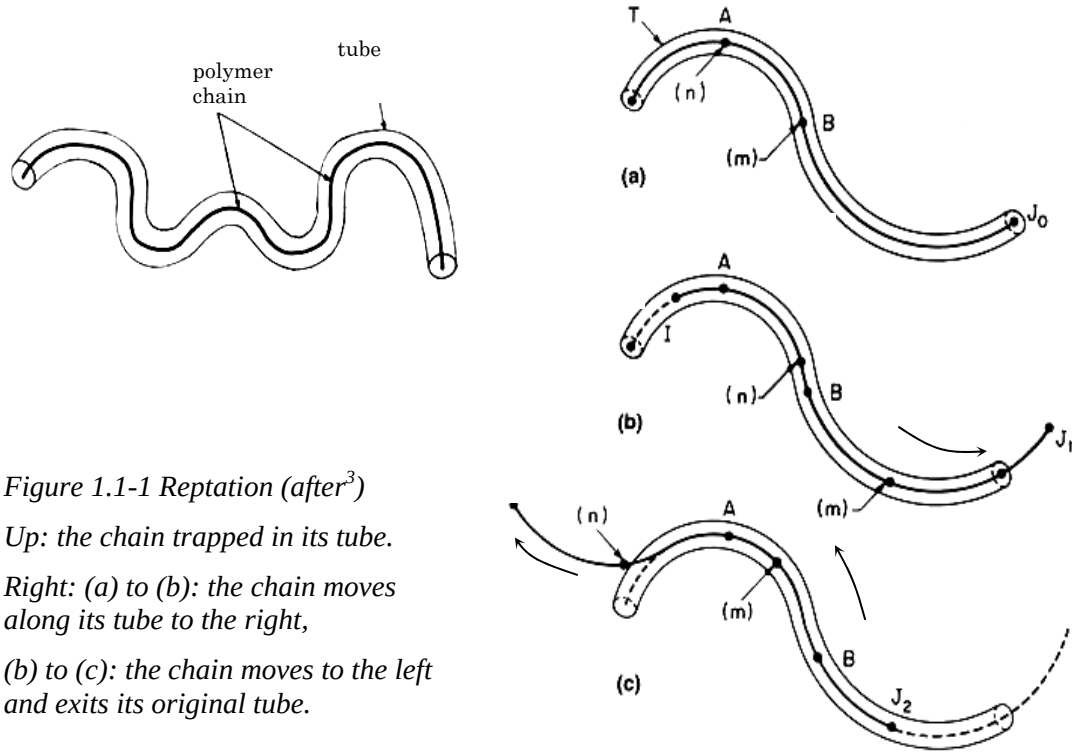

Figure 1.1-1 Reptation (after[3])

Up: the chain trapped in its tube.

Right: (a) to (b): the chain moves along its tube to the right,

(b) to (c): the chain moves to the left and exits its original tube.

The diameter of the tube is given by $d \sim N_e^{1/2} a$, a being the monomer length and N_e the average number of monomers between entanglement points, i.e. between the topogical obstacles.

The tube diffusion coefficient, D_{tube}, is given by the Einstein relationship kT/f where the friction coefficient f is $6\pi\eta_1 Na$:

$$D_{tube} = \frac{kT}{6\pi\eta_1 Na} \qquad \textit{Eq. 1.1-6}$$

where η_1 is a local the viscosity of the polymer melt.

During the reptation time τ_{rept}, the chain moves over L_{tube} along the tube and over R_{tube} in the real space :

$$D_{tube}\tau_{rept} = L_{tube}^2 = \left(\frac{N}{N_e}\right)^2 d^2 = \left(\frac{N}{N_e}\right)^2 N_e a^2 \qquad \textit{Eq. 1.1-7}$$

$$D_{self}\tau_{rept} = R_{tube}^2 = \frac{N}{N_e} d^2 = Na^2 \qquad \textit{Eq. 1.1-8}$$

so :

[1]de Gennes, P. G. *Scaling Concepts in Polymer Physics*. (Cornell University Press, London, 1979)

$$\tau_{rept} = \frac{6\pi\eta_1 a^3}{kT}\frac{N^3}{N_e} \qquad \textit{Eq. 1.1-9}$$

$$D_{self} = \frac{kT}{6\pi\eta_1 a}\frac{N_e}{N^2} \qquad \textit{Eq. 1.1-10}$$

In the case of a polymer with N_e~100 and N~10 000 we get a reptation time of the order of magnitude of 1 sec and a self diffusion coefficient of 10^{-11} $cm^2.sec^{-1}$.

These are the basic equations of the diffusion of a polymer chain in a melt, which will be used later on in the description of interdiffusion at polymeric interfaces.

1.1.1.4.3 The amorphous state

If the melt of a non-crystallizable polymer is cooled, it becomes more viscous and flows less readily. If the temperature is reduced low enough it becomes a transient ("rubbery") network of entanglements and then as the temperature is reduced further, the sample becomes a relatively hard elastic polymer glass. The temperature at which the polymer undergoes the transformation from a transient network to a glass is known as the *glass transition temperature*, T_g. The ability to form glasses is not confined to non-crystallizable polymers. Any material which can be cooled sufficiently fast to avoid crystallization will undergo a glass transition.

Amorphous polymers can be thought of as frozen polymer liquids, in which no well defined order can be found.

The glass transition temperature can be detected experimentally by the variation of the specific volume as represented in Figure 1.1-2 or, as carried out in our study, by differential scanning calorimetry (DSC) (Figure 1.1-3).

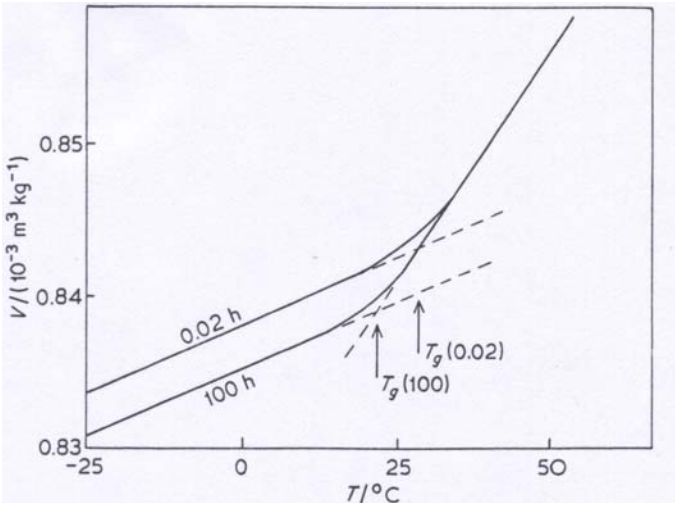

Figure 1.1-2 : variation of the specific volume of poly(vinyl acetate) with temperature taken after two different times (After Kovacs[1])

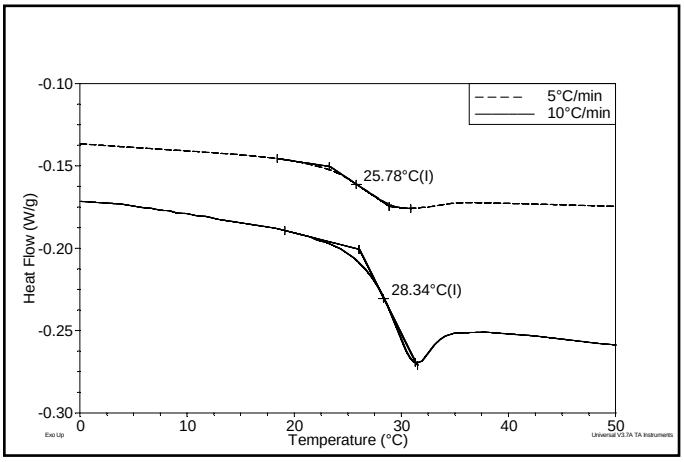

Figure 1.1-3 : variation of the heat flow of poly(butylene terephthalate-co-butylene isophthalate) with the heating ramp

We may consider the amorphous state as an isotropic and out of equilibrium state. More extensive treatments of the amorphous state can be found in textbooks : Gedde[1]

1.1.1.4.4 Mechanical properties of amorphous polymers

Polymers exhibit a wide range of elastic properties depending upon their structure and testing conditions. Figure 1.1-4 shows the variation of Young's modulus, *E*, with temperature for an amorphous polymer. At low temperature, the polymer is glassy with a relatively high modulus of the order of a few GPa. Above T_g, the polymer becomes

[1]Kovacs, A. J. Journal of Polymer Science, 30(121): 131-147, (1958).

viscoelastic with a lower modulus, very rate and temperature dependent. For polymers with relatively high molecular weight, typically higher than the average molecular weight between entanglements, M_e, the polymer can be considered as a transient network, with a modulus remaining approximately constant with increasing temperature. With a very simple molecular theory of rubber elasticity, it can be shown that the shear modulus, G, of a transient network is given by an equation of the form :

$$G = \frac{E}{2(1+\nu)} = \frac{\rho RT}{M_e} \qquad \textit{Eq. 1.1-11}$$

where ρ is the density of the polymer and T the temperature at which the modulus is calculated (ν the Poisson's ratio is typically equal to 0.5 for most polymers above their transition temperature). This expression is remarkably accurate given the assumptions contained in the model.

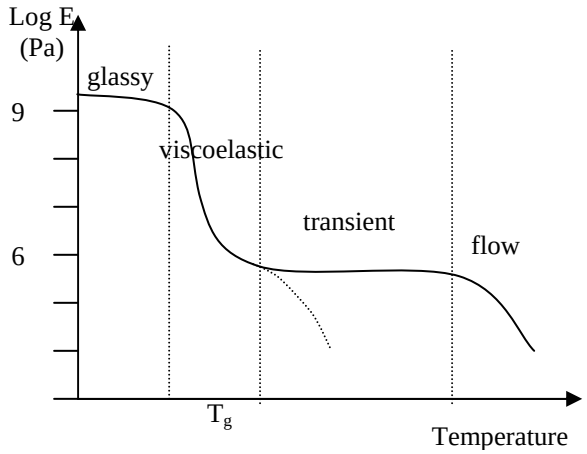

Figure 1.1-4: variation of E for an amorphous polymer

The mechanical behavior of polymers depends upon the testing rate as well as the temperature and it is found that there is a general equivalence between time or frequency of observation and temperature. The mechanical response can be represented in a procedure known as time-temperature superposition. In a series of mechanical measurements made over a range of temperatures at different testing frequencies, the data can be put onto a simple 'master curve' by shifting the data measured at one temperature along the frequency axis by a factor which is a function only of the test temperature, as represented in Figure 1.1-5. This is a very general property of many polymers and is due to the fact that the spectrum of relaxation times of a polymer has typically the same temperature dependence.

In a range of temperatures between T_g and T_g + 100°C, the relationship between the test temperature and this factor a_T is often given by an equation of the form

[1]Gedde, U. W. Polymer Physics. (Kluwer Academic Publisher, 1995)

$$\log a_T = \frac{-C_1\left(T - T_{ref}\right)}{C_2 + \left(T - T_{ref}\right)} \qquad \textit{Eq. 1.1-12}$$

where C_1 and C_2 are constants and T_{ref} is a reference temperature. This equation is normally termed the WLF (Williams-Landel-Ferry) equation and is based on the notion that molecular mobility depends on the available free volume which vanishes for a finite temperature T_∞.

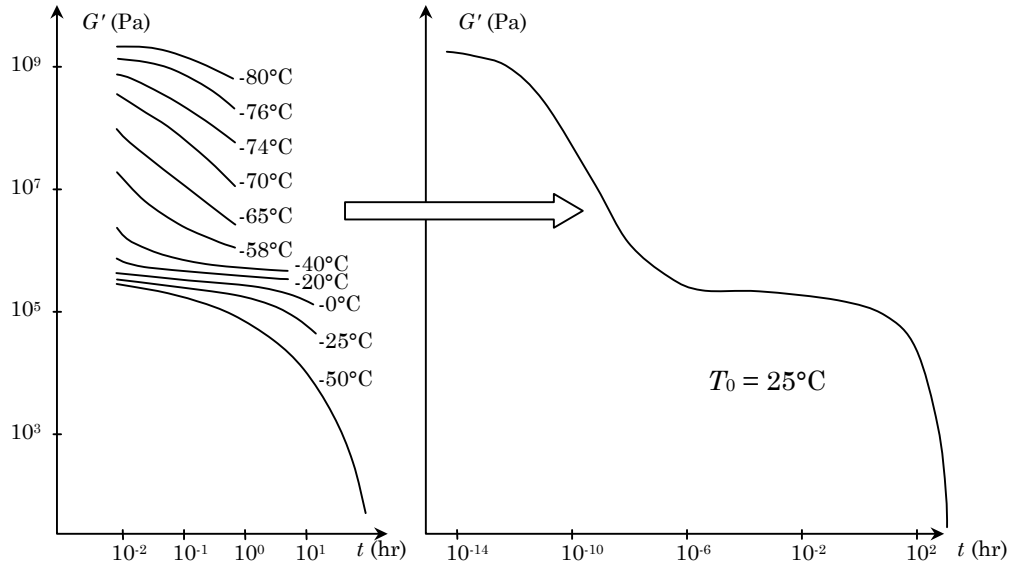

Figure 1.1-5 : Building a master-curve with the time-temperature superposition.

A typical feature of the mechanical behavior of polymers is the way in which their mechanical response to an applied stress or strain depends upon the rate or time period of loading. This behavior can be thought of as being somewhere between that of elastic solids and liquids. The subject of viscoelasticity is covered in several textbooks (Ferry, Ward, Young and Lovell) and so only a very brief review will be given here.

An example of viscoelastic behavior is given in Figures 1.1-6 and 1.1-7 in two particular experimental cases : creep and relaxation.

When a sudden stress is applied to a polymeric sample and maintained, the measured deformation increases with time: This property is called *creep* and it is an indication of the viscoelastic character of the material, as shown on Figure 1.1-6. When a sudden deformation is applied to a polymeric sample and maintained, the measured force decreases as a function of time: This is called *stress relaxation* and is illustrated on Figure 1.1-7.

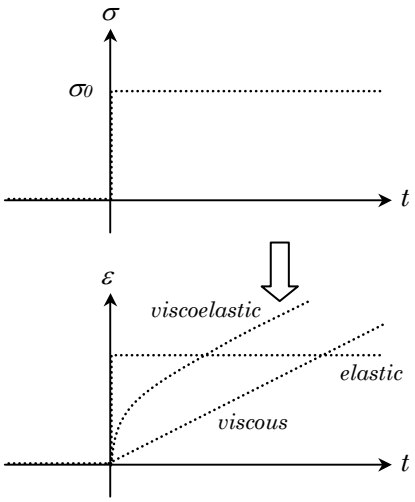

Figure 1.1-6 : Creep of a viscoelastic material at a constant applied stress.

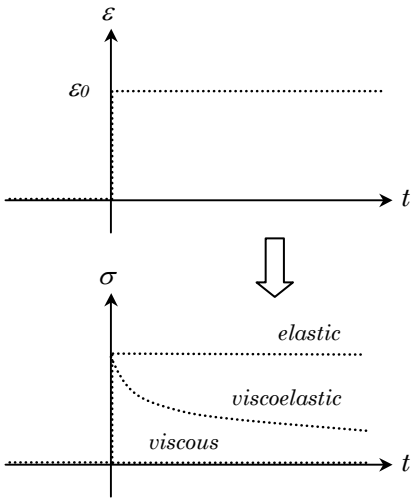

Figure 1.1-7 : Relaxation of a viscoelastic sample submitted to a constant strain.

The viscoelastic behavior of polymers is often examined using a dynamic mechanical testing where the polymer is subjected to an oscillating sinusoidal stress. Unlike an elastic material, the strain lags somewhat behind the stress and so the variation of stress and strain with time can be given by expressions of the type

$$\varepsilon = \varepsilon_0 \sin(\omega t) \qquad \textit{Eq. 1.1-13}$$

$$\sigma = \sigma_0 \sin(\omega t + \delta) \qquad \textit{Eq. 1.1-14}$$

where ε_0 and σ_0 are the strain and stress amplitude, ω is the frequency and δ the phase angle or phase lag. This approach leads to the definition of two dynamic moduli, *G'* which is in-phase with the strain and represents the elastic part of the modulus and *G''* which is π/2 out-of-phase with the strain and represents the viscous part of the modulus. *G'* and *G''* or *E'* and *E''* in uniaxial tension, are sometimes called the storage component and the loss component of the complex modulus respectively. It follows that the loss factor tanδ is given by

$$\tan\delta = \frac{G''}{G'} \qquad \textit{Eq. 1.1-15}$$

and a 'complex modulus *G** can be defined as :

$$G^* = G' + iG'' \qquad \textit{Eq. 1.1-16}$$

The value of *tanδ* like the value of the complex modulus varies with temperature, and peaks are observed at certain temperatures, as shown in the example given in Figure 1.1-8. These peaks of dissipation are attributed to dissipative molecular motions and called transitions. In an amorphous polymer, the most pronounced peak is the α-transition which

corresponds to the onset of molecular motion at the T_g and the β and γ relaxations are due to localized main-chain or side group motion. For semi-crystalline polymers, the interpretation of the transitions can be less obvious but usually a T_g can still be detected in this way.

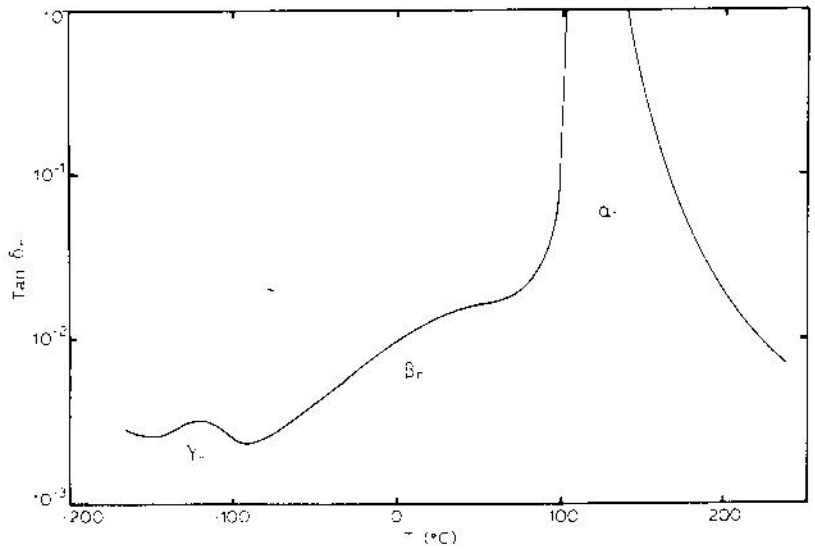

Figure 1.1-8 : variation of tanδ with temperature for amorphous polystyrene (after McCrum et al.[1])

1.1.2 Semi-crystalline polymers

Some polymers, when cooled from the melt, have the ability to form ordered domains, before going through the glass transition temperature below which the motions are drastically reduced, forbidding any more ordering.

A polymer will never be fully ordered, in other words a polymer will never be fully crystallized, from cooling it from melt. In an entangled system of chains, forming ordered regions will largely reduce the entropy. Because of entanglements, a polymer will not fully crystallize within a reasonable time. A mix of ordered and disordered regions will be obtained. Thus, the polymers can be described as *semicrystalline*, since polymers crystallized in the bulk state are never totally crystalline and have both crystalline and amorphous regions.

Both thermodynamics and kinetics govern the crystallization of polymers. For thermodynamics, it is useful to consider the Gibbs free energy of any system related to the enthalpy *H* and the entropy *S* (equation 1.1-17).

$$G = H - TS \qquad \textit{Eq. 1.1-17}$$

The system is in equilibrium when G is a minimum. Below the melting temperature T_m, crystallization may occur as the corresponding large reduction in enthalpy ΔH_m will be greater than that of the product of the melting temperature by the entropy change ($T_m \Delta S_m$).

Crystallization is also controlled by kinetics, as it is possible to obtain a crystallizable polymer in the amorphous state by a rapid cooling from the melt.
The kinetics of crystallization will be discussed in the following sections after a general presentation of the structure of semicrystalline polymers.

We must underline the fact that molecular mobility is needed to achieve ordered regions, thus the *melting temperature, T_m,* of a semicrystalline polymer will always be above its glass transition temperature.

The crystallization of polymers is of enormous technological importance, as many thermoplastics polymers used in the industry will crystallize when the molten polymer is cooled below the melting point of the crystalline phase. The presence of crystals has an important effect upon the polymer properties and indeed on adhesion which is the topic of our study.

We will now concentrate on melt-crystallized polymers. Some general reading on the crystalline state in polymers can be found in the following references : Sperling[2], Tadokoro[3], Wunderlich[4], Young and Lovell[5].

1.1.2.1 General structure of semi-crystalline polymers

Crystalline solids consist of regular three-dimensional arrays of atoms placed at the node of a repeating unit known as the unit cell. In polymers, the mers are placed at those nodes, imposing to the chains to pack together side by side, with their main axis along one of the sides of the unit cell. Usually, the chains are considered to lie along the c-axis of the unit cell.

The structure of a semicrystalline polymer is composed of crystalline domains separated by regions of amorphous polymer. The crystalline morphology is complex and has several levels of structure, as shown schematically in Figure 1.1-9.

[1]McCrum, et al. Anelastic and dielectric effets in polymeric solids. (John Wiley, London, 1967)
[2] Sperling, L. H. Introduction to physical polymer science. (Wiley-interscience, New York, 1992)
[3] Tadokoro, H. Structure of Crystalline Polymers. (Wiley-Interscience, New York, 1979)
[4] Wunderlich, B. Macromolecular Physics. (Academic Press, Orlando, 1973)
[5] Young, R. J. and Lovell, P. A. Introduction to polymers. (Chapman & Hall, London, 1991)

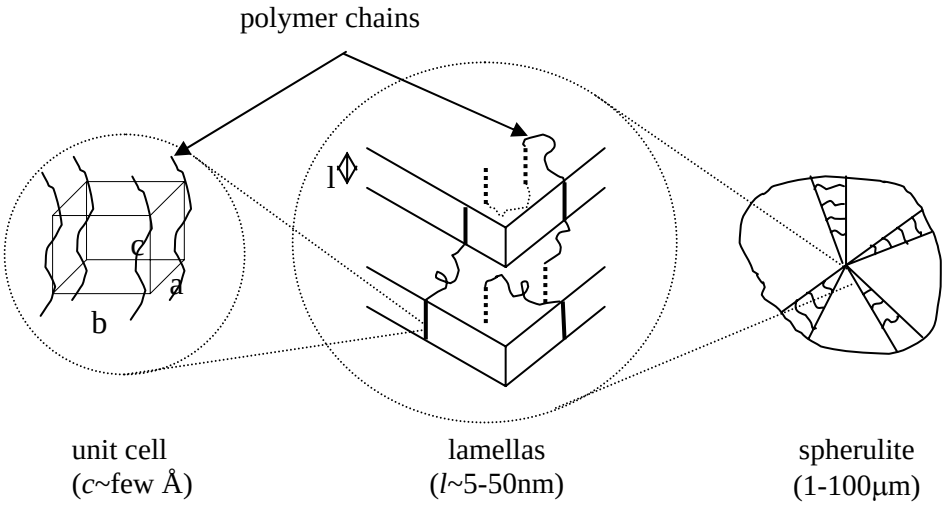

Figure 1.1-9 : Crystalline structure in a melt-crystallized polymer.

The smallest level is the unit cell which can be assigned to one of the seven basic crystal systems (triclinic, monoclinic, etc.). The polymer molecule is generally lying parallel to the *c* axis although there are exceptions. The crystalline domains form then lamellae that grow out from a central nucleation point. The polymer chain which is much longer than the typical thickness of the lamella (from 5 to 50 nm roughly) must reenter several times in the lamella. There are mainly two models that describe the reentry : the folded chain model and the switchboard model. In the first model, the chain folds back and forth with hairpin turns, leading to an adjacent reentry, while in the second model the reentry is more random like an old-time telephone switchboard. In Figure 1.1-9 the second model is represented since, in the case of melt-crystallized polymer, this type of reentry is more likely to occur. The lamellae form a superstructure called spherulite. Under polarized light, this superstructure of typically 5 to 500 μm in diameter, shows the characteristic Maltese cross, as represented in figure 1.1-9.

1.1.2.2 Theories of crystallization kinetics

1.1.2.2.1 General considerations

When the temperature of a polymer melt is reduced below the melting temperature there is a tendency for the random entangled molecules in the melt to become aligned and form small ordered regions. This process is known as *nucleation* and the ordered regions are called nuclei. The second step in the crystallization process is *growth* whereby the crystal nucleus grows by the addition of further chains.

Crystallization is therefore a two step process, nucleation and growth, which can be imaged by raindrops falling in a puddle. These produce expanding circles of waves that

intersect and cover the whole surface. The expanding circles of waves, of course, are the growth fronts of the spherulites and the points of impact are the crystallite nuclei.

In the majority of cases of crystallization from polymer melts, nucleation takes place heterogeneously. The number of nuclei depends upon the temperature of crystallization and upon the presence of foreign bodies or interfaces. The growth of a crystal nucleus can take place in either one, two or three dimensions.

When the radial growth rate is plotted as a function of crystallization temperature, a maximum is observed, due to the competition between the thermodynamic driving force for crystallization, which increases as the temperature is lowered, and the viscosity, which will act against the transport of material to the growth point.

1.1.2.2.2 Overall crystallization kinetics : Avrami's equation

A polymer melt of volume V_L is cooled below the crystallization temperature. If we assume that the nucleation is homogeneous, the number of nuclei formed at a given temperature per unit time per unit volume N is constant. In the time interval dt, $NV_L dt$ nuclei are formed. After a length of time t, these nuclei become spherulites with a volume of $(4/3)\pi r^3$ or $(4/3)\pi g^3 t^3$ with $r = gt$ (g is known as the growth rate). The total volume of spherulitic material, V_S, present at time t, and grown from the nuclei formed in the time interval, dt, is ruled by the differential equation :

$$dV_s = \frac{4}{3}\pi g^3 t^3 N V_L dt \qquad \textit{Eq. 1.1-18}$$

The crystallized fraction is given by $X = V_S/V_L$ and making the assumption that volume of the crystalline phase is small compared to V_L, we have $dX=dVs/V_L$.
dX should be corrected by a factor $(1-V_S/V_L)$ due to the meeting of the developing entities and to the reduction of the volume of liquid. We finally get :

$$\frac{dX(t)}{1-X(t)} = \frac{dV_S}{V_L} = \frac{4\pi g^3 N t^3}{3} \qquad \textit{Eq. 1.1-19}$$

and upon integration

$$1 - X(t) = \exp\left(-\frac{\pi g^3 N}{3} t^4\right) \qquad \textit{Eq. 1.1-20}$$

Equation 1.1-20 is only valid in the initial stages of crystallization ($V_L >> V_S$). If types of nucleation and growth other than those considered here are found, equation 1.1-20 can be expressed as

$$1 - X(t) = \exp\left(-Zt^n\right) \qquad \textit{Eq. 1.1-21}$$

which is the Avrami[1]'s equation. The exponent n is called the Avrami's exponent. Experimentally, it is useful to express the Avrami's equation with the difference in height of a liquid in a dilatometer :

$$\left(\frac{V_t - V_\infty}{V_0 - V_\infty}\right) = \left(\frac{h_t - h_\infty}{h_0 - h_\infty}\right) = \exp\left(-Zt^n\right) \qquad \textit{Eq. 1.1-22}$$

V_0, h_0 and V_∞, h_∞ are the initial and final volume and height respectively, V_t, h_t the volume and height at time *t*.

1.1.2.2.3 Molecular mechanisms of crystallization

Although Avrami's equation provides a useful guide for the overall kinetics of crystallization, it does not give any insight into the molecular process involved in the nucleation and growth of polymer crystals.

The most widely accepted approach at a molecular level, is the kinetic description of Hoffman et al.[2]. It is essentially an extension of the approach used to explain the kinetics of crystallization of small molecules.

Let us consider again the Gibbs equation (equation 1.1-17). In the primary step of crystallization, i.e. nucleation, a few molecules pack together to form a crystalline embryo. This process will change the Gibbs free energy : the creation of a crystal surface will tend to cause *G* to increase while the incorporation of molecules in the crystal causes a reduction of *G*. A schematic representation of the change in free energy is given in Figure 1.1-10.

[1]Avrami, M. Journal of Chemical Physics, 7: 1103, (1939).
[2]Hoffman, J. D et al. Treatise on Solid State Chemistry. (Plenum, New York, 1976)

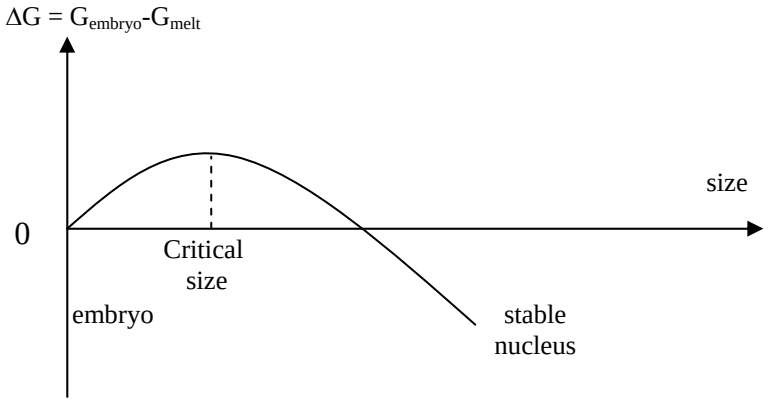

Figure 1.1-10 : Schematic representation of change in free energy for the nucleation process during polymer crystallization

The peak in the curve may be regarded as an energy barrier, which could be overcome by sufficient thermal fluctuation at the crystallization temperature. Once the nucleus is greater than the critical size it will grow spontaneously as this will cause *G* to decrease.

In Hoffman's approach, the polymer crystal is considered to grow on a preexisting crystal surface. We will take as an example the growing on the surface of a lamella (Figure 1.1-11). In this process, new chain segments are added by chain folding on the smooth crystal surface. Assuming that the lamella has a fold surface energy γ_e and a lateral surface energy γ_S, the change in free energy in the lamella involved in laying down *n* adjacent molecular strands or stems of length *l* will be

$$\Delta G_n = 2bl\gamma_S + 2nab\gamma_e - nabl\Delta G_V \qquad \textit{Eq. 1.1-23}$$

the first part $2bl\gamma_S+2nab\gamma_e$ being the increase of free energy due to the increase in surface and $nabl\Delta G_v$ being the reduction in free energy because of the incorporation of stems in the crystal.

At the "equilibrium melting temperature" T^0_m, we have

$$\Delta G_v = \Delta H_v - T_m^0 \Delta S_v = 0 \qquad \textit{Eq. 1.1-24}$$

so, by introducing the degree of under cooling $\Delta T = (T^0_m - T)$, we get

$$\Delta G_v = \frac{\Delta H_v \Delta T}{T_m^0} \qquad \textit{Eq. 1.1-25}$$

For a large number of stems *n*, $2bl\gamma_S$ is negligible, and by introducing a critical length scale l^0, that will be achieved when the nucleus becomes stable $(\Delta G_v = 0)$, equation 1.1-23 becomes

$$l^0 \sim \frac{2\gamma_e T_m^0}{\Delta H_v \Delta T} \qquad \textit{Eq. 1.1-26}$$

which is known as the Thomson-Gibbs's relation (Gedde[1])

The inverse proportionality between l and ΔT which is observed experimentally is therefore predicted theoretically, although this analysis is highly simplified.

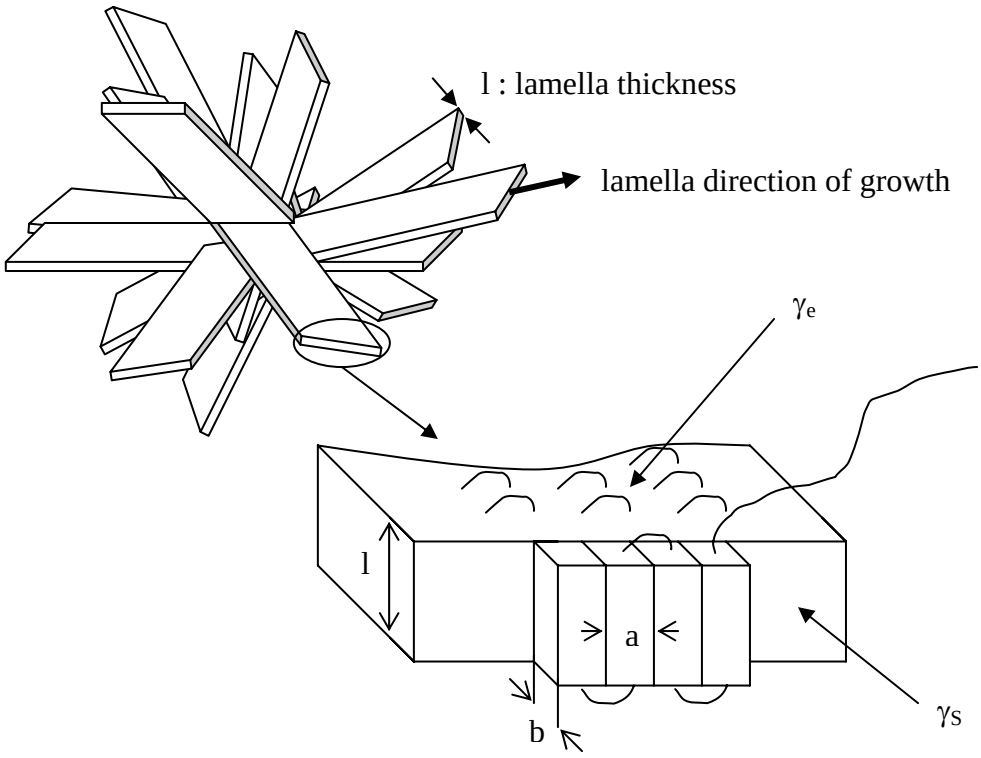

Figure 1.1-11 : Model of the growth of a lamellar polymer crystal through the successive laying down of adjacent stems.

This approach is thermodynamic and in the case of crystallization from a melt, the diffusion of chains toward the growing front is indeed the limiting parameter.

[1]Gedde, U. W. Polymer Physics. (Kluwer Academic Publisher, 1995)

1.1.2.3 Melting

The melting of polymers is far more complicated than the melting of small molecules. The melting takes place over a certain range of temperatures and depends upon the history of the specimen and the rate at which the specimen is heated.

The concept of an equilibrium melting temperature T_m^0 is therefore introduced (Hoffman and Weeks[1]), which corresponds to the melting temperature of an infinitely large crystal. Its value can be estimated by an extrapolation procedure.

The melting temperature T_m is always greater than the crystallization temperature T_c, and a plot of T_m versus T_c is usually linear. Since T_m can never be lower than T_c, the line $T_m=T_c$ represents the limit of the melting behavior. By extrapolating the plot to this line, one obtains T_m^0, the theoretical melting temperature of a polymer crystallized infinitely slowly and for which crystallization and melting would take place at the same temperature, which is called the Hoffman-Weeks plot (see Figure 1.1-12).

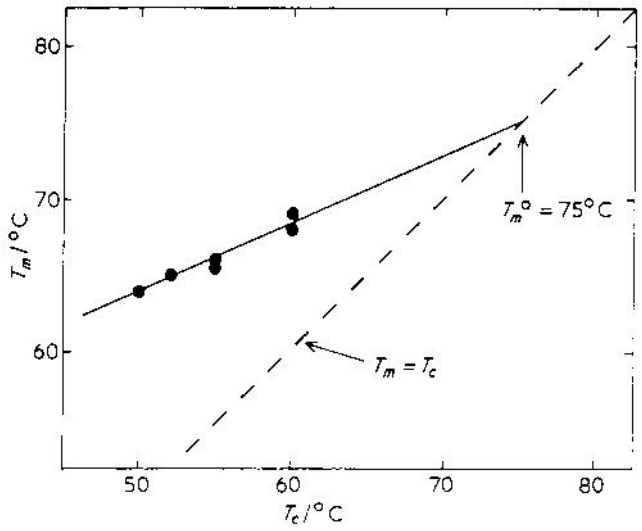

Figure 1.1-12 : plot of the melting temperature, T_m against crystallization temperature, T_c, for poly(dl-propylene oxyde)(after Magill[1]).

There is a strong dependence of the melting temperature on the lamellar thickness, *l*. By considering the thermodynamics of melting of a rectangular lamellar crystal with lateral dimensions x and y, the decrease in surface energy is given by $2xl\gamma_S + 2yl\gamma_S + 2xy\gamma_e$, γ_S being the side surface energy and γ_e the top and bottom surface energy as defined in figure 1.1-11, while the increase in free energy is given by ΔG_v per unit volume due to molecules being incorporated in the melt. The overall change in free energy on melting the lamellar crystal is given by :

[1]Hoffman, J. D. and Weeks, J. J. Journal of Research of the National Bureau of Standards Section a-Physics and Chemistry, 66(JAN-F): 13-&, (1962).
[2]Magill, J. H. *Morphogenesis of Solid Polymers*. (Academic Press, New York, 1977)

$$\Delta G = xyl\Delta G_v - 2l\left(x+y\right)\gamma_S - 2xy\gamma_e \qquad \textit{Eq. 1.1-27}$$

The value of ΔG_v is given by equation 1.1-25, and by considering that the top and bottom are much larger than the sides, we get :

$$T_m = T_m^0 - \frac{2\gamma_e T_m^0}{l\Delta H_v} \qquad \textit{Eq. 1.1-28}$$

where ΔH_v is the enthalpy of fusion per unit volume of the crystals. From equation 1.1-28, it appears that for a finite thickness of the lamellae, T_m is always lower than $T_m{}^0$.

A process which affects the melting behavior of crystalline polymers is annealing. This term, usually used to describe the heat treatment of metals, can be applied to polymers. It was found that when crystalline polymers are heated to temperatures just below the melting temperature, there is an increase in lamellar thickness. This increase in lamellar thickness, l, causes an increase in T_m (see Equation 1.1-28), implying that the measured melting temperature of a given sample will depend upon the time the sample was previously annealed, and then on the heating rate applied.

1.1.2.4 General mechanical behavior of semi-crystalline polymers

We will now briefly describe a typical mechanical behavior of semi-crystalline polymers.

The mechanical response of all polymers is characterized by an elastic part, an anelastic part and a plastic part, the relative magnitude of which depends on the total strain.
At low strains the elastic and the anelastic components dominate while beyond the so-called yield stress, the plastic component becomes dominant.

The plastic deformation of semi-crystalline polymers is particularly complex since they can be assimilated to composite materials with very specific tie molecules between the crystalline domains. A detailed characterization of the plasticity of our semi-crystalline copolymers was beyond the scope of this thesis but some basic concepts of the mechanical properties of solid polymers are useful to keep in mind.

The typical mechanical response of a ductile semi-crystalline polymer to a tensile test is summarized in Figure 1.1-13. At low strains under ε_y, a nearly elastic deformation is observed, where the strain ε is nearly proportional to the applied stress σ. This regime is characterized by an apparent slope E, which is generally taken as the Young's modulus, neglecting the anelasticity. For higher levels of strain, the deformation becomes plastic and preferential orientation can be induced in the sample. The maximum of the stress strain curve is called the yield stress σ_y. When the plastically deformed and oriented part

has extended to the whole sample being tested, a hardening can occur till the breakage of the material.

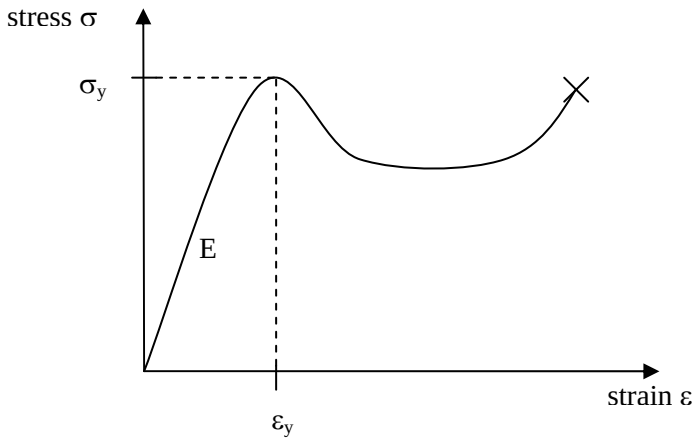

Figure 1.1-13 : schematic stress/strain curves for polymers.

In semicrystalline polymers two cases should be considered in the stress-strain relationships. If the amorphous portion is rubbery, then the polymer will tend to have a low modulus, and the extension to break will be very large. If the amorphous portion is glassy, the polymer will behave much more like a brittle plastic. A schematic stress/strain curves are represented in Figure 1.1-14.

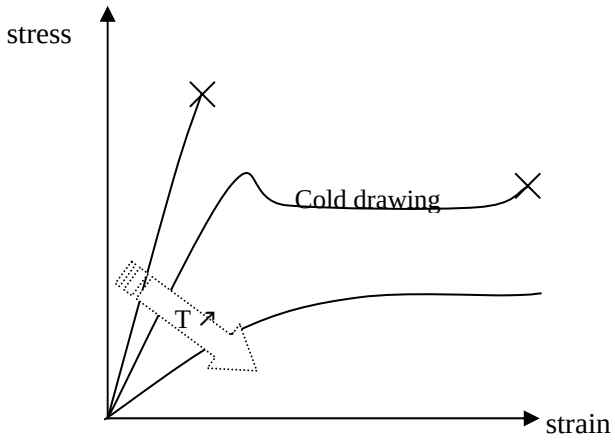

Figure 1.1-14 : schematic stress/strain curves for crystalline polymers

The cold drawing which appears after the yield point in Figure 1.1-14, comes from the rearrangement of the chains in a characteristic and complex manner, beginning with necking. A neck is a narrowing down of a portion of the stressed material to a smaller cross section. The necked region grows, at the expense of the material at either end, eventually consuming the entire specimen.

In the region of the neck, a very extensive reorganization of the polymer takes place. Spherulites are broken up, and the polymer becomes oriented in the direction of the stretch. The number of chain folds decreases, and the number of tie molecules between the new fibrils increases. The crystallization is usually enhanced by the chain alignment. At end of the reorganization, a much longer, thinner, and stronger fiber or film is formed.

The details of this plastic deformation behavior are always greatly dependent on the volume fraction of polymer which is crystallized (the degree of crystallinity), on the average size of the crystallites, and on the so-called tie molecules bridging the crystallites. In particular the yield stress of a semi-crystalline polymer is usually closely related to its degree of crystallinity, with highly crystalline polymers resembling stiff plastics and lightly crystalline polymers having a mechanical behavior resembling that of hard and dissipative elastomers. Therefore the degree of crystallization and hence the thermal treatment can dramatically influence the mechanical properties of a semi-crystalline polymer. This dependence of mechanical properties on the crystalline structure is however very specific of the polymer or copolymer and depends also on the processing conditions. We will discuss this aspect in much more detail for our specific polymer system in chapters 2 and 3.

1.2 Fracture behaviour of polymers

In this section, the fracture behaviour of polymers will be briefly summarized in order to build the theoretical background needed for the study of polymer adhesion. We first introduce some general theoretical concepts which will be useful to interpret the adhesion test we used in our study.

1.2.1 Introduction

The main emphasis of this section is upon the continuum approach where a polymer is considered as a continuum with particular physical properties but for which the molecular structure is mainly ignored.

The theoretical stress to cause cleavage fracture in a brittle solid is of the order of one-tenth of the Young's modulus, *E/10* (Kelly[1]). The modulus of a brittle polymer is typically 3 GPa, so the theoretical strength of such a material should be 300 MPa. Experimental results show that the measured fracture strengths of polymers vary between 10 and 100 MPa. This shortfall in strength was recognized many years ago by Griffith[2] who showed that the relatively low strength of a brittle solid could be explained by the presence of flaws in the material, which act as stress concentrators.

This situation can be easily described for materials which deform in a linear elastic manner. Figure 1.2-1 shows a simple case of an elliptic crack in a polymer sheet under a uniform applied stress σ_0.

[1]Kelly, A. Stong solids. (Charendon Press, Oxford, 1966)

[2]Griffith, A. A. Philosophical Transactions of the Royal Society of London, series A, A221: 163, (1920).

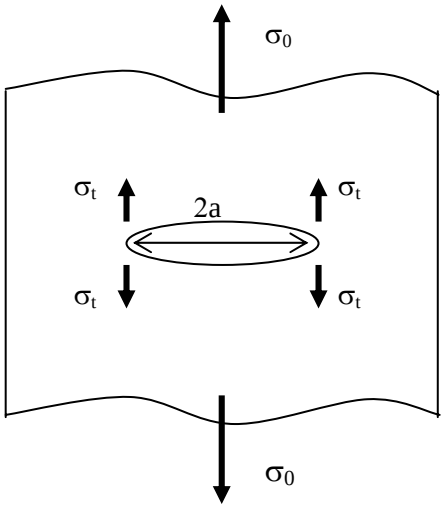

Figure 1.2-1 : model of an elliptical crack of length 2a in a uniformly loaded infinite plate.

The stress σ_t of the crack tip is after Williams[1] :

$$\sigma_t = \sigma_0 \left(1 + 2\sqrt{\frac{a}{\rho}} \right) \qquad \textit{Eq. 1.2-1}$$

where ρ is the radius of curvature of the tip and *2a* the major axis of the ellipse. A singularity appears clearly, when the hole becomes a crack, i.e. for $\rho \rightarrow 0$ the stress goes to infinity. Modified approaches are needed such as the classical energy balance approach of Griffith or the stress intensity factor approach.

1.2.2 Energy balance approach

This approach is based on energy criterion and describes quasi-static crack propagation as the conversion of the work done *W* by an external force and the available elastic energy *U* stored in the bulk of the sample, into a surface free energy γ:

$$\frac{d(W-U)}{da} \geq \gamma \frac{dA}{da} \qquad \textit{Eq. 1.2-2}$$

where *dA* is the increase in surface area associated with an increment of crack growth *da*. For a crack propagating in a thin sheet of thickness *b*, we obtain with *dA = 2b.da* :

$$\frac{1}{b}\frac{d(W-U)}{da} \geq 2\gamma \qquad \textit{Eq. 1.2-3}$$

[1]Williams, J. G. Fracture Mechanics of Polymers. (Ellis Horwood Limited, New York, 1984)

However, for most polymers, the energy to propagate the crack is more than twice the value of the surface energy. This discrepancy comes from the fact that even in the most brittle polymer, a localised viscoelastic or plastic energy dissipation occurs, close to the crack tip, which is not taken into account in the value of 2γ.

The term 2γ may be replaced by the symbol G_c which will encompass all the energy losses incurred around the crack tip. It is therefore the energy required to increase the crack by a unit length in a specimen of unit width. The fracture criterion then becomes :

$$G = \frac{1}{b}\frac{d\left(W-U\right)}{da} \geq G_c \qquad \textit{Eq. 1.2-4}$$

G_c can be written as the sum of an intrinsic fracture energy G_0 which is the energy required solely for bond rupture and a term ψ, which corresponds to the energy dissipated in viscoelastic and plastic deformation at the crack tip. The value of ψ is usually the major contribution to the value of G_c.

$$G_c = G_0 + \psi \qquad \textit{Eq. 1.2-5}$$

We will now concentrate on materials which obey Hooke's law, on which the concepts of linear elastic fracture mechanics (LEFM) can be applied.

Let us consider a crack of length a in the bulk loaded by a generalised force P (Figure 1.2-2).

The loading is represented by the linear load deflection curve (i), then, at point A, the crack grows so that the load and displacement changes ($d\Delta$ and dP), and finally the unloading would give curve (ii).

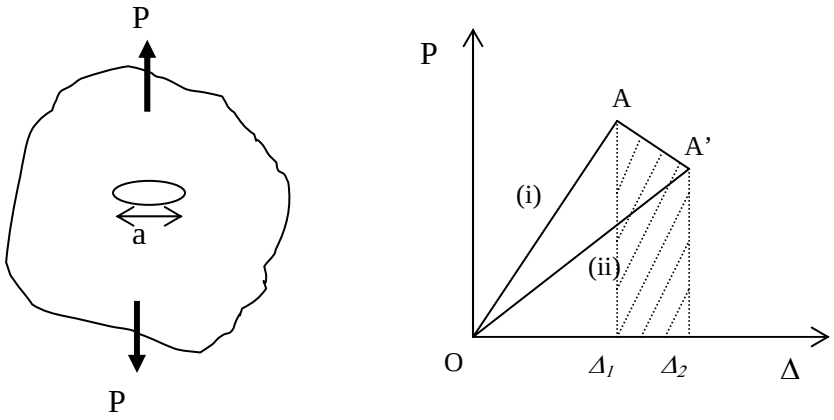

Figure 1.2-2 : generalised loading of a cracked body which exhibits bulk linear elastic behavior.

The change in stored energy is the difference between the two integrated areas under the curves (i) and (ii) (the two triangles $OA\Delta_1$ and $OA'\Delta_2$) :

$$dU = U_2 - U_1 = \frac{1}{2}\left(P + dP\right)(\Delta + d\Delta) - \frac{1}{2}P\Delta \qquad \textit{Eq. 1.2-6}$$

The external work, shown as the hatched area in Figure 1.2-2 is given by :

$$dW = Pd\Delta + \frac{1}{2}dPd\Delta \qquad \textit{Eq. 1.2-7}$$

therefore

$$d\left(W - U\right) = \frac{1}{2}\left(Pd\Delta - \Delta dP\right) \qquad \textit{Eq. 1.2-8}$$

and by putting into equation 1.2-4 the crack propagation criterion becomes:

$$G_c = \frac{1}{2b}\left(\frac{Pd\Delta}{da} - \frac{\Delta dP}{da}\right) \qquad \textit{Eq. 1.2-9}$$

so by using the compliance $C = \Delta/P$ we get

$$\boxed{G_c = \frac{P_c^2}{2b}\frac{dC}{da} = \frac{\Delta^2}{2b}\frac{1}{C^2}\frac{dC}{da}} \qquad \textit{Eq. 1.2-10}$$

with P_c as the load at the onset of crack propagation.

This equation is the foundation for many calculations of G_c, in particular in the case of the double cantilever beam test, described in section 1.2.4.

1.2.3 The stress intensity factor approach

Before presenting the stress intensity factor approach, we should briefly recall the two limitary cases of stress and strain relevant to the fracture of material and the different modes of loading which will be encountered in the fracture of materials.

1.2.3.1 Plane strain, plane stress and different modes of fractures

There are two limitary cases of stress distribution particularly relevant to the fracture of materials. One is plane stress which is obtained in deformed thin sheets as shown in Figure 1.2-3. In a thin body, the stress through the thickness *(σ_z)* cannot vary appreciably due to the thin section. Because there can be no stresses normal to a free surface, $\sigma_z = 0$

throughout the section, a biaxial state of stress results. This is termed a plane stress condition.

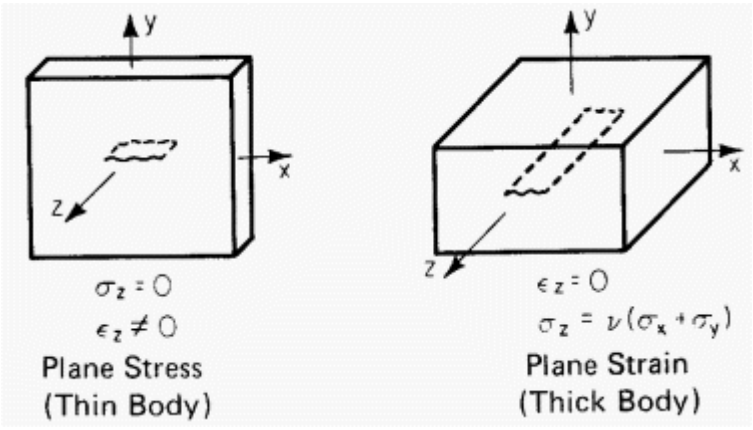

Figure 1.2-3 : schematic representation of plane stress and plane strain.

Another important situation is the case where one of the three principal strains is equal to zero. This is often encountered in the constrained conditions around crack tips in relatively thick sheets. In a thick body, the material is constrained in the z direction due to the thickness of the cross section and $\varepsilon_z = 0$, resulting in a plane strain condition. Due to Poisson's effect, a stress, σ_z, is developed in the z direction.

A crack in a solid may be loaded in three different modes represented in Figure 1.2-4. The following discussion will then mainly be confined to a mode I loading, which is the situation encountered in our work.

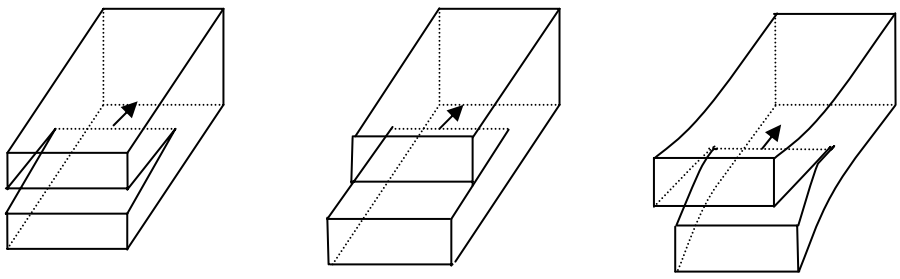

mode I mode II mode III

Figure 1.2-4 modes of loading.

1.2.3.2 Basic principles of the stress intensity factor approach

In the case of a sharp crack in a uniformly stressed infinite sheet shown in Figure 1.2-5 Westergaard[1] has developed stress-function solutions which relate the local concentration of stresses at the crack tip to the applied far-field stress σ_0.

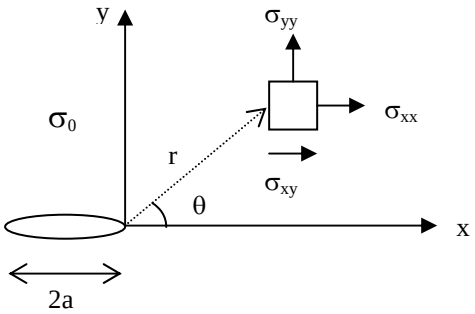

Figure 1.2-5 : sharp crack in a uniformly stressed, infinite sheet.

For regions close to the crack tip the solution takes the form :

$$\sigma_{ij} = \sigma_0 \left(\frac{a}{2r} \right)^{\frac{1}{2}} f_{ij}(\theta) \qquad \textit{Eq. 1.2-11}$$

where σ_{ij} are the components of the stress tensor at a point r, θ in polar coordinates.

Irwin[2] has introduced the parameter K, which is the stress intensity factor. The solution then becomes :

$$\sigma_{ij} = \frac{K}{(2\pi r)^{1/2}} f_{ij}(\theta) \qquad \textit{Eq. 1.2-12}$$

From equation 1.2-12, it is obvious that for $r \rightarrow 0$ the stress goes to infinity, hence it is necessary to have a reasonable local fracture criterion. Irvin postulated that the following condition, $K_I > K_{Ic}$, was a good failure criterion. This criterion has the advantage of being independent of the detailed geometry of the sample far away from the crack tip. Any far-field loading situation would result in the same stress distribution but different intensities reflected by K.

Since the stresses at the crack tip are singular then clearly the yield criterion is exceeded in some zone near the crack tip region. However, if this zone is assumed to be small, the

[1]Westergaard, H. M. Journal of Applied Mechanics, A June: 46, (1939).
[2]Irwin, G. R. Journal of Applied Mechanics, **29**: 651-654, (1962).

elastic stress field will not be greatly disturbed. Dugdale[1] assumed that yielding of the material at the crack tip makes the crack longer by the length of a plastic zone, *R*. The singularity at the crack tip is then cancelled out by a series of internal stresses of magnitude σ_p, usually taken to be the yield stress, σ_y, acting on the boundary of the plastic zone as represented in Figure 1.2-6.

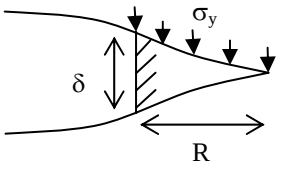

Figure 1.2-6 : the Dugdale line plastic-zone model.

The length of the plastic zone is given by

$$R = \frac{\pi}{8}\left(\frac{K_I}{\sigma_y}\right)^2 \qquad \textit{Eq. 1.2-13}$$

and the thickness $\delta(r)$, of the plastic zone at any distance, r ($\theta=0°$) is given by :

$$\delta(r) = \frac{\pi}{8E^*}\sigma_y R\left[\xi - \frac{r}{2R}\log\left(\frac{1+\xi}{1-\xi}\right)\right] \qquad \textit{Eq. 1.2-14}$$

where

$$\xi = \left(1 - \frac{r}{R}\right)^{\frac{1}{2}} \qquad \textit{Eq. 1.2-15}$$

E^* is the modulus which is equal to Young's modulus, E, in plane stress and $E/(1-\nu^2)$ in plane strain. The crack opening displacement, at the crack tip ($r=0$) is then given by

$$\delta = \frac{8\sigma_y R}{\pi E^*} = \frac{K_I^2}{E^*\sigma_y} \qquad \textit{Eq. 1.2-16}$$

1.2.4 Relationship between G and K

In the case of LEFM a simple relationship exists between G and K, given in mode I by :

[1]Dugdale, D. S. Journal of Mechanics and Physics of Solids, 8: 100, (1960).

$$G_I = \frac{K_I^2}{E} \text{ for plane stress} \qquad \textit{Eq. 1.2-17}$$

$$G_I = \frac{K_I^2}{E}\left(1-\nu^2\right) \text{ for plane strain} \qquad \textit{Eq. 1.2-18}$$

1.2.5 Experimental considerations

A basic aim of fracture mechanics is to provide a parameter, for characterizing crack growth, which is independent of test geometry. We will only present in this section the double cantilever beam geometry, which we used in this thesis. This test has been widely used to measure the fracture toughness at polymer interfaces since its reintroduction by Brown[1] in the late 80's.

In a standard cantilever beam test, a wedge of thickness Δ produces a constant crack opening displacement as shown in Figure 1.2-7. When the crack is at equilibrium, the energy per unit area elastically stored in the deformed beam between the crack tip and the edge is equal to the fracture energy per unit area needed to propagate the crack.

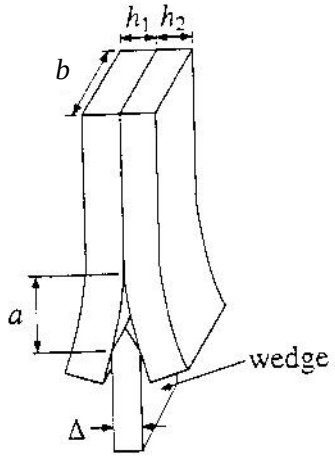

Figure 1.2-7 : the double cantilever beam geometry with a constant opening displacement.

The energy elastically stored in the bent part can be calculated from a classical calculation of the energy stored in a beam, bent by a point load *P*, which can be found in solid mechanics textbooks (Landau and Lifchitz[2]). We will only present the results of the calculation here.

[1]Brown, H. R. Macromolecules, 22: 2859-2860, (1989).
[2]Landau, L. and Lifchitz, E. *Théorie de l'élasticité*. (Mir, Moscou, 1967)

When a prismatic beam of length *a*, width *b* and modulus *E* is bended under the application of a load *P*, the deflection is given by

$$\Delta = \frac{4Pa^3}{Ebh^3} \qquad \textit{Eq. 1.2-19}$$

from 1.2-10 it comes :

$$G_c^{simple} = \frac{3}{8}\frac{\Delta^2}{a^4}Eh^3 \qquad \textit{Eq. 1.2-20}$$

For two beams of different materials we get

$$G_c^{double} = \frac{3}{8}\frac{\Delta^2}{a^4}\frac{E_1h_1^3E_2h_2^3}{E_1h_1^3 + E_2h_2^3} \qquad \textit{Eq. 1.2-21}$$

The formula was simplified in our case of symmetric assemblies where $h_1 = h_2 = h$:

$$G_c^{double} = \frac{3}{16}\frac{\Delta^2 Eh^3}{a^4} \qquad \textit{Eq. 1.2-22}$$

Although the G_c value were found consistent with this model in the case of metals, it appeared that for softer materials, like polymers, Equation 1.2-22 overestimates *G* for short cracks and needs to be modified. A model, developed by Kanninen[1], adds an elastic foundation ahead of the crack tip to the calculation of the bent beam, which leads to a correction factor α :

$$\boxed{G_c^{double} = \frac{3}{8}\frac{\Delta^2}{a^4}\frac{Eh^3}{\alpha^2}} \qquad \textit{Eq. 1.2-23}$$

The determination of the factor α can be found in the pre-cited reference, and depends on the thickness of the beam and on the crack length :

$$\alpha = \frac{1 + 1.92\left(\frac{h}{a}\right) + 1.22\left(\frac{h}{a}\right)^2 + 0.39\left(\frac{h}{a}\right)^3}{1 + 0.64\left(\frac{h}{a}\right)} \qquad \textit{Eq. 1.2-24}$$

It must be pointed out from equation 1.2-23 that knowing the wedge thickness *Δ*, the Young's modulus of the polymer *E* and the thickness of the beam *h*, the only variable to measure is the crack length *a*. This makes the DCB test a particularly convenient test for measuring the fracture toughness.

[1] Kanninen, M. F. International Journal of Fracture, **9**: 83-92, (1973).

This modified beam model was found in good agreement with several experimental studies (Creton et al.[1] and Boucher et al.[2]), even though for very short crack lengths, typically when a/h was less than 4, G_c was still slightly overestimated (Boucher et al.).

This model is based on a calculation at equilibrium. However, experimentally, it appeared more practical to carry out the test in a dynamic way, by pushing the wedge at a constant velocity, in order to see more clearly the artefacts, such as a crack pinned on a defect or the blunting of a crack. Moreover, since the main drawback of this test is the variability in the values of crack length so that a large number of values of crack length are needed on the same assembly in order to get good statistics, waiting for equilibrium would have been extremely time consuming. So, in order to stay in a quasi-static regime, the velocity at which the wedge is pushed was set to a low value experimentally. Boucher et al. checked the validity of the model for different crack velocities and found that G_c was independent of the crack velocity over a range going from 0.3 to 300 $\mu m.s^{-1}$.

To conclude, this test is well adapted for relatively stiff polymers (if not, it is possible to reinforce the beam with another material. This reinforcement has been used in our study for the softer materials) in order to get an elastic deformation of the beam, and a fracture toughness from 1 $J.m^{-2}$ to more than 500 $J.m^{-2}$. For weaker levels of adhesion, it will be difficult to introduce the wedge without delaminating the assembly. For stronger adhesion, the value of the crack length a will be very short and the model will not be accurate anymore.

Crack blunting mechanisms in polymers

In the previous section we described the double cantilever beam test, where the crack is expected to propagate at the same velocity as the wedge. This crack growth is termed “stable” and in those conditions, the crack length is almost independent of the crack velocity, as discussed in the previous section. But in some cases, crack propagation may occur intermittently in a stick-slip manner defining characteristic values for both crack initiation and crack arrest. This is called “unstable” crack propagation. This type of propagation was observed in some of our adhesion experiments. This behavior is summarized in Figure 1.2-8 in a typical load-displacement curve for both stable and unstable crack propagation.

[1]Creton, C., et al. Macromolecules, 25: 3075-3088, (1992).
[2]Boucher, E., et al. Macromolecules, 29(2): 774-782, (1996).

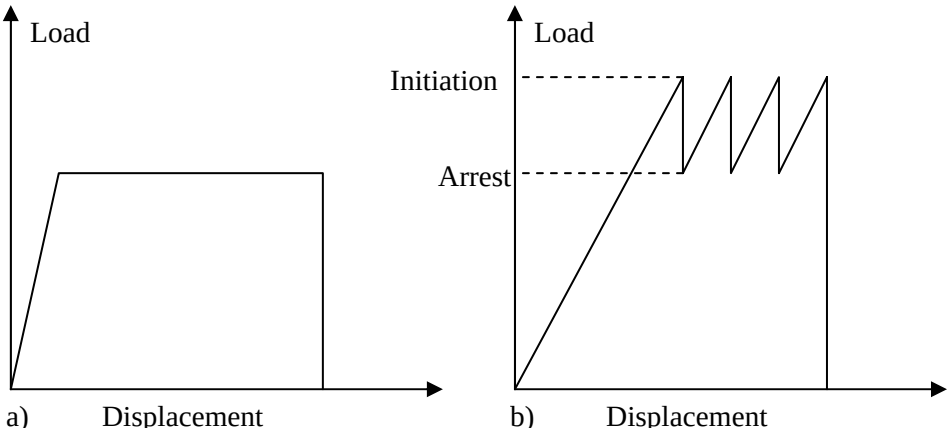

Figure 1.2-8 : typical load-displacement curves for (a) stable, continuous crack propagation ; unstable, stick-slip crack propagation.

The most convincing explanation of the transition from stable to unstable crack propagation stems from the observation of Gledhill et al.[1]. who pointed out that epoxy resins with a low yield stress tend to undergo stick-slip crack propagation whereas the propagation is continuous in high-yield stress resins. They suggested that the low yield stress might promote crack tip blunting and hence unstable propagation.
When a crack blunting mechanism was encountered in our adhesion tests, the fracture toughness was calculated for both crack arrest and crack initiation. More details on the crack blunting can be found in the following reference : Kinloch and Williams[2]

We will now introduce the notion of an interface, i.e. a preferential plane for fracture and focus on the adhesion between polymers in the following sections.

[1] Gledhill, R. A., et al. Polymer, 19(5): 574-582, (1978).
[2] Kinloch, A. J. and Williams, J. G. Journal of Materials Science, 15: 987-996, (1980).

1.3 Adhesion between polymers

In the previous section we reviewed the fracture mechanics of polymers, which is necessary in order to understand the measurement of the fracture toughness of interfaces between polymers. In this section, we will review the different mechanisms that cause adhesion between polymers. A comprehensive view of the studies on polymer adhesion will be given, in a first section for amorphous polymers, and then in the case of semicrystalline polymers which is the bulk of our present study.

1.3.1 Introduction

Adhesion is a complicated process that can be described as the strength of the coupling that can occur between any pair of materials. In a very general thermodynamic sense, however, adhesion can be considered as the reversible energy variation due to the separation of two surfaces :

$$W = \gamma_1 + \gamma_2 - \gamma_{12} \qquad \textit{Eq. 1.3-1}$$

where γ_1 and γ_2 are the surface energies of each material and γ_{12} the interfacial energy.

In this section, we will consider only the adhesion between pairs of polymeric materials, and more specifically the formation of interfaces between non-reactive polymers which are solid at room temperature. In this case, the formation of the interface is non-reversible and the measure of the adhesive strength is carried out via a destructive test, as described in section 1.2, which gives a critical strain energy release rate or fracture toughness of the interface, G_c (see section 1.2).

In glassy polymers, most of the energy necessary to propagate the crack is due to the plastic deformation near the crack tip. When this plastic deformation exists, usually involving a certain volume much larger than the width of the zone of polymer mixing at the interface, it produces a reasonably large G_c. The plastic zone is however also usually much smaller than the characteristic dimensions of the sample, allowing the small scale yielding approximation of linear fracture mechanics to be applied.

In order to produce a reasonable interface reinforcement between polymeric materials, i.e. to activate the plastic deformation mechanisms at the crack tip, a minimum level of stress transfer across the interface is needed.

This stress transfer can be achieved, at a molecular level, by polymer molecules crossing the interface. For two identical polymers it can be due to polymer chains that have crossed the interface by diffusion, they can be due to the crystallization in a single lamella of chains from both sides of the interface, a process we will call co-crystallization, or they

can be due to links created by the chemical reaction between groups from each side of the interface.

In the following review, we will focus on the first two processes, since no chemical reaction can occur in our systems.

In a first section, we will briefly review the different fracture mechanisms for the case of the reinforcement of interfaces between amorphous polymers by connecting chains. The structure of the interface can then be characterized by two parameters: the areal density of connectors Σ, and the degree of polymerization of the connector N.

We will then present some interdiffusion models at polymeric interfaces, illustrated by some experimental studies.

The third part, will be mainly dedicated to experimental studies on interface reinforcement between amorphous and then semicrystalline polymers, in both symmetric and asymmetric cases.

1.3.2 Different fracture mechanisms

These mechanisms have been described in the most detail in the case where the number of connectors and the degree of polymerization of the connectors are known. It is the case usually encountered when the interface between two immiscible polymers is reinforced with a block copolymer. Those mechanisms are reviewed by Creton et al.[1,2]

1.3.2.1 Chain pullout

The chain pull out model, developed specifically for polymer glasses by Xu et al.[3], is described schematically in figure 1.3-1.

[1]Creton, C., et al. Macromolecules, 25: 3075-3088, (1992).
[2]Creton, C., et al. Advances in Polymer Science, 156 : 53-136, (2002)
[3]Xu, D. B., et al. Mechanics of Materials, 11: 257-268, (1991).

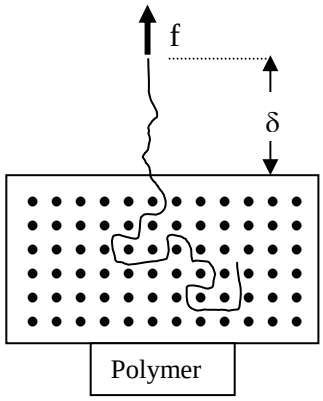

Figure 1.3-1 : a chain, embedded in the polymer, is pulled at one end with a force f.

A chain, embedded in the polymer, is pulled at one end with a force *f*, which is larger than the critical value $f^*=Nf_{mono}$, where *N* is the degree of polymerization of the polymer and f_{mono} the static friction force per monomer. The traction stress component normal to the planar interface (assuming that the chain are pulled out normal to the interface) is related to the force *f* and Σ, the number of chains per unit area of the interface, by $\sigma=f\Sigma$.
Using this model, Xu et al. have demonstrated that for a sufficiently slow crack growth rate, i.e. for $\dot{a} \to 0$, the fracture toughness G_c is given by :

$$G_c(\dot{a}) = G_c^0 = \frac{f_{mono}\Sigma N^2 l_0}{2} \qquad \textit{Eq. 1.3-2}$$

where l_0 is the length of a mer unit.

1.3.2.2 Chain scission

For larger values of *N*, the force required to pull a chain out of the glass, i.e. $f_{mono}N$, will be higher than the force required to break a main-chain bond f_b. In this case, the maximum stress that can be sustained by the interface will be independent of *N*, and equal to $f_b\Sigma$. As long as this interfacial stress is inferior to the crazing stress of both polymers, fracture will occur by simple chain scission and the interface crack will propagate without any significant amount of plastic deformation.

1.3.2.3 Crazing

If the maximum stress that can be sustained by the interface exceeds the crazing stress of the polymer, the propagation of the crack at the interface will be preceded by a craze at the crack tip. The conditions for the nucleation and growth of crazes in a homogeneous polymeric material have been extensively studied, in particular by Kramer and

coworkers[1,2]. We will focus here on the conditions of craze breakdown and on the relationship between the molecular structure at the interface and the macroscopic fracture toughness.

Crazing is a deformation mechanism that can lead to a significant increase in fracture toughness. The energy required to propagate the crack is mainly dissipated by the growth of a craze at the crack tip. This craze corresponds to the plastic zone at the crack tip described in the previous section. The best current model for craze failure at a crack tip is that originally proposed by Brown[3]. In this model, the craze consists of parallel highly oriented, load-bearing fibril, joined by cross tie fibrils. Those cross tie fibrils can have a profound effect on the failure mechanism of a craze since they can transfer stress between broken and unbroken fibrils (see Figure 1.3-2). The existence of such cross-tie fibrils has been confirmed by transmission electron micrographs and electron diffraction (Behan et al.[4], Miller et al.[5])

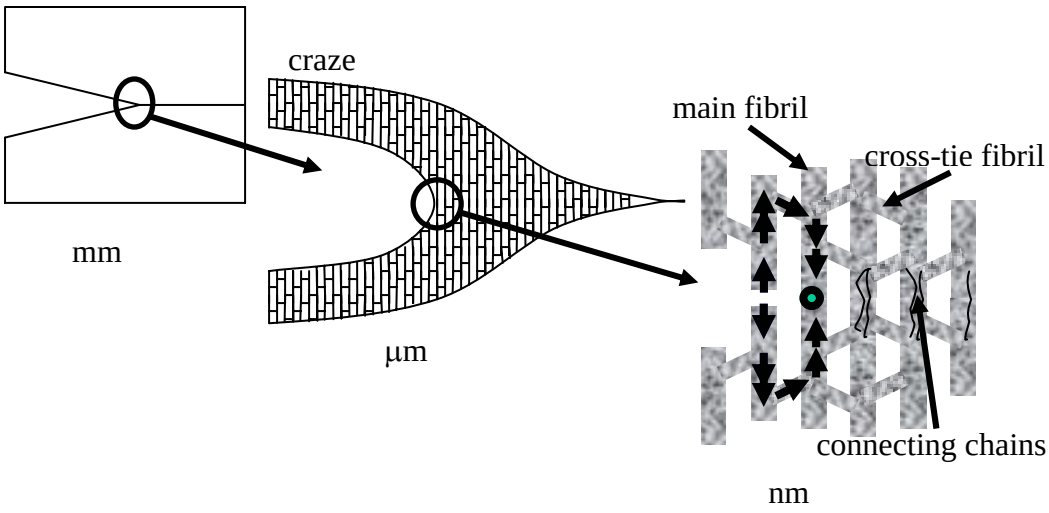

Figure 1.3-2: schematic showing the various structures at different length scales near the crack tip within the craze.

Brown pointed out that this load transfer mechanism allows the normal stress of the fibrils directly ahead of the crack tip to reach the breaking stress of the entangled strands in these fibrils, even if the crazing stress needed for the craze widening and growth σ_c is much lower. By treating the craze as a highly anisotropic continuum with a longitudinal modulus C_{22} and a shear modulus C_{66}, Brown showed that the tensile stress σ_{22} directly ahead of the crack tip (x=0 ;y=0) was :

$$\sigma_{22} = \frac{K_{tip}}{(2\pi x)^{1/2}} \qquad \textit{Eq. 1.3-3}$$

[1]Kramer, E. J. Advances in Polymer Science, 52-3: 1-56, (1983).
[2]Kramer, E. J. and Berger, L. L. Advances in Polymer Science, 91/92: 1-68, (1990).
[3]Brown, H. R. Macromolecules, 24: 2752-2756, (1991).
[4]Behan, P., et al. Proceedings of the Royal Society of London, series A: Mathematical and Physical Sciences, A243: 525, (1975).
[5]Miller, P., et al. Journal of Materials Science, 26: 4445-4454, (1991).

with

$$K_{tip} = A\sigma_c \left(\frac{C_{66}}{C_{22}} \right)^{1/4} \sqrt{h} \qquad \textit{Eq. 1.3-4}$$

where σ_c is the crazing stress, h is the half-width of the craze at the crack tip and A is a constant of order 1.

In further developments of the model, Hui et al.[1] and Sha et al.[2] gave the full field solution of Brown's model directly ahead of the crack tip (y=0 ; x) :

$$\sigma_{22} = \sigma_c \left(1 - \exp\left[-\frac{\pi x \left(C_{22} / C_{66} \right)^{1/2}}{h} \right] \right)^{-1/2} \quad (x>0) \qquad \textit{Eq. 1.3-5}$$

For the case of a craze at an interface, h is related to the continuum opening displacement δ at the crack tip by :

$$\delta = h\left(1 - \nu_{fibrils}\right) \qquad \textit{Eq. 1.3-6}$$

where $\nu_{fibrils}$ is the volume fraction of the fibrils within the craze.

For a craze sufficiently thick, the distance between the main fibrils, *d*, is much smaller than $(C_{66}/C_{22})^{1/2}h$ so the average tensile stress on the continuum fibril structure at a distance $D \sim d/2$ is given by:

$$\sigma_{fibril} = \frac{K_{tip}}{\left(2\pi D\right)^{1/2}} \qquad \textit{Eq. 1.3-7}$$

The failure criterion for the critical opening displacement δ_c at the crack tip is given by $\sigma_{fibril} = \Sigma_{eff} b$, where Σ_{eff} is the number of effective connector strand per unit craze area. If σ_c is assumed to be constant along the craze, we have

$$G_c = \sigma_c \delta_c \qquad \textit{Eq. 1.3-8}$$

$$G_c = h\left(1 - \nu_{fibril}\right)\sigma_c \qquad \textit{Eq. 1.3-9}$$

Using equation 1.3-4, 1.3-6 to 1.3-9 we finally get :

$$G_c = \frac{2\pi D\left(1 - \nu_{fibril}\right)}{A^2} \sqrt{\frac{C_{22}}{C_{66}}} \frac{\Sigma_{eff}^2 f_b^2}{\sigma_c} \qquad \textit{Eq. 1.3-10}$$

[1] Hui, C. Y., et al. Macromolecules, 25: 3948-3955, (1992).
[2] Sha, Y., et al. Acta Materialia, 45(9): 3555-3563, (1997).

which directly relates the macroscopic fracture toughness G_c with the molecular stress transfer at the interface. In the case of connecting chains, the maximum stress that can be transferred at the interface is given by : $\sigma_{fibril}=\Sigma_{eff}.f_{b.}$

We note from equation 1.3-10 that G_c is proportional to σ_{fibril}^2 and inversely proportional to the crazing stress σ_c.

It can be useful now to discuss on the different transitions between these three mechanisms, i.e. the transition from chain pullout to crazing or from chain scission to crazing.

1.3.2.4 Transition between the different mechanisms

In the case of relatively short connectors, typically when $N<N_e$, the most common mechanism for low areal density is the chain pullout described in section 1.3.2.1. For a given chain length, an increase in the areal density will result in a higher value of the stress that can be sustained at the interface without pullout occurring. The maximum stress that can be achieved will be determined either by the saturation of the interface (i.e. when no space is available at the interface for additional block copolymer) or by the plastic yield of one of the polymers, i.e. the formation of a craze. The value of the transition between simple chain pull out and crazing is designated Σ^+. Experimentally, the value of this transition provides a way to estimate the monomer friction force f_{mono}. In the following example of a PVP/PS interface (Poly(2-vinylpyridine)/Polystyrene) reinforced by a dPS-PVP block copolymer (with deuterated PS), the craze occurs on the PS side with a transition from chain scission to failure by crazing, and we get

$$f_{mono_{PVP}} = \frac{\sigma_{craze_{PS}}}{N_{PVP}\Sigma^+} \qquad \textit{Eq. 1.3-11}$$

When N is further increased, the maximum force that is required to pull the chain out of the glass, i.e. $f_{mono}N$, will be higher than the force required to break a main-chain bond f_b. In this case one expects the maximum stress that can be sustained by the interface to be independent of N, and equal to $f_b\Sigma$. As long as this maximum stress remains lower than the crazing stress (or, more generally, the yield stress) of both the homopolymers, the chains will break without much plastic deformation, while when $f_b\Sigma>\sigma_{craze}$, a craze will form and propagate at the interface ahead of the crack, causing a sharp increase in the measured fracture toughness. For a given system, f_b and σ_{craze} are fixed so that the transition should occur at the same value of Σ, defined as Σ^*, provided that the connecting chain is long enough to avoid pullout. Although the jump in G_c is not always clearly seen experimentally, there is always at least a sharp increase in the slope of the measured G_c versus Σ plot.
These transitions are summarized in Figure 1.3-3.

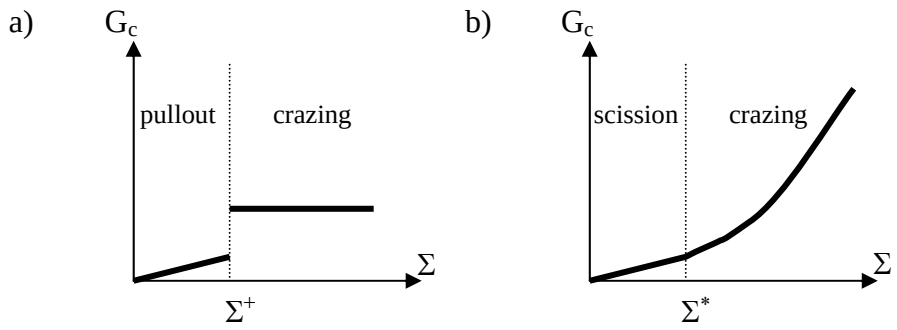

Figure 1.3-3: a) short connectors ($N<N_e$) : transition from pullout to crazing at $\Sigma=\Sigma^+$ b) long connectors ($N>N_e$) : transition from scission to crazing at $\Sigma=\Sigma^*$.

We have reviewed the three main failure mechanisms that can occur at a polymer interface, and the different parameters that influence the transition from one to another. We will now discuss in more detail the thermodynamics and the kinetics of the molecular structure of polymer interfaces.

We will focus on mutual interdiffusion between identical pairs of polymers, which is the case encountered in our study, but we will also briefly present the immiscible case.

1.3.3 Interdiffusion at polymer interfaces

When two surfaces are brought in contact, a preliminary step is needed to allow the interdiffusion to occur. Indeed, intimate contact is the first requirement for further reinforcement of the interface. This process is often named wetting. We will not discuss this point in further detail in this section, since, for melted polymeric interfaces, thanks to the relatively low modulus of polymers, the achievement of intimate contact is relatively fast when a light pressure is imposed. However for very short contact times, this aspect becomes important.

When intimate contact is achieved, the polymer chains can cross the interface by molecular diffusion. The general mechanisms of interdiffusion are based on the well known motion of a polymer chain among other chains described by de Gennes (see section 1.1.1.4).

We will mainly focus our discussion on interfaces between identical polymers where identical chains interdiffuse. For interfaces between two different polymers, which is not the main topic of our study, but which has been extensively studied experimentally, we only present results at thermodynamic equilibrium, i.e. for immiscible polymers.

1.3.3.1 Polymer interdiffusion

1.3.3.1.1 Diffusion and different time scales

Before reviewing the studies on intediffusion at polymeric interfaces, we will first present briefly what is known about the diffusion of polymers in the melt, since in the study of interdiffusion, the different authors have tried to adapt the concept of diffusion to interdiffusion at interfaces.

Polymer self-diffusion in the melt can be described within the framework of the reptation model by Edwards and de Gennes, which was succinctly described in section 1.1.1.4. In this model, the motion of a polymer chain is restricted to a tube formed by the entanglement network of the surrounding chains. Thus different characteristic times are expected for the dynamics of the molecule.

First, there is the Rouse time, τ_e, of the entanglements, which is defined as the time at which the displacement of chain segments of molecular weight M_e becomes comparable to the tube diameter. Second, there is the Rouse relaxation time, τ_R, which is the time when the motion of the single segment becomes coordinated over the entire length of the chain. Finally there is the reptation or tube disengagement time, τ_{rept}, which is the time required for complete disengagement of the chain from its initial tube.

In this time regimes, the predicted mean square displacement of monomers, $<r^2>$, does not evolve with time, t, as in a conventional diffusion process but rather as t^{α}, where $\alpha<1$, becoming 1 only beyond the reptation time. At times $t<\tau_e$, the motion of monomers is essentially the same as in the Rouse model in free space and $\alpha=1/2$. At slightly longer times between τ_e and τ_R, the motion is partly Rouse-like and partly reptative and $\alpha=1/4$. At still longer times, reptation is the dominant motion and $\alpha=1/2$. For $t>\tau_{rept}$ the molecule diffuses effectively as an entity and conventional diffusion behavior ($\alpha=1$) should be recovered.
The molecular weight dependence of the three relaxation times are $\tau_e \sim M_e^2$, $\tau_R \sim M^2$ and $\tau_{rept} \sim M^3$.

A distinctive signature of reptative motion is predicted to occur for the initial stages of interdiffusion of two polymer melts brought in contact, since only the molecules having chain ends at close proximity of the interface can cross it. The interdiffusion process will be now discussed and several studies will be reviewed.

1.3.3.1.2 Interdiffusion at polymeric interfaces

The early stages of polymer interdiffusion across interfaces, are inherently a non steady-state process. The studies on interdiffusion have progressed with the appearance of suitable techniques, like Neutron Reflectivity (NR) or Dynamic Secondary Ion Mass Spectroscopy DSIMS.

Stamm et al.[1] and Kunz and Stamm[2], studied the initial stages of polymer interdiffusion in the case of polystyrene (PS) and poly(methyl methacrylate) (PMMA) respectively. In each study, the interface between two thin films of deuterated and protonated monodisperse polymers have been investigated. The films, of thickness in the range of 50 to 100 nm, were annealed at different temperatures above the glass transition temperature for different times. Annealing times at different temperatures were reduced to a reference temperature using the WLF equation (see section 1.1.4.4 equation 1.1-12). With reflectivity measurements it was possible to determine the interface profile with Ångström resolution. The authors found that the broadening of the interface, which can be taken to be representative of the motion of chain segments, across the initially quite sharp interface, was consistent with a picture given by the reptation model. In particular the power dependence of ¼ was observed in a time range corresponding to the "reptation regime". The time regime of the broadening was found to deviate at small diffusion times from the models proposed in the case of diffusion.

However, deviations from this ideal behavior are expected to be due to the initially distorted chain conformations, the enrichment of ends at the interface, and fluctuation due to capillary waves.

This enrichment of ends at the surface has been proved by Zhao et al.[3], by neutron reflectivity on interfaces between monodisperse PS. The authors used monodisperse PS chains with short blocks of deuterated polystyrene (dPS) at each end. The samples were prepared by spin casting a layer of the triblock copolymer, approximately 240 nm thick, on a silicon wafer. The Si wafer was etched with HF to remove the native oxide, in order to avoid any preferential interactions with either dPS of PS. The segregation of chain ends at either the Si or vacuum interfaces after annealing at 160°C, was probed by neutron reflectivity. The authors found a degree of segregation larger than a factor 2 after annealing at 160°C for 24h.

Almost the same type of material was used in the study of Russell et al.[1], in order to get a direct observation of reptation at polymer interfaces. The authors used two layers of polystyrene, each layer consisted of polystyrene chains that had been 50% deuterated. One layer consisted of a triblock copolymer with the deuterated part at each end, while in the other layer the deuterated part was in the middle, i.e. one layer consisted of a DHD-

[1]Stamm, M., et al. Europhysics Letters, 14(5): 451-456, (1991).
[2]Kunz, K. and Stamm, M. Macromolecules, 29: 2548-2554, (1996).
[3]Zhao, W. et al. Macromolecules, **26**: 561-562, (1993)

labeled PS triblock and the other of a HDH-labeled PS triblock. The length of the deuterated PS end blocks was one-half that of the center protonated PS block for one layer and a HDH polystyrene triblock copolymer of equal molecular weight where the labeling had been reversed, for the other layer. The experiment is schematically shown in Figure 1.3-4.

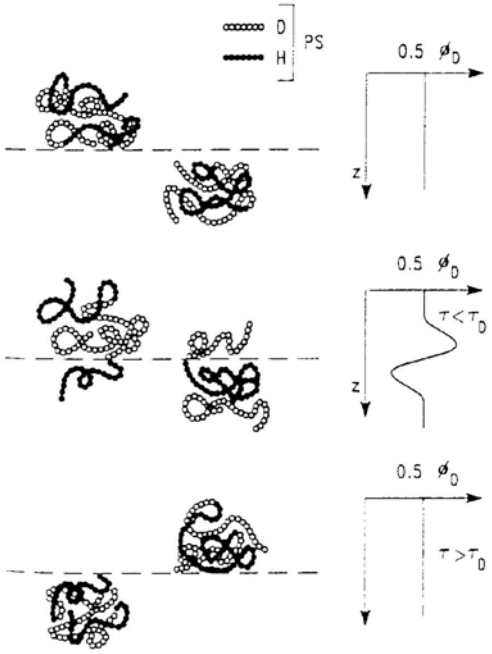

Figure 1.3-4 : diagram of the interface between a layer of HDH- and DHD- labeled polystyrene (PS) showing only a few of the polymer chains (from Russell et al.)

As shown schematically in Figure 1.3-4, it was found that at temperatures above the glass transition (~100°C) the ends of the chains diffused across the interface, leading to an excess of deuterium on the HDH side and a depletion on the DHD side after a certain time t, less than the reptation time τ_{rept}. As the diffusion proceeded, the maximum and minimum in the profile vanished for $t > \tau_{rept}$. The profiles of deuterium and hydrogen across the interface were determined by dynamic secondary ion mass spectroscopy.
In this experiment nearly 120 minutes (slightly less than the Rouse relaxation time) were required before any excess was observable. The amplitude of the excess reached its maximum at t~1 080 min and vanished by 2 880 min which corresponds well to the calculated reptation time at 118°C (2 200 min).
The same group[2] using neutron reflectivity and Dynamic Secondary Ion Mass Spectroscopy, studied the same system with different molecular weights, i.e. high molecular weight HDH/DHD pairs (typically M_w above 100 kg.mol^{-1}) and pairs with a molecular weight of the order of magnitude of the molecular weight between entanglements (30 kg.mol^{-1}). The authors found a maximum in the profile or a “ripple” in

[1]Russell, T. P. et al. Nature, **365**: 235-237, (1993).
[2]Agrawal, G., et al. Journal of Polymer Science: Part B: Polymer Physics, 34: 2919-2940, (1996).

the case of high molecular weight system, while the oscillation were completely missing in the 30 kg.mol^{-1} and 50 kg.mol^{-1} HDH/DHD polymers when the molecular weight was of the order of magnitude of the molecular weight between entanglements. The authors attribute this lack of oscillation to a combination of surface roughness and fluctuations of the order of 30Å.
The authors confronted their results with two models : the Rouse polymer mode coupling (PMC) (Schweizer[1]), which is a tubeless model, and reptation dynamics. The authors found that, the reptation model was a better candidate mechanism of interdiffusion at polymer-polymer interfaces.
This conclusion is in good agreement with the other studies presented above.

We will mention at last the theoretical paper of Brochart-Wyart and Pincus[2]. In this paper the earliest time of contact between two identical polymers A and B is studied (with similar molecular weight higher than the molecular weight between entanglements $N_a=N_b>>N_e$). The asymmetry in left/right interpenetration was simplified to the case where initially ($t=0$) the A side has strong end segregation to the interface while the B side has its ends distributed randomly. The authors define several regimes. First a free interpenetration of the chains ends of A in B occurs, which creates a discontinuity in the concentration profile. For $t>\tau_e$ the end dominance of the interdiffusion creates an asymmetry with more A monomers being dragged into B region. At times between τ_e and τ_R, the B side acts like a transient polymer network and slows down the interdiffusion of A. At time t such as $\tau_R<t<\tau_{rept}$ the profile becomes symmetric and the interdiffusion is controlled by the slow interdiffusion of B in A. At $t>\tau_{rept}$ the initial asymmetry is lost.

This theoretical approach may explain the fast but thin broadening observed experimentally at short times, followed by a slowing down of the interdiffusion.

As a summary, at the earliest times of contact, the chain ends play an important role in the interdiffusion process, producing a fast but very thin broadening of the interfacial region, then the interdiffusion slows down and follows a reptation dynamics, with a good correlation between the observed experimental time and the different time regimes given by the reptation theory.

We will now review the different studies where an attempt of correlation between this interdiffusion process and the toughness of the interface was made.

[1]Schweizer, K. S. Journal of Chemical Physics, 91: 5822, (1989).
[2]Brochart-Wyart, F. and Pincus, P. Comptes Rendus de l'Académie des Sciences de Paris, Série II: 131-138, (1992).

1.3.3.1.3 Fracture toughness and interdiffusion: early studies

In one of the first systematic studies of polymer welding by Voyutskii[1], and Voyutskii and Vakula[2], the authors showed that the buildup of strength at the interface between two polymers involved not only full wetting, but also diffusion of the polymer chains across the interface. It is only twenty years later than the necessity to understand polymer welding motivated a series of more systematic studies on polymer interdiffusion and adhesion. This first series of experiments was typically performed with polydisperse amorphous polymers and often the studies were called crack healing experiments. A homogeneous polymer was fractured at room temperature and the two fractured pieces were then pressed together at a temperature above the T_g of the polymer for different amounts of time.

In these experiments Jud et al.[3] demonstrated that the measured fracture toughness of an interface between identical polymeric species increased with the square root of the time of contact above T_g. This result was taken as a proof that adhesion between two polymers involved molecular interdiffusion. Based on this idea several relatively simple models were proposed.

Along the same lines and at about the same time, an alternative model was proposed. Each time a piece of interdiffusing chain crosses back and forth through the interface, it creates a molecular bridge. The bridge model for welding by de Gennes[4,5] and Prager and Tirrell[6] proposed that the number of bridges crossing the interface (the so-called "crossing density") determines the fracture energy. It is assumed that this crossing density is simply proportional to the fracture energy, which results in the following scaling law with respect to the welding time and molar mass :

$$G_c \sim M^{-3/2} t^{1/2} \qquad \textit{Eq. 1.3-12}$$

In the experimental paper of Jud et al., the authors propose that the fracture energy, in the case of perfect wetting, is determined by the total number of entanglements per chain per unit area. This assumption is actually similar to the bridge model and leads the same dependence as equation 1.3-12.

In both cases, the assumptions on diffusion mechanisms are reasonable but there was simply not a sufficient understanding of the fracture process to propose a relationship between G_c and the molecular structure.

[1]Voyutskii, S. S. Rubber Chemistry and Technology: 748-756 (1959).
[2]Voyutskii, S. S. and Vakula, V. L. Journal of Applied Polymer Science, **7**: 475-491, (1963).
[3]Jud, K. et al. Journal of Materials Science, **16**: 204-210, (1981).
[4]de Gennes, P. G. Comptes Rendus De L Academie Des Sciences Serie Ii, **292**(23): 1505-1507, (1981).
[5]de Gennes, P. G. Physics Today, 36(6): 33-&, (1983).
[6]Prager, S. and Tirrell, M. Journal of Chemical Physics, **75**(10): 5194-5198, (1981).

1.3.4 Polymer adhesion between amorphous polymers: the modern view

1.3.4.1 Introduction

Following these early studies of polymer-polymer adhesion, further progress only came in the early 90's with the advances made in the understanding of the micromechanisms of fracture at interfaces and the development of neutron reflectivity as a technique to measure interfacial width between polymers with Angström resolution.

As discussed in the introduction, the mechanical strength of polymeric interfaces is based on the presence of entangled connectors at the interface, which will allow a certain stress transfer across the interface.

Diffusion of chains across the interface can create such reinforcement, as the chains will act as connectors and will be able to transfer stress.

We will review now different studies on fracture toughness of interfaces between amorphous polymers, and divide them in two main categories. The first type of studies focuses on simple polymer-polymer interfaces. The parameters controlling G_c will be the interfacial width and the average distance between entanglements. It will be shown that the chains need to diffuse over a certain distance, in order to entangle and therefore be able to transfer the stress between those physical links. The second type of studies focuses on the reinforcement of interfaces by the addition of connectors at the interface. Usually this method is used to reinforce interfaces between very immiscible polymers by adding diblock copolymers at the interface, each block being entangled with its respective homopolymer.

1.3.4.2 Direct adhesion between amorphous polymers

In this case, the parameters controlling the mechanical strength of the interface are not independent, but one can still consider the interfacial width a_i and the degree of polymerization N of the chains as the controlling parameter. It has been found by several groups, that the fracture toughness was directly linked to the interfacial width (Schnell et al.[1,2], Brown[3] and Benkoski et al.[4]). The results are summarized in Figure 1.3-5. The direct measurement of the interfacial width was carried out by neutron reflectivity. Note that the polymers of these studies are all monodisperse and not polydisperse. Since the χ parameter has been varied in these experiments by coupling either identical or slightly different polymers (PS/PS, PS and brominated PS, PS and poly(p-methylstryrene)), the

[1]Schnell, R., et al. Macromolecules, 31: 2284-2292, (1998).
[2]Schnell, R., et al. Macromolecules, 32(10): 3420-3425, (1999).
[3]Brown, H. R. Macromolecules, 34: 3720-3724, (2001).
[4]Benkoski, J.-J., et al. Journal of polymer science: Part B: Polymer Physics, 40(20): 2377-2386, (2002).

range of interfacial widths which could be obtained, by varying the molecular weight of the polymers between 150 kg.mol^{-1} and 1250 kg.mol^{-1} and the annealing temperature from 140 to 185°C, was 9-13 nm.

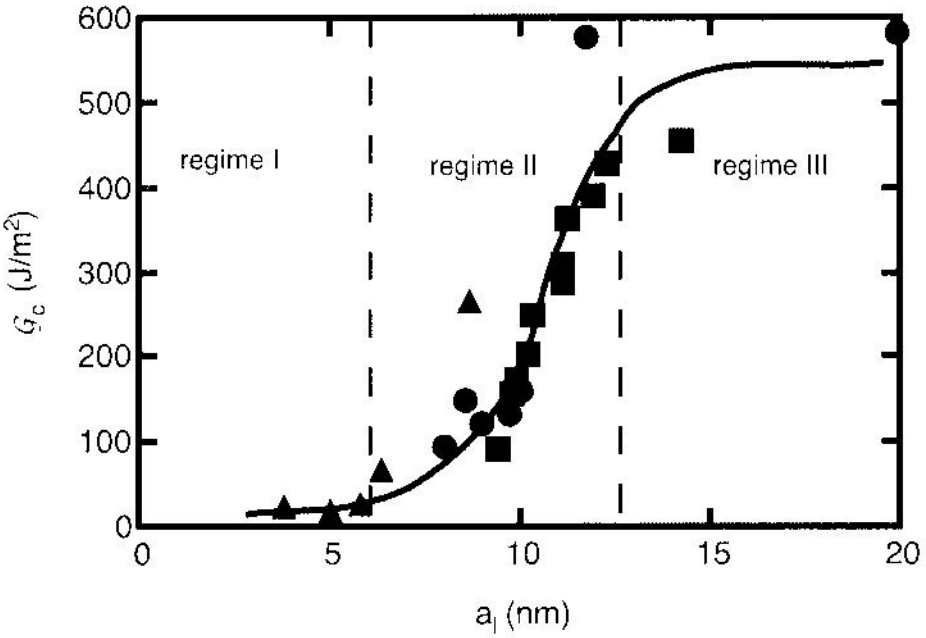

Figure 1.3-5 : fracture toughness G_c of interfaces between several glassy homopolymers as a function of their width a_i. (●) PS/PS interfaces ; (■) PS/PpMS interfaces ; (▲) PS/PBrsS interfaces from Schnell et al.[1]
PpMS : poly(p-methylstryrene) and PBrS : Brominated PS

The results of Figure 1.3-5 clearly show three different regimes which can be interpreted in terms of microscopic failure mechanisms.

- in regime I, G_c is low and presumably the failure mechanism is simple chain pull out or simple chain scission.
- in regime II, G_c increases sharply with interfacial width, suggesting a transition from pullout or scission to crazing.
- in regime III, the failure stress becomes independent of the interfacial width and G_c is that of the bulk homopolymers.

It is quite clear from this data that the variation of G_c with interfacial width is largely non linear at least for monodisperse polymers (compared with the early models).

The transition from chain pullout to crazing can be interpreted as the point where the stress that can be sustained by the interpenetrated chains is higher than the crazing stress. The transition from regime II and III is indicative of the fact that the interface can no longer be distinguished from the bulk by its fracture mechanism.

From these results, an expected fracture mechanism map can be represented (Creton et al.[1]). In Figure 1.3-6 an interfacial width a_i normalized by the average distance between entanglements points d_e is represented as a function of N/N_e, N_e being the average degree of polymerization between entanglements.

For low values of N/N_e, chains will disentangle easily and no crazing will occur (*w*). For a very narrow interfacial width, the interpenetration at the interface is insufficient to activate crazing (*s* or *p* region). By increasing a_i/d_e, crazing appears, with a transition essentially from pullout for low values of N/N_e (c^1 region) and from scission for higher N/N_e (c^2 region). For high a_i/d_e, the fracture toughness is indistinguishable from that of the bulk. However, the fracture toughness is found *N*-dependent for low N/N_e and *N*-independent for high N/N_e.

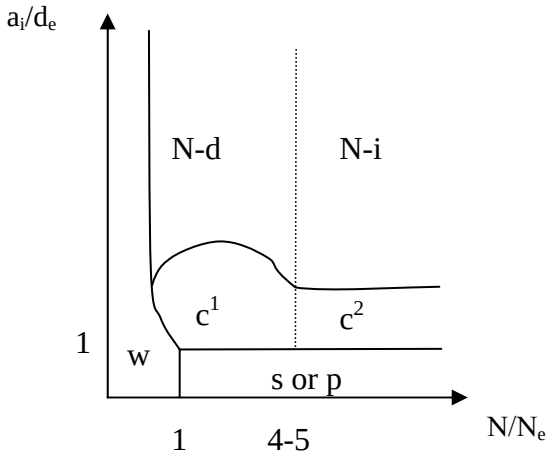

Figure 1.3-6 : fracture mechanisms map for interfaces between glassy polymers as a function of normalized degree of polymerization N/N_e and normalized interfacial width a_i/d_e.

1.3.4.3 Surface reinforcement of interfaces between immiscible amorphous polymers by addition of a copolymer

Since we will focus below on adhesion at interfaces between two immiscible polymers, it is appropriate to describe briefly what is known about such interfaces.

We discussed previously the case of miscible polymers, where the problem of interdiffusion is essentially a kinetic one. In the case of immiscible polymers, we are faced with a thermodynamic problem, where detailed interactions between the segments of two immiscible polymers need to be understood. In this case, the equilibrium structure of the interface is not controlled by the annealing time but rather by the segmental interaction parameter (χ) (introduced by Flory-Huggins (Flory[2] 1953)) of the polymer

[1]Creton et al. Advances in Polymer Science. **156:** 53-136 (2002)
[2]Flory, P. J. *Principles of Polymer Chemistry* (Cornell University Press: Ithaca, New York, 1953).

blend and its molecular weight. The Gibbs free energy of mixing (per segment) of any two homopolymers A and B is given by the Flory-Huggins expression :

$$\frac{\Delta G(\varphi)}{k_B T} = \left(\frac{\varphi}{N_a}\right)\ln\varphi + \left(\frac{1-\varphi}{N_b}\right)\ln(1-\varphi) + \varphi\chi_{AB}(1-\varphi) \qquad \textit{Eq. 1.3-13}$$

where φ is the volume fraction of polymer A, N_A and N_B are the degrees of polymerization of polymer A and polymer B, and χ_{AB} is the Flory-Huggins interaction parameter.

Since χ_{AB} between any two polymers chosen at random is usually positive, equation 1.3-13 implies a strong immiscibility for typical polymer degree of polymerization. In the limit $\chi N >> 1$; the segment volume fraction profile along a coordinate z normal to the interface is given by (Helfand and Tagami[1]) :

$$\varphi(z) = \frac{1}{2}\left(1 - \tanh\left(\frac{2z}{a_i}\right)\right) \qquad \textit{Eq. 1.3-14}$$

where a_i is an interfacial width given by :

$$a_i = \frac{2b}{\sqrt{6\chi}} \qquad \textit{Eq. 1.3-15}$$

and where b is an appropriately averaged statistical segment length of the two polymers.

The very small widths of such immiscible interfaces lead to little penetration of A chains into B chains, and vice versa, and thus very few entanglements are made across the interface. This lack of entanglements across the interface is thought to be responsible for the very low adhesion, as represented by G_c of such interfaces.

Thus, to increase the adhesion it is generally required to replace the entanglements network strands that would naturally span the plane of the interface if the same polymer were on both sides, with some sort of molecular connections. These are produced by block copolymers that reside at the interface and entangle with the polymers on either sides.

When a compatibilizer is added at the interface between two amorphous polymers, it is commonly a diblock copolymer in which each block is miscible with one of the two polymers. In this case, we have access experimentally to two relevant parameters which are the areal density of connectors Σ and the degree of polymerization of the connector N.

Three homopolymers (diblock copolymer) phase boundary systems have been studied extensively : the system polystyrene (PS and poly(2-vinylpyridine) (PVP) reinforced with

[1]Helfand, E. and Tagami, Y. Journal of Chemical Physics, 57(4): 1812-&, (1972).

diblock copolymers of PS-PVP (Creton et al.[1], Xiao et al.[2], Washiyama et al.[3,4,5]), the system of poly(methyl methacrylate) (PMMA) and PS reinforced with diblock copolymer of PMMA-PS (Brown[6,7], Cho et al.[8]) and the system PMMA and poly(phenylene oxide) (PPO) reinforced by diblock copolymer PMMA-PS (Brown et al.[9], Char et al.[10], Creton et al.[11]).

The principal goals of these studies were to determine how the fracture toughness G_c of the interface between two immiscible glassy polymers depends on the areal density of connectors present at the interface and on the polymerization indices of each block of the diblock copolymer of the end-functionalized chain. For that purpose, the diblock copolymers were synthesized by anionic polymerization to produce blocks with controlled polymerization indices where one block was usually labeled with deuterium.
In these studies, one of the homopolymers usually has a lower crazing stress than the other and is able to form a stable craze ahead of the crack tip.

The measurement of the areal density of connector chains was typically done on the fracture surfaces after the fracture had occurred by an ion beam technique, like Forward recoil spectroscopy (FRES).

The results have been interpreted in terms of the three mechanisms detailed in section 1.3.2, i.e. the chain pullout, chain scission and crazing, with the two relevant parameters, i.e. the degree of polymerization of the connector N and the areal density of connectors Σ.

It is convenient to summarize the different results with a map as a function of the main normalized parameters (Figure 1.3-7).

The fracture mechanisms map can be represented as a function of Σ/Σ^*, and N/N_e, Σ^* *being* the value of the transition from chain scission to crazing, and N_e being the average degree of polymerization between entanglements of a homopolymer. The N/N_e domain, where simple chain pullout is active (*p* region), decreases however with increasing Σ with a boundary given by: $\Sigma/\Sigma^* = f_b/f_{mono}N$.

For $\Sigma/\Sigma^* < 1$ and $N/N_e > 1$, the failure mechanism becomes chain scission (*s* region). By increasing Σ/Σ^*, crazing appears, with a transition from pullout for low value of N/N_e (c^+ region) and from scission for higher N/N_e (c^* region). At a certain areal density Σ_{sat}, saturation appears where chains can no longer be accommodated at the interface.

[1]Creton, C., et al. Macromolecules, 25: 3075-3088, (1992).
[2]Xiao, F., et al. Macromolecules, 27: 4382-4390, (1994).
[3]Washiyama, J., et al. Macromolecules, 26: 2928-2934, (1993)
[4]Washiyama, J., et al. Macromolecules, 26: 6011-6020, (1993).
[5]Washiyama, J., et al. Macromolecules, 27: 2019-2024, (1994).
[6]Brown, H. R. Macromolecules, 22: 2859-2860, (1989).
[7]Brown, H. R. Journal of Materials Science, 25: 2791-2794, (1990).
[8]Cho, K., et al. Journal of Polymer Science: Part B: Polymer Physics, 28: 1699-1718, (1990).
[9]Brown, H. R., et al. Nature, 341: 221-222, (1989).
[10]Char, K., et al. Macromolecules, 26: 4164-4171, (1993).
[11]Creton, C., et al. Macromolecules, 27: 1774-1780, (1994).

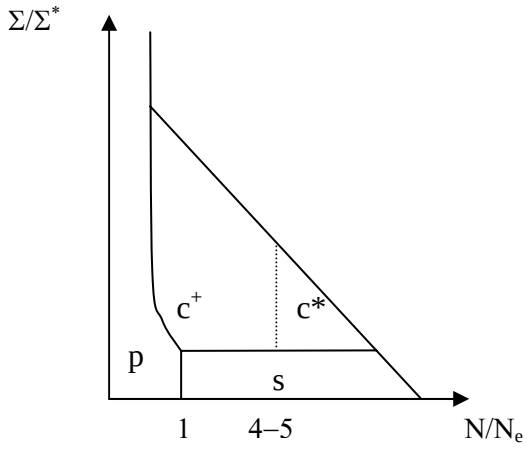

Figure 1.3-7 : fracture mechanics map for interfaces between glassy polymers reinforced with connecting chains. Failure mechanisms are represented as a function of normalized degree of polymerization N/N_e and normalized areal density of connectors Σ/Σ^*.

1.3.5 Adhesion between semicrystalline polymers

While, due to their well-known plastic deformation properties, glassy polymers provide excellent model systems for fracture studies, most engineering plastics are semicrystalline and have plastic deformation mechanisms and adhesion mechanisms which are much less understood.

In the case of semicrystalline polymers, the mechanical reinforcement of the interface can be achieved through either entanglements or through incorporation of polymer chains on both side of the interface in the same crystallite (co-crystallization). The microstructure of the polymer near the interface (highly dependent on thermal treatment) will strongly influence the plastic deformation properties of the polymer near the interface and therefore the measured fracture toughness.

We will first review the studies carried out on the adhesion of semicrystalline polymers. A large part of this work was performed on incompatible semicrystalline polymers, where a copolymer was formed by chemical reaction at the interface. We will then review the work on self-adhesion of semicrystalline polymers which is the topic of this thesis.

1.3.5.1 Reinforcement of incompatible semicrystalline polymers

The reinforcement of incompatible polymers has been widely studied, because of the large number of industrial applications.

Even though incompatible polymers form very thin and mechanically weak interfaces, some attempts were made to reinforce such interfaces, mainly by introducing a copolymer by an in situ reaction.

1.3.5.1.1 Compatibilization by the formation in situ of a copolymer at the interface

The same techniques that were used to study the reinforcement of interfaces between amorphous polymers can in principle be transferred to semi-crystalline polymers. However a number of practical obstacles complicate the life of the experimentalist.

Contrary to amorphous polymers, most semi-crystalline polymers are not soluble, at least below their melting point. This makes it difficult to spin-coat a thin layer of copolymer directly at a planar interface. Furthermore block copolymers may simply not be easy to synthesize. By far the most studied semi-crystalline interface is that between a polyamide and a polyolefin (Bidaux et al.[1],[2], Cho and Li[3], Kalb et al.[4], Kim et al.[5] and Laurens et al.[6]).In this case the copolymer is formed in situ by the reaction at the interface between a maleic anhydride modified polyolefin and the amine of the polyamide. The measurement of the areal density of connectors is more difficult because deuterated polymers are proscribed in an in situ copolymer formation which requires a large quantity of material. In the case of reinforcement between polypropylene (PP) and polyamide-6 (PA6) by a diblock copolymer formed in situ by a chemical reaction, X-ray photoelectron spectroscopy (XPS) appeared as a suitable technique to determine Σ, by monitoring the amount of nitrogen, which originated exclusively from PA6, on the PP surface after removing the PA6 part by an appropriate solvent (Boucher et al.[7]).

On the specific topic of mechanical reinforcement of planar interfaces between semicrystalline immiscible polymers, Bidaux et al.[1], Boucher et al.[7] have both investigated the reinforcement of interfaces between PA6 (T_m = 225°C) and PP (T_m=160°C) with PP-g-MA chains. In this system, a small fraction (1-5%) of functionalized PP (mPP) chains were dissolved in pure PP and reacted at the interface with amine-terminated PA-6 chains. While the first study focused on realistic processing conditions (annealing temperature of a few minutes) and correlated annealing temperature with G_c, the second study focused on correlating the areal density of copolymer chains

[1]Bidaux, J. E., et al. Polymer, 37(7): 1129-1136, (1996).
[2]Bidaux, J. E., et al. Polymer, 39(24): 5939-5948, (1998).
[3]Cho, K. and Li, F. Macromolecules, 31: 7495-7505, (1998).
[4]Kalb, F., et al. Macromolecules, 34(8): 2702-2709, (2001).
[5]Kim, H. J., et al. Macromolecules, 35(4): 1267-1275, (2002).
[6]Laurens, C., et al. Macromolecules, 37(18): 6806-6813, (2004).
[7]Boucher, E., et al. Macromolecules, 29(2): 774-782, (1996).

formed at the interface with the fracture toughness and used lower annealing temperatures and longer annealing times. An additional study was carried out by Cho and Li on the adhesion between amorphous polyamide and PP containing a small percentage of MA functionalized chains. In this case the variables were the annealing time, temperature and concentration of functionalized chains in the PP.

A clear increase in G_c was observed in all three studies when the assembly was annealed at least above the melting point of the PP, implying that the functionalized chains indeed need to diffuse to the interface to react with the amine group of the PA. Bidaux et al.[1] found an increase of G_c with bonding temperature with two well defined transitions corresponding to the melting temperature of grafted-PP (PPg), and to the melting temperature of PA, for a holding time of 9 minutes. Below the PPg melting temperature, there was no significant adhesion. G_c increased gradually with contact temperature between the melting temperature of PP (T_m = 160°C) and the melting temperature of PA (T_m = 221°C). Finally, above the melting temperature of PA, the adhesion was strong (> 600 $J.m^{-2}$). Boucher et al. correlated the fracture toughness with the areal density of connector chains measured by XPS. A square dependence of G_c with Σ was found as predicted by the Brown model (equation 1.3-10) for the case of amorphous polymers, when fracture occurs via a chain scission mechanism. This result was further confirmed by a later study from Kalb et al.[2] where the reinforcement of the interface between a PP-based blend and PA6 gave an identical scaling of G_c with Σ^2.

However, for some annealing conditions, unexpected behaviors were found, and the different authors tried to correlate those behaviors with the morphology at the interface. For PP-aPA6 interfaces, Cho et al. found that G_c became relatively low for contact temperatures above the melting temperature of PP. The authors assumed that above the melting temperature, the mobility of the functionalized PP (mPP) molecules was very high, leading to a phase separation between PP and mPP and then separated lamellae after crystallization, creating the weak part of the assembly. Essentially they found that the mPP must be miscible with the PP to be most effective. This result was also found by Laurens et al.[3].

In the case of PP-PA6 interfaces, Kim et al.[1] using low-Energy Ion beam irradiation to reinforce the interface, found that the fracture toughness increased with the bonding temperature, showed a maximum for a contact temperature of 200°C, and then decreased for a higher contact temperature of 210°C, which is a behavior different from those previously reported. The authors conclude that the adhesive bonding at the interface (i.e. the reaction of maleic anhydride with amine) increases with bonding temperature while the cohesive strength in the bulk in the immediate vicinity of the interface decreases because of less entanglement of reacted chains with the other chains of the bulk PP.

[1]Bidaux, J. E., et al. Polymer, 37(7): 1129-1136, (1996).
[2]Kalb, F., et al. Macromolecules, 34(8): 2702-2709, (2001).
[3]Laurens, C., et al. Macromolecules, 37(18): 6814-6822, (2004).

Boucher et al.[2] by using a higher molecular weight mPP (43 kg.mol^{-1} instead of 23 kg.mol^{-1}), found high values of fracture toughness which no longer uniquely depended on Σ. The authors speculated that the presence of the PP β-phase near the interface could be the main factor responsible for the very high fracture toughness. This argument was however later dismissed by the work of Kalb[3] and Plummer et al.[4], who showed that the high values of the fracture toughness were not due to the presence of the β-phase (identical values of G_c were found for samples with and without β-phase near the interface). Somehow the interfacial structure was able to cause significant amounts of diffuse deformations in the bulk near the crack tip which explained the much higher values of measured toughness compared with the predictions of Brown's model but did not shed light on the reason why these diffuse deformations could develop.

Trying to elucidate the reasons of this anomalous behavior, Laurens et al.[5] investigated the reinforcement of the interface between PA6 and both syndiotactic and isotactic polypropylene (sPP/PA6 and iPP/PA6) by the in situ formation of a sPP-PA6 diblock copolymer. The crystalline orientation at the interface was characterized by grazing angle X-ray diffraction, using thin film assemblies. In both cases epitaxial crystallization of PP on PA6 was observed with a degree of orientation of PP increasing with increasing cooling rates, annealing times, and temperatures. It was found however that sPP-PA6 copolymers were able to mechanically reinforce the sPP/PA6 interface but not the iPP/PA6 interface. The authors demonstrated that the presence of an interfacial orientation of the PP in the vicinity of the interface was not sufficient by itself to promote stress transfer at the iPP/PA6 interface and that a strong mechanical coupling was needed for effective reinforcement. It is likely that the sPP-PA6 copolymer can be incorporated in the sPP homopolymer crystalline lamellae, while the iPP-PA6 cannot.

In another study Laurens et al.[6] used five different types of copolymer with different structures and molecular weights of the PP part, in order to probe the influence of those parameters on the fracture toughness. The authors showed that the most effective reinforcement was achieved when the structure was the most similar to the structure of the bulk, and for sufficiently long PP chains. As all copolymers had a PP block length with M_n greater than 3 M_e, the authors argued that M_e is probably not the key parameter controlling the efficiency of stress transfer, like the situation found for amorphous polymers. The key parameter is more likely the critical length for efficient connections between lamellae, as reported by Benkoski et al.[7] in their study on reinforced interface between amorphous polystyrene and semicrystalline polyethylene by a diblock copolymer. In their study, contact was made at 160°C, well above the melting temperature of PE (low density, T_m = 100°C) for a long time of contact (2h) using diblock

[1]Kim, H. J., et al. Macromolecules, 35(4): 1267-1275, (2002).
[2]Boucher, E., et al. Macromolecules, 30: 2102-2109, (1997).
[3]Kalb, F. *Adhésion, microstructure et microdéformations à l'interface de polymères semi-cristallins*. (Université Paris VI, Paris, 1998)
[4]Plummer, C. J. G., et al. Macromolecules, 31(18): 6164-6176, (1998).
[5]Laurens, C., et al. Macromolecules, 37(18): 6806-6813, (2004).
[6]Laurens, C., et al. Macromolecules, 37(18): 6814-6822, (2004).
[7]Benkoski, J. J., et al. Macromolecules, 36: 3289-3302, (2003).

copolymers (PS-dPE) of different molecular weights and having their PE block deuterated. For relatively short blocks of dPE, i.e. 5 and 7 kg.mol^{-1} (compared to M_n of the polydisperse bulk PE (*I~2*) of 31 kg.mol^{-1}), the fracture energy remained weak and the surface analysis after fracture showed that a pull-out mechanism was active. For longer blocks (30 kg.mol^{-1}) (30PE), a chain pullout to crazing transition was observed for Σ above 0.08 chains.nm^{-2}. For blocks of 85 kg.mol^{-1} (85PE) scission was observed before crazing. In each case, a maximum value for G_c was observed at 0.2 chains.nm^{-2}. Above this areal density, the block copolymers are expelled from the interface due to the entropic penalty of chain stretching. This transition is also observed in TEM by the appearance of cylindrical micelles. The cooling rate of the assemblies has an effect on the G_c values for 30PE but no effect for 85PE. Since the average molecular weight between entanglements, M_e, of PE is about 1 kg.mol^{-1}, much smaller than that of any of the PE blocks, the authors conclude that the major transition in the improvement of the interfacial strength corresponds to the point where the PE block is able to be incorporated in two neighboring crystalline lamellae. This result is in contrast with what occurs for amorphous polymers where entangled chains are able to transfer stress.

In summary, several factors seem to have a great influence on the fracture toughness between immiscible semicrystalline polymer reinforced by the in situ formation of a copolymer, such as the molecular architecture and the molecular weight of the connectors, the annealing conditions, the interfacial density of copolymer, and the crystalline structure at the interface, but none of these parameters, alone, can account for all the observed phenomena, and coupling between these parameters needs to be considered.

1.3.5.1.2 Compatibilizing less immiscible semicrystalline polymers

Some attempts have been made to compatibilize less immiscible polymers without any addition of copolymer at the interface.

Direct compatibilization between polypropylene (PP) and polyethylene (PE) (high density, T_m = 120-130°C) was studied by Yuan and Wool[1] in a butt joint geometry and by Lo et al.[2] in an asymmetric double cantilever beam (ADCB) geometry. In the first study, contact was achieved well above the melting temperature of both polymers for 30 minutes, followed by a cooling stage at 20°C.min^{-1} to room temperature or alternatively cooling to T_c=136°C in order to let the PP crystallize, followed by cooling to room temperature. Yuan and Wool found a poor adhesion in the case of the direct cooling to room temperature, i.e. in non isothermal crystallization, but an increase of the adhesion with the time of isothermal crystallization at 136°C. The authors proposed that during isothermal crystallization, the volume contraction associated with the nucleation of the PP

[1]Yuan, B. L. and Wool, R. P. Polymer Engineering and Science, 30(22): 1454-1464, (1990).
[2]Lo, C. T., et al. Journal of Polymer Science Part B-Polymer Physics, 42(14): 2667-2679, (2004).

spherulites away from the interface allowed PE influxes to be formed between the spherulites and the interfacial region. For a slow crystallization and higher T_c, fewer and larger spherulites nucleated at random. The influxes formed slowly and grew, leading to a mechanical interlocking. In the case of non isothermal crystallization, the authors showed by optical micrographs, that spherulites were formed near the interface. They concluded that crystal nuclei were formed near the interface, during non isothermal crystallization, and blocked the influxes, leading to a weaker adhesion.

In the study of Lo et al., the contact temperature was varied from below the melting temperature of PE, to above the melting temperature of iPP, for different annealing times (from 1h to 24h). The fracture toughness was weak below the melting temperature of PE, increased between the melting temperature of PE and that of iPP, and became strong above the melting temperature of iPP. The authors supposed that between the melting temperature of PE and PP, both the interdiffusion of PE and the crystallization of iPP contributed to the fracture energy.
At low temperatures, PE diffusion is slow since PE and iPP are immiscible (below 143°C, Lo et al.[1])and iPP crystallizes at the interface hindering the interdiffusion of PE. As the temperature increases, PE diffuses faster since PE and iPP become miscible, and crystallization will not hinder the interdiffusion because of nucleation away from the interface.
Above 153°C both PP and PE are miscible and amorphous, G_c depends on the interdiffusion and both interfacial width and G_c, increased.

1.3.5.2 Self-adhesion of semicrystalline polymers

Usually, in the studies on self-adhesion of semicrystalline polymers, compatibilization was carried out in the vicinity of the melting temperature and the adhesion test was performed at room temperature.

Several groups investigated the specificities of self-adhesion of semicrystalline polymers by studying in particular the influence of the temperature gradient (Smith et al.[2]), of the chain mobility (Boiko et al.[3]), of the morphology (Xue et al.[4]) and of the cocrystallization (Xue et al.[5]) and (Gent et al.[6]).

Smith et al. investigated the fusion bonding of PP in both isothermal and non-isothermal conditions in the vicinity of T_m (165°C).
The authors used an experimental set up which allowed short contact times and non-isothermal fusion bonding. Typically, each PP polymer plate was placed in an instrumented matched–die mold installed on a servo-hydraulic load frame, and the system

[1]Lo, C. T., et al. Polymer, 45(11): 3671-3679, (2004).
[2]Smith, G. D., et al. Polymer, 42: 6247-6257, (2001).
[3]Boiko, Y. M., et al. Polymer, 42: 8695-8702, (2001).
[4]Xue, Y.-Q., et al. Macromolecules, 31: 3075-3080, (1998).
[5]Xue, Y.-Q., et al. Macromolecules, 33: 7084-7087, (2000).
[6]Gent, A. N., et al. Journal of Polymer Science Part B-Polymer Physics, 35(4): 615-622, (1997).

was allowed to equilibrate before contact. The temperature of the lower and the upper plate could be varied separately.
The temperature of contact was varied from below the melting temperature of PP; i.e. 150°C to well above tit, i.e.180°C, for relatively short times of contact (from 40 s to 600 s). In the case of the non-isothermal bonding, the interface temperature, T_i, was taken to be equal to the average temperature of each plate prior to bonding, i.e.$(T_1+T_2)/2$, T_1 being the temperature of the upper plate and T_2 of the lower plate. The authors correlated the adhesion measurements with optical microscopy of thin transverse sections through the bond and with SEM of the fracture surfaces.

For T_i below the melting temperature of PP, the adhesion in the non-isothermal condition was found higher than the adhesion in isothermal conditions (100 $J.m^{-2}$ at 150°C instead of 10 for isothermal conditions). In the optical micrographs in the case of non-isothermal conditions with an interfacial temperature of 160°C, a columnar region was observed in the lower plaque (the one initially molten), while in the case of isothermal conditions only very small changes in the sub-surface microstructure compared with the surface structure of as-molded plates was observed. The authors conclude that the solid plate (in the case of non-isothermal bonding) caused a columnar growth in the molten plate, suggesting a certain degree of epitaxy, or at the very least, intimate contact across the interface.

For T_i just above T_m, i.e 170°C, the columnar region was still observed in the lower plate (initially molten) while in the isothermal case, the original morphology was strongly tilted on either side of the interface, reflecting substantial shear of the partly molten material during bonding. Still a difference of one decade was found between the fracture toughness in non-isothermal conditions (1000 $J.m^{-2}$) and the isothermal conditions (100 $J.m^{-2}$). It should be stressed that in these experiments the time of contact in the non isothermal condition was 40 s, while the time of contact was fixed at 600 s in the isothermal case.
The authors argue that the kinetics and temperature dependence of the build up of strength during fusion bonding of a semicrystalline polymer just above T_m may not be simply related to self diffusion in the melt, but also to cocrystallization. These conclusions seem relevant to us, since the columnar region seen in the non-isothermal case may be a proof of an intimate contact between the two sides of the assembly, which can lead to cocrystallization and therefore explain the higher values obtained in the non-isothermal case at temperatures in the vicinity of the melting temperature.
For interfacial temperatures well above T_m, i.e.180°C, the fracture toughness was found identical for the isothermal and non-isothermal case. At this temperature the original surface texture was erased under both isothermal and non-isothermal conditions. Moreover the authors showed TEM images of the interface where lamellae were seen across the interface.

Although this study was of a great interest to us, the role of the amorphous part of the polymers and of the interdiffusion remains unclear. Moreover, we are skeptical of the existence of a direct correlation between the presence of the columnar zone over more

than 10 μm and the enhancement in fracture toughness, since it is well known that in the case of amorphous polymers the fracture toughness reaches the bulk fracture value for interdiffusion over distances of only a few nanometers.

The only study to our knowledge focusing on adhesion of semicrystalline polymers for contacts made between the glass transition and the melting temperature is that of Boiko et al.[1] on PET. Boiko et al. worked on self-adhesion of both amorphous and semicrystalline PET, in a lap shear joint geometry. The amorphous PET was obtained by melting the polymer between thin Teflon sheets in air, then by quenching in ice-water. Some samples were annealed at 180°C for 10 minutes to obtain semicrystalline samples. The samples were bonded in a lap-shear joint geometry at temperatures varying from 64°C (T_g-17) to 108°C (T_g+17) for contact times from 5 minutes to 15 hours, cooled to room temperature, and submitted to a tensile loading at a cross head speed of 0.5 cm.min^{-1} (the contact area of the lap shear bond was 5x5 mm^2). Shear strength was calculated as the measured force at break divided by the contact area.

For amorphous/amorphous interfaces, no discontinuity was seen in the vicinity of the glass transition temperature. The shear strength was found to follow a $t^{1/4}$ dependence with contact time, which suggests a diffusion mechanism causing the strength development. In the vicinity of T_g, the shear strength found for amorphous/amorphous PET interfaces was 5-7 time bigger than for crystalline/crystalline PET interfaces. The authors argue that interdiffusion only occurred over a short distance in the case of crystalline/crystalline interfaces, since the molecules are trapped in the crystals. The possibility of a transesterification was rejected by the author. The authors argue reasonably that in the case of transesterification no differences in the shear strength should be observed between amorphous and crystalline samples.

In this study, the authors did not discuss the possible cold crystallization of PET at temperatures of contact above the glass transition temperature, which can lead to crystalline reorganization at the interface. The occurrence of interdiffusion over a short distance in the case of crystalline/crystalline interfaces, is not proven and the lack of crystalline characterization of the interface in the study of Boiko et al., makes indeed the interpretation of the adhesion results quite difficult.

Xue et al.[2] looked at the influence of different morphologies on self-adhesion, using a quite specific material. They used ultra high molecular weight polyethylene (UHMWPE) with two different morphologies : melt crystallized films and solution crystallized films. In the case of melt crystallized film, the chain dimensions are known to be essentially equal to the random walk values, while in the solution-crystallized films, the chains have a much more compact configuration. In the latter morphology, the chains are expected to rapidly recover their random walk configuration above the melting point, a process known as chain explosion.

[1]Boiko, Y. M., et al. Polymer, 42: 8695-8702, (2001).
[2]Xue, Y.-Q., et al. Macromolecules, 31: 3075-3080, (1998).

The adhesive fracture energy was determined by T-peel testing performed at 5 $mm.min^{-1}$ above and below the melting point, after welding the samples at 145°C, i.e. above the melting temperature. It was found that if the sample was cooled and the adhesive fracture energy was measured at 20°C it was comparable to the fracture energy of the bulk material after a contact time shorter than 3 minutes at 145°C, irrespective of the initial morphology.
By contrast, the initial crystal morphology was found to have a large influence if the adhesive fracture energy was measured above the melting temperature, i.e. in a regime where UHMWPE is an elastomer. The peel force increased only slowly with contact time in the case of melt crystallized films, while the increase of the peel force was almost instantaneous in the case of solution-crystallized films. The authors proposed that the increase of the radius of gyration of the chains above the melting temperature, the so called "chain explosion" which occurs in the case of solution-crystallized films, accelerated dramatically the interdiffusion across the interface compared to the melt-crystallized case.

In another study on the same material, Xue et al.[1] investigated the role of cocrystallization on self-adhesion, by using the properties of a solution-crystallized film of UHMWE which consists of regularly stacked 107 Å thick lamellae that exactly double their thickness upon 15 minutes annealing at 125°C.

In order to get cocrystallization during annealing below the melting temperature at 125°C, the solution-crystallized films were prewetted before removal the solvent. A reference sample was made by preannealing one side of the film. A schematic drawing of those different preparations is given in Figure 1.3-8.

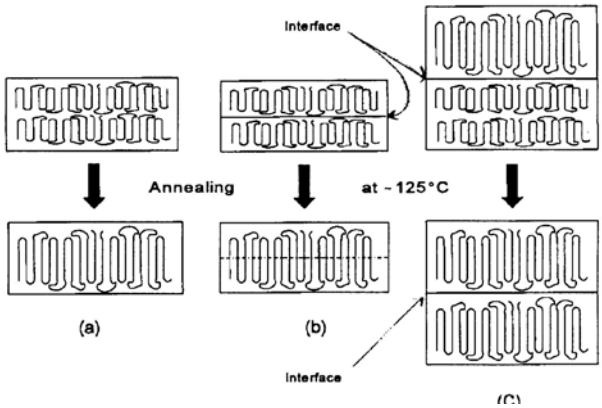

Figure 1.3-8 : schematic drawing of (a) the lamellar doubling process upon annealing at 125°C, (b) cocrystallization across the interface and (c) the reference sample after Xue et al.

It was found that doubling the thickness of the lamellae across the interface enhanced the peel energy to a level such that the films could not be separated anymore. By contrast, reference samples, in which cocrystallization across the interface was prohibited by

[1]Xue, Y.-Q., et al. Macromolecules, 33: 7084-7087, (2000).

“preannealing” one side of the film, could still be separated easily. The authors interpreted this result as a proof that the large-scale chain interdiffusion and , especially at high molecular mass, the long welding times, needed for the buildup of adhesive strength during self-adhesion of amorphous polymers, is not a prerequisite for a good welding performance in the case of semicrystalline polymers, as cocrystallization occurs at relatively short welding times.

It should be noted however that these results focused on solution-crystallized semi-crystalline polymers which crystallized from a dilute solution and hence are completely unentangled. Typical semi-crystalline polymers crystallize from the melt state and show only very limited molecular mobility below their melting point.

Cocrystallization was also studied in the adhesion between crosslinked polyethylene, by Gent et al. Different peeling test geometries were used in this study, and the authors varied the degree of crosslinking. As the degree of crosslinking was increased, the degree of crystallinity at room temperature and the melting temperature decreased. The sheets were bonded at 160°C during 30 minutes. In view of the small extent of molecular interdiffusion expected for crosslinked sheets in contact, the measured adhesion between sheets crystallized in contact was extraordinary high. The authors concluded that cocrystallization may be the cause of the relatively high adhesion.

1.4 Conclusions and objectives of the current study

The studies reviewed in the previous section highlight the fact that for semicrystalline polymers the morphology plays an important role on adhesion. Nevertheless, the way crystallinity acts at the interface remains unclear.

For immiscible polymers reinforced by the addition of a copolymer, the mechanisms now accepted in the case of amorphous polymers, are applicable to a certain extent to the semicrystalline polymers, but are indeed unsatisfactory, since other mechanism such as cocrystallization, crystalline reorganization or epitaxial growth of lamellae are expected to have a great influence on the surface reinforcement between semicrystalline polymers.

These mechanisms seems to largely influence both the strength and kinetics of adhesion buildup between semicrystalline polymers, but still more studies on the subject are needed.

Some questions remain unsolved, like the possibility to obtain a reasonable adhesion below the melting temperature and the role of the amorphous part of the semicrystalline polymer for contact between the glass transition temperature and the melting temperature. It is well known that some semicrystalline polymer can cold crystallize upon heating at temperatures significantly lower than the melting temperature, when the amorphous part is mobile. The influence of this cold crystallization on adhesion has, to our knowledge, never been studied.

In the present study, we tried to get a better idea of the different mechanisms active in the welding process of semicrystalline polymers. We have chosen to work on self-adhesion at temperatures between the glass transition and the melting temperature, in order to get measurable adhesion. The choice of copolymers composed by two slightly different entities, where it was possible to change in a controlled way the degree of crystallinity by changing the ratio between the two entities, appears to us to be the best candidate to investigate the role of crystallinity. We also studied the influence of cold crystallization on the adhesion between semicrystalline polymers prepared and put in contact while in the amorphous state.

Chapter 2

Characterization of PBT, PBI, PBT-PBI copolymers and experimental techniques

This chapter has the dual purpose to characterize the materials we used in my thesis and describe precisely all the experimental procedures applied in our work.

We will first review what is known about PBT, PBI and PBT-PBI copolymers, before presenting our own characterization, both at a molecular level and at a macroscopic scale.

The different experimental procedures linked to the measurement of adhesive strength, which is the bulk of our work, will then be presented.

2.1 Brief review on the structure and properties of PBT, PBI and PBT/PBI copolymers

2.1.1 PBT

2.1.1.1 Introduction

Among semicrystalline polymers, poly(butylene terephthalate) (PBT) nowadays has gained importance as an engineering plastic, and is being used as high performance thermoplastic material for a large number of applications. PBT is often used in blends in order to reduce its main drawback which is a certain sensitivity to crack propagation. PBT has a glass transition temperature around 40°C and a melting point of 225°C roughly. It has some very useful properties for industry, such as its very fast crystallization rate without any nucleating agent, allowing very fast injection cycles, and has also good mechanical properties. We will first review the crystalline structure of PBT, and then briefly some of its mechanical properties.

2.1.1.2 Crystallinity

PBT exists under two different triclinic crystalline forms named α and β, and can change from one form to the other by a reversible transition under strain, as represented in Figure 2.1-1 (Yokouchi et al.[1]).

[1]Yokouchi, M., et al. Macromolecules, 9(2): 266-273, (1976).

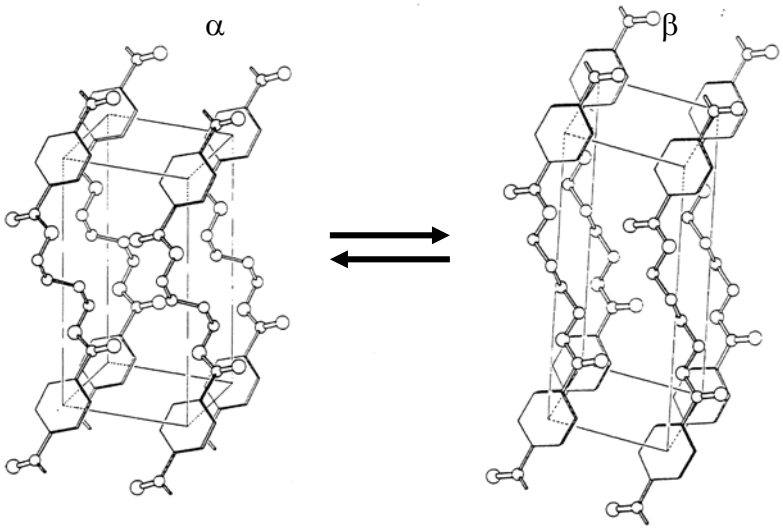

a = 4.83 Å α = 99.7°	a = 4.95 Å α = 101.7°
b = 5.94 Å β = 115.2°	b = 5.67 Å β = 121.8°
c = 11.59 Å γ = 110.8°	c = 12.95 Å γ = 99.9°
V = 260.4 Å^3 d = 1.404 kg.dm^{-3}	V = 285.0 Å^3 d = 1.283 kg.dm^{-3}

Figure 2.1-1 : α and β triclinic crystalline forms after Yokoucshi et al..

The stable form of PBT is the α-form, which is relatively compact if we compare it with the *c* cell parameter of the other polyesters of the group [-O(CH2)$_m$OCOPhCO-] (an extrapolation of the repeat unit from m = 2 to m = 4 gives *c*=13.1 Å, after[1])

2.1.1.3 WAXS study on PBT

The crystalline structure of PBT has been determined by wide angle X-ray diffraction experiments (Desborough and Hall[2] and Stambaugh et al.[3])
As one can see from the cell parameters reported on figure 2.1.1, the characteristic diffraction angles of the β-phase are very close to those of the α-phase. Diffraction patterns of melt crystallized PBT samples obtained from the melt at different cooling rates is given in Figure 2.1-2.

[1]Mencik, Z. Journal of Polymer Science Part B-Polymer Physics, 13(11): 2173-2181, (1975).
[2]Desborough, I. J. and Hall, I. H. Polymer, 18(8): 825-830, (1977).
[3]Stambaugh, B., et al. Journal of Polymer Science Part B-Polymer Physics, 17(6): 1053-1062, (1979).
[4]Yasuniwa, M., et al. Journal ofPolymer Science: Part B, 39: 2005-2015, (2001).

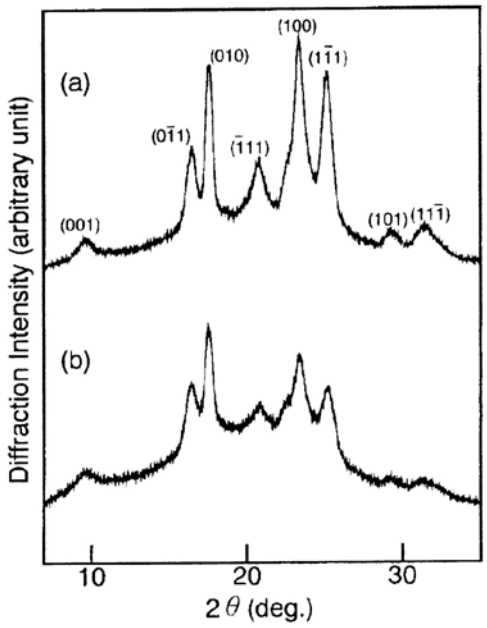

Figure 2.1-2 : diffraction patterns of melt-crystallized PBT samples obtained from the melt at a cooling rate of (a) 0.05 and (b) 24 K.min^{-1}. These diffraction patterns were obtained at room temperature. Miller indices are shown on the diffraction peaks, after[1].

2.1.1.4 The amorphous phase of PBT

The values commonly reported for the glass transition temperature of PBT are between 30 and 50°C. Some authors, tried to extrapolate (Illers[1]) or measure (Cheng et al.[2]) the glass transition temperature of an amorphous PBT. The temperature obtained in the first case, of 15°C, seems reasonable (Cheng et al. obtain -25°C by quenching in liquid nitrogen a glass sphere covered with a 1 mm layer of PBT, where surface effects certainly occur).

For our study we considered the value found for standard PBT : T_g ~ 40 °C, value which was confirmed by our own DSC measurements.

[1]Illers, K. H. Colloid and Polymer Science, 258(2): 117-124, (1980).
[2]Cheng, S. Z. D., et al. Makromolekulare Chemie-Macromolecular Chemistry and Physics, 189(10): 2443-2458, (1988).

2.1.1.5 Spherulitic structure

2.1.1.5.1 Lamellae

From SAXS measurements, the thickness of the lamellae in PBT was found to be between 5 and 20 nm (Huo et al.[1], Tashiro et al.[2] and Peszkin et al.[3])
This thickness strongly depends on thermal history : Huo et al. showed that by increasing the annealing temperature from 68°C to 218°C, the long period increased from 6 to 20 nm.
Most investigators considered that spherulites occupy nearly all the space, and therefore that the amorphous part of PBT is localized in those spherulites. To calculate the lamellar thickness, one can then divide the long period by the degree of crystallinity. A value of 5 to 10 nm for the lamellar thickness seems reasonable according to TEM observations which imply that a lamella contains a few mer units (5 to 8 units).

2.1.1.5.2 Spherulites

As described in section 1.1.2 lamellae are organized in superstructures called spherulites, which are composed of crystalline and amorphous parts.

We can distinguish two types of spherulites by an observation under polarized light. The texture of the spherulite can be positive or negative providing informations on the orientation of the polymer chains in the spherulite. The “negative” spherulite has a tangential refractive index higher that its normal index, implying that the axis of greater polarizability is perpendicular to the spherulite radius, i.e. that the chains are perpendicular to the spherulite radius. On the contrary, the “positive” spherulite implies that chains are oriented parallel to the spherulite radius or without any orientation.

Moreover, spherulites usually exhibit the 0-90° Maltese cross under polarized light. We can distinguish two different patterns : the normal Maltese cross and the unusual or abnormal Maltese cross with a 45° rotation from the normal one.

For PBT, it was shown that the type of spherulite observed depends on the crystallization temperature : below 180°C, abnormal spherulites crystallize, while above 200°C, normal spherulites are formed (Stein and Misra[4]).

A difference in melting temperature was found for the two types of spherulites, i.e. 227°C for normal spherulites and 223°C for abnormal spherulites. The normal spherulites were always found to show positive birefringence.

[1]Huo, P. P., et al. Journal of Polymer Science Part B-Polymer Physics, 30(13): 1459-1468, (1992).
[2]Tashiro, K., et al. Macromolecules, 13(1): 137-145, (1980).
[3]Peszkin, P. N., et al. Journal of Polymer Science Part B-Polymer Physics, 24(12): 2617-2630, (1986).
[4]Stein, R. S. and Misra, A. Journal of Polymer Science Part B-Polymer Physics, 18(2): 327-342, (1980).

2.1.1.6 Crystallization and fusion

2.1.1.6.1 Crystallization

The crystallization kinetics of PBT is among the fastest among polymers (Jadhav[1]). It is the most obvious difference between PBT and PET. PET can be easily obtained in the amorphous state, while it is experimentally very difficult to obtain PBT in the amorphous state. The chain flexibility of PBT may be the reason of its fast crystallization kinetics.

Because of this very fast crystallization, measurements of the crystallization rate of PBT are difficult to perform and results tend to vary. The temperature where PBT was found to have the fastest crystallization rate varied from study to study from 140°C (Runt et al.[2]) to 211°C (Nichols and Robertson[3]). In a non isothermal crystallization experiment analyzed by DSC, the position of the exothermic crystallization peak changed with cooling rate as shown by (Hobbs and Pratt[4]) in Figure 2.1-3.

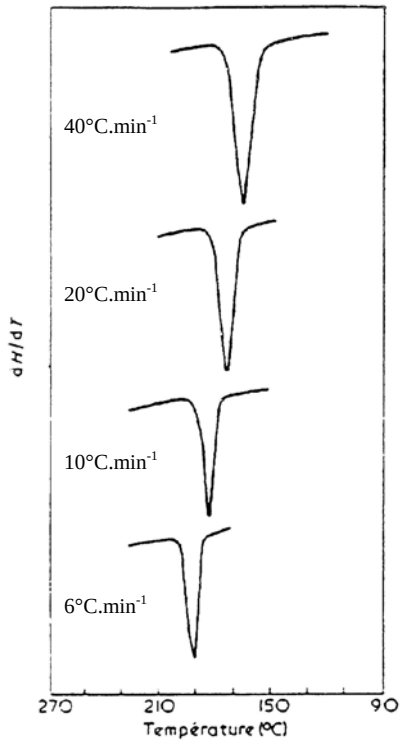

Figure 2.1-3 : influence of the cooling rate on the melting peak after[4].

[1]Jadhav, J. Encyclopedia of polymer science and engineering. (Wiley, New York, 1988)
[2]Runt, J., et al. Macromolecules, 25(7): 1929-1934, (1992).
[3]Nichols, M. E. and Robertson, R. E. Journal of Polymer Science Part B-Polymer Physics, 30(7): 755-768, (1992).
[4]Hobbs, S. Y. and Pratt, C. F. Polymer, 16(6): 462-464, (1975).

Avrami's constants (see section 1.1.2) were calculated by several authors and gave values from 2.0 (at 191°C, Marrs et al.[1]) to 3.1 (at 210°C, Pratt and Hobbs[2]). Most of the authors have found an Avrami's constant around 3, which indicates that the crystallization process is characterized by a heterogeneous nucleation and by three-dimensional spherulitic growth. Nevertheless, in a recent study on isothermal melt crystallization of PBT, Dangseeyun et al.[3] obtained an Avrami's constant around 2.

PBT has an extremely weak fold surface energy γ_e (see section 1.1.2.2.3): 50 to 70 erg.cm^{-2}, compared to the PE (90) or PET (140) (Runt et al.[4]). This folding ability may also explain the fast crystallization kinetics of PBT.

Righetti and Munari[5] showed the influence of branching on the crystallization kinetics of PBT. A decrease in the crystallization rate was observed as the content of branching units increased. The authors also showed that the existence of branching favored the nucleation process.

PBT crystallizes very fast but in a "chaotic" manner which leads to relatively thin lamellae as reported in the previous section, i.e. about 5 nm which correspond to 4-5 mer units only.

2.1.1.6.2 Cold crystallization

The cold crystallization is a secondary crystallization which occurs during heating at a temperature well below the crystallization temperature. Typically, this behavior is seen when a polymer is rapidly cooled below its T_g from the melt and then heated again. PBT has a low ability to cold crystallize, since an incomplete crystallization during cooling is required to get cold crystallization. Nevertheless some attempts have been made to get cold crystallization with PBT samples : Stein and Misra[6] have shown that a transparent quenched sample of PBT, annealed at 120°C, stays transparent but develops an important crystallinity (30%) which can be detected by a density measurement or X rays (Misra and Garg[7]). However, in classical experimental conditions, we can assert that PBT do not cold crystallize.

We can stress the fact that by a copolymerization of PBT with PBI, which was done in our study, the ability to cold crystallize was found to be highly enhanced since the crystallization rate during the cooling phase was considerably retarded.

[1]Marrs, W., et al. Journal of Applied Polymer Science, 23(4): 1077-1093, (1979).
[2]Pratt, C. F. and Hobbs, S. Y. Polymer, 17(1): 12-16, (1976).
[3]Dangseeyun, N., et al. Thermochimica Acta, 409: 63-77, (2004).
[4]Runt, J., et al. Macromolecules, 25(7): 1929-1934, (1992).
[5]Righetti, M. C. and Munari, A. Macromolecular Chemistry and Physics, 198: 363-378, (1997).
[6]Stein, R. S. and Misra, A. Journal of Polymer Science Part B-Polymer Physics, 18(2): 327-342, (1980).
[7]Misra, A. and Garg, S. N. Journal of Polymer Science Part C-Polymer Letters, 20(2): 121-125, (1982).

2.1.1.6.3 Fusion

Upon heating, the PBT thermogram exhibits a main endotherm around 223°C, which can be considered as the main fusion peak of PBT. This endotherm is almost independent of thermal history. This peak is often preceded by smaller secondary peaks. An interesting study was performed by Marrs et al.[1]. They heated PBT well above the melting temperature and then cooled the polymer rapidly to a crystallization temperature that they maintained for one hour. Figure 2.1-4 shows on the left the usual shape of the different endothermic peaks and on the right, the peaks' positions as a function of the crystallization temperature T_c

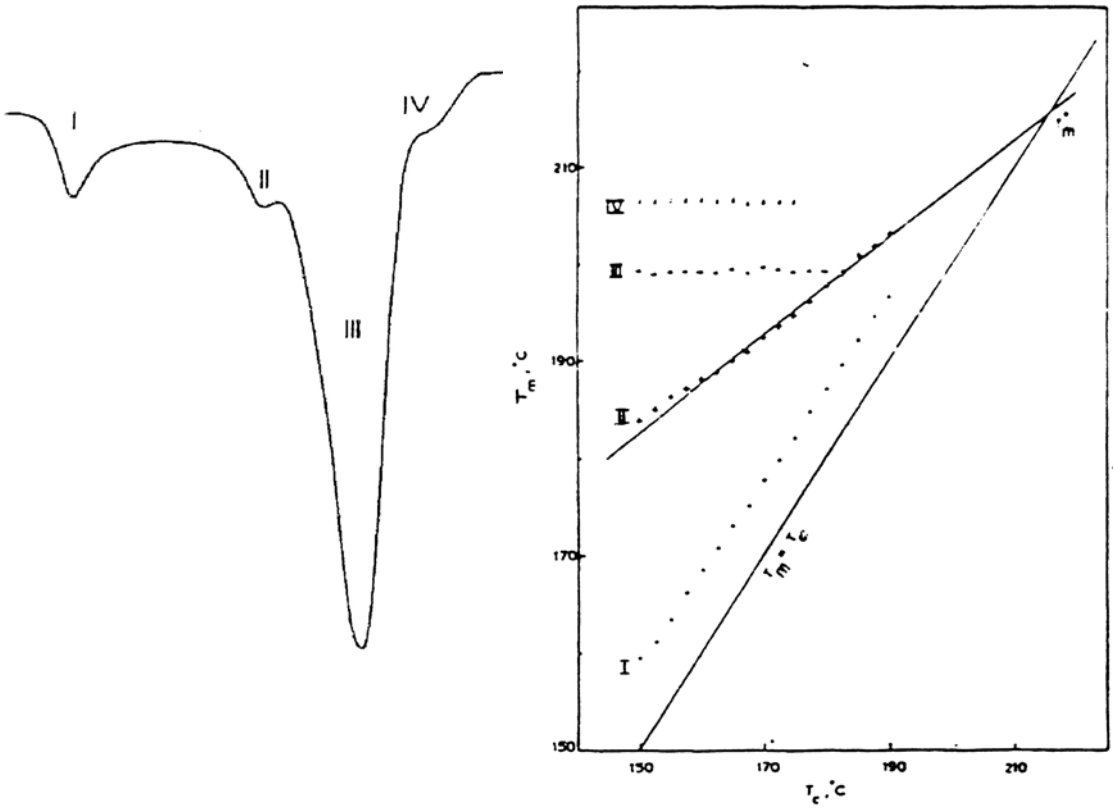

Figure 2.1-4 : different melting peaks of PBT and the evolution of their position (dashed lines) as a function of the crystallization temperature after Marrs et al[1].

The four melting peaks can be interpreted as follows :

- peak I appears 5 to 20 °C above the crystallization temperature T_c. This peak is small but appears, even for very short annealing times. It was attributed to unstable crystals formed during the crystallization time.

[1]Marrs, W., et al. Journal of Applied Polymer Science, 23(4): 1077-1093, (1979).

- peak II, on the contrary, seems to develop quite slowly and is not observed in the case of a continuous cooling, but its intensity increases with the crystallization time. It also corresponds to crystals formed during the crystallization time, but corresponds to crystals which follow the classical laws of the crystallization, i.e. on which the classical Hoffmann-Weeks treatment can be applied (see section 1.1.2.3).
- peak III is always present at the same temperature (~223°C). It is usually the main peak. Its origin is generally attributed to a recrystallization during the heating of the sample. In the case of PBT, at a melting temperature of 223°C, the lamellar thickness can be estimated at 14 nm, i.e. about 10 mer units. As shown on the right hand side of Figure 2.1-4, peak III does not depend on the crystallization temperature, which is usually attributed to an upper limit in the lamellar thickness. This limit can be correlated to the average length between entanglements, which has been estimated from the M_e value of PET (Wu[1]) of 1630 $g.mol^{-1}$, i.e. 8.5 mer units.
- peak IV, appears after long annealing times only. Its attribution remains unclear.

2.1.1.6.4 Equilibrium melting temperature and heat of fusion

As the "stable" crystal follows the classical rules of crystallization, the II peak of fusion in a PBT thermogram is always used to determine the equilibrium melting temperature from the intersection of the melting line with the $T_m = T_c$ line (see the classical Hoffmann-Weeks treatment in section 1.1.2.3). The value of this temperature varied from 233 to 249 °C (Pompe et al.[2] and Huo and Cebe[3]) in the different studies.
The recent study of (Dangseeyun et al.[4]) gives $T_m^o = 235.4$°C.

The heat of fusion of a pure crystal of PBT is, according to Illers[5] : $\Delta H_m^0 = 140$ $J.g^{-1}$.

2.1.1.7 Some mechanical properties of PBT

We will just present some tensile results on PBT, and briefly discuss the influence of temperature.
Figure 2.1-5 shows the stress/strain curve in a tensile test carried out at 23°C at a strain rate of $0.01s^{-1}$. From these data from Gervat[6], we can calculate a Young's modulus of ~ 2 GPa and a yield stress of 57 MPa. Beyond a strain of 0.25, the sample shows a striction which can be attributed to the plastic flow and the destruction of the crystalline structure.

[1]Wu, S. H. Polymer International, 29(3): 229-247, (1992).
[2]Pompe, G., et al. Journal of Polymer Science Part B-Polymer Physics, 34(2): 211-219, (1996).
[3]Huo, P. P. and Cebe, P. Macromolecules, 26(12): 3127-3130, (1993).
[4]Dangseeyun, N., et al. Thermochimica Acta, 409: 63-77, (2004).
[5]Illers, K. Colloid and Polymer Science, **258**(2): 117-124, (1980).
[6]Gervat, L. Structure, propriétés mécaniques et renforcement au choc du Poly(terephthalate de butylene glycol). (Université de Paris VI, Paris, 2001)

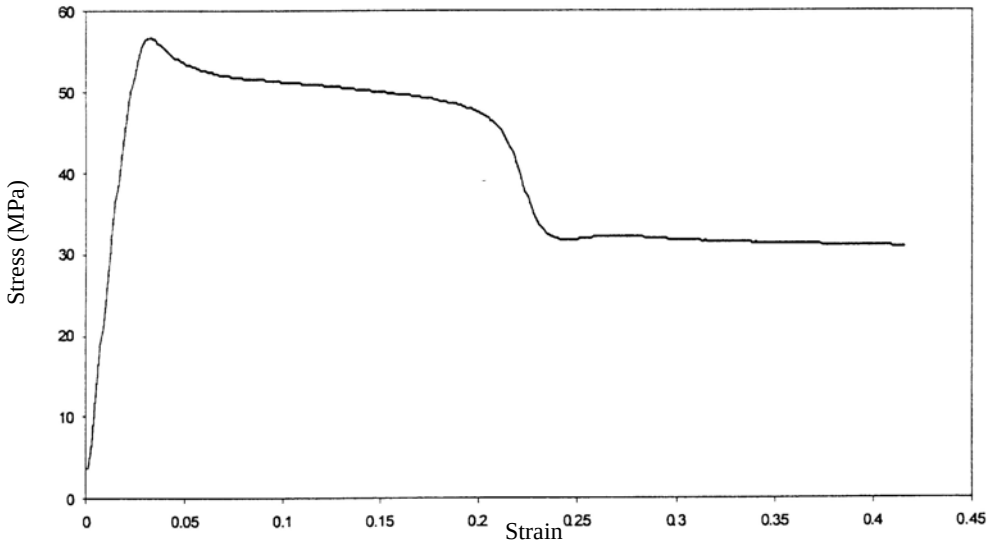

Figure 2.1-5 : PBT stress strain curve in a tensile geometry at 23°C (strain rate : 0.01s^{-1}) after[1].

In figure 2.1-6 the force-displacement curves of PBT obtained by a tensile test at different temperatures are presented.

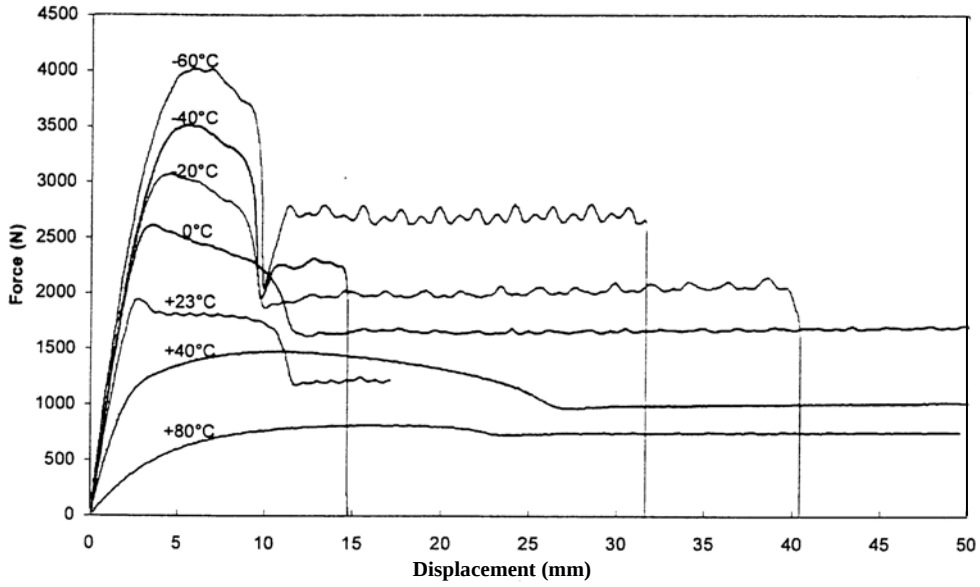

Figure 2.1-6 : PBT force-displacement curves for different temperatures[1].

[1]Gervat, L. *Structure, propriétés mécaniques et renforcement au choc du Poly(terephthalate de butylene glycol).* (Université de Paris VI, Paris, 2001)

Below the glass transition temperature, by decreasing the temperature, the yield stress increases significantly, while the Young's modulus increases slowly. Above T_g the Young's modulus logically decreases sharply. For these temperatures, the striction appears at longer displacements (25 mm corresponding to a strain of 0.4).

From this data, PBT appears as a tough thermoplastic below its T_g and as a more ductile material above its T_g. In our study we never tested interfaces above the glass transition temperature of the material. Since it is not the purpose of our study, we will not go into further detail here on the mechanical properties of PBT.

Table 2.1-1 summarizes the different data which can be useful for our study (data obtained from the literature).

Table 2.1-1

Density		Fusion			Crystallization			
Amor. ($g.cm^{-3}$)	Cryst(α) ($g.cm^{-3}$)	T_m(III) (°C)	T_m^0 (°C)	ΔH_m^0 ($J.g^{-1}$)	n_{avrami}	kinetics	ν (Poisson)	M_e ($kg.mol^{-1}$)
1.28	1.4	225	230-249	140	2-3.1	196°C : 69s 198°C : 105s 200°C: 150s	1/3	1.63

2.1.2 PBI

Poly(butylene isophthalate) differs from poly(butylene terephthalate) only by the position of the carboxyl group on the benzene cycle :

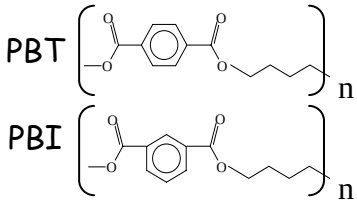

The studies on PBI are far less numerous than those on PBT. We will very briefly report the few data on PBI and insist on the differences with PBT.

To start with, the amorphous part of PBI has a glass transition temperature of roughly 25°C (Righetti et al.[1]), which is above the extrapolated glass transition temperature of amorphous PBT (see section 2.1.1.4).

The crystallization kinetics of PBI is much slower than the crystallization kinetics of PBT. Hence it is quite easy to obtain PBI amorphous by quenching a sample from the

[1]Righetti, M. C., et al. Macromolecular Chemistry and Physics, 199: 2063-2070, (1998).

melt and PBI can cold crystallize easily upon reheating. As for PBT, the Avrami's exponent was found close to 3, indicating that the crystallization process originates from predetermined nuclei and is characterized by three-dimensional spherulitic growth.

The heat of fusion of perfectly crystalline PBI was found to be in the range of 125 $J.g^{-1}$ by Righetti et al.[1], a value slightly lower than what is found for PBT (140 $J.g^{-1}$), and an equilibrium melting temperature in the range of 156 to 165°C, which is much lower than the melting temperature of PBT.

Although PBI has a much slower crystallization kinetics than PBT, due to the rigidity of the PBI chains (Phillips et al.[2]) and the asymmetry induced by the meta-position of the aliphatic chain on the aromatic cycle, the melting behavior of PBI presents some similarities with the melting behavior of PBT. In Figure 2.1-7, the DSC melting endotherms are represented for different crystallization temperatures, after a crystallization time of one hour. The DSC melting endotherms were scanned at a heating rate of 10°C.min^{-1}.

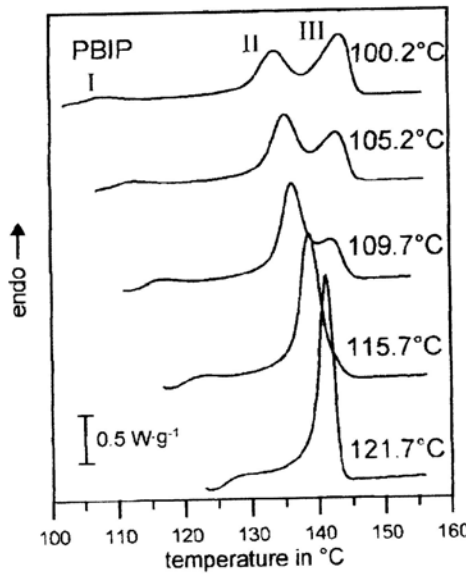

Figure 2.1-7 : DSC scan on PBI crystallized at different temperatures after[1].

Different melting peaks can be seen in Figure 2.1-7. The first peak (I) is usually attributed to the melting of crystals formed during a secondary crystallization process. This peak is barely visible. The second melting peak (II) can be associated with the crystals grown at T_c by a normal primary crystallization and strictly depends on the crystallization temperature, as reported for PBT (see section 2.1.1.6.3). On the contrary, the location of the highest (III) melting endotherm, shows no dependence on the crystallization temperature.

[1]Righetti, M. C., Pizzoli, M., Lotti, N. and Munari, A. Macromolecular Chemistry and Physics, **199**: 2063-2070, (1998).
[2]Phillips, R. A., et al. Journal of Polymer Science Part B-Polymer Physics, 32(5): 791-802, (1994).

2.1.3 PBT-PBI copolymers

Studies on Poly(butylene terephthalate-co-isophthalate) copolymers can be found essentially in the following papers : Bandiera et al.[1,2] and Finelli et al.[3]
Bandiera et al. synthesized and characterized copolymers of various compositions. Calorimetric measurements were carried out with a Perkin-Elmer DSC instrument. The DSC curves were recorded at a scanning rate of 20°C.min^{-1} over a temperature range -50/250°C. Two different procedures were used by the authors. In a first procedure the specimens were compression molded at 230°C, slowly cooled to room temperature and then annealed at 90°C for 8 days in vacuum, while in a second procedure the specimens were quenched after molding. The results are given in Figure 2.1-8.

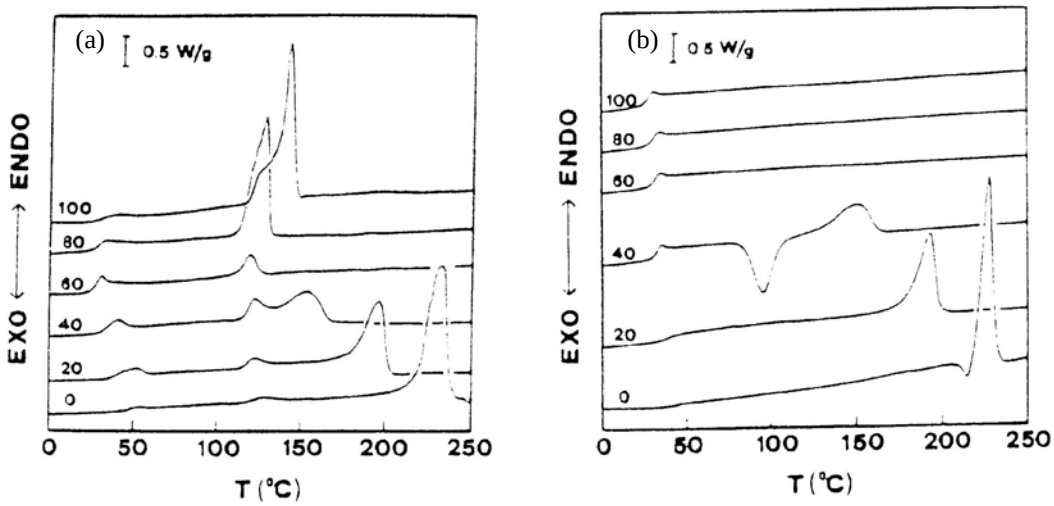

Figure 2.1-8 : calorimetric curves of PBT/PBI random copolymers annealed at 90°C (a) and quenched after molding (b) after Bandiera et al[1].

In the case of annealed samples (a) for PBT, 20PB (20%PBI, 80%PBT) and 40PB, Bandiera et al. found a separate peak or a shoulder at 120-130°C, certainly due to the melting of crystals produced upon annealing, either by crystallization from the amorphous phase or by reorganization of the pre-existing crystals formed during cooling. The DSC curves indicate than an increase in the amount of comonomer added to PBI or to PBT leads to a marked reduction of the heat of fusion, and therefore to a reduced level of crystallinity in the copolymers with respect to the homopolymers.

[1]Bandiera, M., et al. European Polymer Journal, 30(4): 503-508, (1994).
[2]Bandiera, M., et al. European Polymer Journal, 33(4): 497-500, (1997).
[3]Finelli, L., et al. European Polymer Journal, 37: 2039-2046, (2001).

For the quenched samples, pure PBT and the sample with 20% of PBI are still crystalline, while the other copolymers and PBI are amorphous. The copolymer with 40% of PBI shows a cold crystallization peak at 94°C.

In the case of annealed samples, the composition dependence of T_m and ΔH_m is given in Figure 2.1-9.

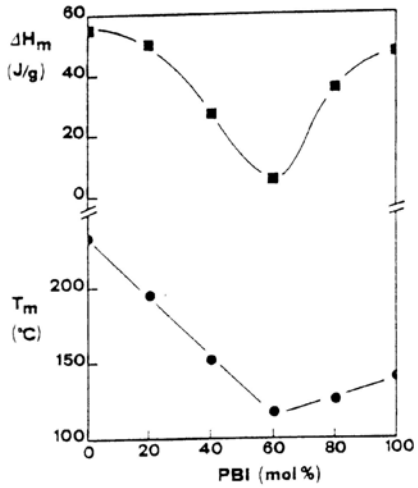

Figure 2.1-9 : composition dependence of T_m (●) and ΔH_m (■) in PBI/PBT random copolymers (after Bandiera et al.).

The minimum heat of fusion and melting temperature was found near a composition with a similar proportion of PBI and PBT.

Finelli et al. characterized the crystalline structure of these copolymers by using Wide-angle X-rays (Figure 2.1-10). Going from pure PBT to 60PB, the crystalline peaks are severely reduced but still appear roughly at the same position. The overall degree of crystallinity is reduced from PBT to 60PB and the lamellar thickness is certainly also reduced (see Figure 2.1-9) but the incorporation of a certain amount of PBI up to 60% does not seem to change the cell parameters. The story is quite different for 80PB, which crystallizes with the same structure as PBI.

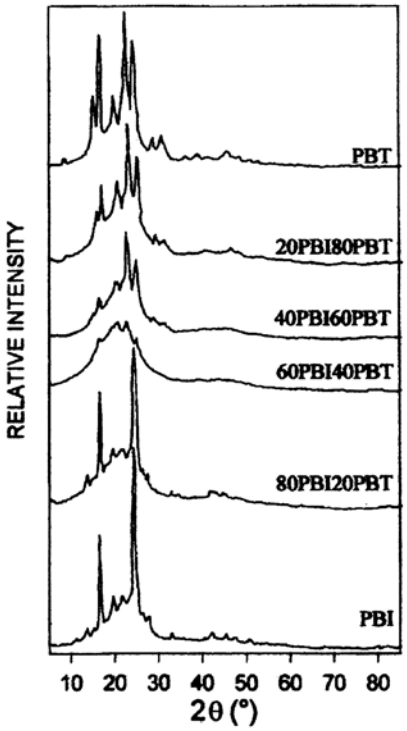

Figure 2.1-10 : Wide-angle spectra of PBT, PBI and PBT/PBI copolymers after Finelli et al.

We may draw several conclusions from this review of the structure and properties of PBT, PBI, and PBT-PBI copolymers. The crystalline structure of PBT has been largely studied but still, because of its complexity, the different parameters which describe the crystallization or fusion behavior change from one study to the other.

What should be kept from this review of PBT is the very high crystallization kinetics, the chaotic growth of the crystallites, the difficulty to obtain amorphous samples, the poor aptitude to cold crystallize and the quite complex melting process.

PBI has a much slower crystallization kinetics. PBI crystallizes in a different structure from PBT, and has a much lower melting temperature. PBI can very easily be obtained in the amorphous state and can easily cold crystallize.

By copolymerization between PBT and PBI, the different properties change in a continuous manner. For a PBI content up to 60%, the crystalline structure of the copolymers remains identical to the PBT structure. Both the melting temperature and the heat of fusion (and as a consequence the degree of crystallinity) decrease with an increasing content of PBI. For a PBI content beyond 60%, the copolymers crystallize in the PBI structure and both the melting temperature and the heat of fusion increase slightly with increasing PBI content.

We will now present our own characterizations of the materials, which focus on the important data for our study, i.e. the characterization of the average molecular weights (M_n and M_e) and of the degree of randomness of our copolymers at the molecular scale, and its effect on the extent and structure of the crystalline phase and on the mechanical properties needed to interpret adhesion results.

2.2 Synthesis and molecular characterizations

2.2.1 Synthesis

The copolymers were synthesized by double condensation by M. Dahrouch (DSM research), and A.-C. Koch (PPMD), according to the procedure published by Bandiera et al.[1]. Three copolymers of weight fraction in PBI of 15, 35 and 45% were obtained (named 15PB, 35PB and 45PB). Pure PBT was synthesized industrially by DSM.

Poly(butylene isophthalate-co-butylene terephthalate) samples were synthesized starting from dimethyl terephthalate (DMT), dimethyl isophthalate (DMI) and 1,4 butanediol (BDO), with Titanium(IV) butoxide $Ti(OBu)_4$ {ca 0.47g/kg of (DMT+DMI)} as a catalyst. Following reference 1, we supposed that in all cases the copolymer composition was identical to the feed composition. The total amount of DMT+DMI was always 705,16 g; the amount of BDO was 412,95 g and the amount of $Ti(OBu)_4$ was 331,6 mg. The synthesis was carried out in a 1.8 L pyrex reactor according to the usual two-stage polycondensation procedure.

The first stage, at atmospheric pressure, is a transesterification. The temperature was raised between 220°C and 230°C under nitrogen atmosphere. The second stage is carried out under a reduced pressure of 0.5 bars, at a temperature of 245°C. This stage is a polycondensation.

Figure 2.2-1 summarizes the two stages in the case of an isophthalate group.

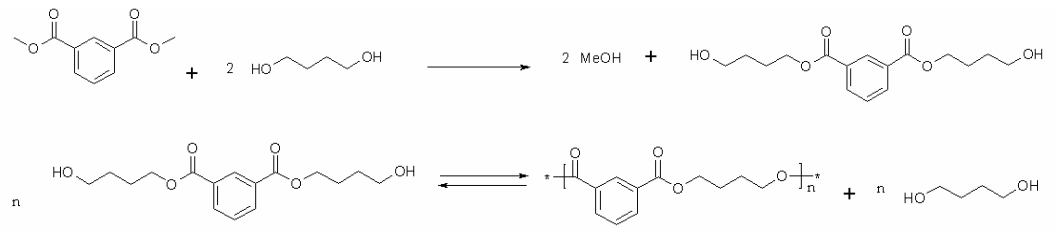

Figure 2.2-1 : two stage polycondensation for the formation of Poly(butylene isophthalate).

[1]Bandiera, M., Munari, A., Manares, P. and Pizzoli, M. European Polymer Journal, 30(4): 503-508, (1994).

Roughly 600g of each copolymer have been obtained. The polymers obtained, because of the use of $Ti(OBu)_4$ as a catalyst and the high reaction temperature which favor redistribution reactions (Pilati[2]) are essentially random. The molecular mass of the monomer is 220.2 $g.mol^{-1}$.
From these syntheses, we finally obtained one homopolymer, PBI and three copolymers : 15% PBI – 85% PBT (15PB), 35%PBI – 65% PBT (35PB) and 45% PBI – 55% PBT (45PB).

2.2.2 End group analysis : determination of M_n

An end group analysis was used to determine the number average molecular weight M_n. When the end groups are chemically distinguishable from the backbone of the polymer, measuring the concentration of the end group allows you to measure the number of end groups. Thus dividing the number of end groups by two will give the total number of molecules. Knowing the global mass of the polymer, it is then possible to deduce a number average molecular mass by dividing by the number of chains.:

$$\frac{Total\ Weight}{Number\ of\ Polymers} = \frac{\sum_i N_i M_i}{\sum_i N_i} = \overline{M}_n \qquad \textit{Eq. 1.2-1}$$

The limitation of this technique is the low ratio of end-groups to total amount of polymer, which requires an extremely sensitive detection method. The sensitivity problem becomes worse as the molecular weight increases, since obviously the concentration of end groups decreases as the molecular weight increases. As a result, end-group analysis is limited to relatively low molecular weight polymers (M_n < 30$kg.mol^{-1}$).

The following formula was used in our case :

$$\overline{M}_n = \frac{2000000}{E_c + E_{OH} + E_{vinyl}} \qquad \textit{Eq. 1.2-2}$$

with E_c = COOH (meq/kg) et E_{OH} = OH (meq/kg)

The results obtained by E. Bijleveld (DSM research) are summarized in table 2.2-1.

[2]Pilati, F. Comprehensive Polymer Science. (Pergamon Press, Oxford, 1989)

Table 2.2-1

	OH (meq/kg)	COOH (meq/kg)	M_n
PBT	71	30.1	19.8
15PB	83	11.4	21.2
35PB	71	13.9	23.6
45PB	70	11.6	24.5
PBI	46	17.1	31.7

2.2.3 Rheology

The linear viscoelastic properties of PBT, PBI and the three copolymers PBT-r-PBI were obtained from small strain rheological measurements in oscillatory shear. We performed these tests on a parallel plates rheometer (Rheometric Scientific ARES)) with the help of J. Palmen (DSM research). Measurements could be performed in the 60°C – 200°C temperature range and the $\omega = 10^2$ to 10^{-3} rad.s^{-1} frequency range (3.10^{-4} – 80 Hz).

The different samples (granules of each polymers and copolymers) were dried under vacuum for 24 hours at 95°C, then placed on the bottom plate which had been preheated above the melting temperature of the polymer. The amount of granules was adjusted to fit the plate diameter (21 mm) and the width between the two plates (1.8 mm). The furnace was then closed and the temperature fixed at $T_{ini} > T_m$.

When the temperature was equilibrated at T_{ini}, the sample was quickly cooled (40°C.min^{-1}) to the temperature of the test. The measurement were performed over the range of frequency mentioned above, starting with the high frequency measurements (3 points per decade). The tested temperatures are summarized in table 2.2-2.

Table 2.2-2 : initial temperatures and tested temperature for each copolymer.

	T_{ini} (°C)	Tested temperatures
PBT	240	240, 220
15PB	240	230, 210, 190
35PB	220	200, 180, 157, 140
45PB	220	120, 100, 80
PBI	200	140, 120, 100, 80, 60

The gap between the plates was adjusted depending on the thermal expansion of the plates and portion of the support heated by the furnace (Invar stainless steel).

The data obtained were the storage modulus *G'*, the loss modulus *G''* and consequently the loss tangent $tan(\delta) = G''/G'$ as a function of ω. For each sample, the master curve was built using the time-Temperature superposition (see equation 1.1-12).

For PBT in figure 2.2-2 the rubbery plateau was not seen because of the very fast crystallization. At temperatures below 220°C, we observed an elastic response (fall of tanδ due to the crystallization.

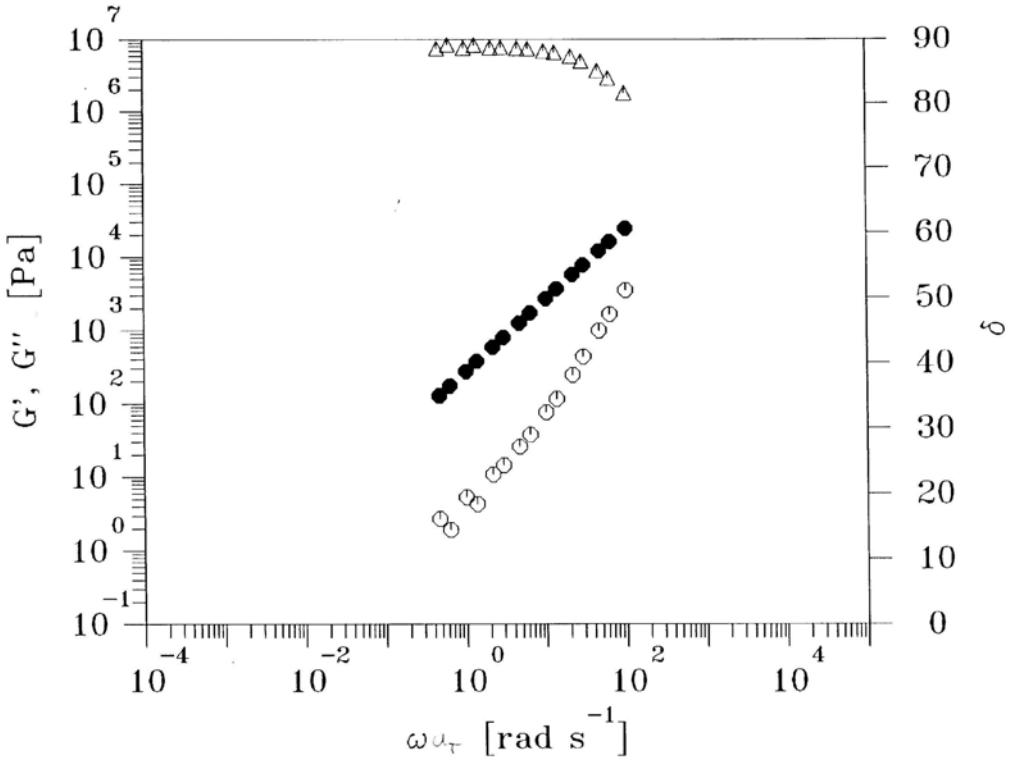

Figure 2.2-2 : time-temperature superposition (○ storage modulus G', ● loss modulus G'' and △ tanδ) for pure PBT (T_{ref} = 220°C).

The behavior of 15PB in Figure 2.2-3 was found very similar.

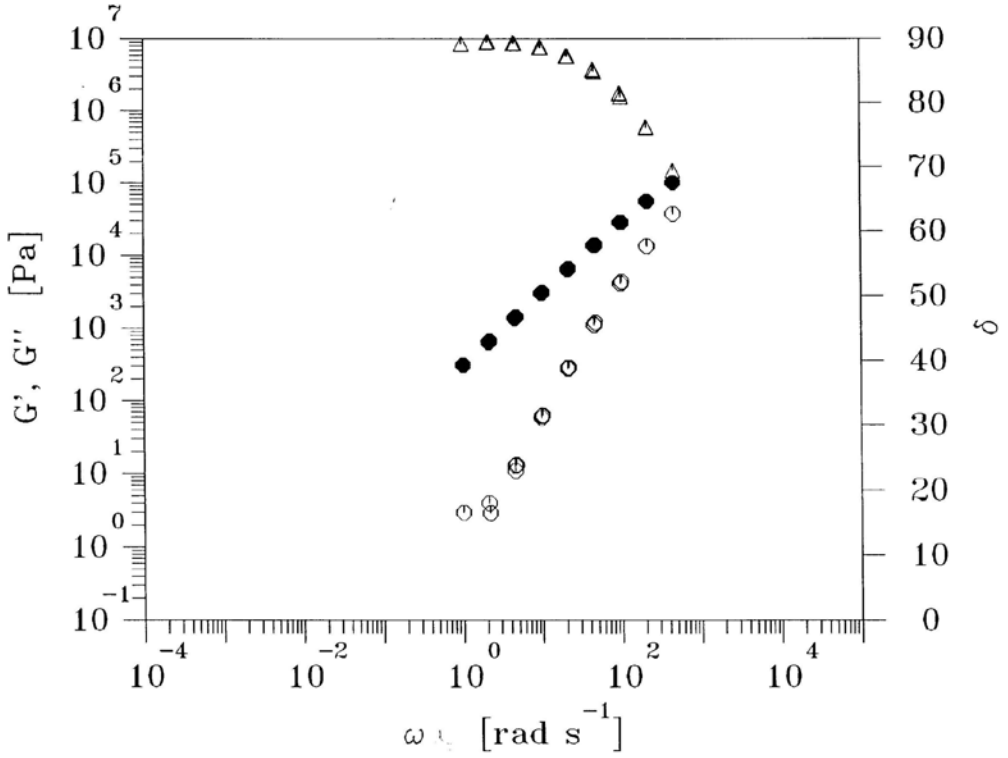

Figure 2.2-3 : time-temperature superposition (○ storage modulus G', ● loss modulus G'' and △ tanδ) for 15PB (T_{ref} = 230°C).

For 35PB in Figure 2.2-4 it was possible to see the beginning of the rubbery plateau and then to determine the storage modulus value at the minimum of tanδ on this plateau. By analogy to crosslinked polymers, the modulus at this point is proportional to the average molecular weight between entanglements, according to the following equation :

$$\overline{M}_e = \frac{\rho RT}{G'} \qquad \textit{Eq. 2.2-1}$$

At the intersection between G' and G'' it is possible to get the Maxwell's relaxation time, which will be used as the reptation time in our following discussions.

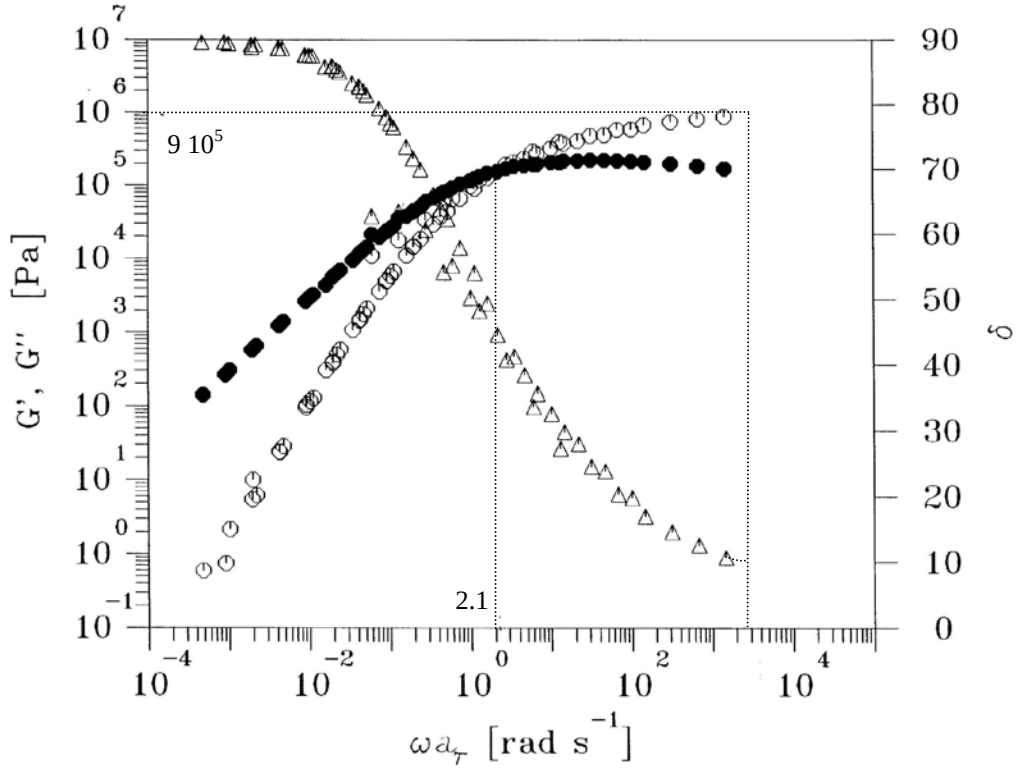

Figure 2.2-4 : time-temperature superposition (○ storage modulus G', ● loss modulus G'' and △ tanδ) for 35PB (T_{ref} = 100°C).

In figure 2.2-5 and 2.2-6 are represented the time-temperature superposition for 45PB and PBI respectively. Their rheological behavior is quite similar.

We extract from the data, the terminal relaxation time and the average molecular weight between entanglements. The different values of M_e and τ_{rept} are summarized in table 2.2-2. For the calculation of M_e we take ρ = 1.2 10^3 kg.m^{-3}, R = 8.314 and T = 373K. It is interesting to note that all three copolymers have very similar behaviors in the melt both in terms of M_e and in terms of terminal relaxation time. Essentially the only difference is the crystallization behavior. Also in comparison to the reported values for M_e of PBT, we find values which are distinctly higher. There may be some experimental errors in the absolute value of the plateau modulus. However, given the difficulty to measure reliable values of M_e for pure PBT, we feel that our values are quite reasonable and that probably values of M_e and relaxation times for the more crystalline copolymers and the PBT homopolymer are not very different from what we measure.

Table 2.2-3 : average molecular weight between entanglements and reptation time at the reference temperature (100°C).

	M_e (g.mol^{-1})	τ_{rept} (s) at 100°C
35PB	4 100	3
45PB	3 900	1.4
PBI	4 100	2

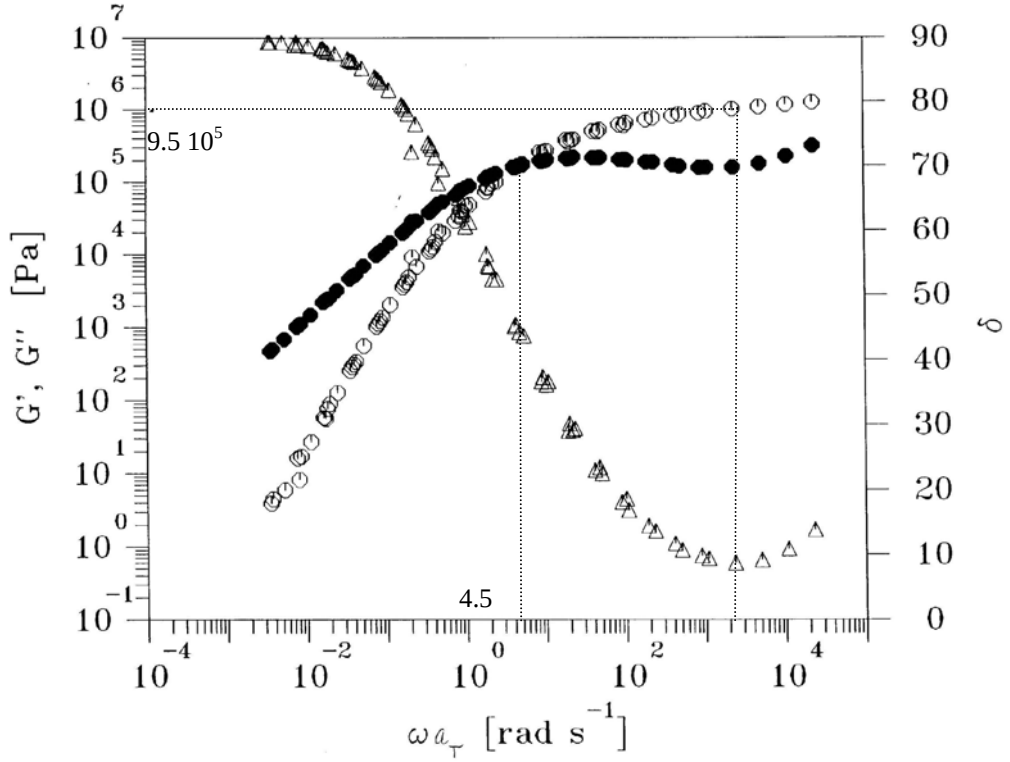

Figure 2.2-5 : time-temperature superposition (○ storage modulus G', ● loss modulus G'' and △ tanδ) for 45PB (T_{ref} = 100°C).

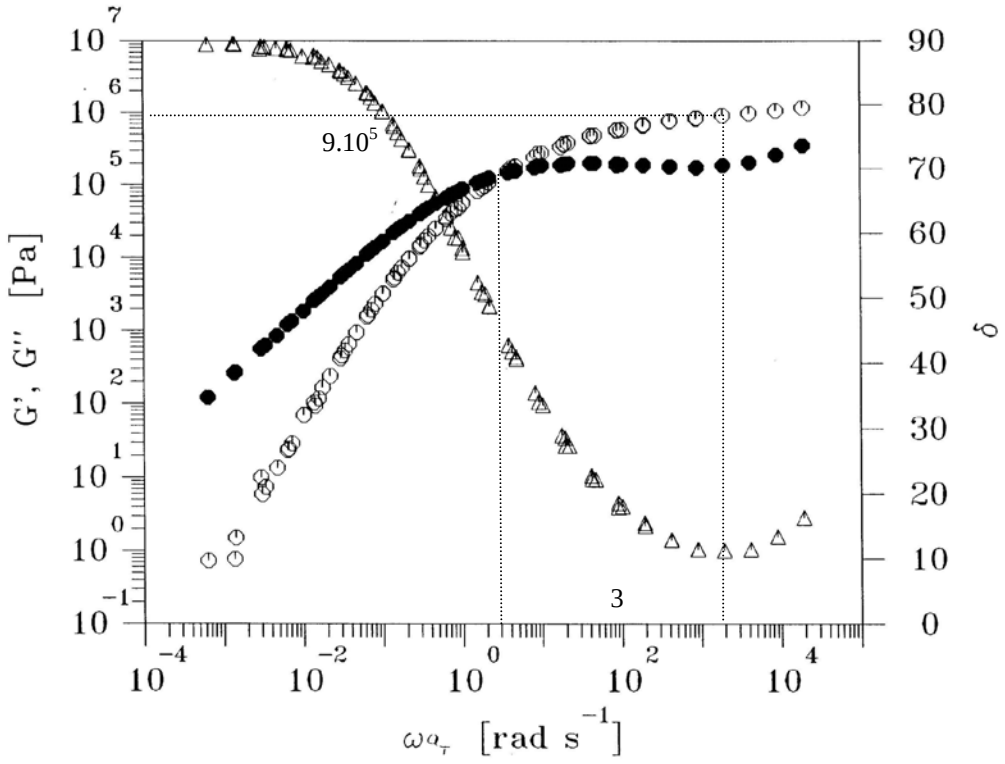

Figure 2.2-6 : time-temperature superposition (○ storage modulus G', ● loss modulus G'' and △ tanδ) for PBI (T_{ref} = 100°C).

2.2.4 NMR experiments

NMR C_{13} spectra were acquired for the three copolymers (15, 35 and 45PB) and the homopolymers PBT and PBI by H-AJ. Linssen (DSM research). The samples were dissolved in $C_2D_2Cl_4$ at 120°C and then placed in a 5 mm NMR tube, before acquiring the spectra on the ARX 400 apparatus according to a DSM standard protocol.

In the C_{13} spectra a small chemical shift difference is expected for the aliphatic carbon atoms of the butanediol ester of PBI and PBT. In the spectra of the block copolymers these differences, although very small are indeed observed.

TPZ-0-C**H**$_2$-CH_2-CH_2-C**H**$_2$-O-TPZ has a chemical shift of 65.06 ppm
IPZ-0-C**H**$_2$-CH_2-CH_2-C**H**$_2$-O-IPZ has a chemical shift of 65.01 ppm
TPZ-0-CH_2-C**H**$_2$-C**H**$_2$-CH_2-O-TPZ has a chemical shift of 25.87 ppm
IPZ-0-CH_2-C**H**$_2$-C**H**$_2$-CH_2-O-IPZ has a chemical shift of 25.90 ppm

The resonances of IPZ-0-CH_2-C**H**$_2$-C**H**$_2$-CH_2-O-TPZ are expected between 25.87 and 25.90 ppm while those of IPZ-0-C**H**$_2$-CH_2-CH_2-C**H**$_2$-O-TPZ are expected between 65.05 and 65.06.

For a random copolymer with 15% PBI we would have expected 4 lines with intensity ratio 0.72 : 0.13 : 0.13 : 0.02. We observed only two lines in all three copolymers, as represented in Figure 2.2-7 for 15PB. This shows the predominance of the TT of the II diade. We may conclude that our copolymers are not completely random.

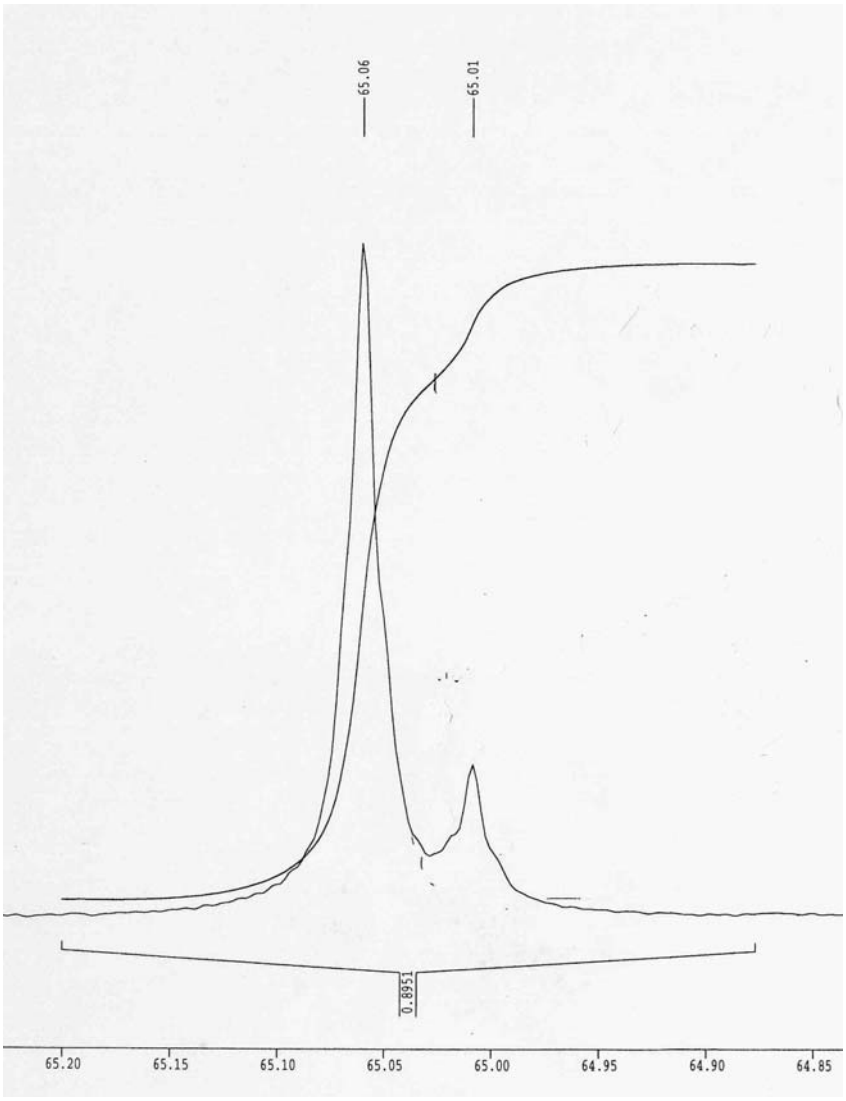

Figure 2.2-7 NMR spectra

In summary, the number average molecular weight was found in the range of 20 to 25 kg.mol^{-1} for PBT and the copolymer and up to 30 kg.mol^{-1} for pure PBI, which are values roughly five to ten times higher than the average molecular weight between entanglement, depending whether one uses 1.6 kg.mol^{-1} for PBT (from literature) or 4

$kg.mol^{-1}$ for 35PB, 45PB and PBI (from the rheology data). As a result all polymers are well entangled and diffuse in the melt by reptation. The typical reptation time at 100°C was of the order of 2 s for 35PB, 45PB and PBI (from the rheology data). Using the T-t superposition we could also extract some shift factors which can be used to extrapolate the reptation times to temperatures well below the crystallization temperature where a direct rheological measurement is no longer possible. This extrapolation will be used in the discussion.
NMR experiments showed that our copolymers were not completely random but probably constituted of short blocks of PBT and PBI.

We will now present bulk characterizations on crystallinity, mechanical behavior and crystalline structure.

2.3 Bulk characterization

2.3.1 Temperature modulated Differential Scanning Calorimetry

2.3.1.1 Basic theory

The theory supporting modulated DSC can be easily understood by comparing it to conventional DSC. In conventional DSC, the difference in heat flow between a sample and an inert reference is measured as a function of time and temperature as both the sample and reference are subjected to a controlled environment in terms of temperature and pressure. The common instrumental design for making those DSC measurements is the heat flux design shown in Figure 2.3-1.

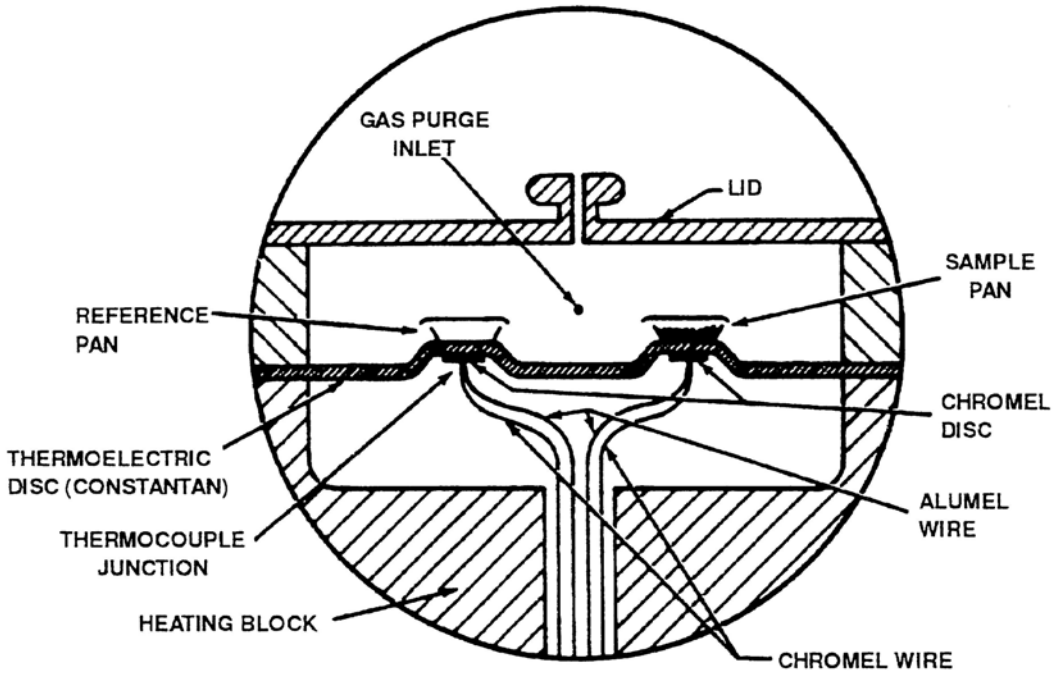

Figure 2.3-1 DSC schematic view : heat flux design, from TA instrument compendium.

In this design, a metallic disc (made of constantan alloy) is the primary means of heat transfer to and from the sample and reference. As heat is transferred through the disc, the differential heat flow to the sample and reference is measured by a thermocouple formed by the junction of the constantan disc and the chromel disc which cover the underside of the heating block. These thermocouples are connected in series and measure the differential heat flux using the thermal equivalent of Ohm's law :

$$\frac{dQ}{dt} = \frac{\Delta T}{R_D} \qquad \textit{Eq. 2.3-1}$$

ΔT being the temperature difference between reference and sample and R_d the thermal resistance of the constantan disc.
Modulated DSC is a technique which also measures the difference in heat flow between a sample and an inert reference as a function of time and temperature. However, in TM-DSC a different heating profile is applied to the sample and the reference. Specifically, a sinusoidal modulation is overlaid on the conventional linear heating ramps to yield a profile in which the average sample temperature continuously changes with time but not in a linear fashion. The net effect of imposing this more complex heating profile on the sample is the same as if two experiments were run simultaneously on the material – one experiment at the traditional linear (average) heating rate and one at a sinusoidal heating rate as represented in Figure 2.3-2.

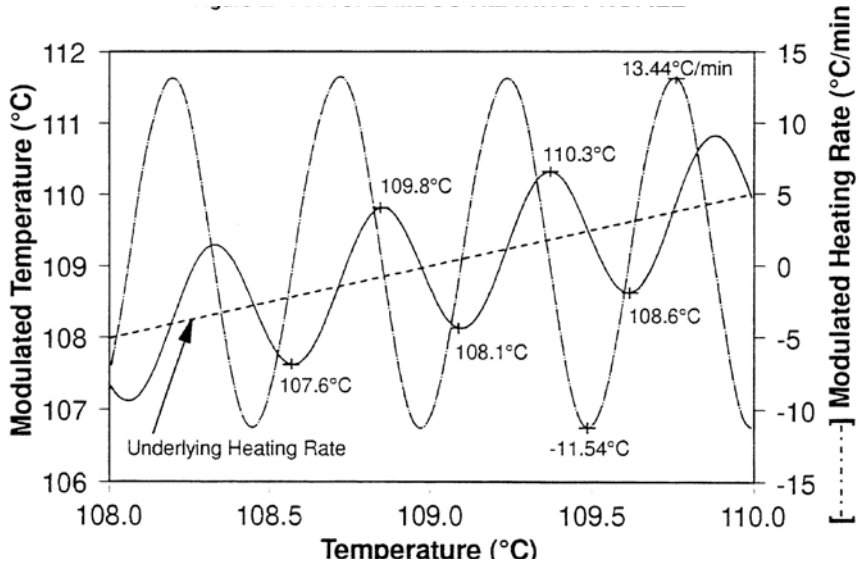

Figure 2.3-2 : sinusoidal modulated temperature superimposed to a linear heating ramp from TA instrument compendium.

The general equation which describes the resultant heat flow at any point in TM-DSC experiment is :

$$\frac{dQ}{dt} = C_p\beta + f(T,t) \qquad \textit{Eq. 2.3-2}$$

where *dQ/dT* is the total heat flow, C_p the heat capacity, β the heating rate and *f(T,t)* the heat flow from kinetic processes.

From equation 2.3-2, the heat flow is composed of two terms which are the "*reversing heat flow" ($C_p\beta$)* and the "*nonreversing heat flow" (f(T,t))*. These TM-DSC heat flows signals are calculated from three measured signals : time, modulated heat flow, and modulated heating rate.

In TM-DSC, the *reversing heat flow* and the *total heat flow* are calculated from the three measured signal. The *nonreversing flow* is determined by the arithmetic difference between the *total heat flow* and the *reversing heat flow*.
The *total heat flow* is continuously calculated as the moving average of the raw modulated heat flow signal.

The *reversing heat flow* is calculated by the determination of the heat capacity and converting it into heat flow by using the following equation where β is the average heating rate used in the experiment: Reversing heat flow = (-Cp)β

C_p is determined by dividing the modulated heat flow amplitude by the modulated heating ramp amplitude.

2.3.1.2 Experimental procedure

In order to characterize our samples, we chose to apply to each polymer and copolymer the same experimental procedure. A granule of each polymer or copolymer was placed in the DSC pan, heated to 260°C in order to cancel any previous thermal history, cooled at 5°C. min^{-1} to -50°C and reheated again at 5°C.min^{-1} with a temperature modulated ramp to above the melting temperature. In figure 2.3-3 are shown the total heat flows obtained in the last heating ramp.

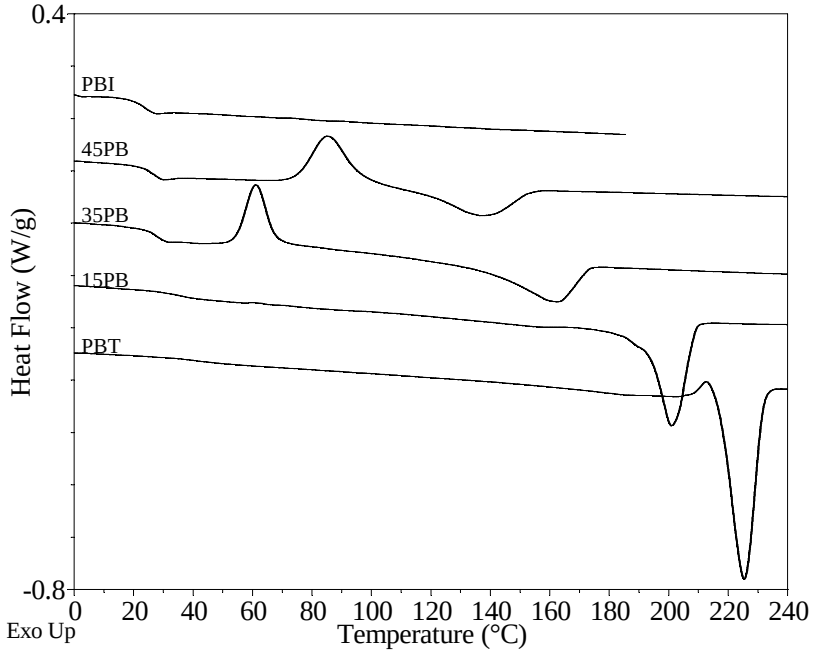

Figure 2.3-3 : total heat flow for PBT/BPI samples. Scan ramp : 5°C.min^{-1}.

PBT, and 15PB were already crystallized before the last heating ramp, since no cold crystallization occurred, while 35PB and 45PB present a cold crystallization peak during

the last heating. PBI was found fully amorphous and no cold crystallization was seen. These results are consistent with the results found by Bandiera et al. and presented in section 2.1.3.
We can obtain additional information by examining the nonreversing flow in Figure 2.3-4. As explained in the previous section, the nonreversing flow, which corresponds to the term *f(T,t)* in equation 2.3-2, is the heat flow of the processes governed by kinetics. One can see the nonreversing flow as the out of phase signal, which can be compared to the signal used for the calculation of G'' in Dynamic Mechanical Analyses. As a first approximation, the kinetics-dependent processes, like cold crystallization or crystalline reorganization, will appear in the nonreversing flow while the non kinetics-dependent processes, typically the fusion, will be seen in the reversing flow.

The nonreversing flow of PBT in Figure 2.3-4 is of great interest, since we obtained information on the melting behavior of PBT. Hence, an exothermic peak is clearly seen at temperatures where the total heat flow showed only multiple endotherms. We can conclude that in the early stages of melting, fusion and recrystallization or reorganization all occur at the same time. This recrystallization process corroborates very well the interpretation made for the main melting peak of PBT (see section 2.1.1.6.3), which was attributed to the melting of lamellae crystallized during the heating of the sample. The case of 15PB is similar, although the amplitude of the phenomenon is reduced. For 35PB and 45PB, the cold crystallization logically appears in the nonreversing flow.

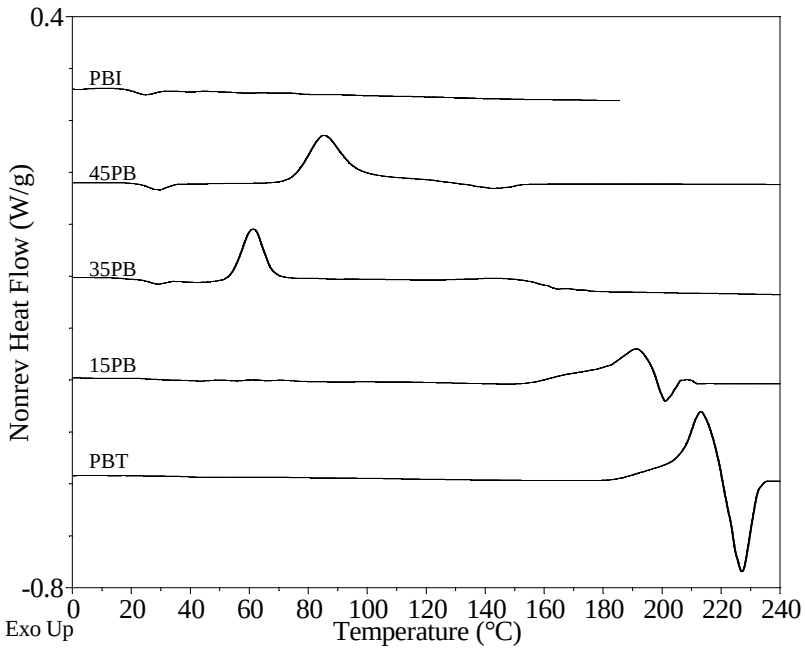

Figure 2.3-4 : nonreversing flow for PBT/BPI samples. Scan ramp : 5°C.min^{-1}.

In table 2.3-1 are summarized the different temperatures and specific heats extracted from Figure 2.3-3. The degree of crystallinity has been calculated from equation 2.3-3. The

heat of fusion of a pure crystal of PBT (ΔH_m^0 = 140 J.g^{-1}) was taken for the calculation in the case of PBT, 15PB and 35PB and 45PB and a value of ΔH_m^0 = 125 J.g^{-1} was taken for PBI (see section 2.1.1.6.4 and 2.1.2). The crystal morphology of PBT, 15PB, 35PB and 45PB was found very similar (only very small shifts for some peaks in the WAXS spectra given in section 2.3.1.4). Hence the same value of ΔH_m^0 was assumed for 15PB, 35PB and 45PB.

$$\chi_c = \frac{\Delta H_m}{\Delta H_m^0} \qquad \textit{Eq. 2.3-3}$$

Table 2.3-1: different temperatures and specific heats obtained in the case of a standard procedure.

	T_g (°C)	T_{cc} (°C)	ΔH_{cc} (J.g^{-1})	T_m (°C)	ΔH_m (J.g^{-1})	ΔH_m-ΔH_{cc} (J.g^{-1})	χ_c (%)
PBT	41	-	-	225	40	40	29
15PB	36	-	-	201	36	36	26
35PB	27	61	16	162	25.5	9.5	6.9
45PB	26	85	17	137	17.7	0.7	0.43
PBI	24	-	-	-	-	-	-

2.3.2 Dynamic Mechanical Analysis

2.3.2.1 Experimental procedure

In this section, Dynamic Mechanical Analyses (DMA) were carried out on our polymers and copolymers, in order to get the linear viscoelastic properties from below T_g up to the temperature of fusion.

We used the Q800 Dynamic Mechanical Analyzer from TA Instruments, which can operate over a large range of temperatures (-145→600°C), force (0.0001N→18N), frequency (0.01→200 Hz) and amplitude (0.5→10 000 μm).

In our experiments, the samples were mounted on a single cantilever clamp, one part of which is stationary while the other is movable and connected to the drive motor, which directly affects the deformation of the sample.

The sample preparation was identical to the one used for adhesion experiments (see section 2.4). PBT, 15PB and 35PB were molded at T_m+20°C and cooled at 2.5°C.min^{-1}. For 35PB two different cooling rates were applied : 2.5°C.min^{-1} or quenched in ice water. 45PB and PBI were molded at 180°C, and quenched in ice water.

The samples were cut in the following dimensions : 25x10x2 mm^3. A general schematic of the sample mounted on the clamp is given in Figure 2.3-5. In our experiments, we used the clamp in a single cantilever geometry, i. e. only two clamps were used.

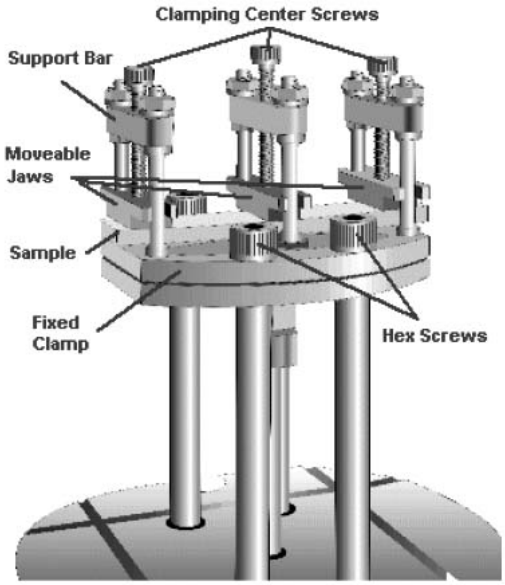

Figure 2.3-5 : schematic of the sample mounted on a single or dual cantilever clamp (from TA instrument compendium).

The amplitude of motion of the mobile part was set at 15 μm and the frequency at 1 Hz in all our experiments. Measurements were carried out every 3 minutes, after 3 minutes of isotherm in order to stabilize the temperature.

2.3.2.2 Results

In figure 2.3-6 the storage modulus of PBT, 15PB and 35PB, molded and cooled at 2.5°C.min^{-1} are plotted as a function of temperature. The three copolymers have a similar behavior, with a decrease of G' at the glass transition temperature. The value of G' is given in table 2.3-2 at 20 and 100°C, together with the glass transition temperature determined by the inflection point of G'. The values obtained for the glass transition temperature pointing this way were slightly higher than those obtained by DSC (see table 2.3-1)

Table 2.3-2 : values of G' at 20 and 100°C, glass transition temperature.

	G' (MPa) at 20°C	G' (MPa) at 100°C	T_g(°C)
PBT	2050	390	46
15PB	1940	215	35.5
35PB	1920	120	33.5

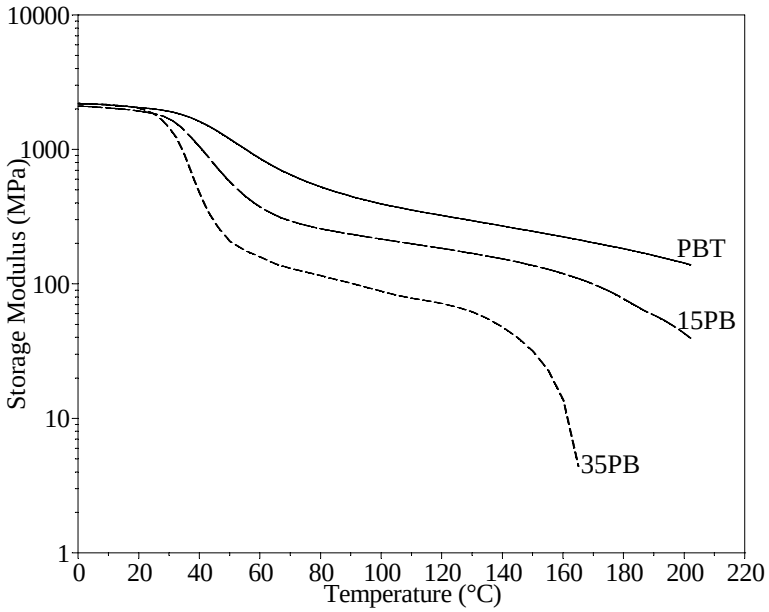

Figure 2.3-6 : storage modulus measured at 1Hz as a function of temperature.

Figure 2.3-7 shows the storage modulus as a function of temperature for 35PB prepared with two different experimental procedures. The sample was molded then slowly cooled (2.5 °Cmin^{-1}) to room temperature in one case, and molded then quenched in ice water in the second case. The quenched sample, which was amorphous at room temperature, has a completely different behavior. Both the modulus at 20°C and the glass transition temperature was found lower for 35PB in the amorphous state. Above the glass transition temperature, a sharp decrease in G' is seen, followed by a sharp increase due to the fast cold crystallization of the sample. The final modulus remains however lower than what is measured for the slowly cooled sample implying that the crystalline structure and maybe the degree of crystallinity is probably different.

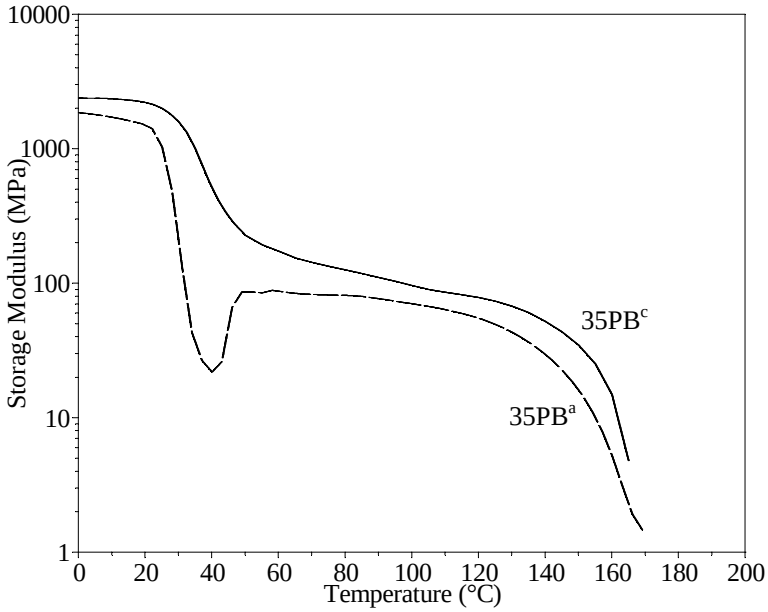

Figure 2.3-7 : storage modulus measured at 1Hz as a function of temperature for 35PB slowly cooled after molding (35PB^c) and 35PB quenched after molding (35PB^a)

Figure 2.3-8 shows the variation of the storage modulus for 35PB, 45PB and PBI, prepared in the same conditions, i.e. the samples were molded at 180°C, then quenched in ice water. For each sample, G' increases for temperatures above the glass transition temperature because of the cold crystallization of the samples. The temperature of cold crystallization can be extracted from these data: 44°C for 35PB, 54°C for 45PB and 68°C for PBI. These values indeed differ from the values obtained by DSC In the DSC experiments, the copolymers were cooled at 5°C.min^{-1}. In these conditions 35PB was partly crystallized. Also at high temperature the modulus of pure PBI is higher than that of the copolymers suggesting a slower kinetics but a higher final degree of crystallinity.

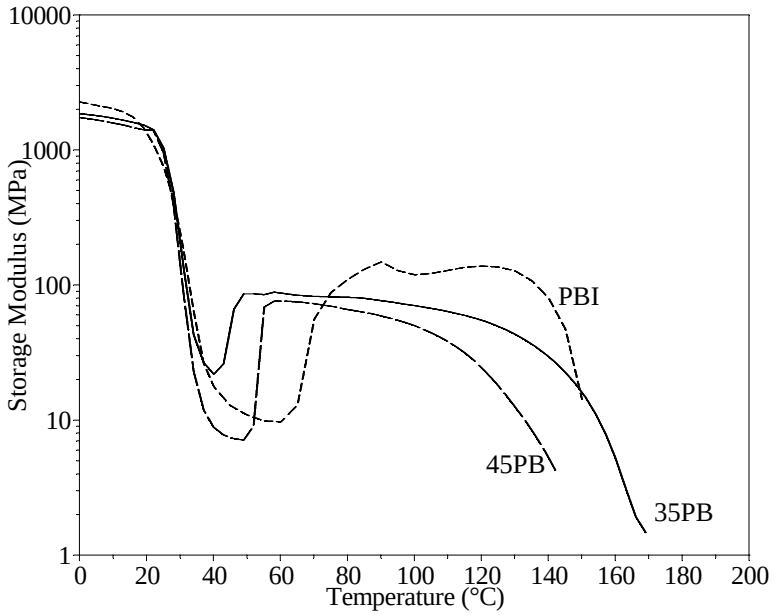

Figure 2.3-8 : storage modulus measured at 1Hz as a function of temperature in the case of quenched samples.

2.3.3 X-rays

We used Wide Angle X-ray scattering (WAXS) to characterize the crystalline structure in our different copolymers and also to calculate the degree of crystallinity in our copolymer.

X-ray diffraction can be used as a technique for estimating the degree of crystallinity. Several methods have been devised for the calculation of the degree of crystallinity from a WAXS spectrum. Basic principles of these methods can be found in the textbook of Alexander[1]). By these methods, one can obtain the degree of crystallinity at room temperature directly, while in the DSC experiment, the sample must be heated in order to obtain the melting peak and complex changes that can occur during heating. Nevertheless, the deconvolution between the amorphous halo and the crystalline peaks in a WAXS spectrum is the difficult part of the analysis.

2.3.3.1 Sample preparation and results

These experiments were performed in the laboratory of "Céramique et Matériaux Minéraux" with the help of Pr. Nicolas Lequeux.

In our experiments, we used an X-ray diffractometer from Philips (XPert instrument) using CuK_α radiation (1.54056 nm) with a graphite monochromator in the diffracted

[1]Alexander, L. E. X-ray Diffraction Methods in Polymer Science. (Wiley-Interscience, New York, 1969)

beam. Data where collected by counting typically 15 seconds at each 0.05° step in 2q from 5° to 40°.

In a first set of experiments, PBT, 15PB, 35PB, 45PB and PBI 2 mm thick disks were molded at T_m+20°C, then cooled at 2.5°C.min^{-1} (the same experimental procedure was used for adhesion in section 2.5). In the case of 45PB and PBI, the disk was annealed at 100°C for 120 minutes in order to reach the complete crystallization.

Each disk was placed in the diffractometer and scanned with an incidence angle between 5 and 40°. The spectrum is given in Figure 2.3-9.

The crystalline structure is roughly the same for PBT, 15PB, 35PB and 45PB, since the crystalline peaks appear at the value of 2θ. The degree of crystallinity however is clearly decreasing from PBT to 45PB. The crystalline structure of PBI on the other hand, is rather different. The crystal structure of PBT has been reported by many authors and has been determined to be a monoclinic crystal. The Miller index for the reported monoclinic crystal system was indexed on every diffraction peak. The diffraction peaks of PBT are distinctly sharper than those of 45PB. The width of the diffraction peak increases from PBT to 45PB, which indicates that the crystalline size decreases, as suggested by the Scherrer equation (Warren[1]).

The height of the peaks is also decreasing from PBT to 45PB, which indicates that the overall degree of crystallinity is decreasing from PBT to 45PB which is indeed consistent with the DSC results.

[1]Warren, B. E. X-Ray Diffraction. (Dover, New York, 1969)

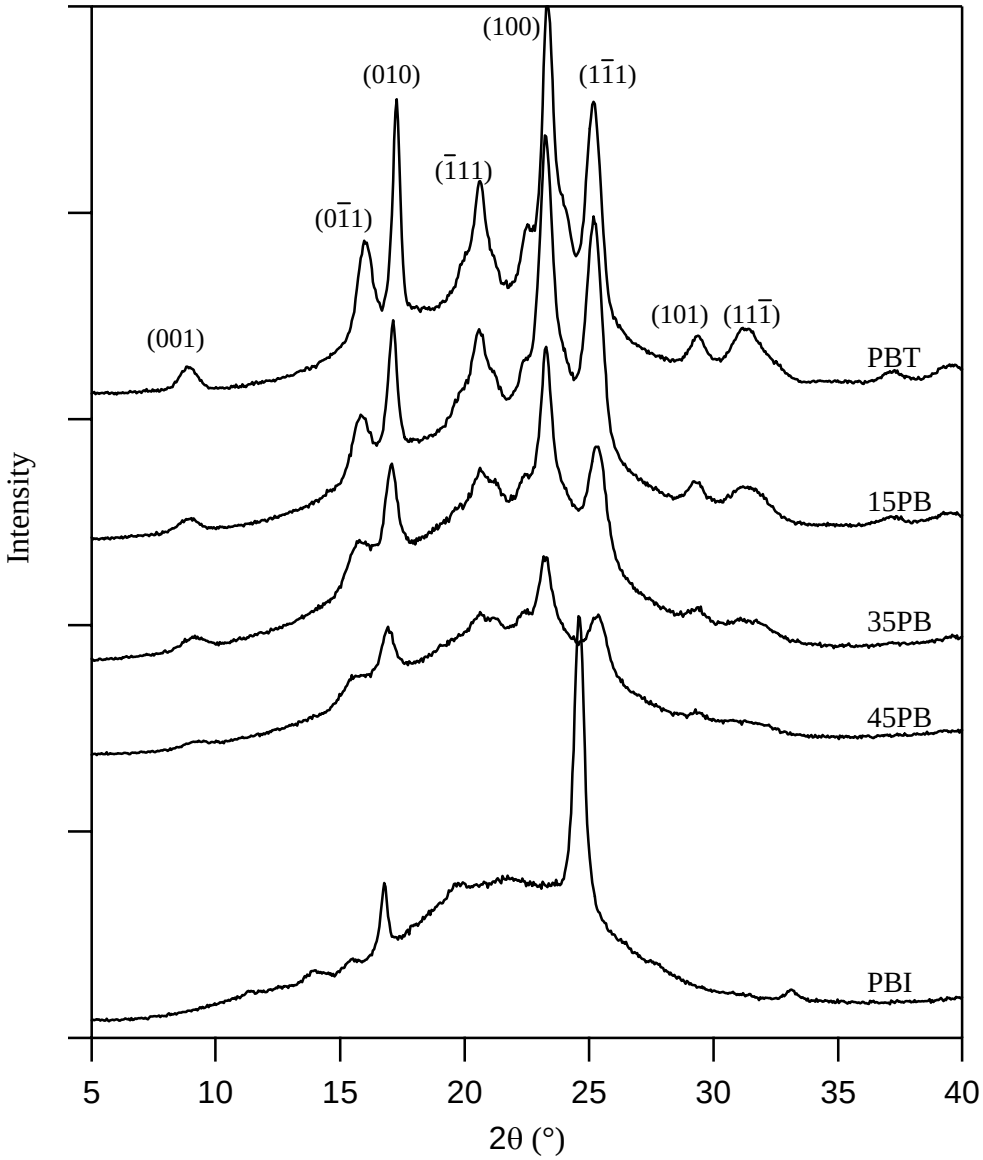

Figure 2.3-9 : Diffraction patterns of melt-crystallized PBT, 15PB, 35PB at a cooling rate of 2.5°C.min^{-1} and cold crystallized 45PB and PBI at 100°C for 120 min. Miller indices are shown on the diffraction peaks of PBT.

We will now quantify the degree of crystallinity in the following section.

2.3.3.2 Calculation of the degree of crystallinity

The calculation of the degree of crystallinity from the X-ray spectrum is based on the deconvolution of the spectrum into an amorphous halo and crystalline peaks (Murthy and Minor[1]).

[1]Murthy, N. S. and Minor, H. Polymer, 31: 996-1002, (1990).

In order to deconvolute, we used two different fit functions. The first fit function *($f_1(2\theta)$)* was composed of an arithmetic sum of Gaussian functions, while the second fit function *($f_2(2\theta)$)* was the sum of a Gaussian function and Lorentzian functions :

$$f_1(2\theta) = A_0 + I_0 \exp\left\{-\left(\frac{2\theta - P_0}{W_0}\right)^2\right\} + \sum_{i=1}^{nb\ of\ peaks} I_i \exp\left\{-\left(\frac{2\theta - P_i}{W_i}\right)^2\right\} \quad \textit{Eq. 2.3-4}$$

$$f_2(2\theta) = A_0 + I_0 \exp\left\{-\left(\frac{2\theta - P_0}{W_0}\right)^2\right\} + \sum_{i=1}^{nb\ of\ peaks} \frac{I_i}{1 + \left(\frac{0.4142}{(W_i/2)^2}\right)(2\theta - P_i)^2} \quad \textit{Eq. 2.3-5}$$

Where A_0 is a constant, I_0, P_0 and W_0 are respectively the height, the position and the full-width at half-maximum of the amorphous halo, I_i, P_i and W_i are respectively the height, the position and the full-width at half-maximum of the crystalline peaks.

The fitted curves are given in Figure 2.3-10.

The amorphous halo was subtracted from each spectrum (upper curves) then an amorphous 45PB (quenched after molding) was fitted with a Gaussian function (lower curve) in order to have the amorphous reference needed for the calculations.

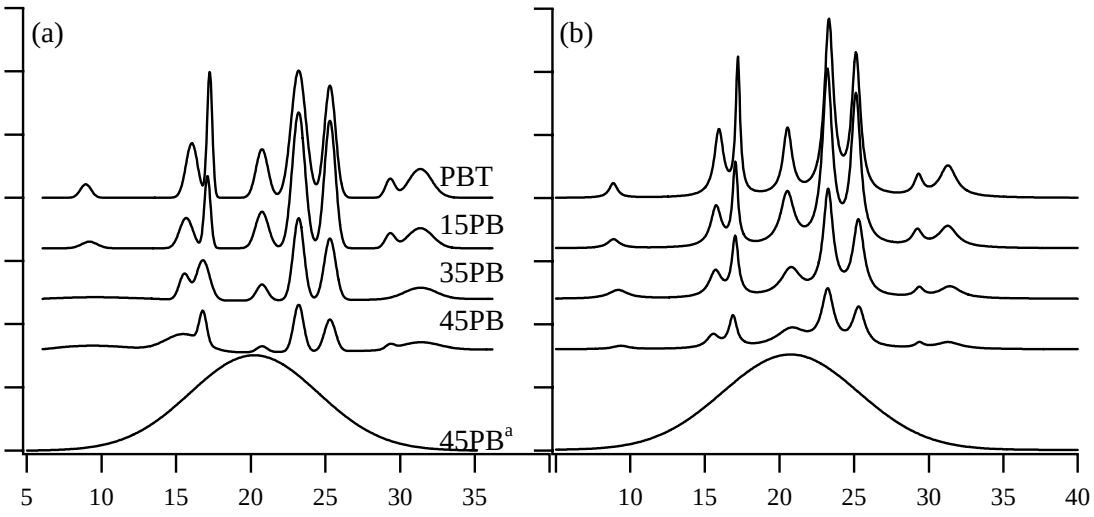

Figure 2.3-10 : result of the fit with f_1 (a) and f_2 (b) for PBT, 15PB, 35PB, cold crystallized 45PB and amorphous 45PB (45PB^a).

The calculation was made using the following equation

$$\chi_j = \frac{\int_{2\theta=5}^{40} C_j(2\theta)}{\int_{2\theta=5}^{40} A_{45PB^a}(2\theta) + \int_{2\theta=5}^{40} C_j(2\theta)} \qquad \textit{Eq. 2.3-6}$$

with

$$C_1(2\theta) = \sum_{i=1}^{nb\ of\ peaks} I_i \exp\left\{-\left(\frac{2\theta - P_i}{W_i}\right)^2\right\} \text{ and } C_2(2\theta) = \sum_{i=1}^{nb\ of\ peaks} \frac{I_i}{1+\left(\frac{0.4142}{(W_i/2)^2}\right)(2\theta - P_i)^2}$$

and

$$A_{45PB^a}(2\theta) = B_{45PB^a} + I_{45PB^a} \exp\left\{-\left(\frac{2\theta - P_{45PB^a}}{W_{45PB^a}}\right)^2\right\}$$

$B_{45PB}{}^a$ being a constant. The results of the calculation are given in figure 2.3-11.
After scanning the samples by WAXS, a small part of each polymer disc was placed in a DSC pan, and a heating ramp of 5°C.min^{-1} to above the melting temperature was applied in order to also quantify the degree of crystallinity by DSC ($(\Delta H_m - \Delta H_{cc})/\Delta H_m{}^0$, see section 2.3.1.2). The obtained results are also plotted in Figure 2.3-11.

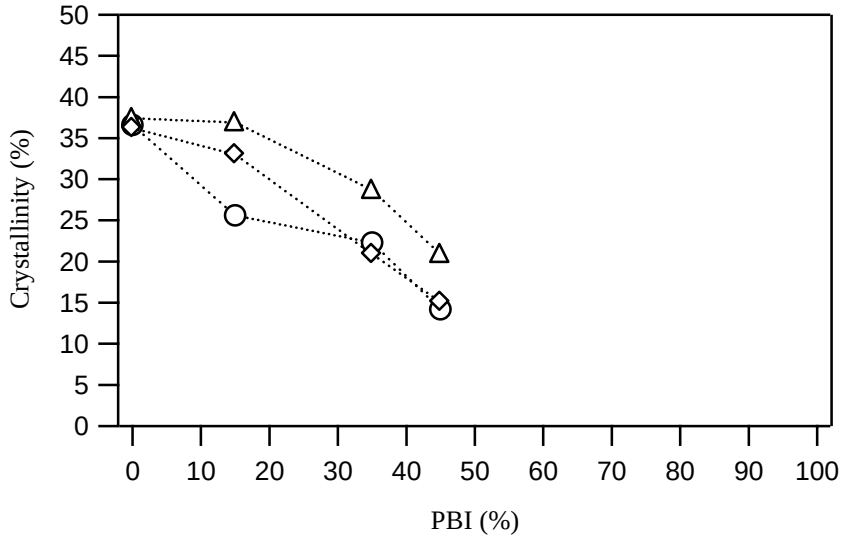

Figure 2.3-11 : degree of crystallinity as a function of PBI content, obtained from X-ray measurements, with the fit function f_1(◇), f_2(△) and obtained by DSC (○)

The degree of crystallinity obtained with the f_1 fit function was found in better agreement with the DSC results, excepted for 15PB. The heat of fusion of 15PB in DSC was probably underestimated.

The calculation has not been carried out in the case of PBI, because the tested sample (annealed at 100°C for 60 minutes) had not reached its maximum degree of crystallinity, as showed later in DSC and DMA experiments in section 3.4.2.

Several conclusions can be drawn from the characterization results. From TM-DSC experiments, we can classify the different polymers and copolymers we used in two main categories. In the first category, PBT and 15PB have a fast crystallization kinetics and showed a quite complex melting behavior. During melting, we observed a recrystallization or a crystalline reorganization, which was more pronounced in the case of PBT. 35PB, 45PB, and PBI have a much slower crystallization kinetics and tend to cold crystallize upon heating. Both 35PB and 45PB exhibit an exothermic peak of cold crystallization in a standard TM-DSC experiment, i.e. after melting at 206°C, cooling at 5°C.min^{-1} to -50°C and heating at 5°C.min^{-1}. The crystallization kinetics of 35PB is relatively faster than that of 45PB, since after the cooling at 5°C.min^{-1} the first sample was partly crystallized while 45PB was fully amorphous. PBI cold crystallizes very slowly, since it was not detectable in the last heating ramp in our standard procedure.

The mechanical properties, characterized by a Dynamical Mechanical Analysis, depended strongly on the degree of crystallinity unlike the situation observed at high temperature in the melt (see section 2.2.3) where all copolymers behave more or less in the same way. The mechanical response of the cold crystallization was seen for 35PB, 45PB and PBI samples, made amorphous by quenching them after compression molding.

X-Ray measurements showed that PBT, 15PB, 35PB and 45PB crystallize in the same structure, while PBI crystallizes in a different structure.

In summary, we have calculated the degree of crystallinity, from both X-Ray diffraction patterns, and DSC on the same samples. Our materials can all crystallize but with large differences in overall degree of crystallinity and even larger differences in crystallization kinetics. This will provide us with a specific set of variables to tune molecular mobility and mechanical properties in our polymer systems. In other words, the crystallinity of our samples strongly depends on thermal history.

Thus, in our adhesion measurements, we paid a special attention to the way we prepared our samples for the adhesion tests, by controlling the different cooling rates or annealing times. Additional specific DSC experiments were carried out, when necessary, in order to exactly simulate the thermal history of the samples prepared for adhesion tests. These results will however be presented together with the adhesion data for coherence.

This section will present the experimental techniques used for the characterization of adhesion, from the sample preparation and testing, to the different techniques used for the observation of the interface. This section can be considered as the core of the present work.

2.4 Adhesion : sample preparation and testing

2.4.1 Molding and assembling

The preparation of the assemblies can be divided in two steps: The first step consists in molding the polymer plates and the second in making the assembly by applying a certain pressure ($P_{contact}$, held constant) between two plates at a specified contact temperature ($T_{contact}$) and during a specified contact time ($t_{contact}$). A special attention was paid to the thermal history, which is known to influence the crystallization process in these semi-crystalline materials.

2.4.1.1 Temperature controlled press

Sheets of homopolymers or copolymers were molded and assembled in a temperature controlled press (Darragon SE 10T), showed in Figure 2.4-1.

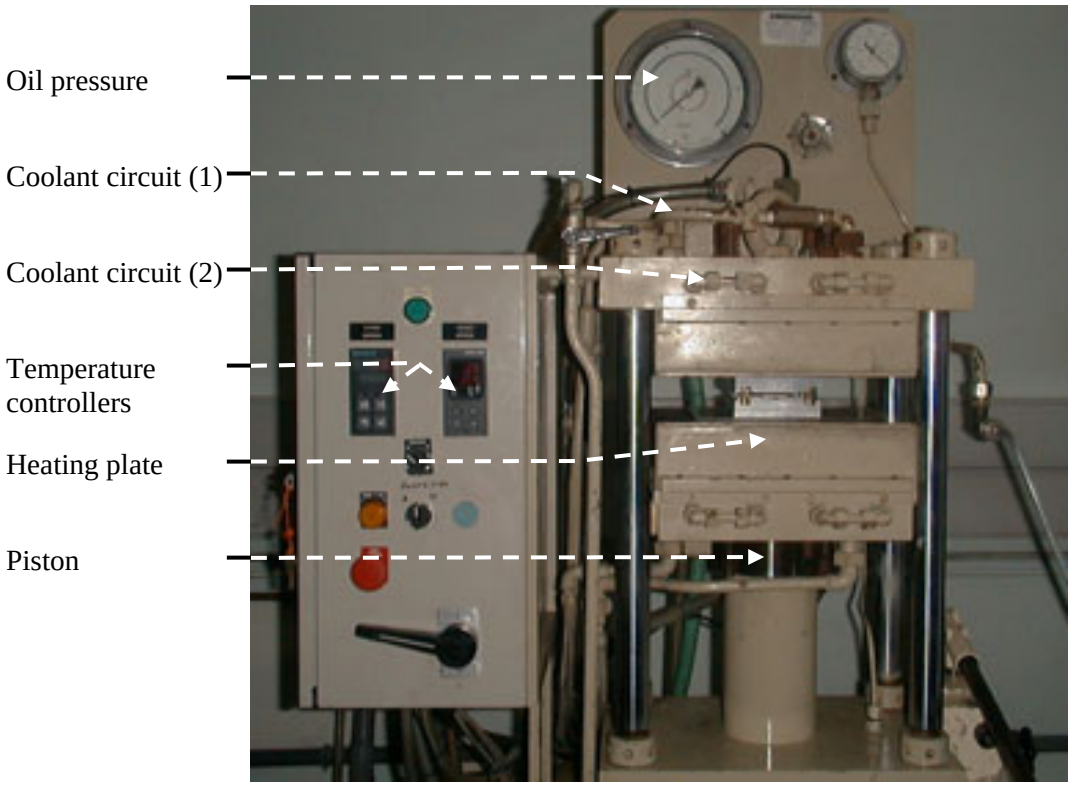

Figure 2.4-1 : general view of the temperature controlled press

This press is composed basically of two parallel plates, each plate containing a heating element. The temperature controllers of the press which accepts a temperature sensor such as a thermocouple as input, provide an accurate control of the temperature of the upper and lower heating element. The pressure between the two plates is raised by increasing the oil pressure under a piston. The pressure of the oil can be read on the press.

The press was equipped with two different cooling circuits, which could impose different cooling rates.

Cooling the sample after molding was found to be a crucial step to control the microstructure of all polymers as mentioned earlier. Hence, we used the different cooling devices of the press in order to control the cooling rate of the samples. The primary coolant circuit (1), directly connected with the heating plate of the press, can receive either water or air. A secondary circuit, connected to the frame, runs with water (Figure 2.4-2). As an example, water cooling in both circuits leads to a cooling ramp of around 20°C.min^{-1}, while air in the primary circuit and water in the secondary circuit leads to a 2.5°C.min^{-1} cooling ramp.

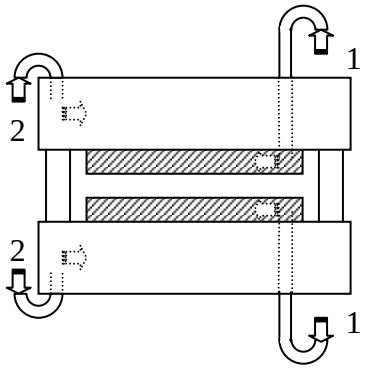

Figure 2.4-2: press primary and secondary coolant circuit
1 → ∅/ water /air ; 2 → ∅/ water

2.4.1.2 Molding

The polymer granules were placed in a window steel mold (50x30x2 mm^3). In order to obtain clean demolding of the plates and a smooth surface finish, two procedures were used: For the PBT, the steel window mold was placed between two smooth stainless steel plates (Weber metals, 0.5 mm thick, optical finish) while for all the other polymers, a polyimide film (Kapton® from DuPont, 0.3 mm thick) was placed on top of each steel plate. The polyimide film was added to avoid adhesion between the polymer and the stainless steel plate. The molding temperature was selected such as $T_{mold} = T_m + 20°C$.

In the case of 45PB and PBI, which exhibit a lower modulus than the other polymers, we overmolded a 300 µm thick layer of these polymers on top of a 2mm thick polycarbonate

(PC) plate to keep a reasonable modulus for the DCB test. The molding procedure can be described as follows : first the molding of a PC plate, 2 mm thick, at a molding temperature of 200°C, then the overmolding of a 45PB or PBI layer on top of the PC plate in a 2.3 mm mold. The adhesion between PC and our copolymers was found to be good. The best results for the second molding procedure was obtained by imposing a different temperature on each side of the 2-layers molded plate, i.e. 180°C for the upper heating plate which was in contact with 45PB or PBI and 150°C for the lower heating plate in contact with PC.

The molding procedure is summarized in Figure 2.4-3. The thickness checked after molding was 1.85 mm +/-0.05 for PBT, 15PB and 35PB and 2.3 mm +/- 0.1 for 45PB/PC and PBI/PC.

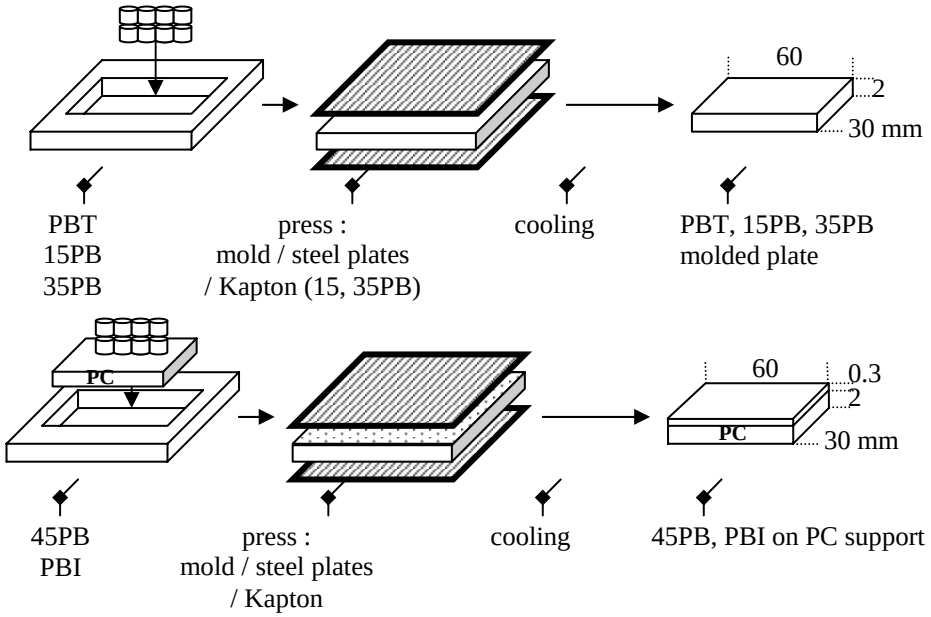

Figure 2.4-3: molding process for each polymer and copolymer

P_{mold} = *60 bars*

$T_{mold} = T_m + 20°C$

2.4.1.3 Cooling procedure

We applied a controlled cooling rate of 2.5°C.min^{-1} (1→air, 2→water) for PBT, 15PB and 35PB. For 45PB and PBI, two different cooling procedures were applied in order to obtain these polymers in two different crystalline states. These copolymers are indeed very sensitive to the thermal history, and one can obtain them fully amorphous or semi-crystalline depending on the heat treatment. We chose mainly two different cooling procedures : one was the same as the procedure used for PBT, 15PB and 35PB and the other was a quench in ice-water. For this latter case, a controlled cooling of 20°C.min^{-1} (1→water, 2→water) was applied during 1 min before quenching (the upper heating plate

was then cooled from 180°C to 160°C) to minimize mechanical residual stresses between the 2 layers due to the difference in thermal expansion between PC and our polymers (direct quench after t_{mold} led to bent samples).

A careful temperature check was performed during the molding for each polymer and each molding procedure. In order to perform this verification, the complete molding cycle was reapplied to a polymer plate (as it was difficult to place thermocouples directly on the polymer granules). Two thermocouples were placed with a thermoconductive paste, on each face of the polymer plate previously placed in the mold. The molding procedure was then followed. One example of a recorded temperature as a function of molding time is given in Figure 2.4-4 (molding of a 15PB plate). The temperature was recorded with a thermometer (Hanna Instruments), at sampling intervals of 1 second.

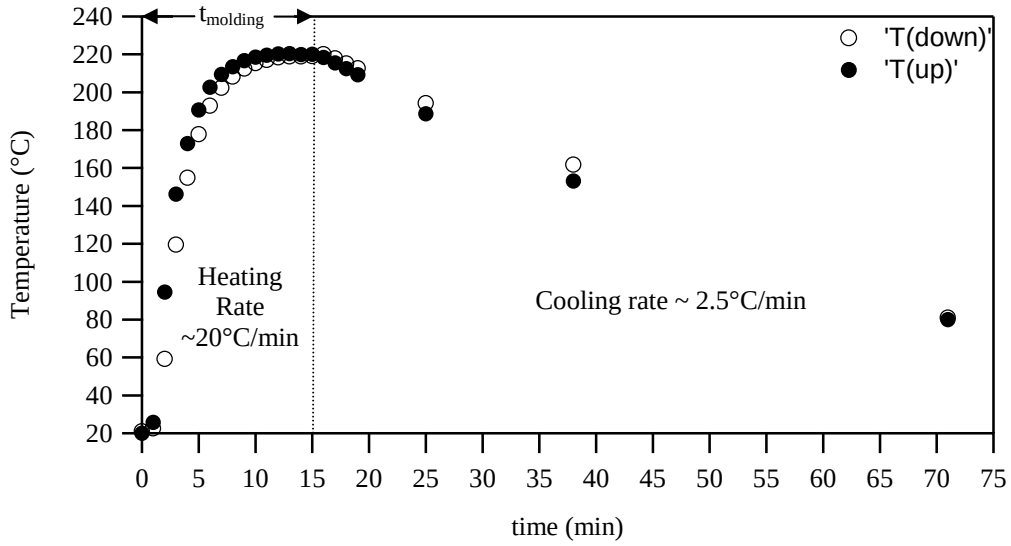

Figure 2.4-4 : temperature on each face of the polymer during the molding process

If assembling was not carried out immediately after molding, the samples were stored at -20°C.

A schematic view of the different thermal histories applied to the polymers during molding is given in Figure 2.4-5

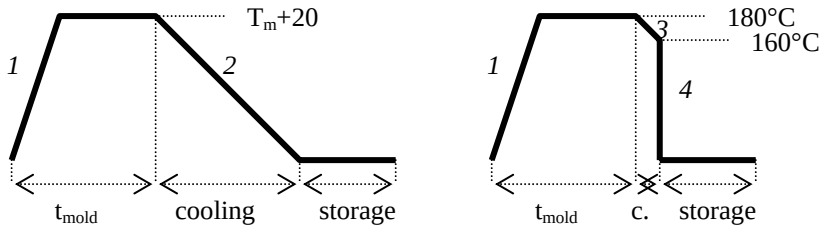

PBT, 15PB, 35PB, 45PB 45PB, PBI

Figure 2.4-5: thermal history undergone during molding.
1 → 20°C/min ; 2 → 2.5°C/min ; 3 → 20°C/min ; 4 → quenched

2.4.1.4 Assembling

After molding, two polymer plates were placed in a home-made set up, designed by Philippe Sergot in our laboratory, which gives the possibility of preheating each individual plate independently and at different temperatures before contact is established under a pressure of 200 bars (Figure 2.4-6).

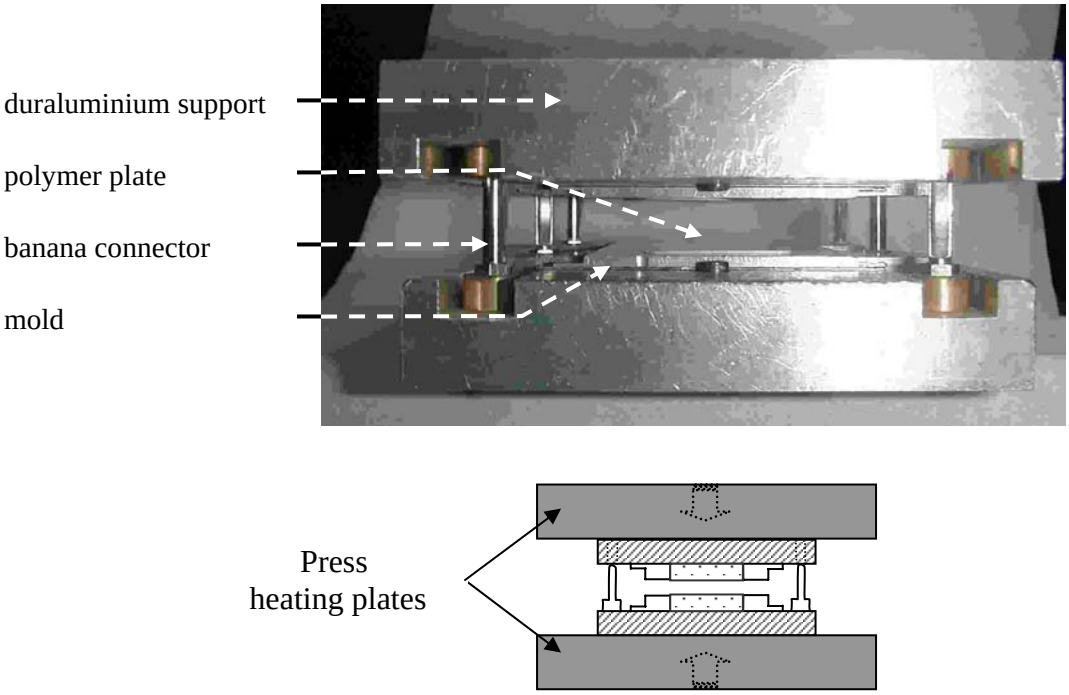

Figure .2.4-6 : home-made set up for assembling under the press

The banana connectors maintain the set up open, even under the light pressure imposed by the press in order to obtain a good thermal contact between the heating plate of the press and the set up during the preheating step. Moreover, when the set up is closed, these

banana connectors maintain the set up closed, making it possible to withdraw the set up from the press in the closed position if necessary.

Contact was made after a certain time of preheating t_{ph} by increasing the oil pressure under the press piston (diameter of 10 cm) to P_c = 50 bars. The pressure of contact was kept constant for all experiments, while the temperature of contact $T_{contact}$ and the time of contact t_c were variables. After contact, the set up was placed between the two plates of a water heat exchanger made of copper (Figure 2.4-7), in order to obtain a fast cooling of the assembly (40°C.min^{-1}). The contact between the polymer plates was maintained during the cooling step, thanks to the specific design of the set up with the banana connectors.

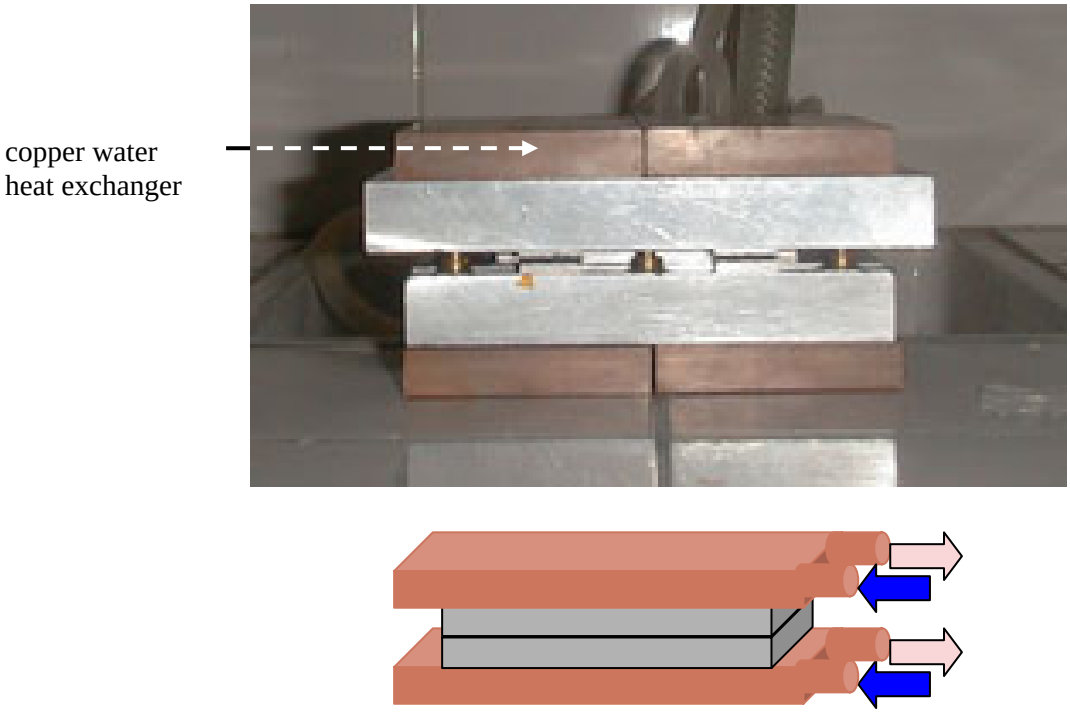

Figure 2.4-7 : cooling the assembling set up

In our first experiments, a problem of oxidation was observed for PBT during the preheating near the melting temperature. In order to avoid oxidation, the whole set up was placed in a vacuum box (Figure 2.4-8). The box was placed between the heating plates of the press, evacuated and refilled with nitrogen at least three times.

This vacuum box was used for PBT and 15PB only.

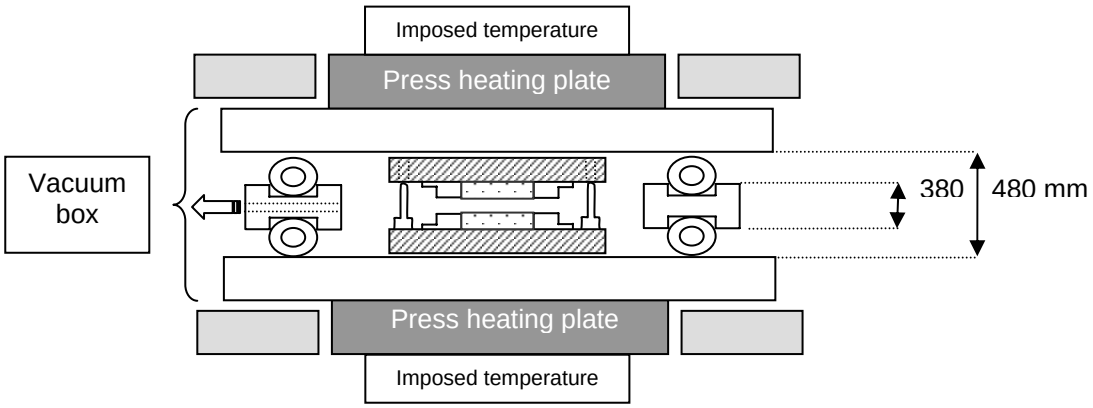

Figure 2.4-8 : set up for assembling in the vacuum box between the heating plates of the press

For each polymer, the temperature at the surface of the polymer was checked several times for each temperature cycle. Experiments with a surface thermocouple ("Cement-On" CO3-K, Omega) glued (with a heat conductive paste) on the surface of the polymer were performed following the same experimental procedure as assembling. Data were recorded with a digital thermometer (HI 98801, Hanna Instruments) with a sampling interval of one minute. It was then possible to follow the temperature at the polymer surface during the assembling process. It was found that after a certain time, the temperature remained constant but stayed below the set temperature (in the heating plates), about 5°C below in the case where assembling was performed without the vacuum box and 10°C below with the vacuum box. In each case, the temperature finally reached the set temperature (equal to $T_{contact}$) within several minutes and remained constant, until the cooling, at an average rate of 40°C.min^{-1}, was applied. An example is given in Figure 2.4-9 in the case of PBT and 15PB (with the vacuum box). A general view of the assembling set up in the press is given in Figure 2.4-9.

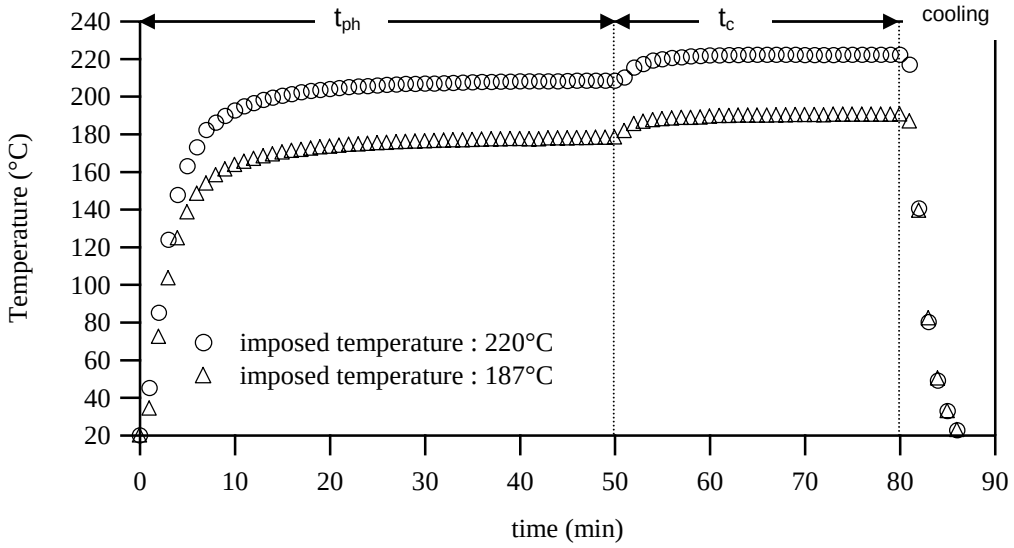

Figure 2.4-9 : temperature at the polymer surface during assembling
Set temperature : temperature of the press heating plates

2.4.2 Measurement of the fracture toughness

2.4.2.1 DCB test

Prior to the adhesion test, the assemblies were cut in three parts with a precision sectioning saw (Isomet 1000, Buehler) using a diamond wheel (30HC diamond, Buehler). This procedure allows more independent measurements on the same assembly and is necessary to remove the edge of the samples (Figure 2.4-10).

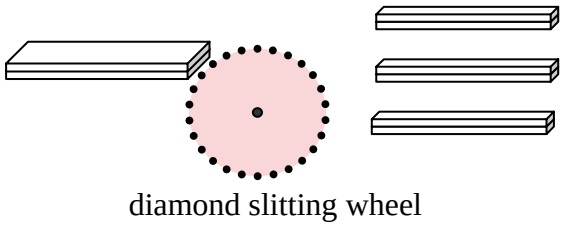

Figure 2.4-10 : sample preparation for DCB test

The adhesion test we used was the so called DCB test which relies on a mechanical model to calculate the fracture toughness G_c *(*see section 1.2.4*)*, from a measurement of crack length *a*. The length of the crack was measured with a video camera, monitoring the evolution of the assembly from the side (Figure 2.4-11). The DCB test was carried out at fixed crack opening of 0.32 mm and at a constant crack velocity of 0.5 mm/min. The test was carried out at room temperature for PBT, 15PB and 35PB assemblies and respectively at 15°C and 10°C for 45PB and PBI.

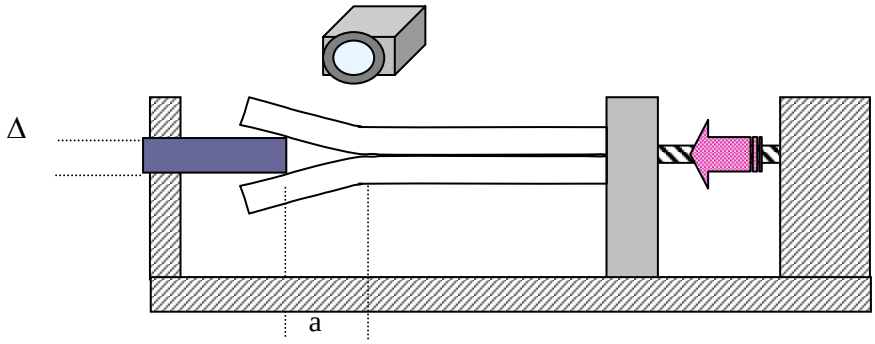

Figure 2.4-11: double cantilever beam test

Kanninen[1]'s model (see section 1.2.5) (Equation 1.2-23) has been used to calculate G_c from the dimensions of the assembly and the elastic modulus of the polymers on both sides of the interface i.e. a, Δ, E_1, E_2, h_1, h_2, α_1 *and* α_2 respectively, the length of the crack, the opening displacement, the Young's modulus, the thickness of each arm, and the correction factors of the model. More details on this model can be found in chapter 1.

The crack length a was measured from the acquired image of the video, at least 20 times during the progressive advance of the razor blade imposing the opening displacement. From the examination of the images, it was possible to remove some data points where clearly a macroscopic defect appeared and pinned the crack. The mean value and the standard deviation were calculated from all the remaining data points (about 2x3x20 values).

2.4.2.2 Measurements of the Young's modulus

We measured the Young's modulus with a three point bending test on one of the two beams of the assembly which had been separated during the DCB test. We used a dynamic mechanical analyser (DMA Q800, TA instruments) to carry out those experiments (Figure 3.1-12).

The following equation was used to calculate the stress and the strain (equation 2.4-1 and 2.4-2) :

[1] Kanninen, M. F. International Journal of Fracture, 9: 83-92, (1973).

$$\sigma_x = \frac{P \cdot L \cdot t}{4 \cdot I} = \frac{3 \cdot P \cdot L}{w \cdot t^2}$$

$$\varepsilon_x = \frac{6 \cdot \delta \cdot t}{2 \cdot L^2 \cdot \left[1 + \frac{6}{10} \cdot (1 + \nu) \cdot \left(\frac{t}{L}\right)^2\right]}$$

σ_x = stress
ε_x = strain
P = applied force
δ = amplitude of deformation
L = 1/2 sample length (span)
t = sample thickness
w = sample width
ν = Poisson's ratio
I = moment of inertia $I = \frac{w \cdot t^3}{12}$

Eq. 2.4-1
Eq. 2.4-2

The ramp in displacement was set at 0.5 mm/min. Except for a corrective factor which is needed to go from the vertical displacement to the displacement of a wedge, this rate is supposed to be of the order of magnitude of the rate used in the DCB test (0.5 $mm.min^{-1}$). Ten cycles were performed for each sample and no change in the young's Modulus was detected. The strain range was chosen in order to keep the stress below the yield stress of the polymer.

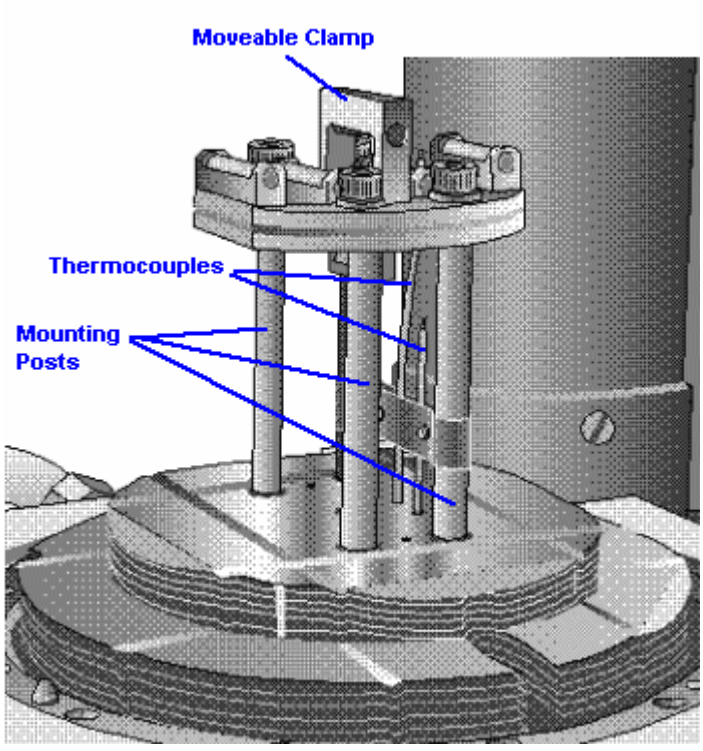

Figure 3.1-12: DMA with the 3-points bending clamp

2.5 Tensile tests

Tensile behavior was studied in the case of the two softer polymers, i.e. 45PB and PBI which can both be obtained in the amorphous state. Tests were carried out on amorphous polymers and on polymers annealed at several temperatures and times of annealing.

2.5.1 Sample preparation

Sheets of 45PB and PBI were molded in a temperature controlled press (Darragon SE 10T) by placing the polymer granules in a window steel mold (50x20x1 mm^3) placed between two smooth stainless steel plates. A polyimide film was added between the polymer and the stainless steel plates to avoid adhesion between the polymer and the plates (see section 2.4.1.1). The molding temperature was fixed at T_{mold} = 180°C. The sample was molded for 10 minutes, then cooled from 180°C to 160°C at 20°C.min^{-1}, and finally quenched in ice water (see section 2.4.1.2 and figure 2.4-4).

The samples were then cut in a bone shape as represented in Figure 3.2-1. After cutting, some samples were annealed at different annealing temperatures T_{ann} and for two different annealing times t_{ann} (10 and 60 minutes).

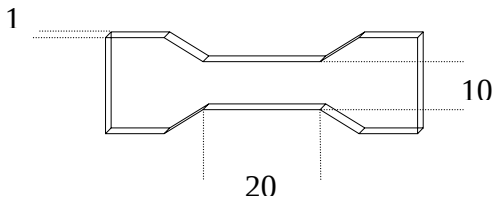

Figure 2.5-1 : sample dimensions for the tensile test, in millimeters.

2.5.2 Tensile test

The tests were carried out on an MTS hydraulic testing machine. The compliance of the machine, tested before our tensile test (0.4 μm.N^{-1}), was found negligible compared with the range of forces and displacements used in our experiments, since the maximum load was 300 N and the final displacement 20 mm. The force sensor has a full scale of 1.5 kN. The displacement rate was set at 0.5 mm.min^{-1}.
The force F and displacement L data were directly obtained from the tensile tester. The nominal stress (σ_N) and the deformation (ε) data were calculated using the initial values of the width w_0, the thickness and the length L_0 (20 mm in our case) of the usable portion of the sample (Equation 2.5-1):

$$\sigma_N = \frac{F}{w_0 e_0} \quad \text{and} \quad \varepsilon = \frac{L - L_0}{L_0} \qquad \text{Eq. 2.5-1}$$

2.6 Study of the crystallinity at the interface

The crystalline morphology of the samples near the interface was studied at two different length scales by optical microscopy and transmission electron microscopy (TEM). Those observations were typically made by selecting a specific region of the assembly which was assumed to be representative of the morphology of the sample.

2.6.1 General procedure for optical and electron microscope observations

In order to carry out optical and TEM observations, thin polymer sections (typically 1 to 5 μm thick for optical and 80 to 100 nm thick for electron microscopy) had to be prepared. To obtain those sections, a precise cutting tool, called microtome, is needed. To use the microtome to cut the slices, the samples have to be specifically prepared to present a 1 mm square face at the end of a pyramid. In order to obtain these samples, two different preparations methods were used : one for the observation of the surface and interface of the assemblies, the other for the observation of the crack tip.
For the surface and interface observations, a parallelepiped of more or less 2x2 mm^2 of cross section was cut from the non damaged part of the assembly with a diamond saw (see paragraph 2.4.2.1). The cube edges were then removed to obtain a block containing the surface or the interface, with a trapezoidal shape at the top in order to get a 1 square mm planar face for sectioning (Figure 2.6-1).

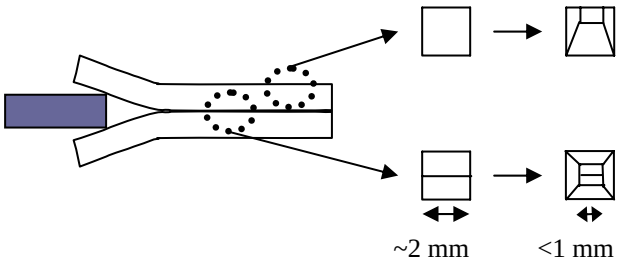

Figure 2.6-1 : sample preparation → surface and interface observations

For the crack tip observations, the assembly was first embedded in a resin to fill the crack tip region (the assembly was taken directly from a DCB test). A mix of 1/5 (percentage by mass) of hardener (HY 956) and 4/5 of epoxy resin (Araldite D) was used. The mix was degassed in vacuum for half an hour, then poured on the assembly. The transformation of the embedded DCB sample into a trapezoidal block containing the crack tip and suitable for microtome cutting, was made as reported in the previous paragraph at least 24 hours after the embedding step in the epoxy (Figure 2.6-2).

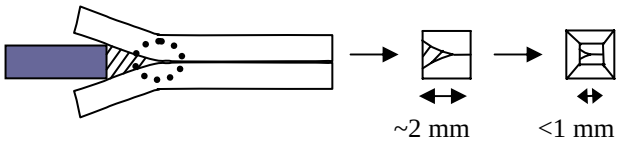

Figure 2.6-2 : sample preparation → crack tip observations

2.6.2 Optical observations

2.6.2.1 Microtoming the sample

A Reichert-Jung Ultracut microtome equipped with a glass knife was used to make the 3 μm thick sections (Figure 2.6-3). The polymer block with its trapezoidal top was firmly gripped in the microtome arm. Before cutting a precise alignment between the 1 mm square face and the knife edge was made. Sections were collected with tweezers and put on a microscope slide. A drop of immersion oil (n_D = 1.515) from Cargille was positioned on the section and everything was then covered with a microscope cover glass.

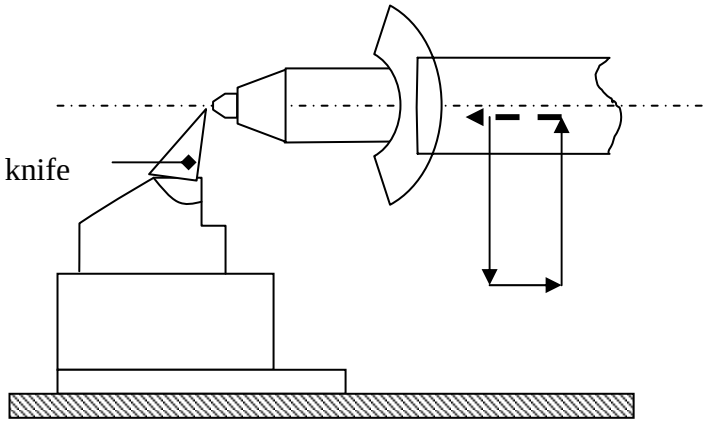

Figure 2.6-3:polymer block with its pyramidal shape mounted on the microtome arm
The microtome arm is moved backwards from the knife edge during the return stroke.

2.6.2.2 Observation in polarized light microscopy

Polarized light microscopy is a useful tool for morphological observations of semicrystalline polymers. It can distinguish between isotropic and anisotropic (birefringent) materials. The technique exploits optical anisotropic properties to reveal detailed informations about the structure and composition of the materials.
We used an Olympus OM2 optical microscope with a Nikon camera to take micrographs.

2.6.3 Observation in transmission electron microscopy

the TEM observations were performed in the Laboratoire de Technologie des Composites et Polymères (EPFL, Lausanne) with the help and the expertise of Christopher Plummer on polymer observations with electron microscopy (Plummer et al.[2], 1998 and Plummer and Kausch[3], 1996).

2.6.3.1 Sample preparation for TEM

The TEM is a very useful instrument to reveal the microstructure of heterogeneous materials at a high level of resolution. However, for polymeric materials, which are typically only composed of C, O and H , it is important to obtain a sufficient mass contrast among the different phases of the structure. Staining with heavy elements is a good method to increase the electron contrast between the crystalline and the amorphous phase. In this study, we stained our sample with Ruthenium tetroxyde RuO_4, which gave good results according to previous studies on POM (Li et al.[4], 1996), PET (Haubruge et al.[5], 2003), PP(Li and Cheung[6], 1999) and PBT (Janik et al.[7], 1992). Staining methods are designed to produce a differential absorption of the staining agent in the different phases to be observed. Such a differential absorption is not always easy to predict ab initio and as a result, many staining techniques are the result of empirical optimization.

A ruthenium tetroxide solution was prepared in situ, following the procedure proposed by Montezinos et al.[8]. The tetroxide was prepared through a reaction between ruthenium (III) trichloride hydrate from Fluka and aqueous sodium hypochlorite (NaOCl) from Fluka. The dark red fresh mixture was used immediately as it deteriorates with time.
Before staining the trapezoidal top prepared samples (see paragraph 2.6.1) were trimmed with an ultramicrotome (Reichert-Jung) equipped with a Diatome 35° diamond knife. An extremely smooth trapezoidal top was obtained with the cross section of the polymer strip parallel to the top surface.

We tried three different staining procedures in order to optimize the contrast. In the first experimental procedure, the sample block was soaked in the staining solution for 24 hours, then washed in a 3% aqueous solution of sodium hydrogen sulphate and finally in distilled water. The cutting was performed at room temperature at 1mm/sec and the sections were picked up from distilled water. The very first sections were discarded, but after a few cuts, it was possible to obtain ultrathin sections (between 80 and 100 nm

[2]Plummer, C. J. G., Kausch, H. H., Creton, C., Kalb, F. and Léger, L. Macromolecules, 31(18): 6164-6176, (1998)
[3]Plummer, C. J. G. and Kausch, H. H. Macromolecular Chemistry and Physics, 197(6): 2047-2063, (1996).
[4]Li, J. X. and Cheung, W. L. Journal of Applied Polymer Science, 72: 1529-1538, (1999).
[5]Haubruge, H. G., Jonas, A. M. and Legras, R. Polymer, 44: 3229-3234, (2003).
[6]Li, J. X., Ness, J. N. and Cheung, W. L. Journal of Applied Polymer Science, 59: 1733-1740, (1996).
[7]Janik, H., Walch, E. and Gaymans, R. J. Polymer, 33(16): 3522-3524, (1992).
[8]Montezinos, D., Wells, B. G. and Burns, J. L. Journal of Polymer Science, Polymer Letters Edition, 23: 421-425, (1985)

thick). Those very thin sections were recovered by a wire loop and put on a copper grid covered with a thin carbon film for the TEM observations (Figure2.6-4)
In a second procedure, the block was stained in vapors at 40°C.
The third procedure, consisted in sectioning the non stained sample block, then staining the section in vapors of RuO_4 at room temperature for 24 hours.
The first and the third procedure gave the best staining results in terms of contrast and less damage.

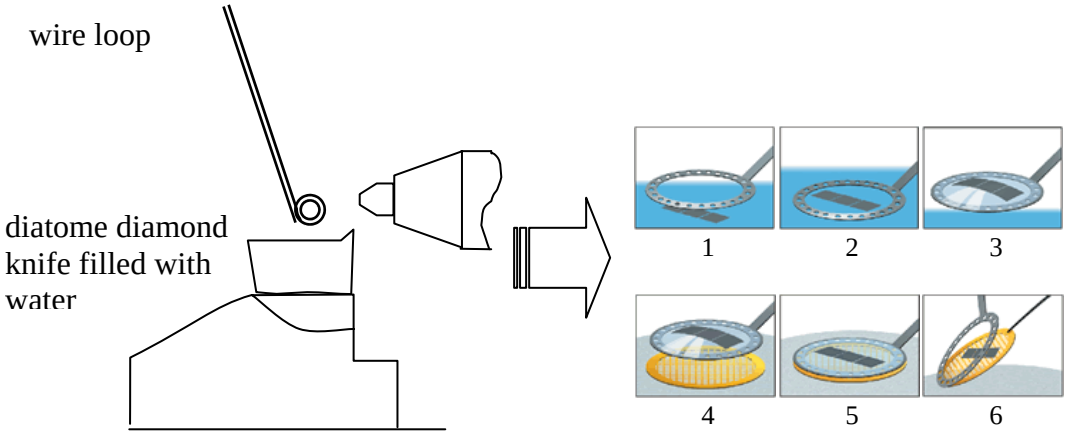

Figure 2.6-4:Ultramicrotome equipped with a diatome diamond knife.
Procedure to recover the ultra thin sections :

1. *Center the loop above the sections*
2. *2. Slowly lower the loop over the sections and touch the water*
3. *Gently lift up the loop with the sections in a droplet of water*
4. *Lower the loop onto a grid placed onto a filter paper*
5. *water is removed*
6. *Separate the grid from the loop with an eyelash*

2.6.3.2 Transmission electron microscope observations

The TEM observations have been carried out with Christopher Plummer. We used a Philips EM 430 microscope with a 300kV acceleration voltage and a magnification from 10^4 to 2.10^4.

Chapter 3

Results

126

Table of contents

In this chapter, the main experimental results of the thesis are presented in detail. As discussed in the introduction, the focus of the work is the investigation of the experimental conditions necessary to obtain a measurable self adhesion between semi-crystalline polymers, when they are put in contact at a temperature lower than the melting point of the crystalline phase. In order to reach this goal in a systematic way we needed, first to work with a system where the degree of crystallinity and the kinetics of crystallization could be varied, and second to develop experimental techniques to form the bond in a controlled and reproducible way and characterize the level of adhesion and the crystalline morphology as a function of the material and processing parameters.

The technique to measure self-adhesion we used is the well-known double cantilever test, which has been widely used to evaluate the fracture toughness of polymer-polymer interfaces. In order to get a better understanding of the role of the crystallinity in the case of self adhesion below the melting point, the recrystallization kinetics and the melting behaviour were also studied with the Temperature Modulated DSC. The morphology near the interfaces was observed by optical or electron transmission microscopy. Whenever it is relevant, these results will be presented and compared with the adhesion results.

For the sake of clarity, the results are presented by types of materials. As discussed in chapter 2, the characterisation of the different copolymers leads naturally to a classification in three groups in terms of their crystallinity, recrystallisation kinetics and melting behaviour. The relative homogeneity in properties within these groups makes the adhesion results easier to compare. In a final section, the entire set of results will be compared. Hence, results on PBT and 15PB are first described, followed by results on 35PB and 45PB, then the results on pure polybutylene isophthalate (PBI). The reasons for this separation stem mainly from the kinetics of crystallization: PBT and 15PB crystallize fast and even at the faster cooling rate experimentally available, samples at room temperature are highly crystalline. Our tests of self-adhesion will therefore only take place between crystalline samples. On the other hand 35 PB, 45PB and PBI crystallize increasingly slowly, making it possible, depending on the cooling conditions to obtain nearly amorphous samples or fully crystalline samples. All three of these samples can cold-crystallize, meaning that crystallization can occur during the heating phase of the preparation of the assemblies. In the case of 45PB and PBI, it is even possible to get amorphous samples after molding and before assembling. 35PB could be obtained in amorphous state but not in a reproducible manner because of the still relatively high crystallization kinetics. Detailed results of self-adhesion between amorphous, but crystallizable samples will be shown for the 45PB and PBI copolymers.

3.1 PBT and 15PB

In terms of crystallinity, crystallisation kinetics and mechanical properties, the behaviour of PBT and 15PB is quite similar as was shown by the characterization presented in Chapter 2 (DSC, WAXS, DMA and other mechanical results). PBT and 15PB have a relatively high degree of crystallinity if compared to the other copolymers (from 25 to 35 %) and a fast crystallisation kinetics. We have not been able to obtain amorphous samples by changing the cooling rate of melted samples. The crystallization during cooling is clearly visible in a standard DSC run (sample annealed at high temperature to erase the thermal history then cooled at 5°C.min^{-1} and heated again at 5°C.min^{-1}). We now present the results obtained for polymer-polymer adhesion along with the results on the bulk degree of crystallinity (obtained by the TM-DSC technique) and the characterizations of the crystalline morphology at the interface as observed by optical and electron microscopy.

3.1.1 Adhesion measurements

The assemblies were formed at different temperatures of contact. We started with an interface temperature corresponding to the melting point T_m or slightly above, down to a temperature where adhesion became null.
After a certain time of preheating t_{ph}, a contact time $t_{contact}$ of 10 minutes was applied to the two PBT plates, while two contact times of 10 and 30 minutes respectively were tested for the 15PB material. The contact pressure was held constant at $P_{contact}$ = 200 bars. For each temperature of contact and time of contact, two assemblies were made. Each assembly was then cut in tree parts as described in section 2.4.2.1. Table 3.1-1 summarises the experimental conditions and recalls the different characteristics of the polymers which are relevant for the molding and assembling processes (see characterisation in Chapter 2 and section 2.3.1 for the melting temperature obtained in the standard procedure from a polymer granule).

Tableau 3.1-1 : experimental conditions of the formation of assemblies, and polymer characteristics

polymer	T_{mold} (°C)	Cooling molding (°C.min^{-1})	T_g *(°C)*	T_m *(°C)*	t_{ph} (min)	$P_{contact}$ (bars)	$t_{contact}$ (min)	Cooling assembling (°C/min)
PBT	240	2.5	*40*	*225*	50	200	10	40
15PB	220	2.5	*32*	*201*	50	200	10, 30	40

Figure 3.1-1 represents the fracture toughness G_c, calculated with Kanninen's model (see section 1.2.5), as a function of temperature of contact, for a constant contact time, equal to 10 minutes.

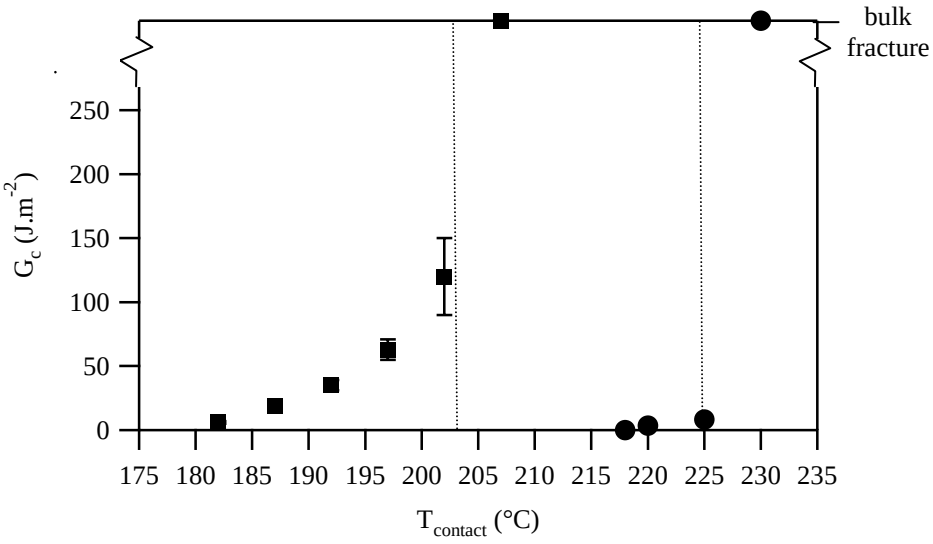

Figure 3.1-1: fracture toughness after 10 minutes of contact : ✸PBT ■15PB. The dashed lines represent T_m for 15PB (203°C) and PBT (225°C)

Very strong adhesion is obtained for both PBT and 15PB for a contact temperature above their melting temperature, i.e. at 207°C for 15PB and 230°C for PBT. Here the crack no longer propagates along the interface between the two plates but deviates, leading to a bulk fracture. When the temperature of contact is lowered, the two polymers have a different behaviour : for PBT, adhesion drops when the temperature of contact becomes smaller than the melting temperature, while the decrease for 15PB is more progressive. In other words, polymer-polymer adhesion for PBT depends strongly on the distance to T_m, while a significant polymer-polymer adhesion is observed for joining temperatures below T_m for 15PB. It should be noted however that when the temperature is lower than T_m - 15°C, the fracture toughness becomes very low although the contact is still established well above the glass transition temperature of the polymers.

Figure 3.1-2 shows the influence of contact time between 10 and 30 minutes on fracture toughness. Below T_m, the same self-adhesion is obtained after 10 or 30 minutes of contact, while in the vicinity of T_m, the level of self-adhesion increases between 10 and 30 minutes. However, the two error bars overlap each other in this case.

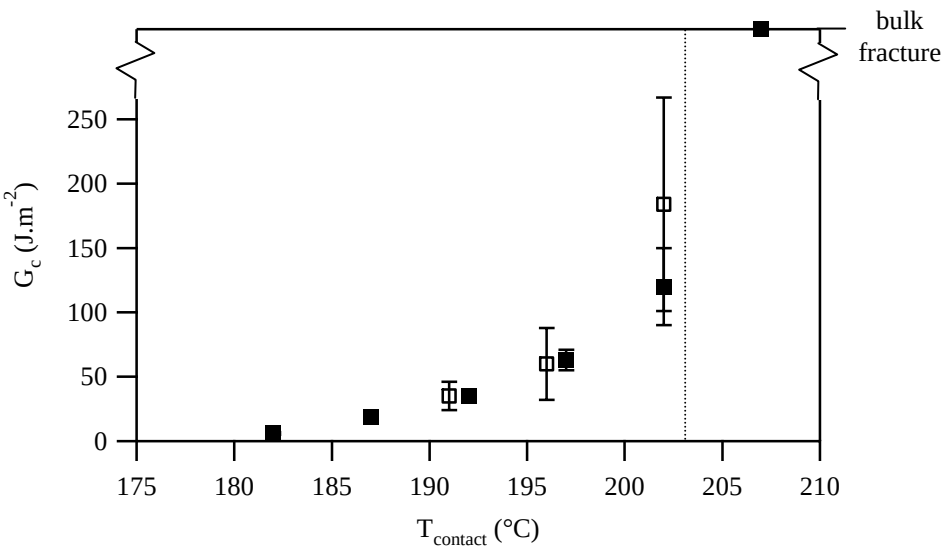

Figure 3.1-2: fracture toughness for 15PB after 10 minutes contact (full symbol) and 30 minutes (open symbol)

In this temperature range, close to the melting peak in DSC, local melting and recrystallization play a significant role. A study of the crystallinity and melting/recrystallisation behaviours is carried out in the next section with the Temperature Modulated DSC technique (TMDSC).

3.1.2 DSC results

For the results presented in section 2.3.1, a TMDSC scan had been performed on granules using a classical procedure where the previous thermal history of the sample was erased by annealing at high temperature (well above T_m, i.e. 260°C in the case of PBT and 15PB). In the following series of experiments, our purpose was different : we wanted to characterize the bulk crystallinity of the polymer after molding and before contact. We had therefore to reproduce exactly the thermal history of the molding conditions.

The complete procedure was the following: A polymer plate was molded according to the molding experimental procedure (see section 2.4). After cooling at 2.5°C.min^{-1} to room temperature, a small part (typically 5-10 mg) of polymer was taken from the plate, a few millimetres from the edge of the plate to avoid artefacts, and directly placed in the DSC pan. (The ablation of the DSC sample from the plate was made with a razor blade to obtain a flat surface which gave a large surface for the thermal conduction inside the DSC pan). A single 5°C.min^{-1} heating ramp was then imposed (more detail on DSC can be found in section 2.3.1).

In Figure 3.1-3 and 3.1-4, a comparative view of the total heat flows for the two procedures (i.e. the characterization procedure carried out on granules annealed at 260°C

and the procedure followed for the molded polymer) is given. Similar results were found for the two procedures.

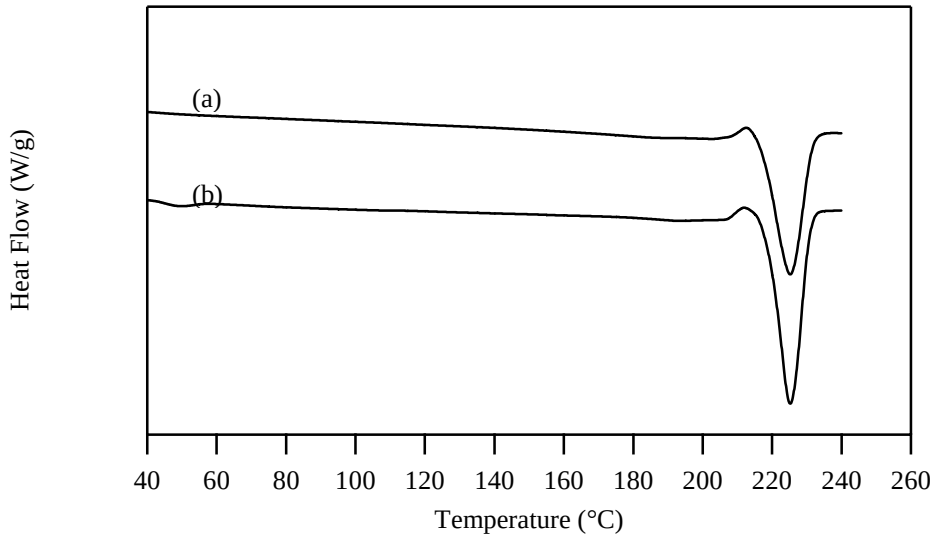

Figure 3.1-3: Total heat flows as a function of temperature for PBT scanned at 5°C/min, (a) standard procedure (polymer granule heated at 260°C and cooled at 5°C/min before scanning, (b) from a polymer plate molded at 240°C, cooled at 2.5°C/min.

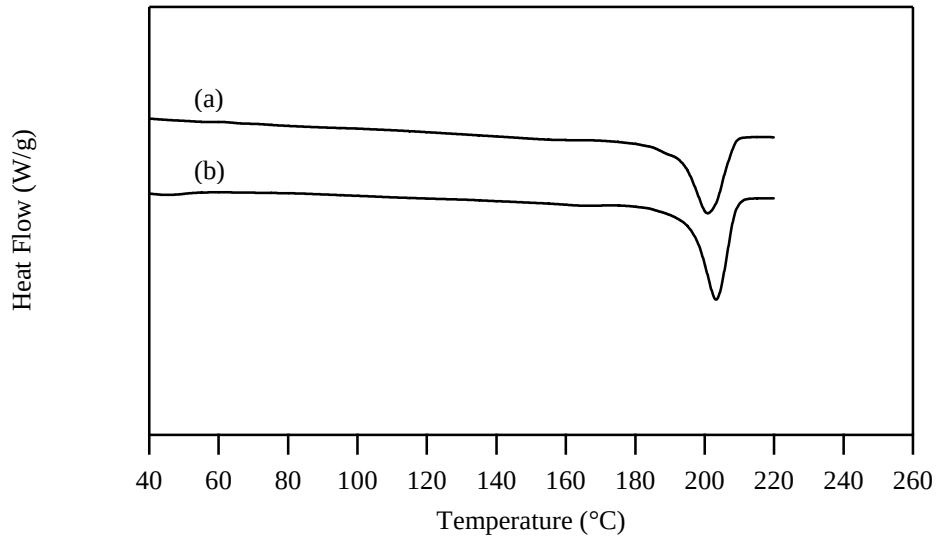

Figure 3.1-4: Total heat flows as a function of temperature for 15PB scanned at 5°C/min, (a) standard procedure (polymer granule heated at 260°C and cooled at 5°C/min before scanning, (b) from a polymer plate molded at 220°C, cooled at 2.5°C/min.

In table 3.1-2, the melting temperature and the heat of fusion are given in each case. The degree of crystallinity has been calculated from equation 2.3-4 in section 2.3.1. The heat of fusion of a pure crystal of PBT is, according to Illers[1] (1980) : ΔH_m^0 = 140 $J.g^{-1}$. According to the WAXS results given in section 2.3.3 the crystal morphology of 15PB and PBT was found very similar (only very small shifts for some peaks in the WAXS spectra). Hence the same value of ΔH_m^0 was assumed for 15PB.

The heat of fusion was calculated by integrating the peak from T_s. This temperature corresponds to the onset of the fusion process and was obtained with the help of the reversible and non-reversible flow curves (see Figures 3.1-5 and 3.1-6).

Table 3.1-2

Polymer	Type	Thermal history	T_s	T_m	ΔH_m	χ_c
PBT	Granule	260°C ↘ 5°C/min	183	225	44	31
PBT	**Molded plate**	**240°C ↘ 2.5°C/min**	**189**	**225**	**52**	**37**
15PB	Granule	260°C ↘ 5°C/min	152	201	34	24
15PB	**Molded plate**	**220°C ↘ 2.5°C/min**	**163**	**203**	**36**	**26**

In conclusion, after the molding procedure, the overall degree of crystallinity is larger for both polymers, which is in agreement with the cooling rates. In the case of the molding procedure, more time is given to the polymer to crystallise from the melt. Nevertheless, the shape of the curves remains similar and the melting point does not change

More details on the TM-DSC results in the case of the molded plate are given in Figure 3.1-5 and 3.1-6, where the reversing and nonreversing flows are shown. Each graph shows three different heat flows : the total heat flow, the reversible heat flow and the nonreversing heat flow. The total heat flow exhibits a small exothermic peak in the case of PBT, which is very apparent in the nonreversing flow curve. This peak does not appear in the total heat flow of 15PB but is present in the non-reversible flow curve. Nevertheless the exothermic peak in the nonreversing flow of 15PB is far less pronounced than the one of PBT. The irreversible processes such as recrystallization or reorganisation, which usually appear in the nonreversing heat flow, are more obvious in the case of PBT. The reversing flow shows in both cases the classical double melting behaviour of PBT with the two endothermic peaks. This behaviour can be compared with results obtained by Righetti and Munari[2] on linear and branched PBT, which point out the double melting behaviour of PBT. The authors get multiple endotherms, which suggest a primary fusion of the less perfect crystallites followed by the melting of more perfect material. The difference in our experiment is a slower heating rate (5°C.min^{-1} instead of 10°C.min^{-1}) and the use of the temperature modulation. According to Schawe[3], the total heat flow in a temperature modulated experiment is approximately equal to the heat flow

[1]Illers, K. Colloid and Polymer Science, **258**(2): 117-124, (1980).
[2]Righetti, M. C. and Munari, A. Macromolecular Chemistry and Physics, 198: 363-378, (1997).
[3]Schawe, J. E. K. Thermochimica Acta, 260: 1-16, (1995).

in a conventional DSC. A possible interpretation of the exothermic peak is the presence of a melt-recrystallization process : the fusion of the less perfect crystallites allows a recrystallization into thicker crystal, eventually melted at higher temperature. The presence of this exothermic peak is clear in the work of Yasuniwa et al.[4]

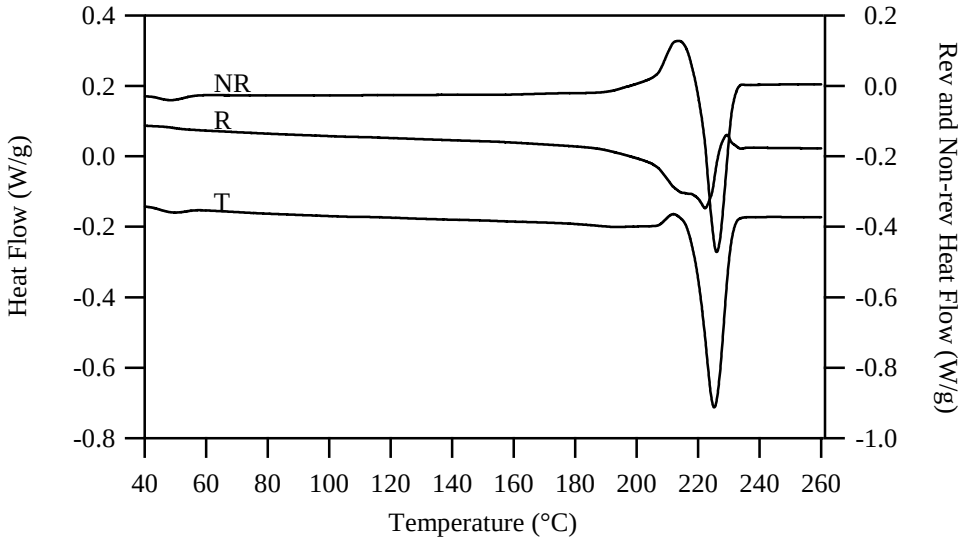

Figure 3.1-5 : MDSC results for PBT scanned at 5°C.min^{-1}, with oscillations of ± 0.796°C every 60s (Heat Only). Total (T), Reversing (R) and non-reversing heat flows vs. temperature.

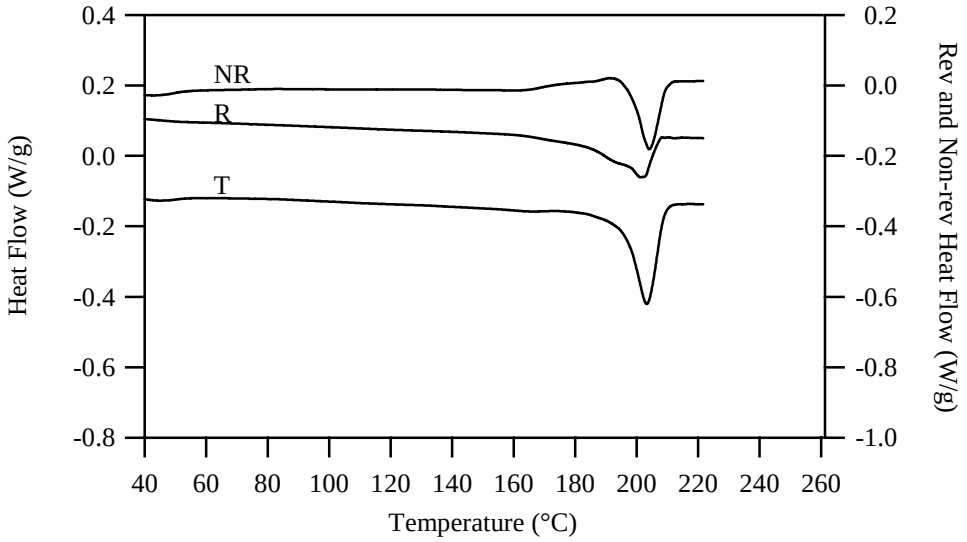

Figure 3.1-6 : MDSC results for 15PB scanned at 5°C.min^{-1}, with oscillations of ± 0.796°C every 60 s (Heat Only). Total (T), Reversing (R) and nonreversing heat flows vs. temperature.

[4]Yasuniwa, M., Tsubakihara, S., Ohoshita, K. and Tokudome, S. Journal ofPolymer Science: Part B, 39: 2005-2015, (2001)

3.1.3 Microstructure

3.1.3.1 Optical observations

The microstructure at the interface was studied with optical microscopy and transmission electron microscopy. The sample preparation in both cases can be found in section 2.6. The following pictures have been done under polarised light. The thickness of the microtome slices was 3μm. Observation of a PBT section in Figure 3.1-7 shows mainly two different structures. A spherulite structure is observed in all the micrographs with spherulites of 50-100 μm in diameter, and in some pictures, we notice a transcrystalline zone at the surface or at the interface. It is hard to see any difference between the transcrystalline zone of the reference section (from a non assembled sample), and the surface and the interface of the assembled samples at 220°C and 225°C. According to this observation, at the microscopic scale, nothing major happened during assembling at 220°C and 225°C in terms of crystalline morphology. The micrograph of the sample assembled at 230°C shows a completely different pattern. Here, no transcrystalline zone can be seen and the interface is hard to detect. The spherulites appear less distinct than in other pictures, as if the spherulite structure seen in the sample assembled at 220 °C had melted and imperfectly recrystallized during the rapid cooling after assembling (40°C/min, see section 2.4.1.4).

In the case of 15PB, we also observed a transcrystalline zone for a contact below T_m (Figure 3.1-8, a and b) for 10 and 30 minutes of contact. For a contact at 202°C, which is roughly the melting temperature, no transcrystalline zone was observed at the interface. The spherulites seem to cross the interface. For a contact above T_m, the structure is different, similar to the structure observed above T_m for PBT. At this temperature of contact, the melting is significant, and the spherulites do not have enough time to grow in a proper way during the rapid cooling after assembling. We can notice a very bright line at the interface, which may due to the formation of a very small transcrystalline zone during cooling.

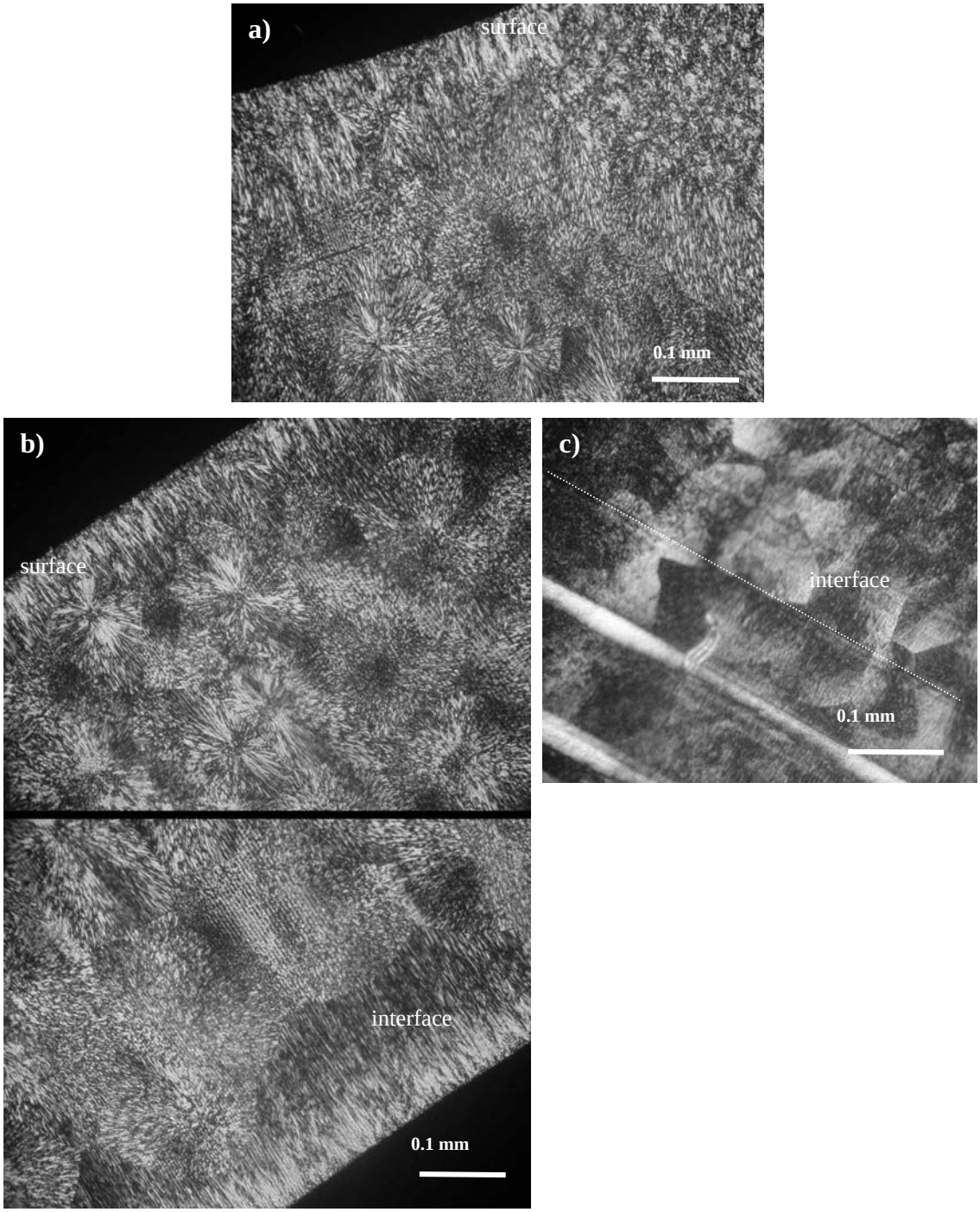

Figure 3.1-7: Optical micrographs of PBT (3 µm thick sections) under polarised light. a) reference sample : surface of a molded plate ,b) surface and interface of a PBT assembly at 220°C during 10 min and c) interface of a PBT assembly made at 230°C during 10 min.

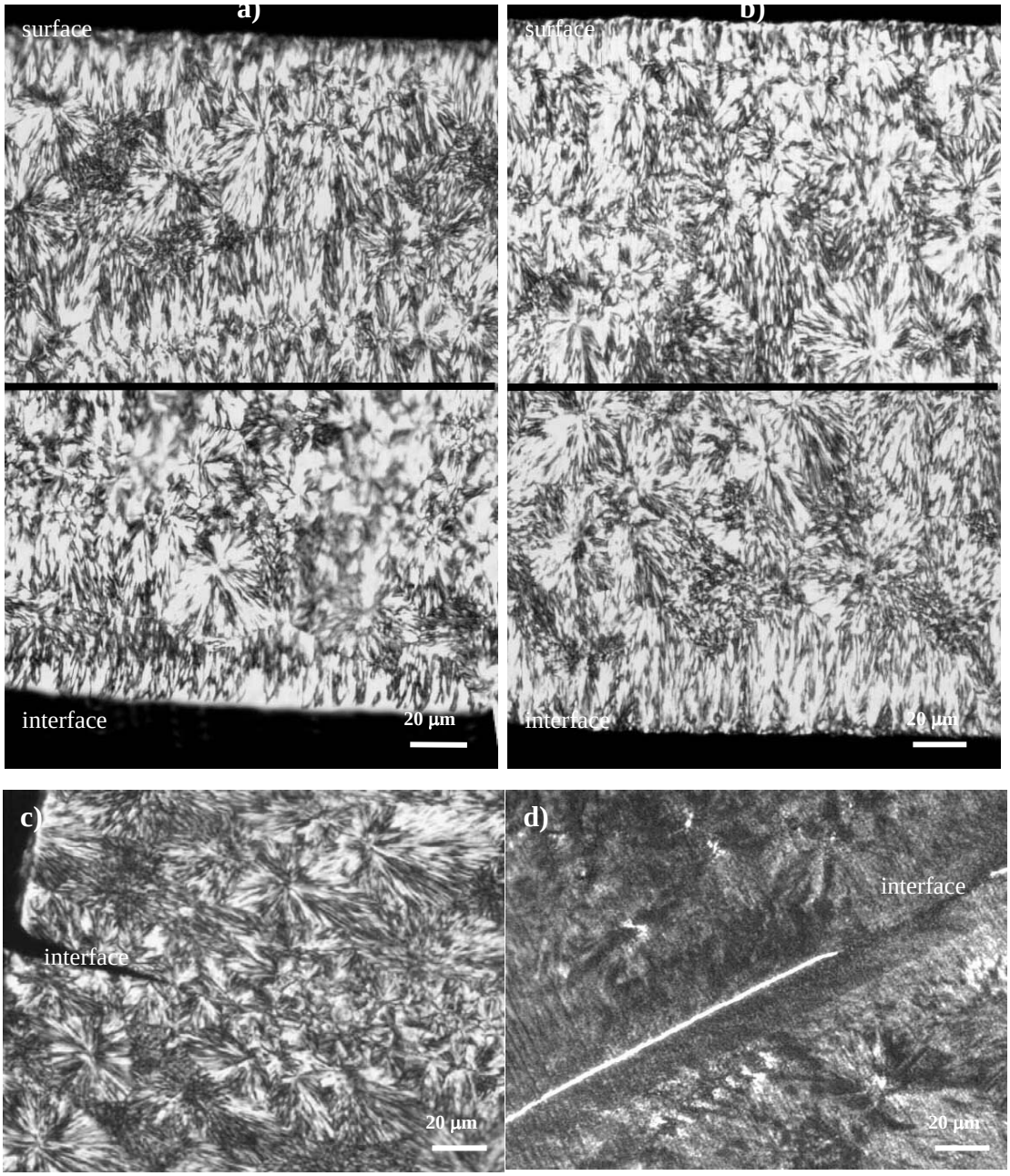

Figure 3.1-8: Optical micrographs of 15PB (3 µm thick sections) under polarised light. a) surface and interface of 15PB assembled at 197°C during 10 min, b) surface and interface of 15PB assembled at 197°C during 30 min, c) interface of 15PB assembled at 202°C during 30 min, d) interface of 15PB assembled at 207°C during 30 min.

3.1.3.2 TEM observations

TEM observations were carried out on a 15PB sample near the crack tip by preparing the sample with the procedure described in section 2.6. The assembly chosen for the TEM observations had a medium fracture toughness and the assembling conditions were : a temperature of contact of 197°C and a time of contact of 10 minutes. An optical observation is shown on the left side of Figure 3.1-9. No plastic zone can be distinguished near the crack tip. The transcrystalline zone described in the previous paragraph is seen at the interface. The right side of Figure 3.1-9 shows the TEM micrograph. The lamellas are clearly visible and have a thickness of 9±1 nm which is in good agreement with previous studies (Liu and Geil[5], 1997). We focused on two zones, one after the crack has passed in a , near the previous interface, and the other just before the crack has advanced in b, across the interface. Despite the high level of local strain near the previous interface, lamellas are visible. However, it is hard to see any particular structure since this zone is quite damaged. The general direction of the lamellas is perpendicular to the previous interface as if they were going through the interface before the crack propagated. Figure b confirms that some lamellas cross the interface (white arrow). Contrary to the optical observations where nothing revealed the level of adhesion in terms of crystalline structure since the surface and the interface looked the same, electron microscopy shows lamella going trough the interface.

[5] Liu, J. and Geil, P. H. Journal of macromolecular Science - Physics, B36(2): 263-280, (1997).

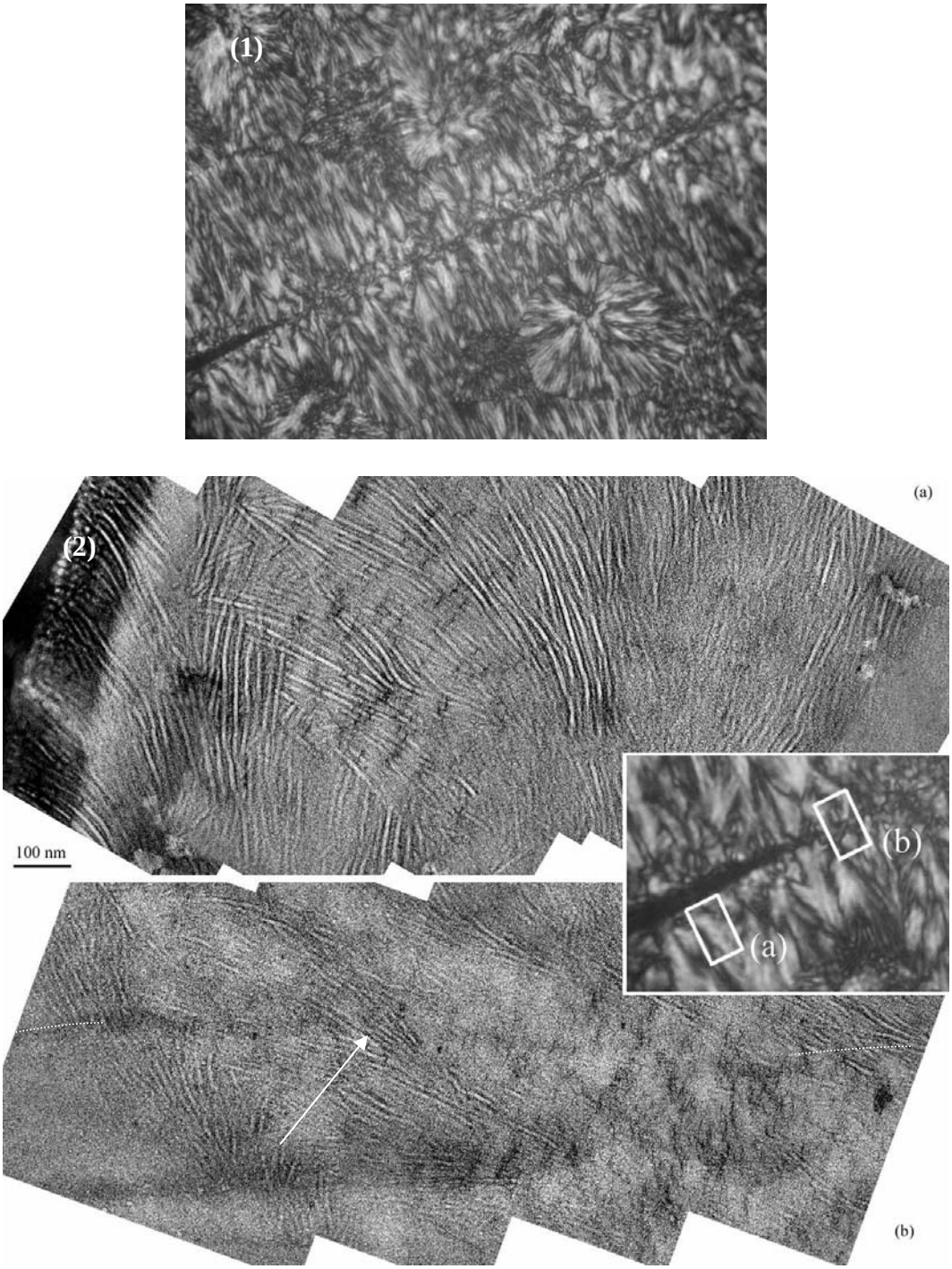

Figure 3.1-9: Optical (1) and TEM (2) observation of 15PB assembled at 197°C during 10 min, crack tip area.

3.1.4 Simultaneous analysis of the different techniques

In Figures 3.1-10 and 3.1-11 the adhesion measurements and the TM-DSC results on the molded plates are shown together with the optical micrographs. For contact temperatures above the melting point, i.e. above the maximum of the melting peak on the total heat flow, both PBT and 15PB develop a strong self-adhesion. The micrographs associated with strong adhesion differ from the other micrographs. For both PBT and 15PB, the transcrystalline zone observed at lower temperatures of contact is no longer present. This change in the microstructure is due to the melting of the spherulites observed in the micrographs of the samples put in contact below T_m. At this temperature (230°C for PBT and 207°C for 15PB) we are indeed well above the maximum of the melting peak of the DSC curve. On the other hand, for a contact T in the vicinity, but lower than the melting temperature (225 for PBT and 202°C for 15PB), a very weak adhesion is obtained for PBT, while 15PB exhibits a reasonably good adhesion. The micrographs show different structures at the interface between PBT and 15PB. For PBT, the structure looks like the one at a lower temperatures of contact, with a transcrystalline zone. For 15PB, we see spherulites going through the interface. This may explain the good adhesion obtained at this temperature of contact for 15PB. But for yet lower temperatures of contact in the case of 15PB the adhesion is still acceptable (at 197°C) while a transcrystalline zone is now seen on the micrographs.

If we now analyze the TM-DSC curves, for PBT and 15PB, the initial fusion (T_s) starts at a temperature where adhesion is null (189°C for PBT and 161°C for 15PB). In the case of PBT, the adhesion remains very weak until the temperature of contact becomes higher than the maximum of the total heat flow peak, whilst adhesion increases continuously in the case of 15PB.

Of course, the DSC curve gives the response of the bulk, while adhesion is sensitive to what occurs at the interface. We can just say that the melting-recrystallization process is more pronounced in the case of PBT if one look to the nonreversing curve. This may reduce the mobility at the interface.

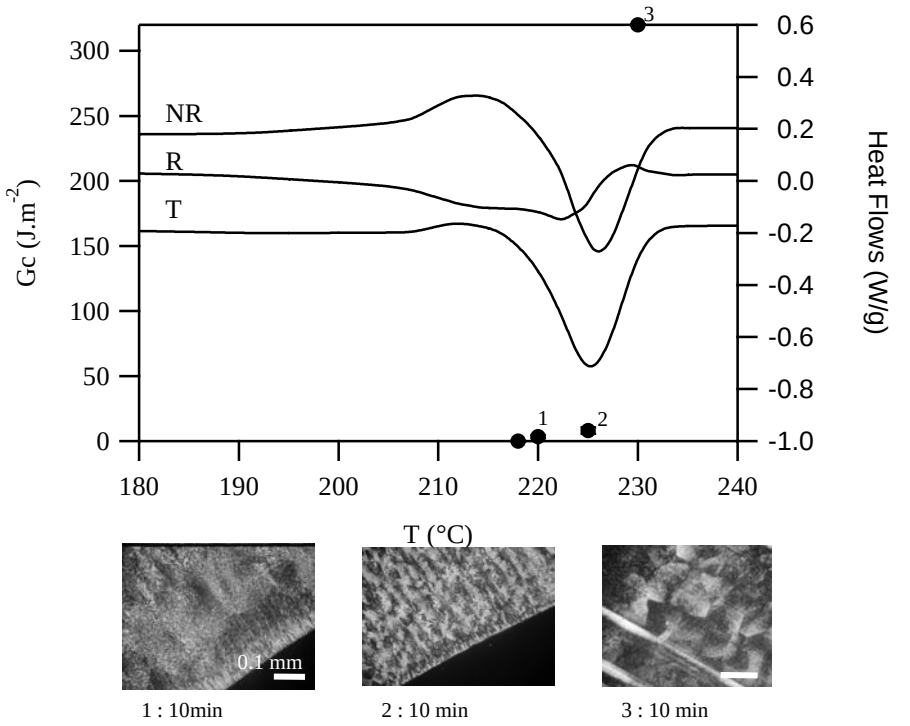

Figure 3.1-10: Adhesion, TM-DSC and optical micrographs (previously presented in section 3.1.3.1) for PBT

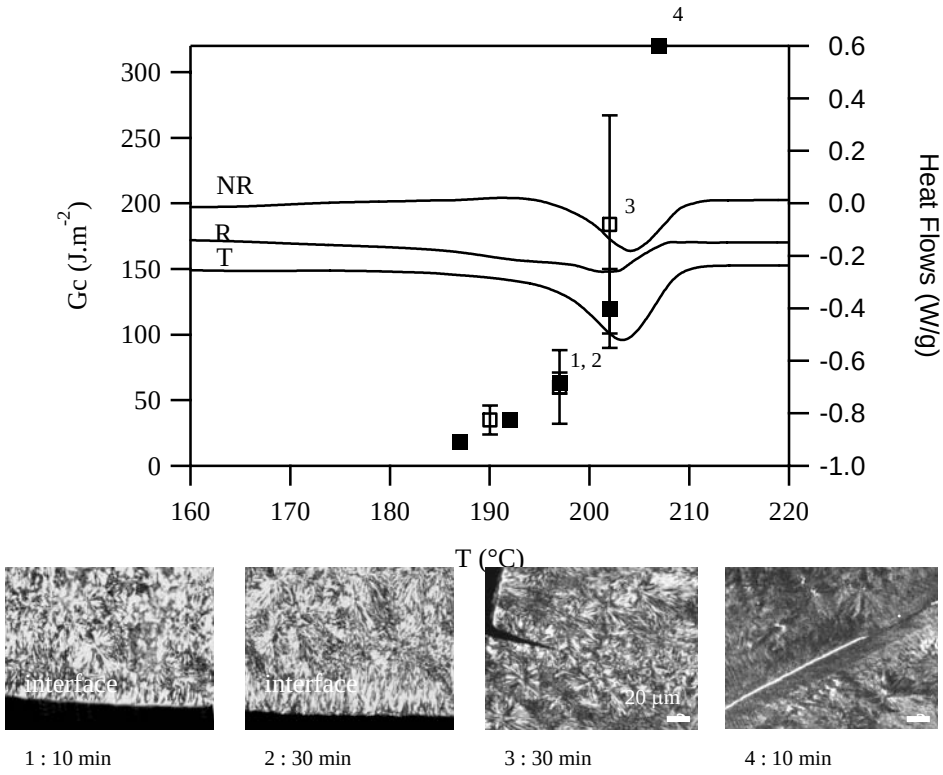

Figure 3.1-11: Adhesion, TM-DSC and optical micrograph (previously presented in section 3.1.3.1) for 15PB

3.1.5 Partial conclusions

Polymer self-adhesion was found strong just above the melting temperature and null for contact 20°C below T_m, for both polymers. In the case of PBT, the adhesion decreases sharply when the temperature of contact goes below the melting temperature, whilst there is a more progressive decrease in the case of 15PB down to a temperature of contact of T_m-15°C. The temperature modulated DSC reveals that non-reversible recrystallization effects upon heating are much more present in the case of PBT. This could be a reason for the very low adhesion for contact T below Tm obtained for PBT. The micrographs provide also some clues for interpretation, as the transcrystalline zone which is seen at the surface and at the interface in the case of contact below T_m, disappears for contact T above T_m. This large scale melting results in a strong adhesion. In the case of weaker adhesion, the electron microscopy has been of great help since nothing is visible optically, and reveals that lamellas can cross the interface (15PB assembled at 197°C during 10 min).

Next section will now focus on less crystalline copolymers, 35PB and 45PB, with a similar approach (adhesion results, TM-DSC and microscopy).

3.2 35PB and 45PB

35PB and 45PB, which have similar mechanical and structural properties, have both a relatively low degree of crystallinity and slow crystallisation kinetics compared to pure PBT and to 15PB. However, the crystalline structure, as determined by WAXS in section 2.3.3, remains roughly the same between PBT and the three copolymers 15, 35 and 45PB. On the other hand, PBI crystallises in a different structure, with different cell parameters. The presence of the isophthalate monomer in the copolymers 15PB, 35PB and 45PB introduces defects in the crystal structure which influence the degree of crystallinity and the crystallisation kinetics but do not change so much the cell parameters (see Chapter 2).

The main particularities of 35PB and 45PB compared to PBT and 15PB are revealed in the standard DSC characterization (melting well above the melting temperature, cooling at 5°C.min^{-1} and heating at 5°C.min^{-1}). By comparing the different curves, we notice that no crystallisation peak is visible during cooling for 35PB and 45PB contrary to PBT and 15PB, but a peak appears during heating prior to the melting peak (see section 2.3.1). Hence the adhesion results of 35PB and 45PB will be presented together, followed by results on crystallisation studied with the TM-DSC technique. In a final section, adhesion and DSC results will be compared.

3.2.1 Adhesion results

The assembly was made at different temperatures of contact (from T_m down to the temperature where adhesion was found null) and with two different times of contact. These conditions of formation of the samples and the main copolymer properties are summarised in table 3.2-1. The molding and assembling procedure can be found in section 2.4.1. The polymer plates were cooled slowly at 2.5°C.min^{-1} in order to obtain crystalline polymers after the molding step (see section 2.4.1.3).

Table 3.2-1 : experimental conditions and polymer characteristics

polymer	T_{mold} (°C)	Cooling molding (°C/min)	T_g (°C)	T_m (°C)	t_{ph} (min)	P_c (bars)	t_c (min)	Cooling assembling (°C/min)
35PB	180	2.5	27	165	25	50	10/30	40
45PB	180	2.5	26	140	10	50	10/30	40

Figure 3.2-1 shows the fracture toughness after 10 minutes of contact as a function of the temperature of contact for 35PB and 45PB.

For both polymers, a very good adhesion is obtained when the temperature of contact is in the vicinity of T_m and even below T_m, i.e. 160°C for 35PB and 129°C in the case of

45PB. When the temperature of contact is further decreased, the adhesion also decreases for both polymer but in a different manner, since the fracture toughness becomes progressively null within a temperature range of 50°C for 35PB and 30°C for 45PB. The level of adhesion drops faster with contact temperature in the case of 45PB than for 35PB. It must be pointed out that the temperature at which adhesion becomes null is still much higher than the glass transition temperature (about 100°C above T_g).

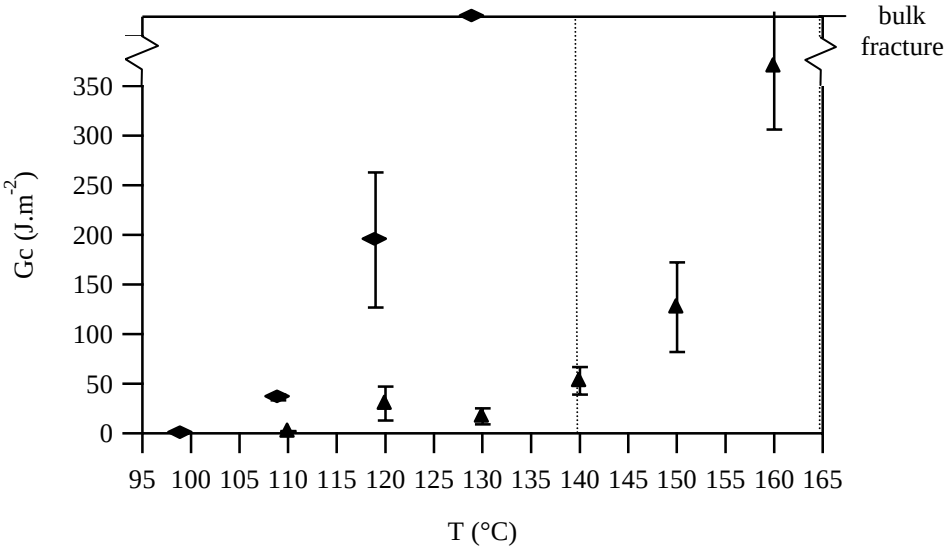

Figure 3.2-1: fracture toughness after 10 minutes contact : ▲35PB ◆45PB. The dashed lines represent T_m for 35PB (164°C) and 45PB (140°C)

Figures 3.2-2 and 3.2-3 show the effect of the contact time (between 10 and 30 min) for respectively 35PB and 45PB. For 35PB, the fracture toughness remains the same for 10 and 30 minutes of contact time and temperatures of contact below T_m, i.e. for 120°C, 130°C and 140°C. At 150°C, the adhesion becomes stronger for 30 minutes of contact. For 45PB at 109°C and 119°C the fracture toughness was found the same after 10 or 30 minutes. It was not possible to observe any difference at 129°C since the adhesion was too high, to allow obtaining quantitative result.

These results imply that for both polymers, the structural rearrangement causing adhesion (interdiffusion, crystallization) occur at relatively short times and are then blocked even at fairly high temperatures of contact (far above T_g). A fully amorphous system would show a marked dependence of adhesion on contact time in this range of temperatures.

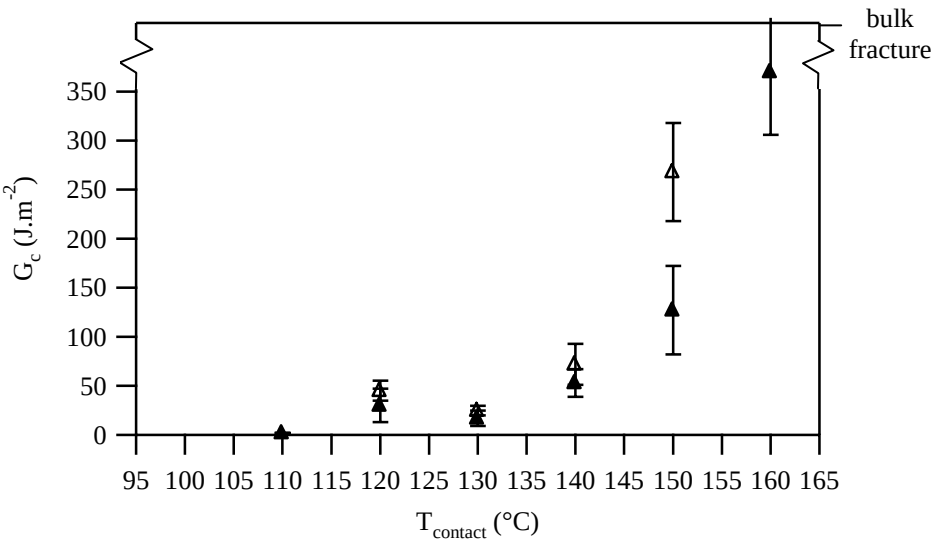

Figure 3.2-2: 35PB fracture toughness as a function of temperature after 10 min of contact (full symbol) and 30 min contact (open symbol).

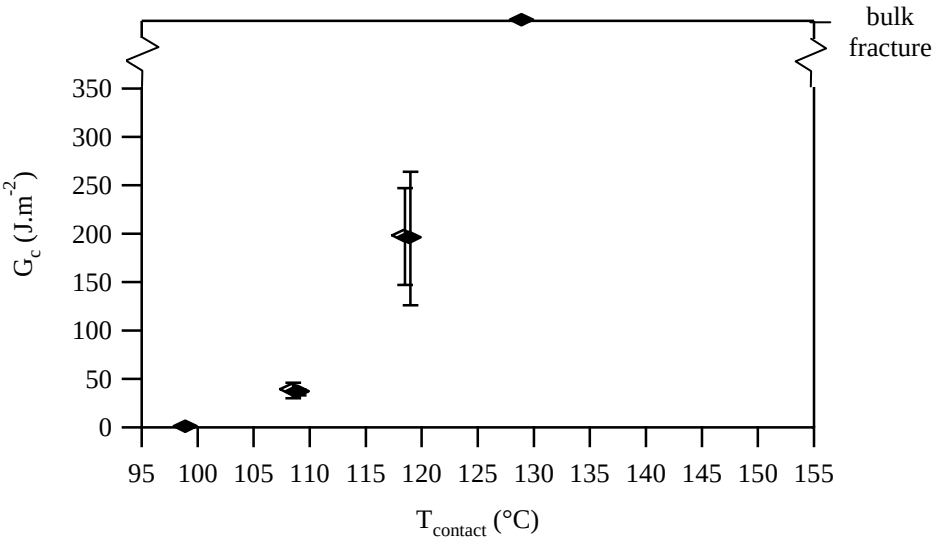

Figure 3.2-3: 45PB fracture toughness as a function of temperature after 10 min of contact (full symbol) and 30 min contact (open symbol).

3.2.2 DSC results

The crystallization and melting behaviour of 35PB and 45PB are rather complex, as indicated by their slow crystallization kinetics. To get a better idea of the crystallinity of the materials before the formation of the interface, different thermal histories were applied to the copolymers before recording the DSC runs. Figures 3.2-5 and 3.2-6 show a

comparative view of the total heat flow scanned at 5°C.min^{-1} after those different thermal histories were applied on 35PB and 45PB respectively :

- curve (a) corresponds to the standard procedure where a granule (5 to 10 mg) is placed in the DSC pan, heated at high temperature (260°C) in order to erase the thermal history and cooled at 5°C.min^{-1} before scanning.
- curve (b) presents the DSC scan of a molded sample. The sample was molded under the press according to the molding experimental procedure described in section 3.1.1.1 (180°C, cooling rate : 2.5°C.min^{-1}). A small sample (5 to 10 mg) was then taken from the molded plate, a few millimetres from the plate edge to avoid any artefacts, and placed in the DSC pan.
- curve (c) is the DSC scan of a molded sample preheated before contact. A polymer plate was removed from the set up designed for assembling after the preheating time (t_{ph}, see table 3.2-1) and just before contact at 100°C (see the experimental procedure for assembling in section 2.4.1.4). This corresponds to the annealing of a molded plate at 100°C (during 25 min in the case of 35PB and 10 min in the case of 45PB)
- in curve (d), the same procedure as curve (c) was followed with longer annealing times (55 minutes for 35PB and 70 for 45PB), in order to simulate the time of contact and look for possible change in the crystallinity changes over this time range.

The different thermal histories of cases a, b and c are summarized in Figure 3.2-4 :

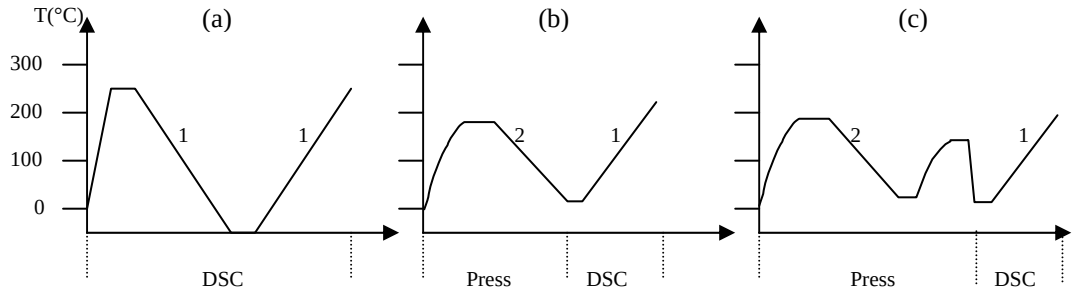

Figure 3.2-4: different thermal history undergone by the samples before scanning in the DSC at 5°C.min^{-1}. The main ramps are 1 : 5°C.min^{-1} and 2 : 2.5°C.min^{-1}

The curves in Figure 3.2-5 show one exothermic and one endothermic peak in curve (a), one endotherm in curve (b) and two in curves (c) and (d). The exothermic peak in curve (a) corresponds to a cold crystallization, while the endothermic peaks correspond to a fusion. The absence of cold crystallization in curve (b) and (c) is due to the fact that the sample has already recrystallized during the molding and molding/annealing step. For 45PB in Figure 3.2-6, the exothermic peak is present in curves (a) and (b) and disappears in curve (c).

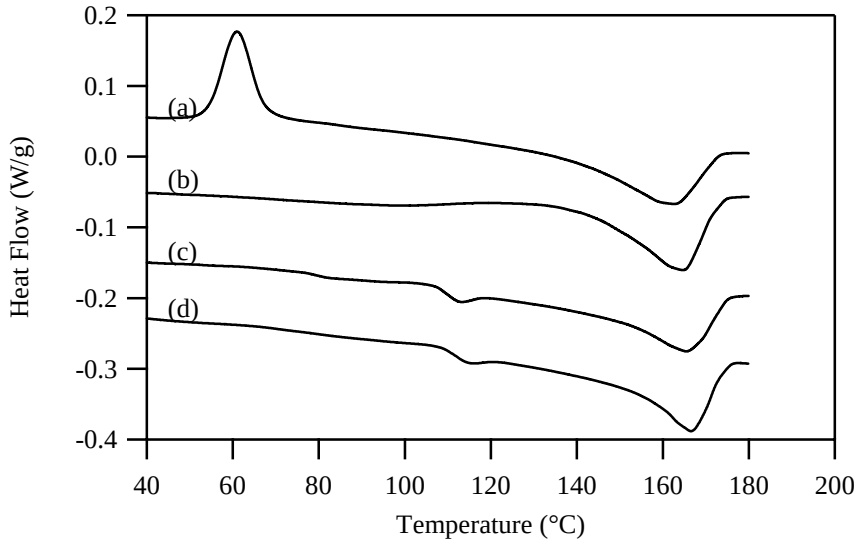

Figure 3.2-5: total heat flow as a function of temperature for 35PB scanned at 5°C.min^{-1}
(a) standard procedure (polymer granule heated at 260°C and cooled at 5°C.min^{-1})
(b) from a polymer plate molded at 180°C and cooled at 2.5°C.min^{-1}
(c) from a polymer plate molded, then annealed at 100°C for 25 min.
(d) from a polymer plate molded, then annealed at 100°C for 55 min.

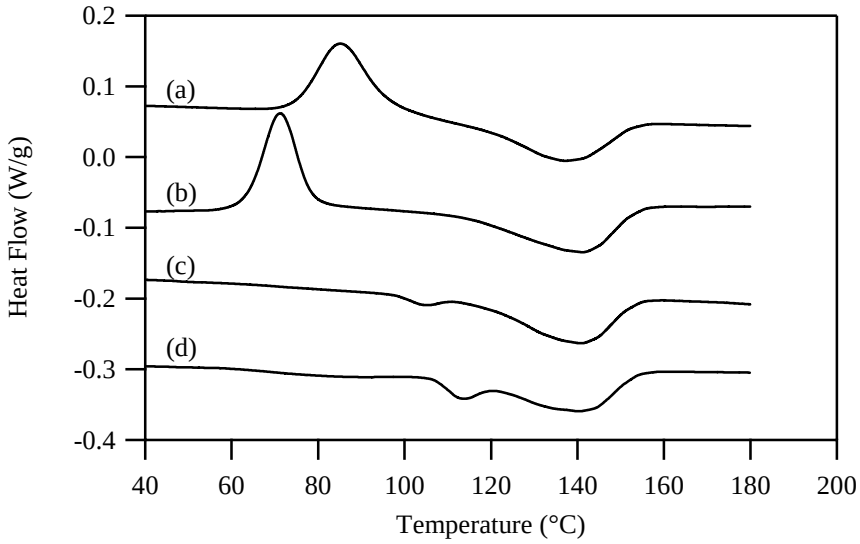

Figure 3.2-6: total heat flow as a function of temperature for 45PB scanned at 5°C.min^{-1}
(a) (b): see Figure 3.2-5
(c) from a polymer plate molded, then annealed at 100°C for 10 min.
(d) from a polymer plate molded, then annealed at 100°C for 70 min.

In table 3.2-2 is given the integrated peak area in each case, the onset of the fusion process T_s, T_{cc}, T_m^1 and T_m respectively the cold crystallization temperature the temperature of the first melting point and the main melting point.

Table 3.2-2 : cold crystallisation and melting temperatures and heats

polymer	Curve	T_{cc} (°C)	ΔH_{cc} ($J.g^{-1}$)	T_s (°C)	T_m^1	T_m (°C)	ΔH_m ($J.g^{-1}$)
35PB	(a)	61	15.9	100	/	162	25.5
	(b)	/	0	130	/	165	24.5
	(c)	/	0	104	113	165	31.3
	(d)	/	0	105	116	167	32.9
45PB	(a)	85	17.5	106	/	137	17.1
	(b)	71	17.5	93	/	141	21.6
	(c)	/	0	99	105	141	21.2
	(d)	/	0	105	113	140	19.9

In the case of 35PB, a slower cooling rate, i.e. 2.5°C.min^{-1} under the press instead of 5°C.min^{-1} in the DSC in the case of curve (a), gives time for crystallization during cooling. This crystallization during cooling prevents the sample from cold crystallization during the heating ramp. However, for curve (a), the heat of cold crystallization is smaller than the heat of fusion, strongly suggesting that the sample was not fully amorphous even after cooling at 5°C/min.

In curves (a) and (b), we have not reached the maximum degree of crystallinity or at least a near equilibrium value. The heat of fusion obtained in curves (c) and (d) are indeed bigger and the shape of the endothermic peaks changes. The annealing process has increased the degree of crystallinity of the sample. Therefore, cold crystallisation can occur during the annealing step at 100°C. An annealing time of 25 min was chosen for 35PB, equal to the time of preheating for assembling in the adhesion tests. Then curve (c) gives a good idea of the onset of the fusion process T_s, the first and the main peak of the melting process, respectively T_m^1 and T_m and the heat of fusion at the moment of contact, if we consider that nothing really happens during the heating ramp in the DSC at 5°C.min^{-1}.

In curve (d), we applied a longer annealing time to the sample in order to check how stable was the structure on further annealing. The differences in terms of the two melting peaks and heat of fusion are very small for the 35PB.

In the case of 45PB, the exothermic peak is observed in curve (a) and in curve (b). The crystallisation kinetics of 45PB is slower than that of 35PB, and the sample has not enough time to crystallize during the cooling step even at a relatively slow cooling rate, i.e. 2.5°C.min^{-1}. However, the sample crystallizes during the annealing step as shown in curves (c) and (d).

Contrary to 35PB, we get roughly the same value for the heat of fusion in curves a, b, c and d in the case of 45PB, but we can notice a few additional changes between curves (c) and (d) mainly in the position of the first peak. This implies that some changes occur in the crystalline morphology of 45PB between 10 and 70 minutes of annealing at 100°C. The first melting peak is shifted to higher temperatures for a longer annealing time, which implies that thicker crystallites are formed after a longer annealing time.

These simulations of preheating give a general idea of the melting behaviour (onset of the fusion process, position and shape of the melting peaks), but are indeed not representative of the exact crystallinity before contact, since the temperature is not constant during the preheating step of the assembling procedure. Since the shape of the DSC curve remains roughly the same by applying different annealing times to the sample, we can estimate that roughly the same pattern would be obtained for the samples before contact at different temperatures.

We will then consider that curve(c) for 35PB and 45PB represents well the behaviour of the (bulk) sample just before contact. Hence, in the following discussion, we will use curve (c).

In Figure 3.2-7 and 3.2-8 are represented the heat flow, the reversing heat flow and the non-reversing heat flow for respectively 35PB and 45PB. The differences which appeared in the total heat flow between 35PB and 45PB, are clearly shown in the non-reversing flow. This flow represents the kinetic component of the flow. In Figure 3.2-7, a flat peak appears between 50 and 90°C. This peak can correspond to a residual cold crystallisation, but its amplitude is very small. Then the first melting peak appears followed by a weak reorganisation. The non-reversing flow in the case of 45PB is quite different. Contrary to 35PB, there is no exothermic peak before the first melting peak. Moreover, the first melting peak is followed by a real exothermic peak. This peak is due to recrystallization or reorganisation, which thus appears to be much more pronounced for 45PB than for 35PB.

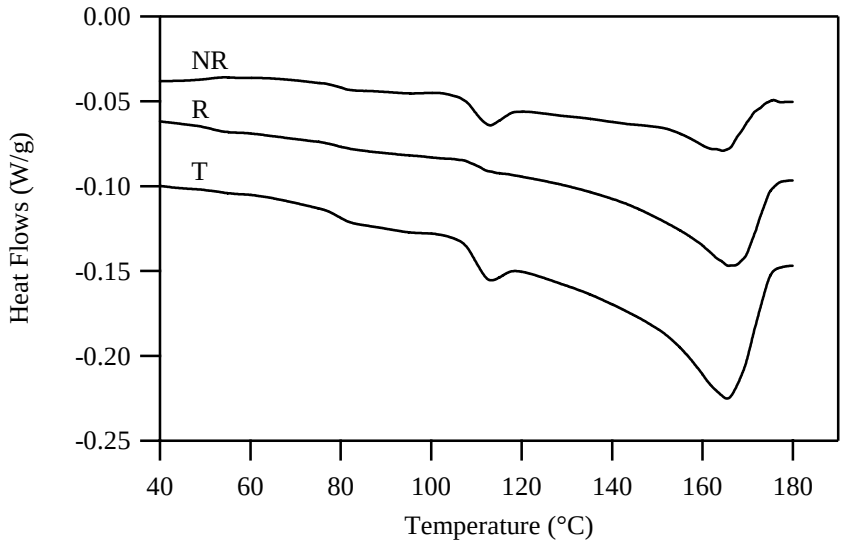

Figure 3.2-7: TM-DSC results for 35PB scan at 5°C.min^{-1}, with oscillations of 0.796°C every 60s (Heat Only). Total (T), Reversing (R) and non-reversing heat flow vs. temperature.

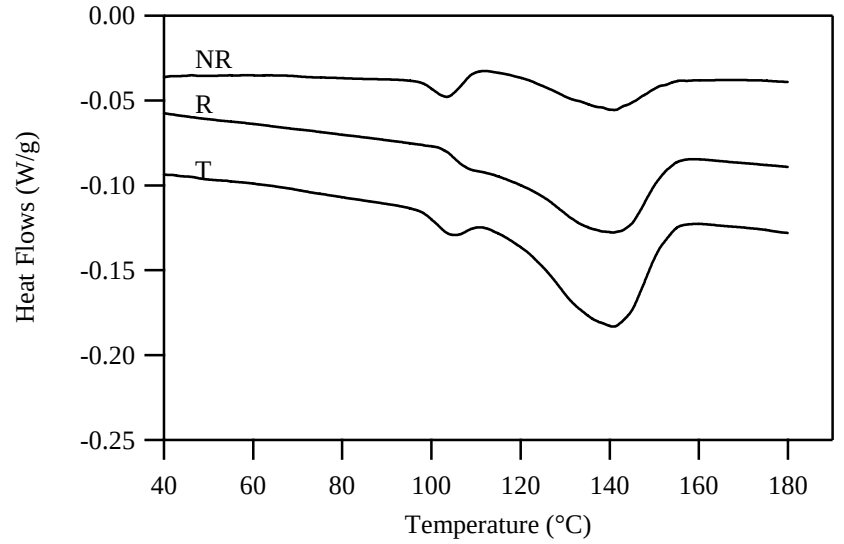

Figure 3.2-8: TM-DSC results for 45PB scan at 5°C.min^{-1}, with oscillations of 0.796°C every 60s (Heat Only). Total (T), Reversing (R) and non-reversing heat flow vs. temperature.

3.2.3 Discussion

In Figures 3.2-9 and 3.2-10, adhesion and DSC results for respectively 35PB and 45PB are presented on the same graph as a function of temperature. The DSC curve was scanned at 5°C.min^{-1} on a molded and annealed sample (during 10 minutes for 35PB and 10 for 45PB) as described in section 3.2.2 (curve (c)).The same temperature range was chosen and the melting peaks of 35PB and 45PB were placed one above the other to make the comparison easier. As discussed in section 3.2.1, fracture toughness falls from high to null over a range of 50°C in the case of 35PB, while its drops over a range of 30°C in the case of 45PB. The observation of the DSC curve may give some clues to explain this difference, since the melting peak of 35PB is clearly broader than that of 45PB. The difference between T_s and T_m (see previous section) is 60°C for 35PB and 45°C for 45PB.

For each copolymer, the contact temperature at which the self-adhesion level becomes measurable corresponds more or less to the onset of the fusion process T_s. Both 35PB and 45PB have a double melting behaviour according to the DSC curve. In the case of 35PB G_c goes through a maximum at 120°C, decreases a little at 130°C and levels up again at 140°C. On the DSC curve, 120°C corresponds to the end of the first melting peak. Thanks to the preheating, the temperature of the polymer plate when the contact is established is the temperature of contact (see section 2.4.1.4). At 120°C, the first melting is completed but the reorganisation is not yet achieved. At 130°C, a certain reorganisation has already taken place, which could possibly influence the chain mobility and by consequence, self-adhesion. In the case of 45PB, the melting peak is quite narrow and it is quite difficult to observe the phenomena. Another experiment with a temperature of contact of 114°C might help.

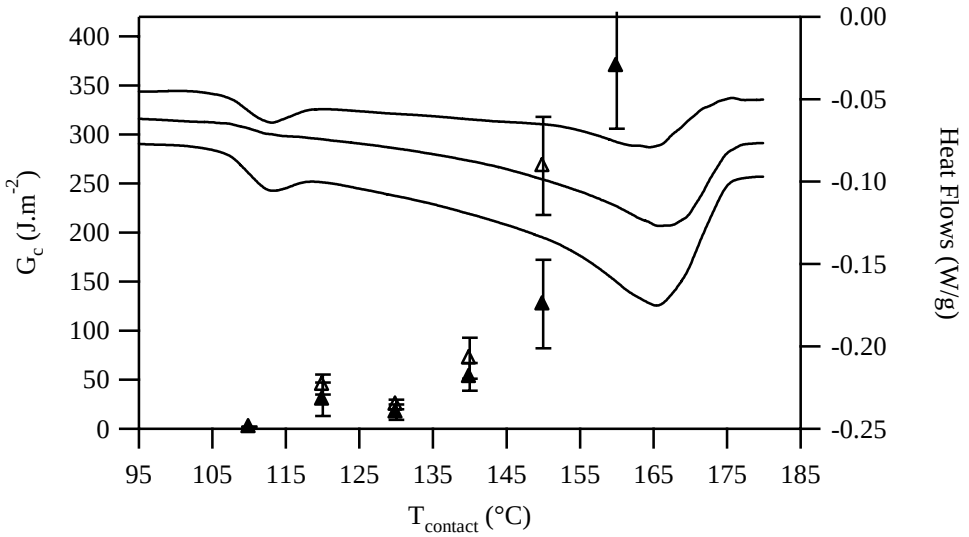

Figure 3.2-9: Adhesion and TM-DSC results for 35PB as a function of temperature after 10 minutes of contact (full symbol) and 30 minutes of contact (open symbols).

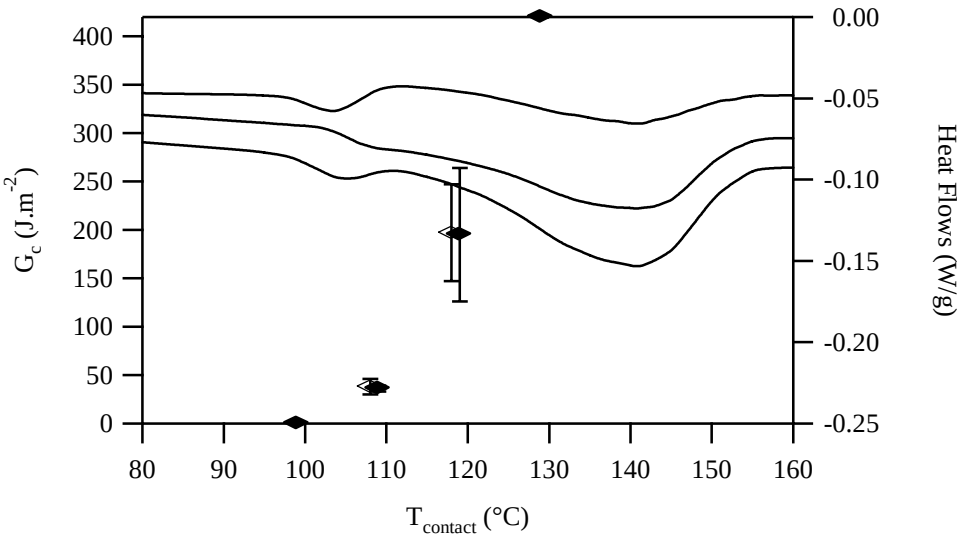

Figure 3.2-10: Adhesion and TM-DSC results for 45PB as a function of temperature after 10 minutes of contact (full symbol) and 30 minutes of contact (open symbols).

3.2.4 Conclusions

Similarly to what was observed for the 15PB (section 3.1), a certain fusion, at least of the first crystallites, is a required condition to obtain some self-adhesion in the case of 35PB and 45PB. Even with a low degree of crystallinity (15%), it was not possible to get any adhesion with 45PB below T_s. This temperature seems to control the possibility to develop adhesion. If we choose the thermal history of the sample before it is placed in the DSC, to simulate the thermal history undergone during molding and preheating, we obtain a relatively good correlation between the TM-DSC curves and the resulting values of G_c.

Of course, TM-DSC results just provide general guidelines for a better understanding, but their limitations are obvious: adhesion is clearly an interfacial problem and TM-DSC only provides bulk properties. Unfortunately, for crystalline 35PB and 45PB, the optical and TEM observations were not very meaningful so we remain with a lack of information about crystallinity at the interface. The next section, however, which concentrates on amorphous 45PB, will offer some additional insight about the crystallinity at the interface.

3.3 Amorphous 45PB : 45PB^a

In section 3.2, we reported that, even for the copolymers with a low degree of crystallinity, it was not possible to obtain adhesion for a contact temperature below the onset of the fusion process T_s, the temperature where the first crystallites melt.

In this section a different set of experiments was carried out : 45PB samples made amorphous by rapid quenching (45PB^a) , were then put in contact at room temperature, i.e. when they are still amorphous, before heating them to the contact temperature $T_{contact}$. The increase in temperature is expected to favour both cold crystallization of the copolymer in the bulk and mutual diffusion of the copolymer chains across the interface. The main idea of this set of experiments was to try to investigate the relative contributions of molecular interdiffusion and cold crystallization to the interfacial adhesion. In principle, a range of temperatures should exist (above T_g but below T_{cc}) where polymer chains could interdiffuse without being frozen in position by the crystallization process.

Because of the slow crystallization kinetics of 45PB, amorphous 45PB samples could be obtained, by quenching the samples from the melt. In practical terms, this entailed some small changes in the preparation procedure of the sample since amorphous 45PB has a low modulus. We actually overmolded a 300 μm thick layer of 45PB on top of a stiff 2 mm thick polycarbonate plate in order to keep a reasonable modulus for the beam of the DCB test (see section 2.4.2.1). It should be noted that the same procedure was used in the case of 35PB, which shows a similar crystallization behaviour (relatively slow crystallization kinetics and cold crystallization during heating) but even after quenching, the sample was still partially crystalline. We should stress that by molding a 2 mm thick 35PB sample without the PC substrate, we managed to obtain amorphous 35PB. Hence the PC has probably a nucleating action.

Contrary to previous sections where the temperature of contact was varied from the melting point down toward the glass transition temperature until adhesion was found null (typically at a temperature well above T_g, i.e. 100°C), the following experiments with 45PB^a samples were carried out from a temperature of contact just above T_g (40°C) up to a temperature of contact just below the melting point. Indeed, for an amorphous sample, the important temperatures are the glass transition temperature and the cold crystallization temperature.

Since the properties of 45PB^a will change during the time where contact is established at the interface, a comprehensive characterization of the variation in crystallinity and mechanical properties of the 45PB^a as a function of thermal history is necessary. The amorphous state is indeed out of equilibrium, making the adhesion results quite difficult to interpret without a detailed understanding of the crystalline structure as well. Hence we chose to start this chapter by the study of the evolution of the degree of crystallinity, crystalline structure and mechanical properties with the thermal history of the bulk

polymer, before presenting the results of fracture toughness of the interfaces as a function of contact temperature and contact time.

3.3.1 Characterization of the crystallinity of 45PBa by DSC

The overall crystallization behaviour of 45PB has been already discussed in chapter 2. Because of its slow crystallization kinetics, it is possible to obtain amorphous 45PB at room temperature by quenching the sample from the melt.

DSC experiments were used to monitor the crystallinity of the bulk sample after quenching and to simulate the crystallization behavior of the amorphous sample occurring during the formation of the interface. We were particularly interested in the degree of crystallinity of the sample at the onset of the contact and at the end of the contact.

Before entering in the description of the DSC experiments, we will first briefly recall the experimental procedure scrupulously applied in the adhesion experiments :

- we kept for all the experiments, the same cooling rates for the molding procedure of the 45PB samples (on a PC substrate see section 2.4.1.1), i.e. a first ramp at 20°C.min^{-1} from 180°C to 160°C followed by a quenching in ice water (see section 2.4.1.2).
- we always formed the contact at room temperature between amorphous samples, i.e. prepared as described before, and then quickly heated the assembly to the contact temperature. Contact was held at the nominal temperature of contact until the time of contact $t_{contact}$ was elapsed, then the assembly was rapidly cooled (about 40°C.min^{-1}) to room temperature. In the adhesion experiments, the time of contact begins at the onset of contact (at room temperature) and ends at the onset of cooling, i.e. the temperature of the interface is not constant during the 1 or 2 first minutes of contact (see section 2.4.1.3 for more details).

We used two different methods to study the crystallization kinetics: one method was to fully simulate the assembling process in the DSC (by molding an amorphous plate and placing a small sample of it in the DSC, where a temperature history can simulate the assembling process), the other method was to analyze in the DSC a small sample of an assembly after fracture of the interface with the DCB test.

More specifically :

In protocol one, a 45PB^{a} polymer plate, 2 mm thick, was molded according to the procedure described in section 2.4.1.3 (molding at 180°C, cooling at 20°C.min^{-1} to 160°C and quenching in ice water to obtain an amorphous sample). A small part of 5 to 10 mg taken from the edge of the plate was placed in the DSC pan. To simulate the thermal history undergone by the sample during the assembling procedure, the polymer was heated in the DSC pan to an annealing temperature T_{ann}, during an annealing time t_{ann}, which correspond respectively to the contact temperature $T_{contact}$ and the contact time $t_{contact}$. The heating and cooling ramp chosen to reach the annealing temperature were of

20°C.min^{-1}. The final heating, during which the scan was recorded, was carried out at 5°C.min^{-1} (Temperature modulated DSC, +/- 0.796°C every 60 seconds). The annealing time was measured from the onset of the isotherm to the end of the isotherm in order to have a good control of both the temperature and time of annealing. This measurement of the annealing time differs a little from the measurement of the contact time, as shown in Figure 3.3-2, but still we considered that this difference would not change the results too much, especially for a time of annealing or of contact of 60 minutes.

In protocol two, 45PB^{a} was taken from an assembly after the DCB test and directly placed in the DSC. The scan was recorded in the same conditions as the first set (5°C.min^{-1}, +/- 0.796 every 60s).

The main advantage of the second procedure is to give results on the polymer which had undergone the real assembling procedure. Moreover, in the second procedure, the polymer was taken from a region near the interface, while in the first procedure the polymer was more bulk like (see figure 3.3-1). Hence, we may obtain some information on the influence of the interface on the crystallization.

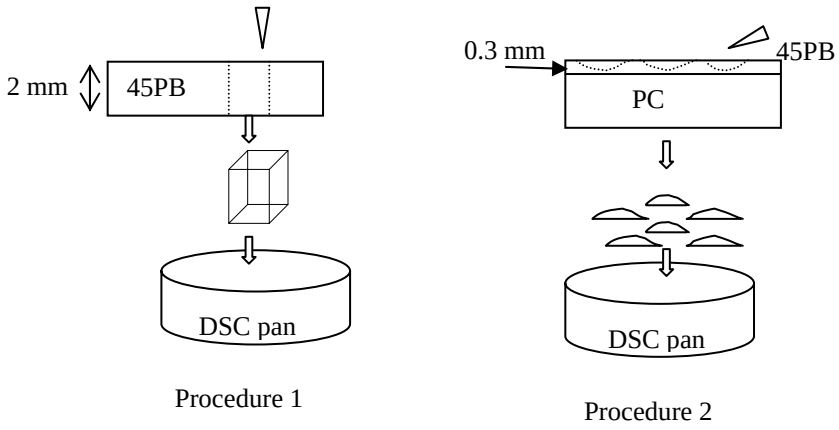

Figure 3.3-1 : difference between the two procedures in the sample localisation

The two procedures are summarized in Figure 3.3-2 together with the standard procedure used for the characterization in chapter 2.

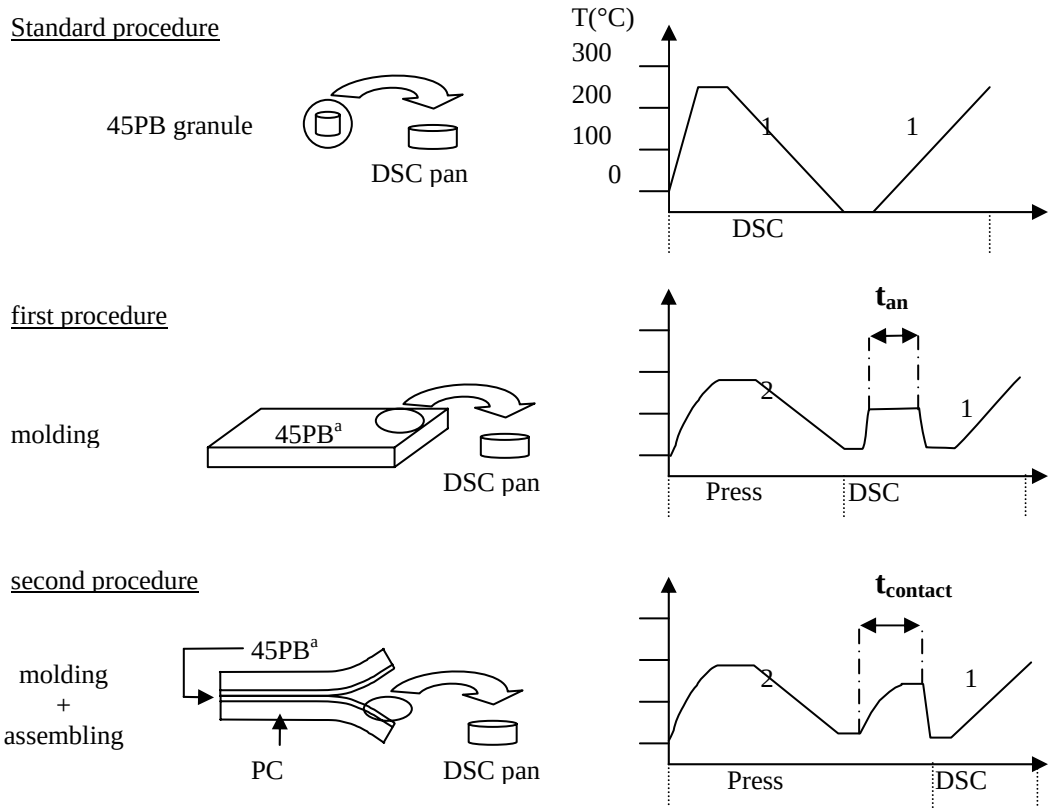

Figure 3.3-2 different thermal histories undergone by the samples before scanning at 5°C.min^{-1}. The main ramps are 1 : 5°C.min^{-1} and 2 : 2.5°C.min^{-1}

A series of DSC heating scans are shown in figure 3.3-3 for samples annealed at different temperatures and for different times. The two upper curves are the scans obtained for a granule and for a molded plate. All annealings were performed using the first procedure. For unannealed or slightly annealed samples, a pronounced peak of cold crystallization is observed around 60°C to 80°C. The amplitude of this peak as well as its temperature clearly decreases with increasing annealing temperature, while the heat of fusion around 140°C remains unchanged.

These results show that the crystallization occurs in two steps: Some crystallization occurs during the annealing procedure and if it is not completed after the annealing time, cold crystallization occurs during the final heating scan. It is then possible to determine the actual degree of crystallinity after annealing, by subtracting the heat of cold crystallization from the heat of fusion.

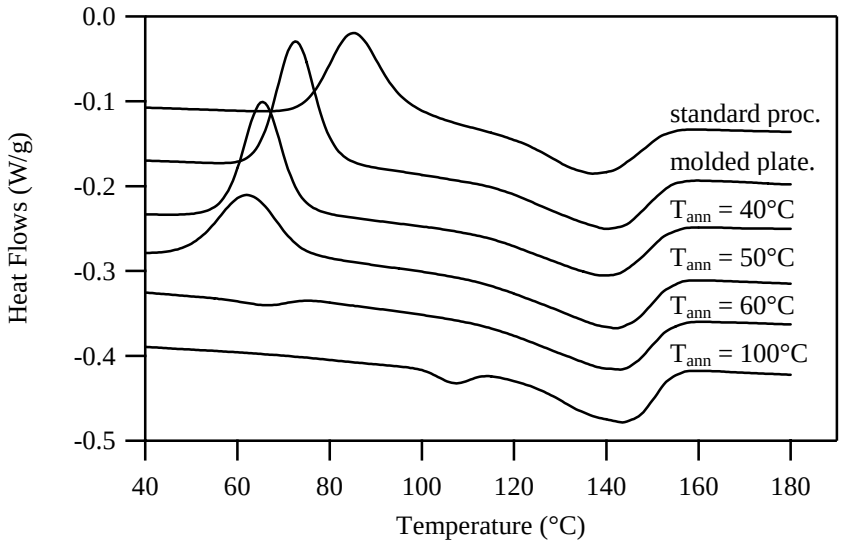

Figure 3.3-3: DSC scans at 5°C.min^{-1} ; effect of the annealing temperature (annealing time : 10 minutes)

A second issue is the difference between the two procedures, i.e. DSC simulation and the results obtained for the sample taken from the fractured surface. Figure 3.3-4 shows a direct comparison between these two procedures. A sample annealed at 100°C during 10 minutes and a sample assembled at a temperature of contact of 100°C during 10 minutes were scanned during heating at 5°C.min^{-1}. Both samples show the same profile indicating no sign of cold crystallization and a small melting peak appearing before the main melting peak. The first melting peak appears however at a lower temperature in the case of the assembled sample, indicating the presence of a population of smaller crystallites.

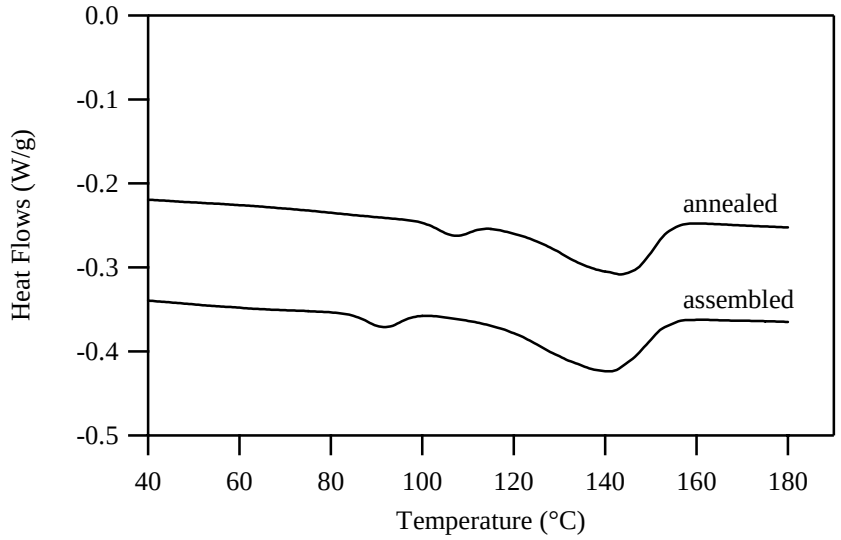

Figure 3.3-4: difference between a DSC simulation (T_{ann} = 100°C, $t_{a\,nn}$ = 10 min) and an assembled sample ($T_{contact}$ = 100°C and $t_{contact}$ = 10 min)

Figure 3.3-5 is given as an example of the quantitative determination of the different critical temperatures and specific heat capacities : the glass transition temperature T_g, the temperature of cold crystallization T_{cc}, the heat of cold crystallization ΔH_{cc}, the onset of the melting process T_s, the temperature of the first melting peak T_m^1 if it exists, the temperature of the main melting peak T_m and the heat of fusion ΔH_f. In the rest of the text, these temperatures will be referred to with these symbols and determined as shown on Figure 3.3-5.

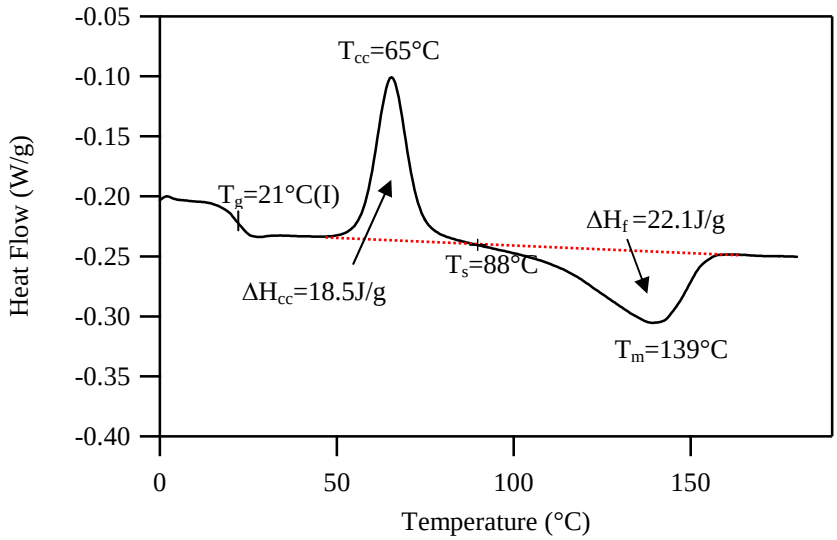

Figure 3.3-5: critical temperatures and characteristic heat capacities for 45PB[a] annealed at 40°C for 10 minutes.

The variation of these characteristic quantities with thermal history is now presented. The glass transition temperature is plotted in Figure 3.3-6 as a function of the annealing or contact temperature. The values of the glass transition temperature fluctuate from 21°C to 28°C with the T_g of the most crystallized sample being slightly higher. Those fluctuations are however quite small and do not affect much the results of adhesion experiments, since the interfaces were always formed at temperatures well above the average value of the glass transition (24°C).

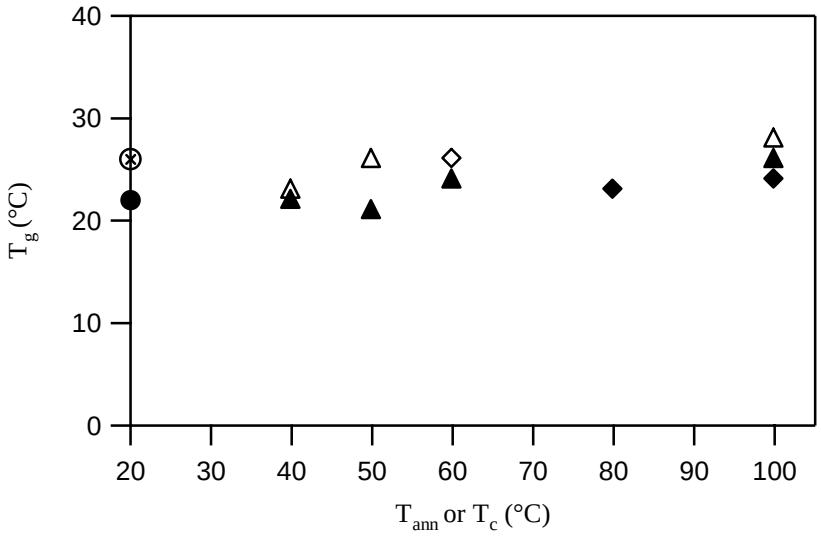

Figure 3.3-6: glass transition temperature.
samples annealed ▲ or assembled ◆ for 10 minutes
samples annealed △ or assembled ◇ for 60 minutes
unannealed sample ● and standard procedure ⊗

As seen qualitatively in figure 3.3-3 and shown in Figure 3.3-7, the temperature of cold crystallization (maximum of the peak) varies from 62°C to 73°C.
T_{cc} is distinctly higher for the sample cooled with the standard procedure in the DSC. The value of T_{cc} for the unannealed sample is higher than the values obtained for samples which were previously annealed at a temperature of 40°C and 50°C. For an annealing time of 10 minutes, T_{cc} goes to a minimum at 50°C. At this temperature, T_{cc} increases with annealing time.

These differences in the value of T_{cc} as a function of annealing procedure surely reflect differences in the nucleation process of the crystallites, between a granule placed in a DSC pan, and a molded sample, where the interface is present. Nucleation effects are always very sensitive to the presence of seeds. In the case of the standard procedure, few crystalline seeds may be present initially and the nucleation starts at a higher temperature. More nuclei are present in the unannealed sample. During the annealing time, both nucleation of new crystallites and growth of the nuclei already present in the sample can take place. In the case of an annealing at 50°C during 60 minutes or at 60°C during 10 minutes, most nuclei have probably already grown to give crystallites and only few opportunities to grow new crystallites remain. From Figure 3.3-8, we can notice that for those temperatures, the heat of cold crystallization is very low, meaning that the crystallization is almost completed after the annealing step.

The integral of the peak, i.e. the heat of cold crystallisation shown in Figure 3.3-8, logically decreases with increasing annealing/contact temperature or time showing the progressive crystallization of the copolymer during the annealing time. This reveals

clearly that the kinetics of crystallization is strongly temperature activated and cold crystallization occurs within an hour at 50°C but probably within a few minutes at 60°C.

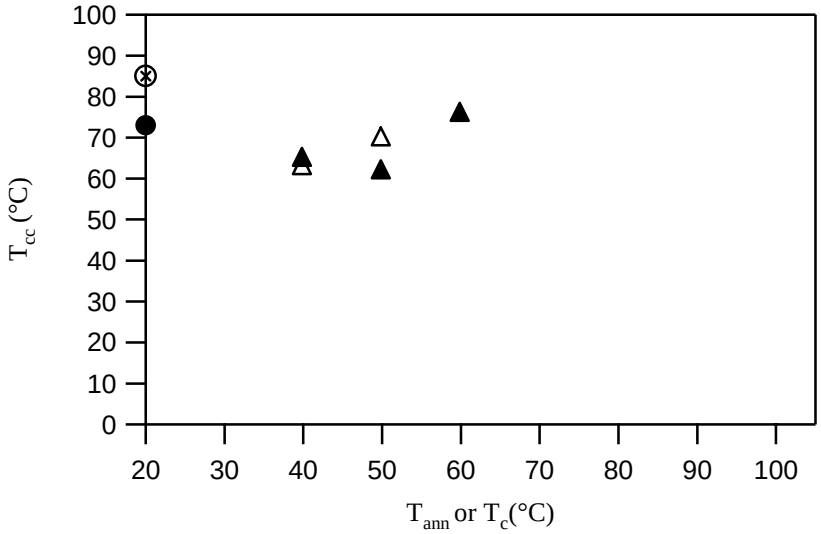

Figure 3.3-7: cold crystallization temperature.
samples annealed ▲ or assembled ◆ for 10 minutes
samples annealed △ or assembled ◇ for 60 minutes
sample not annealed ● and standard procedure ⊗

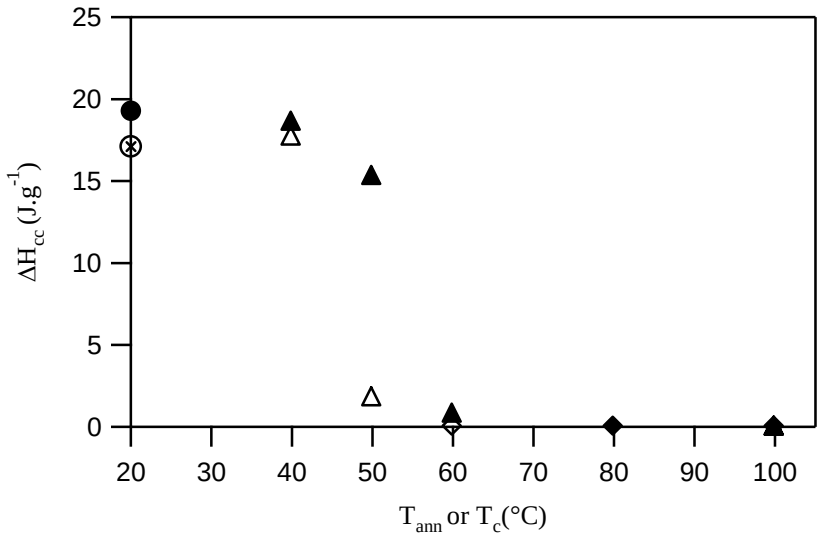

Figure 3.3-8 : heat of cold crystallization.
samples annealed ▲ or assembled ◆ for 10 minutes
samples annealed △ or assembled ◇ for 60 minutes
sample not annealed ● and standard procedure ⊗

The onset of the fusion process, plotted in Figure 3.3-9, is almost constant in the case of the first procedure, where the amorphous 45PB is annealed in the DSC, with a mean value of 90 +/- 2°C. This temperature becomes lower in the case of assembled samples. Here the crystallization occurs during the time of contact and the interface must play an important role in the nucleation of the crystallites. A low onset of the fusion process suggests the presence of less perfect and smaller crystals. In other words, in the case of assembled samples, the nucleation process has been favoured compared to the growth process.

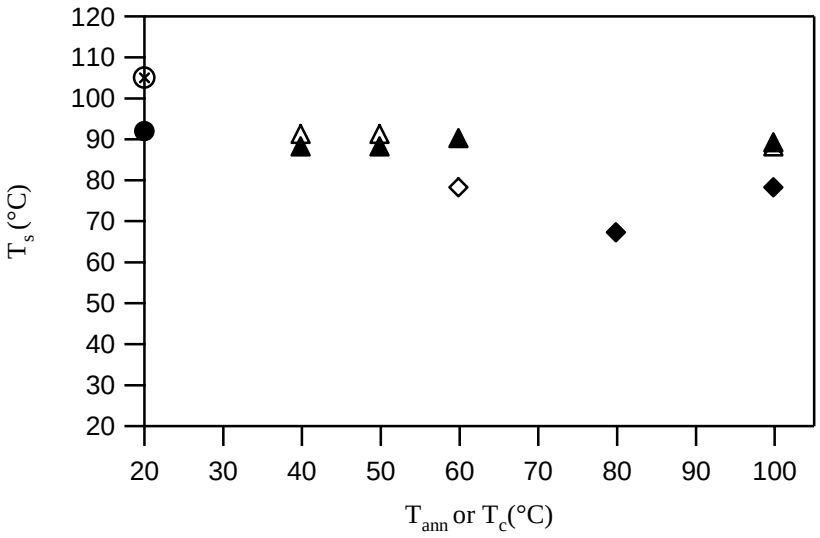

Figure 3.3-9: onset of the fusion process.
samples annealed ▲ or assembled ◆ for 10 minutes
samples annealed △ or assembled ◇ for 60 minutes
sample not annealed ● and standard procedure ⊗

For an annealing/contact temperature above 80°C, a small peak of fusion appears before the main melting peak. Figure 3.3-10 shows the temperature of this peak as a function of T_{ann} or $T_{contact}$. The temperature of this first melting peak is lower in the case of assembled samples, for an annealing or contact temperature of 100°C. This result is consistent with result shown in figure 3.3-9 on the onset of the fusion process.

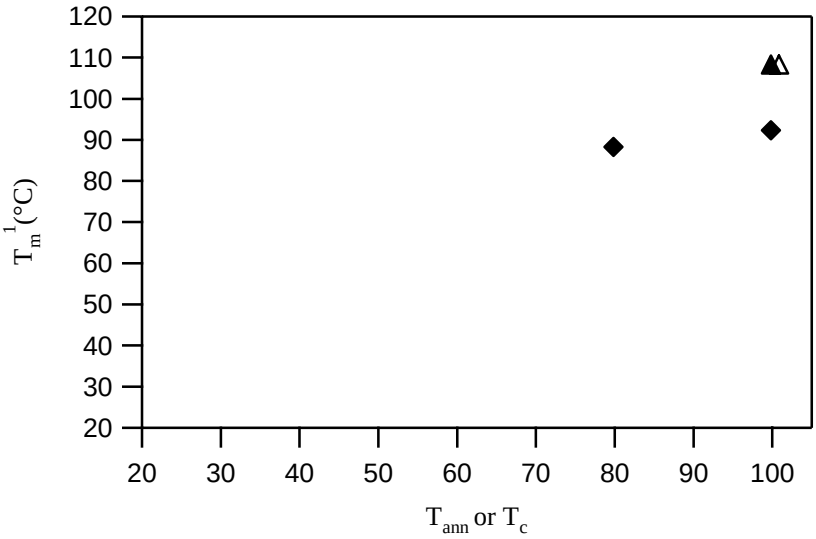

Figure 3.3-10: temperature of the first melting peak.
samples annealed ▲ or assembled ◆ for 10 minutes
samples annealed △ or assembled ◇ for 60 minutes.

In Figure 3.3-11, the position of the melting peak is plotted as a function of annealed or contact temperature. The melting point appears quite constant : 140 +/- 2 °C independent of the previous thermal history.

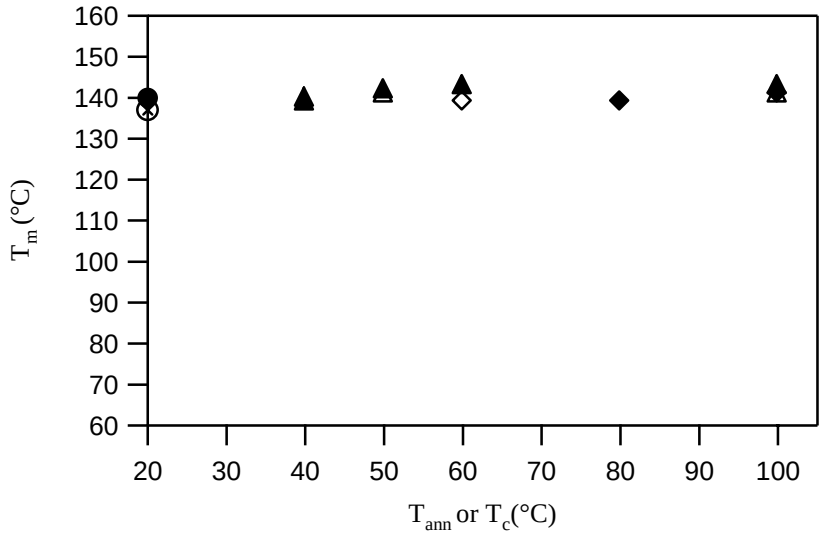

Figure 3.3-11: melting point
samples annealed ▲ or assembled ◆ for 10 minutes
samples annealed △ or assembled ◇ for 60 minutes
sample not annealed ● and standard procedure ⊗

Finally, Figure 3.3-12 shows the heat of fusion as a function of annealing or contact temperature. The values appear almost constant for the annealed or assembled samples. The value in the case of the standard procedure is lower. This implies again that the molding process produces a large amount of seeds which will enhance the total degree of crystallinity.

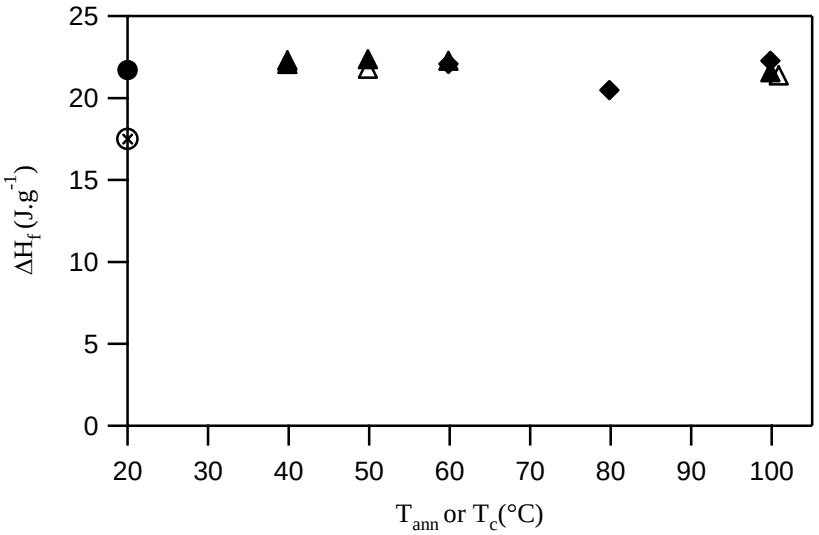

Figure 3.3-12: heat of fusion.
samples annealed ▲ or assembled ◆ for 10 minutes
samples annealed △ or assembled ◇ for 60 minutes
sample not annealed ● and standard procedure ⊗

Another interesting result for the interpretation of adhesion experiments, is the degree of crystallinity of the sample at the beginning of the contact when forming the interface. The calculation of χ_c is based on equation 3.3-1 with the heat of fusion of the perfect PBT crystal ΔH_m^0 = 140J.g^{-1} (after Illers[1]). From the WAXS experiments in section 2.3.1.3 which show the same crystalline peaks from PBT to 45PB, we assumed that the crystalline part in all copolymers was mainly the PBT part. To obtain the degree of crystallization as it was before the last heating ramp (where the DSC curves were recorded) the heat of cold crystallization has been subtracted to the heat of fusion (Equation 3.3-1):

$$\chi_c = \frac{\left(\Delta H_m - \Delta H_{cc}\right)}{\Delta H_m^0} \qquad \textit{Eq. 3.3-1}$$

Figure 3.3-13 represents the degree of crystallinity χ_c as a function of the annealing or contact temperature.

The degree of crystallinity of the amorphous, unannealed sample (1.7%) is slightly above the error bar of our experiments (roughly 1%). We can then stress that this value is slightly higher than the value found in the case of the standard procedure (0.4%) which can be considered as a baseline for a nearly amorphous sample. Hence, if we trust the accuracy of the DSC experiments, the molded-quenched sample is not fully amorphous.

At 40°C, the degree of crystallinity remains low, after 10 or 60 minutes. The real change occurs at 50°C, where the degree of crystallinity after 60 minutes of annealing is much higher than the degree of crystallinity obtained after 10 minutes. At 60°C, the degrees of

[1]Illers, K. Colloid and Polymer Science, **258**(2): 117-124, (1980)

crystallinity after 10 or 60 minutes are similar. Above 60°C, the crystallinity appears to be constant within experimental error although the shape of the peak varies as one can see in figure 3.3-2.

Finally, the two procedures give almost the same degree of crystallinity at 100°C after 10 minutes.

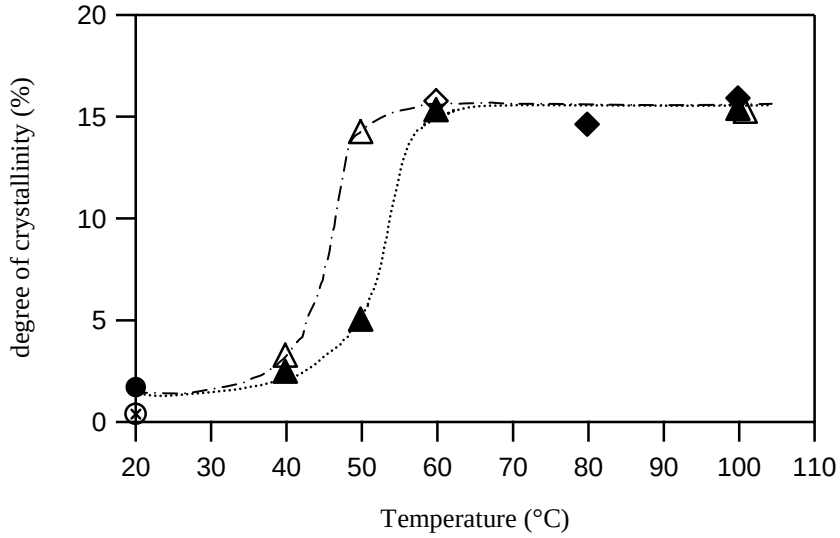

Figure 3.3-13: degree of crystallinity.
samples annealed ▲ or assembled ◆ for 10 minutes
samples annealed △ or assembled ◇ for 60 minutes
sample not annealed ● and standard procedure ⊗

- **<u>conclusions of the DSC experiments</u>**

- in the case of samples unannealed or annealed at low temperature, the overall degree of crystallinity obtained is very small but not null, compared to the one obtained in the standard procedure (not molded sample). Moreover, those molded-quenched samples show a cold crystallization at a significantly lower temperature than for the standard procedure. Hence, the very small degree of crystallinity may be due to the presence of nuclei, which will then enhance the cold crystallisation process
- 50°C appears to be the temperature where the growing process of the crystallites really starts : after 10 minutes, the degree of crystallinity remains small and cold crystallization occurs at a low temperature while after 60 minutes, the crystallinity is close to the maximum and the cold crystallization occurs at higher temperature.
- at higher temperature, the apparent maximum of crystallinity is reached within 10 minutes for both the annealed and the assembled sample.
- The main differences between the annealed and the assembled sample, shown in Figure 3.3-9 and 3.3-10, are the lower onset of fusion process and the lower first

melting peak obtained in the case of assembled samples. This suggests the presence of less perfect or smaller crystals which is typical of a predominance of the nucleation process against the growth process. The presence of the interface is surely playing an important role in that competition.

3.3.2 Crystallization kinetics

The previous section gave some results on the degree of crystallinity of the samples before and after contact, which stressed the important role played by the crystallization kinetics. In order to further investigate this point, we annealed the samples in isothermal conditions in the DSC, while recording the heat flow as a function of time. Figures 3.3-14 and 3.3-15 show the heat flows recorded during isothermal annealing for different annealing temperatures.

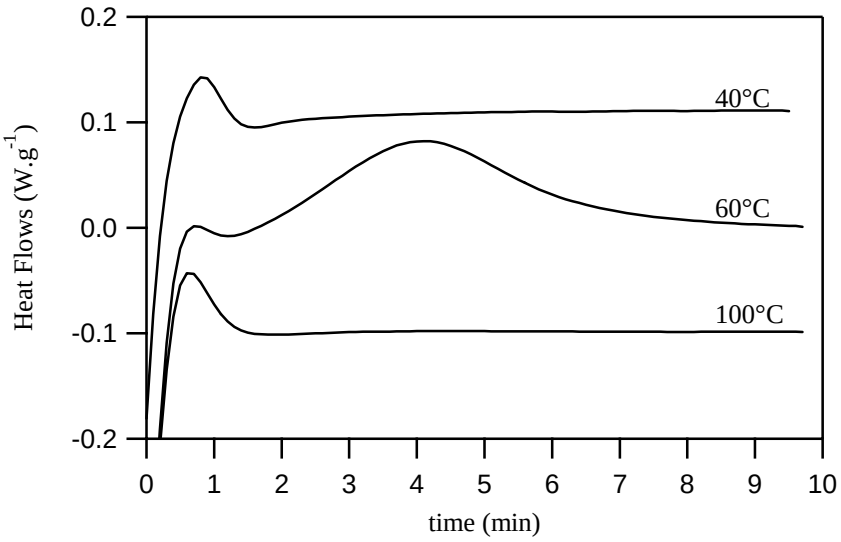

Figure 3.3-14: Heat Flows during a 10 minutes isotherm. Annealing temperatures : 40, 60 and 100°C.

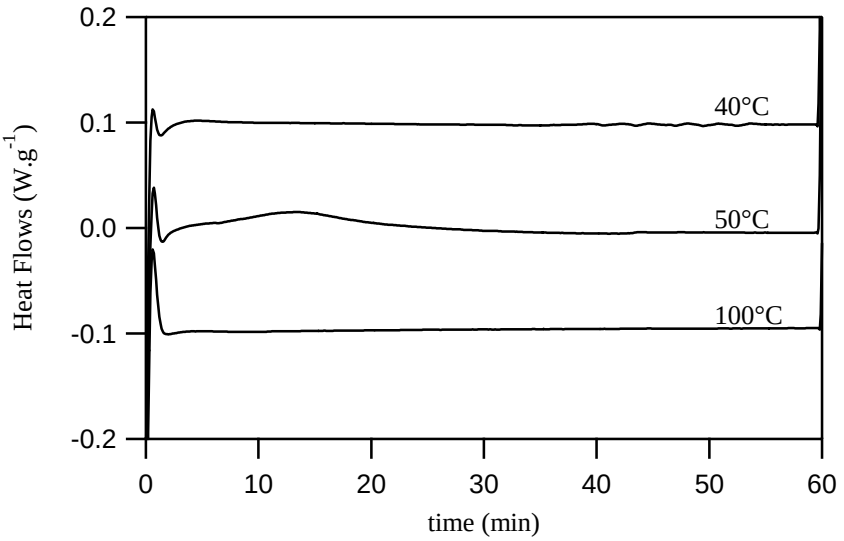

Figure 3.3-15: Heat Flows during a 60 minutes isotherm. Annealing temperatures : 40, 50 and 100°C.

The beginning of the cold crystallization process was in some cases masked by the initial transient signal that is observed after a sudden change of the scanning rate, typically in the first minute of the annealing time. In figure 3.3-14, no cold crystallization is observed for an annealing temperature of 40°C. At 60°C, an exothermic peak appears, with a maximum at 6.1min. At 100°C, due to the fast crystallization kinetics, the crystallization peak is masked.

In Figure 3.3-15 no crystallization is visible at 40°C after 10 minutes. At 50°C a crystallization peak appears, with a maximum at 15.1 min.

The sum of the heat of cold crystallization during annealing and the heat of crystallization during the final reheating of the same sample to the melting temperature should be equal to the heat of fusion (we make the assumption that the cold crystallization which could occur when heating the sample to the isotherm is almost null). For isothermal annealing at 50°C during 60 minutes and 60°C during 10 minutes, the heats of cold crystallization were respectively 17.1 and 15.6 $J.g^{-1}$. The heats of cold crystallization obtained during the final heating were respectively 1.8 and 0.8 $J.g^{-1}$. The sum gives respectively 18.9 and 16.4 which is slightly below the heats of fusion for annealing at 50°C, 60 min and 60°C, 10 min: 21.7 and 22.2 $J.g^{-1}$.

The heat of cold crystallization during the isotherm is probably underestimated because of the initial transient signal and because of the fact that it was not possible to estimate the crystallization during the heating ramp before the isotherm.

This method did not work for fast crystallization kinetics, as reported from results on annealing at 100°C. We then tried to study the crystallization kinetics by using a method probing the changes in mechanical properties of the sample with increasing degree of

crystallinity. In semi-crystalline polymers, the storage modulus is very sensitive to the degree of crystallinity of the sample, at least for temperatures between T_g and T_m.

A 45PB[a] polymer plate was molded and quenched. The sample was then placed in a DMA apparatus configured in single cantilever beam geometry.

In Figure 3.3-16 the storage modulus of 45PB[a] is plotted as function of time. The polymer plate was placed in the DMA at t = 0 at room temperature. A fast heating rate was then applied. During heating, the storage modulus decreases sharply down to a minimum, as the temperature of the sample becomes higher than the glass transition temperature. At t = 2 min, the storage modulus increases till t = 7.7 min, where the modulus remains almost constant.

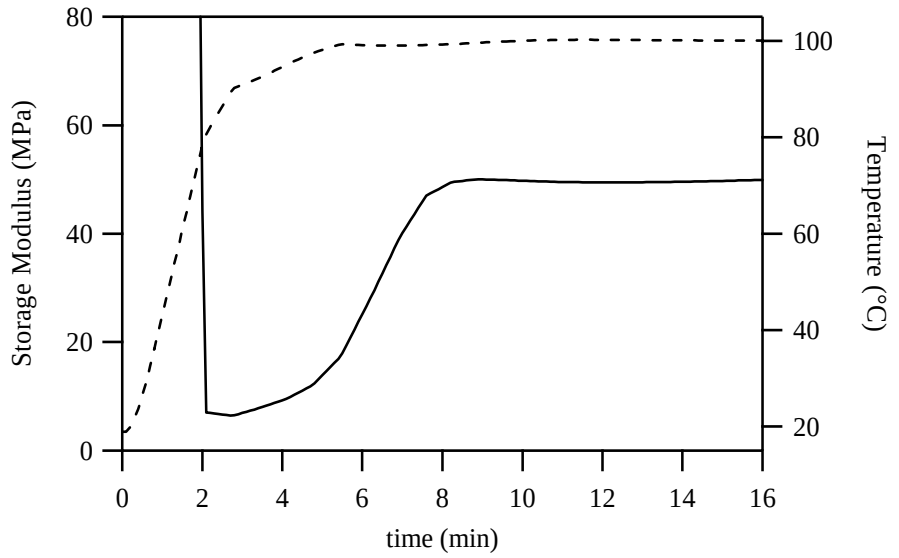

Figure 3.3-16: Storage modulus (——) and temperature (- - - - -) as a function of time.

The modulus obtained at the plateau in Figure 3.3-16 can be compared with the modulus obtained in section 2.3.2 for the sample characterization. Figure 2.3.8 in section 2 showed the variation of the storage modulus with the temperature. The sample preparation for the characterization was the same as the present one. A 45PB plate was molded at 180°C, cooled at 20°C.min-1 to 160°C and quenched in ice water. In section 2, the DMA experiment was carried out from 0°C to the melting temperature, with an average heating ramp of 0.3°C.min^{-1}, while in the present experiment the temperature was held constant at 100°C.

In Figure 2.3.8, we obtained at 100°C a storage modulus of 50 MPa, i.e. after a non isothermal cold crystallization of the sample from 50°C (onset of the cold crystallization process) to 100°C, in other words a non isothermal crystallization of 167 min. In figure 3.3-16, a plateau value of 49.5 MPa is obtained after 5.7 min of isothermal cold crystallization. Thus, we may assume that in isothermal condition the cold crystallization is almost complete after 5.7 minutes.

Figure 3.3-17 shows a comparison between the modulus data and the crystallinity obtained by DSC. We assumed that the crystallization started in the DMA experiment at t = 2.1 min, which corresponds to the minimum of the storage modulus. At this point was then plotted the degree of crystallinity obtained for the reference sample (unannealed sample) by DSC.

In the DSC experiments, the annealing time was measured from the onset of the annealing isotherm to the moment of cooling. In DMA experiments, the isotherm starts at t = 5.3 min. We have then plotted the crystallinity of the sample annealed at 100°C for 10 minutes at 5.3+10, i.e. at t = 15.3 min, and the crystallinity obtained in the DSC for a sample annealed at 100°C for 120 min at t= 125.3 min.

The storage modulus reaches a maximum at t=7.7 min after a huge increase from the point at 5.3 min (onset of the isotherm). We can consider that at this point the sample almost reaches its maximum of crystallinity. Therefore, the time to crystallize at 100°C is close to 2.4 min.

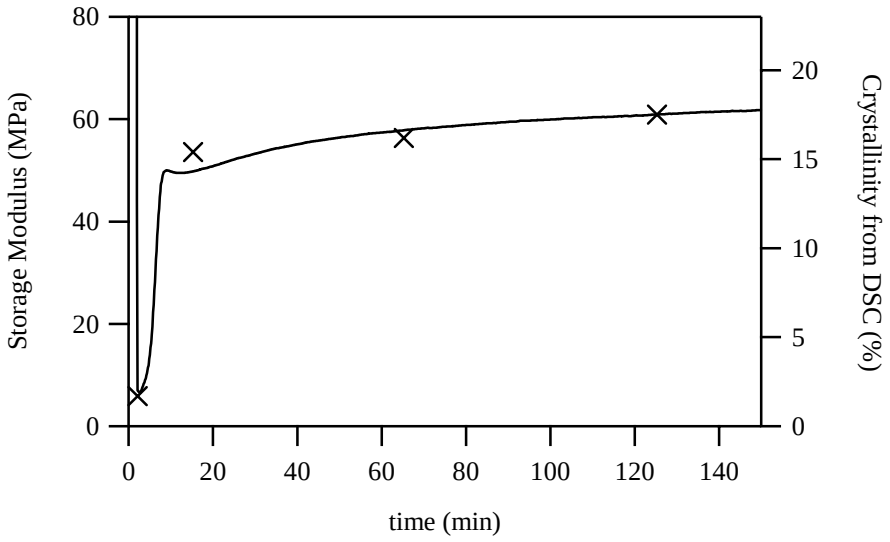

Figure 3.3-17: Storage modulus from DMA and crystallinity from DSC.

This is of course a coarse approximation, but it provides an order of magnitude of this time of crystallization at 100°C.

By making the assumption of a linear relationship between the degree of crystallinity and the storage modulus and by measuring the slope of the storage modulus as a function of time between 5.3 and 7.7 minutes, we can get an idea of the crystallisation kinetics :

1.7% ⇔ 7 MPa
17.5% ⇔ 60.9 MPa
Slope 4%.min^{-1} ⇔ 14MPa.min^{-1}

3.3.3 Observations of the samples

The microstructure at the interface of the assemblies was studied by optical microscopy. The sample preparation in both cases is described in section 2.6. For optical microscopy, the pictures have been taken under polarised light. The thickness of the microtome slices was approximately 3μm.

We will present in this section samples microtomed after the DCB test, meaning that we examined the crystalline morphology near the crack surfaces after the crack propagated through all the assembly. These results are shown in Figure 3.3-18 together with the images of the DCB test which give an idea of the degree of transparency of the sample.

The reference sample shown in figure (1), molded in the conditions used for the adhesion measurements (cooling from 180°C at 20°C.min^{-1} to 160°C then quenched in ice water), which correspond to the unannealed sample in the DSC experiments, appears optically fully amorphous, at least in the bulk, while the DSC gave a slight degree of crystallinity. The sample is transparent and no optical birefringence is observed. The difference in Young's modulus between the 45PB^{a} and the PC support makes the 45PB^{a} layer warp a little bit. However, on the left-hand side we can observe a thin bright line at the interface with the PC support. This could be a thin crystalline zone, introduced by the nucleant effect of the PC. The degree of crystallinity found in DSC can not be related to that thin layer as the unannealed sample used for the DSC experiment was composed of only one layer of 45PB^{a}. Moreover, in the DSC experiment on assembled samples, only the top layer was taken out, i.e. the first 0.2 mm. In the right hand side picture, the surface appears slightly brighter, but it is quite hard to conclude on the presence of thin crystalline layer.

In figure (2), for a contact temperature of 40°C and a contact time of 10 minutes, both the top view of the assembly during the DSC test (2a) and the optical micrograph of one part of the assembly after testing (2b), appear clearly transparent. The slight degree of crystallinity found in DSC can not be observed in the bulk but bright spots are clearly seen close to where the interface was before fracture, which could indicate some crystalline areas.

For samples assembled at 80°C for 10 min, in Figure (3a), a very slight crystallinity can be observed. In the top view taken during the DCB test, the sample appears no longer transparent. In the microtome slice (3b), a very fine spherulitic structure can be observed close to where the interface was before fracture. The bright line close to the interface is now undoubtedly present.

For a contact at 100°C for 60 minutes in Figure (4), the top view is whiter than in the previous picture and the spherulitic structure appears clearly in the side view. Furthermore another line, close to the interface, appears, which can be related to the formation of a different population of crystallites.

We may conclude from those observations that a very thin layer of crystallites is present at the very surface of the 45PB[a] sample after molding and quenching, or at least some nuclei, which will be there even for a low temperature of contact (40°C). On the other hand, for low temperatures of contact, the growth process will not really occur and the bulk will remain amorphous. At higher temperatures of contact, the crystalline zone can then spread from the interface all over the sample. The nucleating effect of the interface appears clearly from these observations and is likely to affect both the formation of the interface by molecular interdiffusion and the build up of adhesion strength.

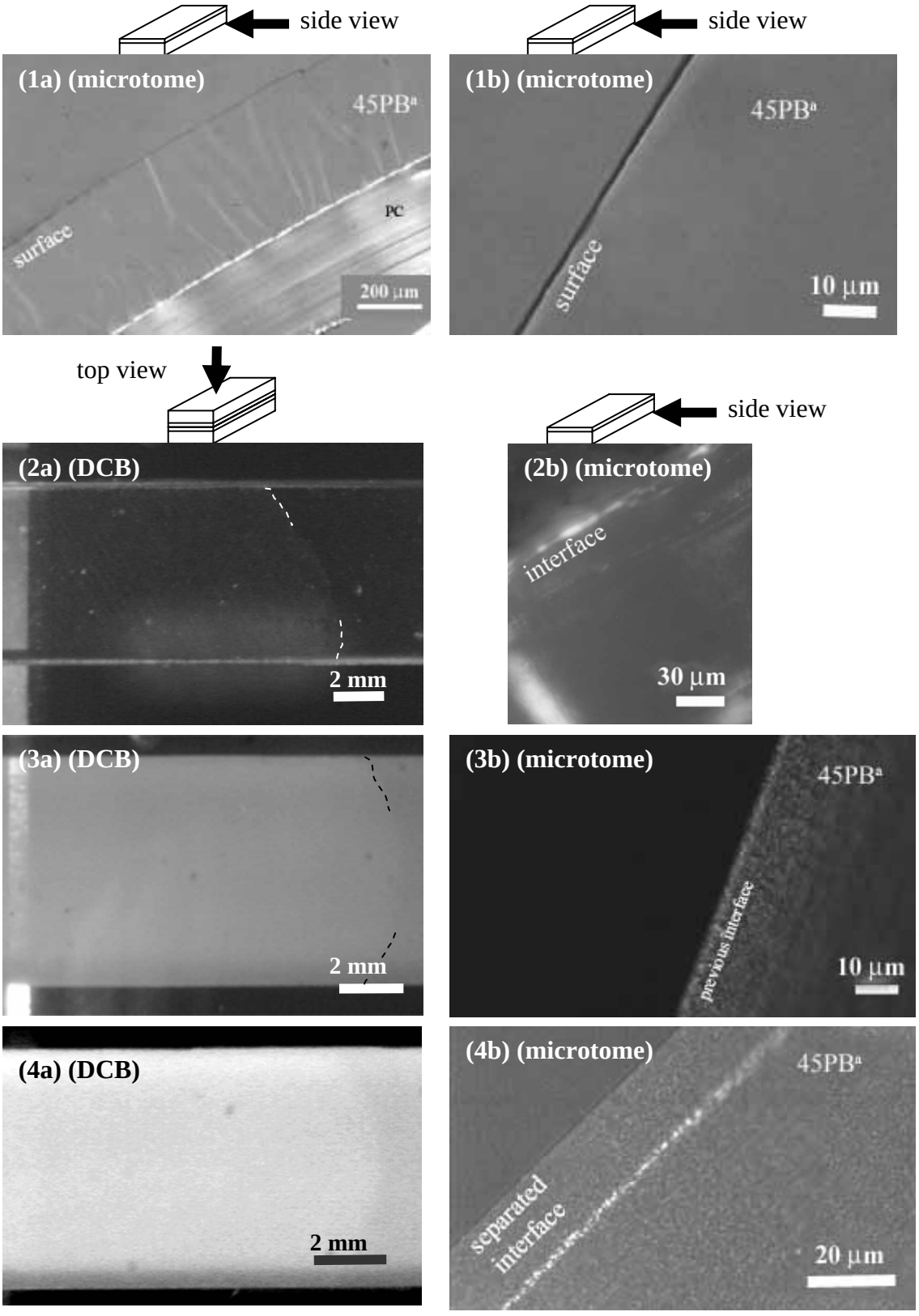

Figure 3.3-18 : images from DCB test (a) and optical micrographs of microtomed samples(b). 1 : molded sample (reference) ; 2 : assembled at 40°C for 10 minutes ; 3 : assembled at 80°C for 10 minutes ; 4 : assembled at 100°C for 60 minutes.

3.3.4 Tensile tests

In order to interpret correctly the results of the fracture tests, it is essential to obtain more information about the mechanical properties of 45PB[a] as a function of the degree and nature of the crystallinity. We performed tensile tests on bulk samples for that purpose. The details of sample preparation can be found in section 2.5 (1 mm thick plate molded at 180°C, cooled to 160°C at 20°C.min^{-1} then quenched in ice water)
After cutting the sample in a bone shape, some samples were annealed in the press in order to simulate the thermal history undergone by the polymer layer of 45PB[a] during assembling.

The tensile tests were carried out in a temperature controlled chamber at the same temperature used for the double cantilever beam tests. This temperature was chosen sufficiently below the glass transition temperature (mean value of 24°C from section 3.3-2) to avoid the changes in the mechanical properties.

Figure 3.3-19 shows the stress strain curves obtained for the reference sample (not annealed) and the annealed samples at 60 and 100°C. Table 3.3-3 summarizes the main results obtained from Figure3.3-19.

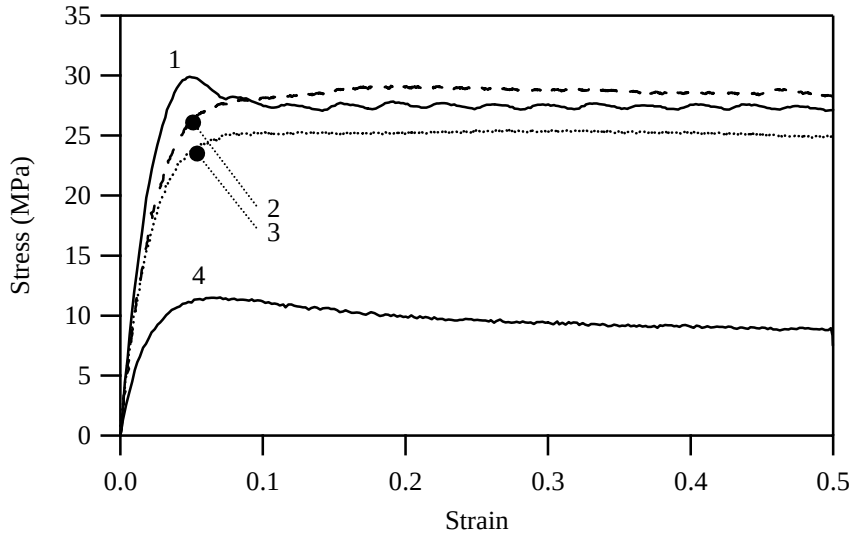

Figure 3.3-19: stress/strain curves in traction experiments.
1 : annealed at 100°C during 60 minutes
2 : annealed at 60°C during 60 minutes
3 : annealed at 60°C during 10 minutes
4 : unannealed

Table 3.3-1

T_{an}	t_{an}	σ_y	E
/	/	12	320
60	10	25	625
60	60	28	685
100	60	30	820

A real change in mechanical properties occurs between the unannealed and the annealed samples. Both the yield stress and the Young's modulus increase by about a factor of two from the reference sample to the annealed samples. This change in mechanical properties is connected of course with the cold crystallization of the sample during the annealing stage. Several additional features of figure 3.3-19 deserve further comment. First of all the absolute value of the modulus for the unannealed sample is rather high. One has to keep in mind however that the test has been performed at 15°C slightly below the T_g of the amorphous phase. It is difficult hence to infer a degree of crystallinity from this measurement alone.

Then the differences between the three annealed samples are interesting because in terms of total degree of crystallinity, they are rather similar (see figure 3.3-13). However the sample annealed at 100°C for 60 minutes has a distinctly higher and more marked yield stress than the other two samples. The plasticity after yield, although showing very little strain hardening, is different for the three annealing treatments. This result combined with the DSC curves clearly points to a reorganization of the crystalline structure without much change in the total fraction of crystallized matter. It is very likely that these changes in crystalline structure will also have effects on the fracture properties at the interface.

3.3.5 Partial conclusions on the different results on crystallinity and mechanical behavior

From sections 3.3-1, 2, 3 and 4, it appears that both the crystallinity and the mechanical properties of 45PB[a] change with thermal history and are hence likely to change during the assembling process, depending on the temperature and time of contact.

Before presenting the adhesion results, some conclusions can be drawn :

The quenched-molded sample has a very low, but not null, degree of crystallinity. However, there is no clear evidence of a presence of crystallites in the optical observations.
In the optical observation of a sample assembled at 40°C for 10 minutes, no crystallinity is revealed in the bulk but a bright line is seen at the interface, probably due to a thin layer of crystallites, which have grown from the nuclei already present in the quenched molded sample.
For a contact temperature above 60°C, the sample is crystalline, but still a brighter line appears at the interface.

Although above 60°C, the degree of crystallinity remains the same in the DSC experiments, both optical observations and tensile tests show that changes still occur (in the morphology and in the mechanical response of the sample)

3.3.6 Adhesion results

The following experimental procedure was followed for all the adhesion experiments : contact at room temperature between "amorphous" samples (molded and quenched) under a pressure of contact $P_{contact}$ and fast but not controlled heating to the contact temperature $T_{contact}$ (within 2 minutes) (see section 2) : the assembly was placed in the press which was previously heated to the temperature of contact. A controlled cooling was then applied after a certain time of contact.

The time of contact was taken from the moment of contact at room temperature to the beginning of the cooling (see section 2.4.1.3). The DCB tests were carried out at a controlled temperature of 15°C in order to be below the glass transition temperature (~24°C). The effect of the temperature of contact was studied over a 70°C range, i.e from 40°C to 110°C for two different times of contact, 10 and 60 minutes. The conditions are summarized in table 3.3-2. Detailed description of the the molding and assembling procedure can be found in section 2.4.

Table 3.3-2: experimental conditions

polymer	T_{mold} (°C)	Cooling molding (°C/min)	t_{ph} (min)	P_c (bars)	t_c (min)	Cooling assembling (°C/min)
45PB	180	2.5	10	50	10/30	40
45pb[a]	180	Quenched[(1)]	0	50	10/60	40

[(1)] the polymer plate was first cooled under the press at 20°C.min^{-1} to 160°C then quenched (see section 2.4.1.3)

During the fracture tests, the crack propagation often occurs intermittently in a stick-slip manner exhibiting characteristic G_c values for crack initiation and crack arrest. An example of this "unstable" crack growth is given in Figure 3.3-20 for a sample assembled at 40°C for 10 minutes and a sample assembled at 110°C for 10 minutes. The camera takes one picture every 2 minutes, and the opening displacement was fixed at 0.5 mm.min^{-1}.

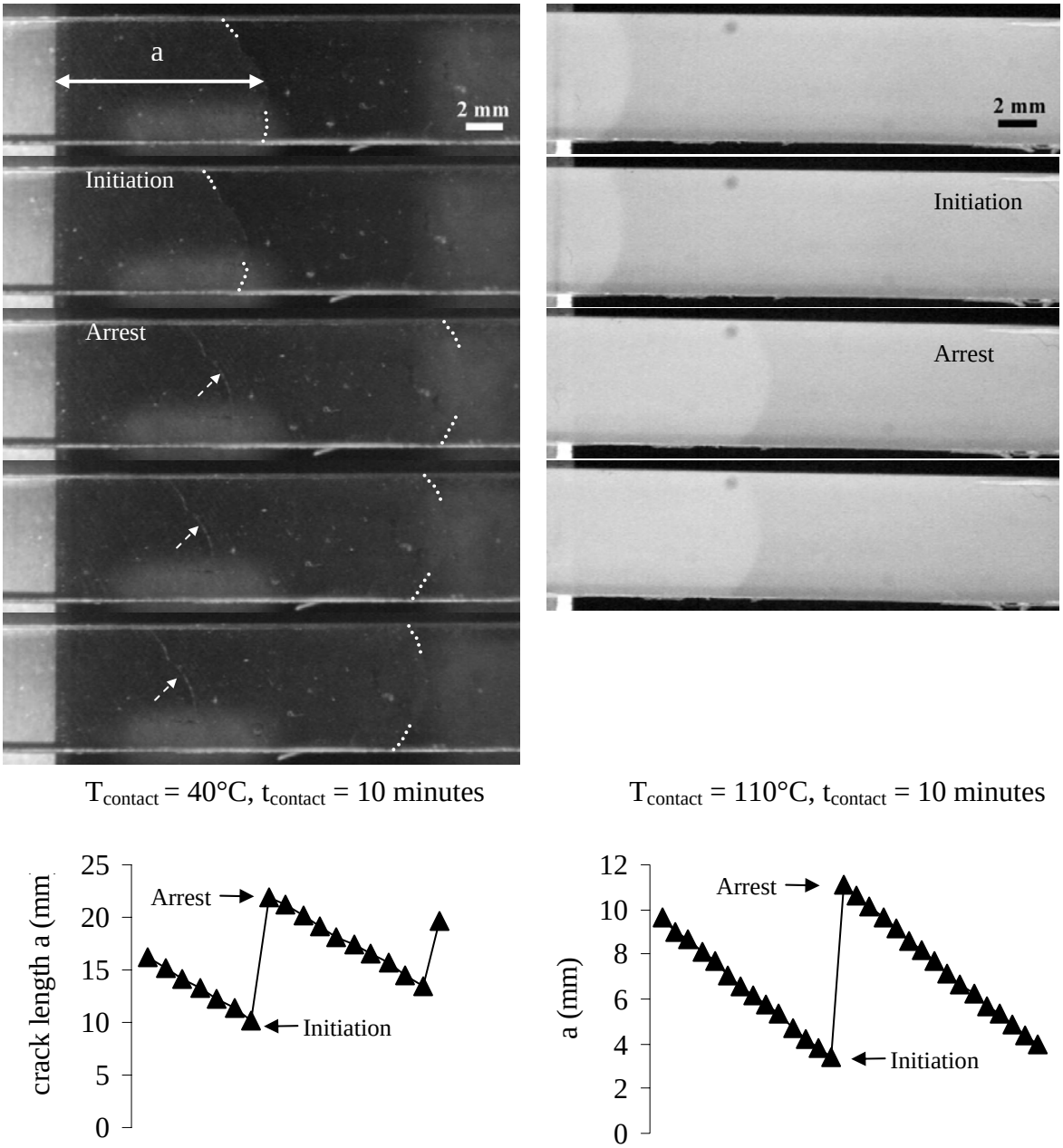

Figure 3.3-20 : Stick slip behavior during the DCB test (carried out at 15°C).

The behaviour schematically described in Figure 3.3-21 is typically what causes the stick slip behavior. Based on figure 3.3-20, the crack does not move at all until the initiation point and then moves rapidly toward a new position, within less than one second. This behaviour is caused by what is called crack blunting . The crack remains pinned at the same position but its shape changes and progressively blunts as schematically represented in Figure 3.3-21.

Figure 3.3-21 : schematic representation of the crack blunting phenomena.

In figure 3.3-20 after the first initiation of the crack, the deformation caused by the previously blunted crack is clearly visible (white arrow).

In the case of a stick-slip behavior, both the values of G_c for crack initiation and for crack arrest are meaningful. We have chosen to discuss first the G_c values for the crack arrest.

In Figure 3.3-22 the G_c values for crack arrest are reported as a function of the contact temperature for 10 minutes of contact time. The two open symbols correspond to the G_c result of "crystalline" 45PB shown in section 3.2.

As expected, a certain degree of self-adhesion is obtained for 45PB^a at temperatures for which the self adhesion of crystalline 45PB is null. However, the measured fracture toughness is surprisingly low for all temperatures of contact. For contact temperatures going from 40°C to 80°C, the adhesion remains very weak. The samples are almost amorphous and after the fast heating, when the temperature reaches the temperature of contact, the temperature at the interface is well above T_g and interdiffusion should in principle occur rather rapidly.
At 40°C and 50°C, DSC results have shown that the sample was still rather amorphous after 10 minutes (for isothermal crystallization at 50°C, the cold crystallization peak reaches its maximum after 15 minutes only). Hence, interdiffusion is not efficient in that case for the interface reinforcement.
At 60°C and 80°C, the sample does crystallize during the 10 minutes of contact. The adhesion remains very weak. The cold crystallization does not reinforce the interface. The fracture toughness levels up only at 90°C. The adhesion at 100°C for 45PB^a is small but not null, while the adhesion of "crystalline" 45PB is equal to zero. At 110°C G_c for "crystalline" 45PB is higher.

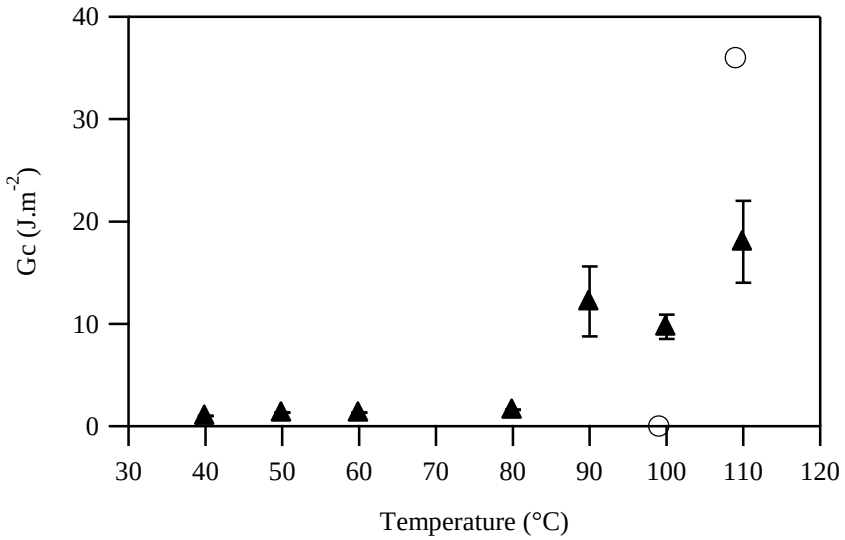

Figure 3.3-22a : fracture toughness after 10 minutes of contact:
◢ 45PB[a] crack arrest value
⬭ "crystalline" 45PB.

In figure 3.3-22b, the fracture toughness after 10 minutes of contact is presented in logarithmic scale along with the DSC curve of "crystalline" 45PB (see section 3.2 : sample molded, cooled at 2.5°C.min^{-1} and annealed in the press at 100°C for 10 minutes) and the curve obtained for a sample assembled at 100°C during 10 minutes.
We can stress that the fracture toughness goes through a maximum at 90°C, which corresponds to the first melting peak in the DSC curve for 45PB[a].

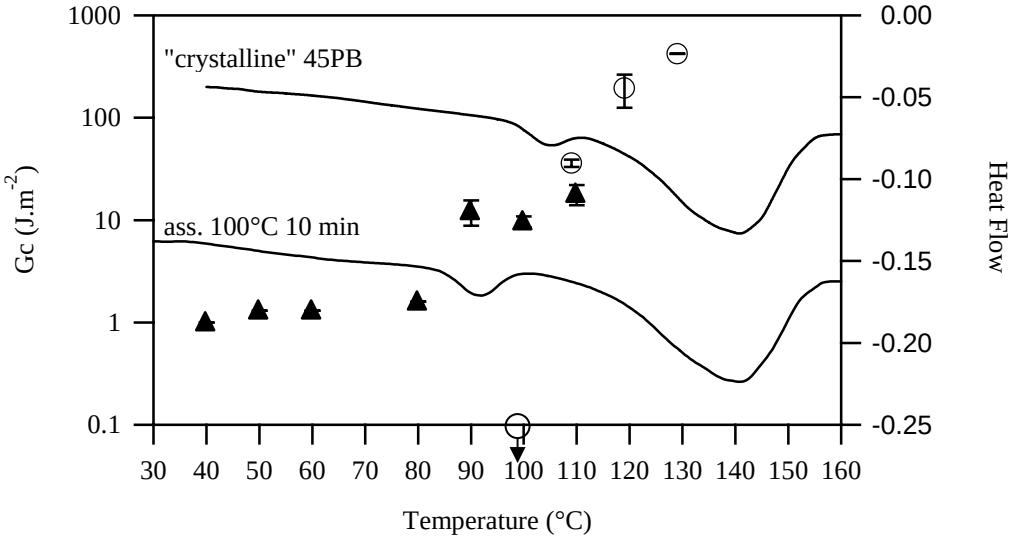

Figure 3.3-22b : DSC curves for 45PB and 45PB[a]
and fracture toughness after 10 minutes of contact:
◢ 45PB[a] crack arrest value
⬭ "crystalline" 45PB.

Figure 3.3-23 shows the effect of increasing the time of contact from 10 to 60 minutes. At 40 and 50°C, the values of the fracture toughness after 10 and 60 minutes annealing time are identical. At 40°C, the bulk crystallinity after 10 minutes is close to the crystallinity after 60 minutes contact, but at 50°C, the bulk crystallinity changes completely between 10 and 60 minutes. This has no effect on the value of G_c for the crack arrest. At 60°C and above, the difference in G_c between 10 and 60 minutes of contact increases. At 110°C, the fracture toughness after 60 minutes is even larger than the adhesion after 10 minutes for the "crystalline"45PB. Above 80°C, the sample starts melting and recrystallizing (see Figure 3.3-23b), and the time becomes an important parameter. After the first melting peak is over however, the degree of adhesion decreases and we get the same result after 10 or 60 minutes of contact (the point at 100°C).

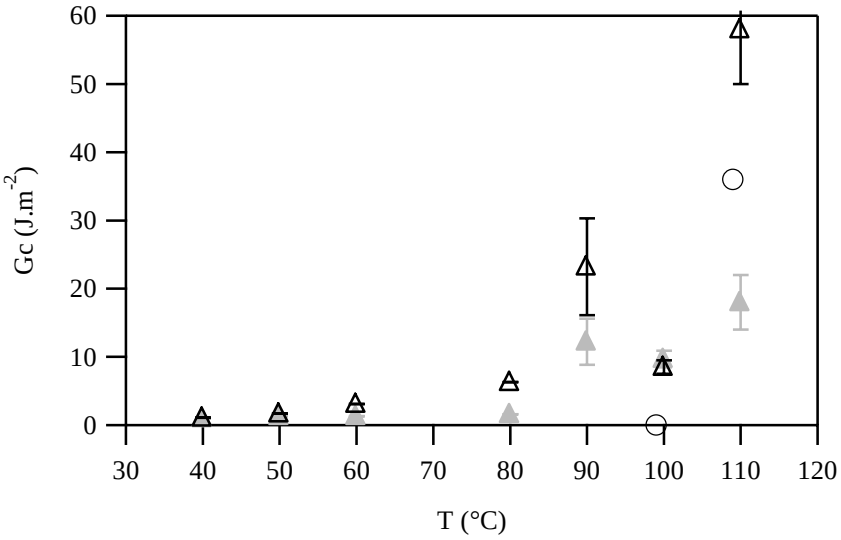

Figure 3.3-23a : fracture toughness for 45PB[a] after 10 minutes contact ▲ and 60 minutes contact △ (crack arrest)

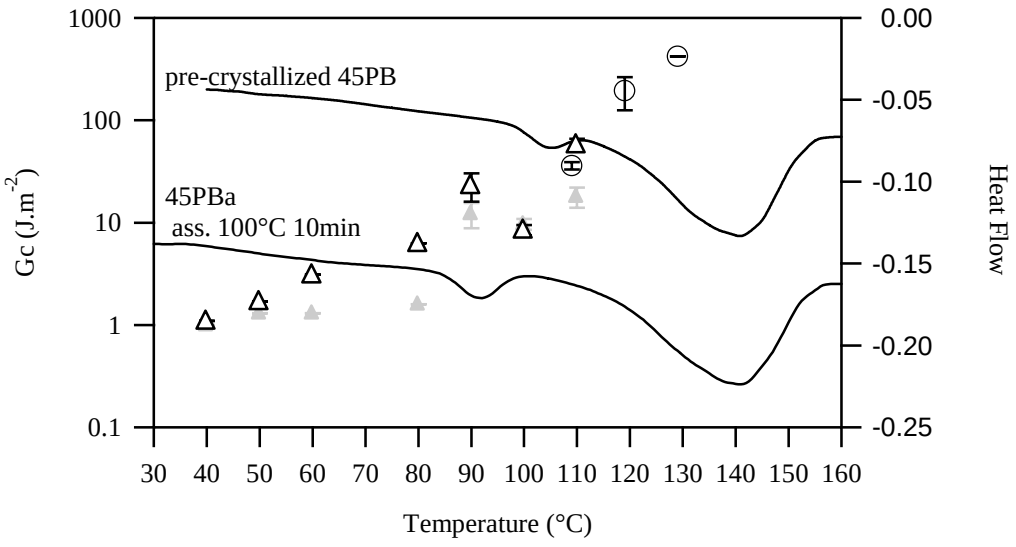

Figure 3.3-23b : DSC curve for 45PB and 45PBa and fracture toughness after 10 minutes contact ▲ and 60 minutes contact △ (arrest)

In figures 3.3-24 (a) and (b) both the crack initiation and the crack arrest values are represented in a logarithmic scale, for respectively 10 minutes and 60 minutes of contact time. The amplitude of the stick-slip process (i.e. the difference between crack arrest and crack initiation) varies with the temperature of contact. The difference in fracture toughness between crack initiation and crack arrest goes through a minimum around 60°C for 10 minutes of contact time and 50°C for 60 minutes of contact time.

The fracture toughness for crack arrest is more representative of the intrinsic strength of the interface because the system is at equilibrium and we think that the deformed region at the crack tip is small and localized. On the contrary, when the crack initiates, the system is indeed out of equilibrium, and the deformation at the crack tip is important. However the magnitude of the stick slip process indicates the propensity of the bulk to develop blunting.

From Figures 3.3-24ab, three main regions can be distinguished. In region I, the samples are amorphous, at least in the bulk according to both the DSC results and the optical observations in figure 3.3-18. The fracture toughness for the crack arrest is very weak but not null, and increases very slowly for 10 minutes of contact time and a little bit faster for 60 minutes of contact. The Yield stress and Young's modulus are close to the value obtained for the unannealed sample, and are relatively low compared to the values obtained for a crystalline 45PB. Hence, even if the adhesion is weak, the crack can blunt more easily than for the crystalline 45PB, leading to a surprisingly high value for the crack initiation. The fracture toughness for the crack initiation decreases with the temperature of contact, and a minimum value is obtain at 60°C for 10 minutes of contact and 50°C for 60 minutes of contact. This behavior is certainly linked to the mechanical properties of the 45PB[a], as we showed that both the Yield stress and the Young's modulus increased with the degree of crystallinity (see Figure 3.3-19). With almost constant interfacial strength, the increase in the bulk mechanical properties hinders the blunting of the crack.

In region II, the maximum degree of crystallinity is reached. No discontinuity was found in the fracture toughness for the crack arrest, while the value for the crack initiation goes through a minimum. Above 60°C, the toughness obtained for crack initiation changes with the temperature of contact in a rather complex way. We have a competition between the increase in interfacial strength with the temperature of contact, which can enhance the blunting of the crack, and the change in bulk properties by an slight increase or a reorganization of the crystallinity, which can in some cases reduce the degree of blunting. Although the degree of crystallinity does not change so much above 60 °C, the mechanical properties still change as seen in figure 3.3-19.

The beginning of region III correspond to the onset of the fusion process of the DSC curve obtained for an assembled sample at 100°C for 10 minutes. At this point the fracture toughness for the crack arrest value increases sharply, breaking the continuous increase of the region I and II. We assume that the DSC curve obtained for the assembled sample gives a reliable onset of the fusion process for the sample assembled at 90°C and

above. In this regime, the melting of the smallest crystals gives sufficient mobility for the chains to interdiffuse somehow.

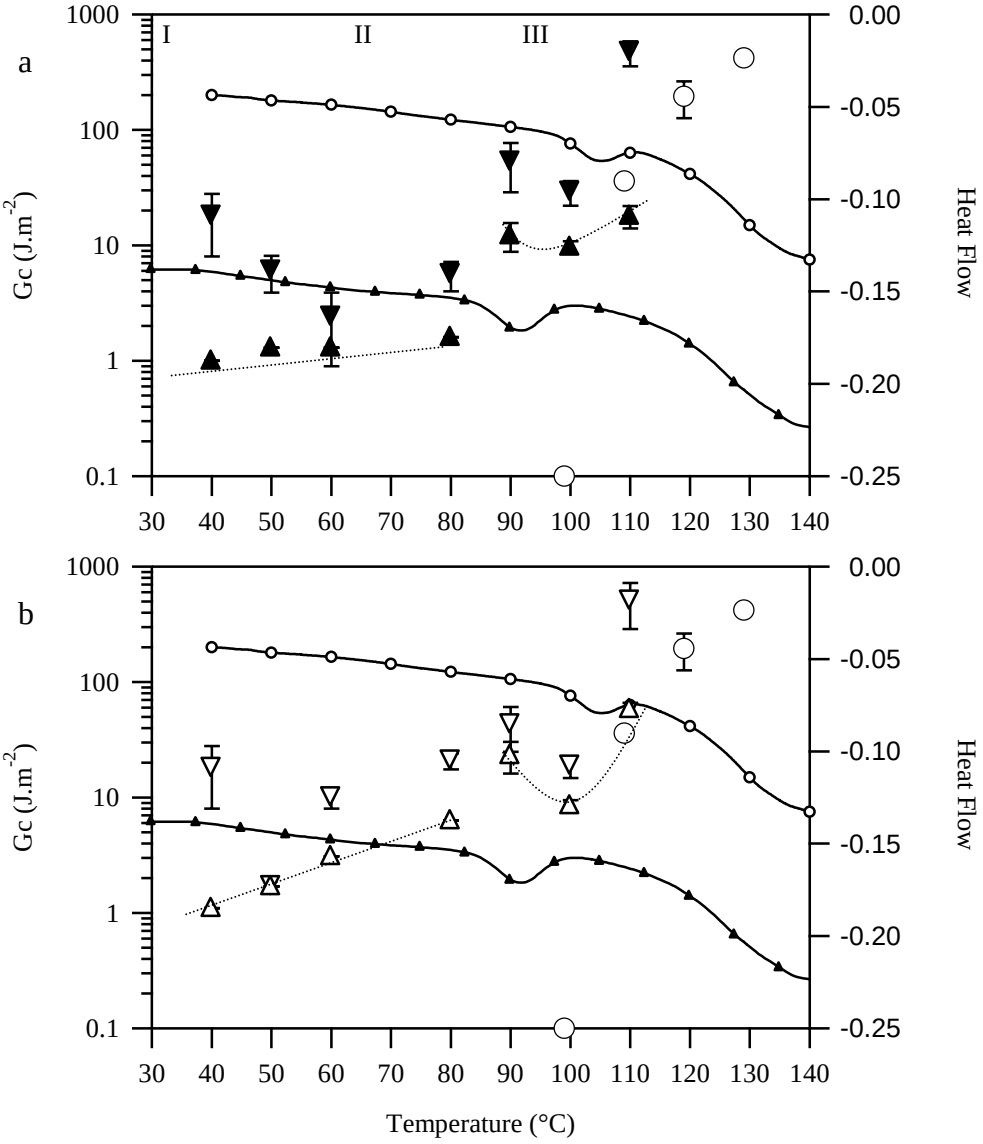

Figure 3.3-24 : fracture toughness after 10 (a) and 60 (b) minutes contact :
◢△ 45PB[a] crack arrest value ◤▽45PB[a] crack initiation value
○ "crystalline" 45PB.

3.3.7 Crack tip observations (optical and TEM)

Crack tip observations were made on assemblies welded at different temperatures. The experimental procedure can be found in section 2.6.
We used both optical and electron microscopy.

Figure 3.3-25 shows an optical micrograph for a temperature of contact of 40°C and a time of contact of 10 minutes. Due to the difference between the Young's modulus of 45PB[a] and the PC, we did not succeed in obtaining a flat surface of 45PB[a]. Despite the presence of waves, the crack can be observed. In the image on the right, the crack tip is far from being straight.

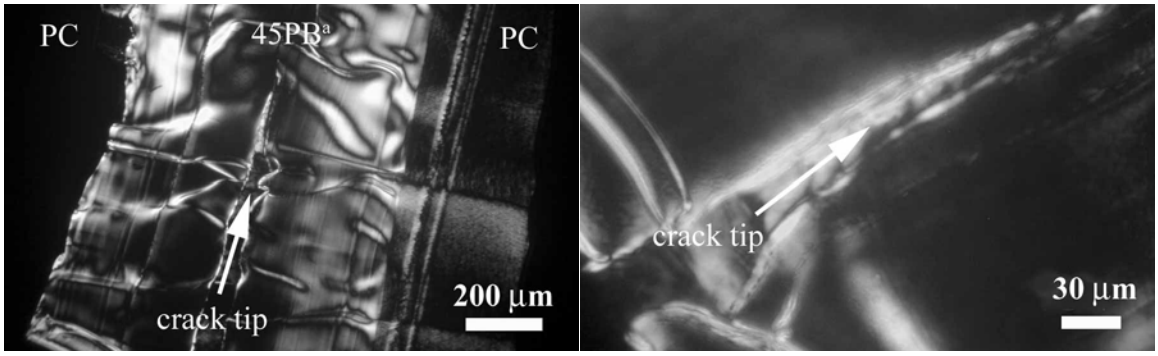

Figure 3.3-26: assembly ($T_{contact}$ = 40°C, $t_{contact}$ = 10 min), crack tip view.

Figure 3.3-25 shows the crack tip for a sample where the contact was made at 100°C for 10 minutes. The crack tip appears to be sharper than for a contact made at 40°C. No plastic zone is visible ahead of the crack tip.

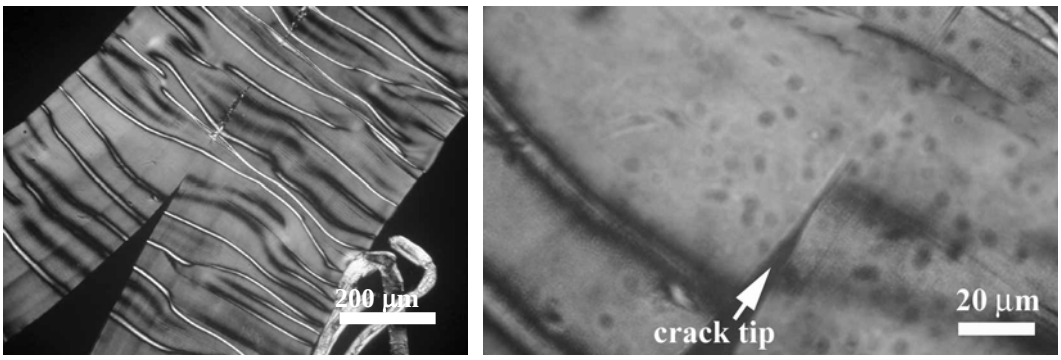

Figure 3.3-26: assembly ($T_{contact}$ = 100°C, $t_{contact}$ = 10 min) crack tip.

In Figure 3.3-27, the crack tip for a contact at 110°C during 10 minutes is shown. In that case, the crack has a blunt shape and the interface was found to be very strong.

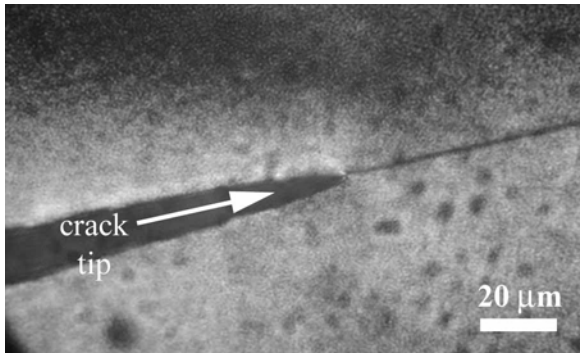

Figure 3.3-27: assembly ($T_{contact}$ = 110°C, $t_{contact}$ = 10 min), crack tip

The sample assembled at 110°C for 10 minutes has been also observed in TEM (see the sample preparation in section 2.6). The micrographs are shown in Figure 3.3-28. An important deformed area is visible around the crack tip (part b). This part has been degraded by the etching process and is quite damaged. The crack tip is not sharp but blunted. The interface, ahead of the crack (part a) appears to be quite rough. No lamellas seem to cross the interface. The area of the crack looks quite damaged. This can explain a high level of energy dissipation near the crack tip and therefore the high value of fracture toughness obtained in section 3.3.6 for that sample.

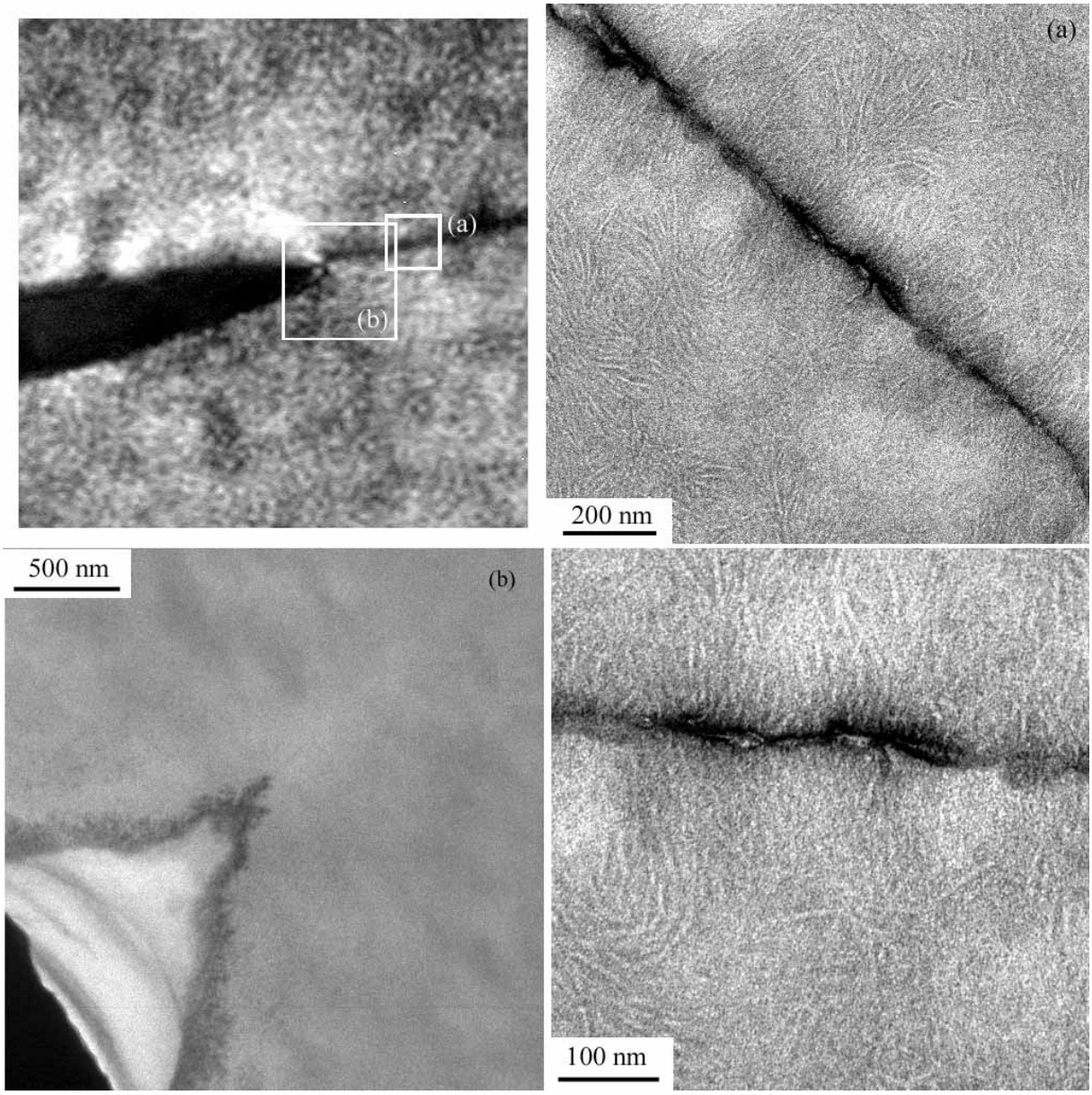

Figure 3.3-28: TEM micrographs (sample assembled at 110°C during 10 min)

3.3.8 Conclusions

In order to get self adhesion between “crystalline” 45PB, the temperature of contact should be above the onset of the fusion process. At 100°C, the adhesion was found null for 45PB, while well above Tg.
Since 45PB crystallizes very slowly, we could prepare nominally amorphous plates (transparent) of 45 PB. For these amorphous samples, a weak adhesion was obtained for all contact temperatures below 100°C.

Interestingly, when the temperature of contact was between 20°C and 40°C above Tg, the adhesion after 10 or 60 minutes contact was still found very weak, while nominally, the DSC results showed that the sample remained almost amorphous at those temperatures. Interdiffusion at the interface seems to be inefficient for the reinforcement of these interfaces.

The presence of a very thin crystalline layer at the interface, which could prevent, or at least strongly hinder interdiffusion, is hence a possibility which has been investigated. The DSC revealed a very low degree of crystallinity even for the molded-quenched sample. The optical evidence of the existence of such an interfacial crystalline layer is not clear in the case of the “unannealed” sample but is more obvious in the sample assembled at low temperature.
The low values of G_c measured for the samples put in contact between 40°C and 90°C strongly suggests that there is no “co-crystallization” across the interface but rather an independent crystallization on each side of the interface with some limited interpenetration in the amorphous phase.

It is important to point out that we observed a stick-slip propagation in all fracture tests in the case of 45PB^a, presumably because of its low yield stress due a low degree of crystallinity, which favours crack blunting. However the magnitude of the stick slip effect varied significantly depending on the exact conditions under which the interface was formed. This suggests a subtle coupling between bulk and interface properties which both vary with the interface annealing conditions. Given this complexity, a detailed model of the influence of annealing conditions at the interface on the fracture propagation behaviour remains beyond our reach.

Above the onset of the fusion process, adhesion in the case of “crystalline” 45PB was found bigger than the adhesion for 45PB^a if we take the fracture toughness for the crack arrest. If the crack blunts, we get indeed a bigger adhesion (G_c value for the crack initiation). This result suggests again that the details of the bulk properties of the polymer near the interface matter for the self-adhesion properties.

3.4 PBI

PBI has a crystalline structure (see WAXS experiments in section 2.3) and a crystallisation behavior (see standard DSC experiments in section 2.3) different from those of PBT and PBT-PBI copolymers.

Contrary to what was found for the PBT and for the copolymers, it was experimentally difficult to obtain crystalline PBI simply by cooling it from the melt, even very slowly. This results from the extremely slow crystallisation kinetics observed for this polymer. Hence, the self-adhesion experiments reported in this section were all carried out following the same experimental procedure as for the 45PB^a samples (see section 3.3), i.e. we overmolded a 300 μm thick layer of PBI on top of a stiff 2 mm thick polycarbonate plate in order to keep a reasonable modulus for the beam of the DCB test (see section 2.4.2.1).
PBI individual reinforced plates were quenched from the melt state (30°C above the melting temperature), then the DCB samples were prepared by putting two of those reinforced plates in contact at room temperature, i.e. presumably in the amorphous state, and heating them to the contact temperature $T_{contact}$. In this situation, the increase in temperature while the interface is formed should favour both cold crystallization and mutual diffusion.

As for 45PB^a, adhesion experiments were carried out from a temperature of contact just above T_g (40°C) up to a temperature of contact below the melting point.

The preliminary remarks on 45PB^a about the changes of the polymer properties during the time where contact is established at the interface, are indeed relevant in the case of PBI. Because of the very slow crystallization kinetics of PBI, a detailed understanding of the crystalline structure and the mechanical properties is even more vital in the case of PBI, if one hopes to interpret the adhesion results. Hence we chose to start this chapter by the study of the evolution of the degree of crystallinity, crystalline structure and mechanical properties with the thermal history of the bulk polymer, before presenting the results of fracture toughness of the interfaces as a function of contact temperature and contact time.

3.4.1 Characterization of the crystallinity of PBI by DSC

In section 2.3 PBI appeared fully amorphous and no cold crystallization was seen in the standard DSC curve (granule melted at 260°C, cooled to -50°C at 5°C.min^{-1} and heated at 5°C.min^{-1} to 200°C).

Additional DSC experiments were carried out to characterize the degree of crystallinity of the PBI samples before and after contact. The experimental procedure is very similar to the one used for 45PB^a, as the experimental procedure used for adhesion was similar to

the one used for 45PB[a] (contact between amorphous PBI at room temperature, rapid heating to the contact temperature and cooling) (see section 3.3.1 for more details).

The two DSC procedures applied to PBI can be found in section 3.3.1 and are summarized in Figures 3.3-1 and 3.3-2 with PBI instead of 45PB[a]. In the first procedure, a polymer plate, 2 mm tick was molded-quenched and a part of it was annealed in the DSC, while in the second procedure the PBI upper layer was taken from a fractured assembly and directly placed in the DSC.

In Figure 3.4-1, the DSC curve obtained in the case of a molded-quenched sample unannealed is compared to the curve obtained for a granule in a standard procedure. No fusion peak appears in the standard curve, while the curves for the molded-quenched samples, unannealed, show a small endothermic peak. The unannealed sample is clearly not fully amorphous. Moreover, in this case, a very flat exothermic peak is seen, meaning that the sample has a tendency to cold crystallize a little. We may think that in the case of the unannealed sample, nuclei were formed during the cooling step in the press. Those nuclei allowed a cold crystallization during the heating ramp in the DSC.

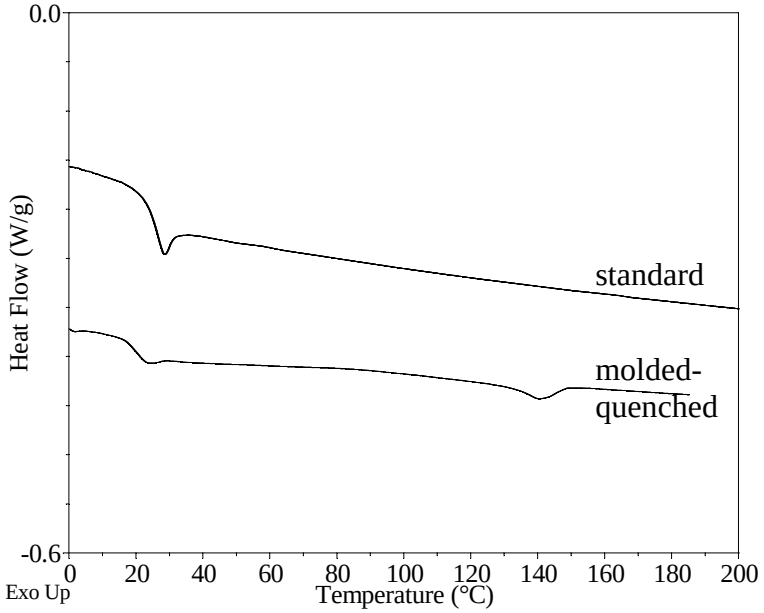

Figure 3.4-1 : DSC scans at 5°C.min^{-1}: standard procedure and molded-quenched plate (unannealed)

Figure 3.4-2ab shows the total heat flows obtained in the case of annealed samples (a) (in the DSC from a molded-quenched sample) and assembled sample (b) at different temperatures and times. For the annealed sample, no cold crystallization seems to occur, thus the melting peak corresponds to the fusion of the crystals already present after the annealing step, while for the assembled sample, cold crystallization appears at each temperature but with a different magnitude. From the presence of a cold crystallization in the assembled samples only, we can conclude that the interface enhanced the formation of nuclei, which promoted cold crystallization during the last heating ramp.

The cold crystallization peak has a maximum value for the assembled sample at 70°C for 10 minutes. After assembling the sample at 70°C for 60 minutes, the cold crystallization peak is smaller and shifted to higher temperatures. We think that the cold crystallization really starts between 10 and 60 minutes at 70°C, and then, after 60 minutes of contact, a first cold crystallization had already occurred, and it becomes more difficult to cold crystallize in the time of the heating ramp in the DSC.

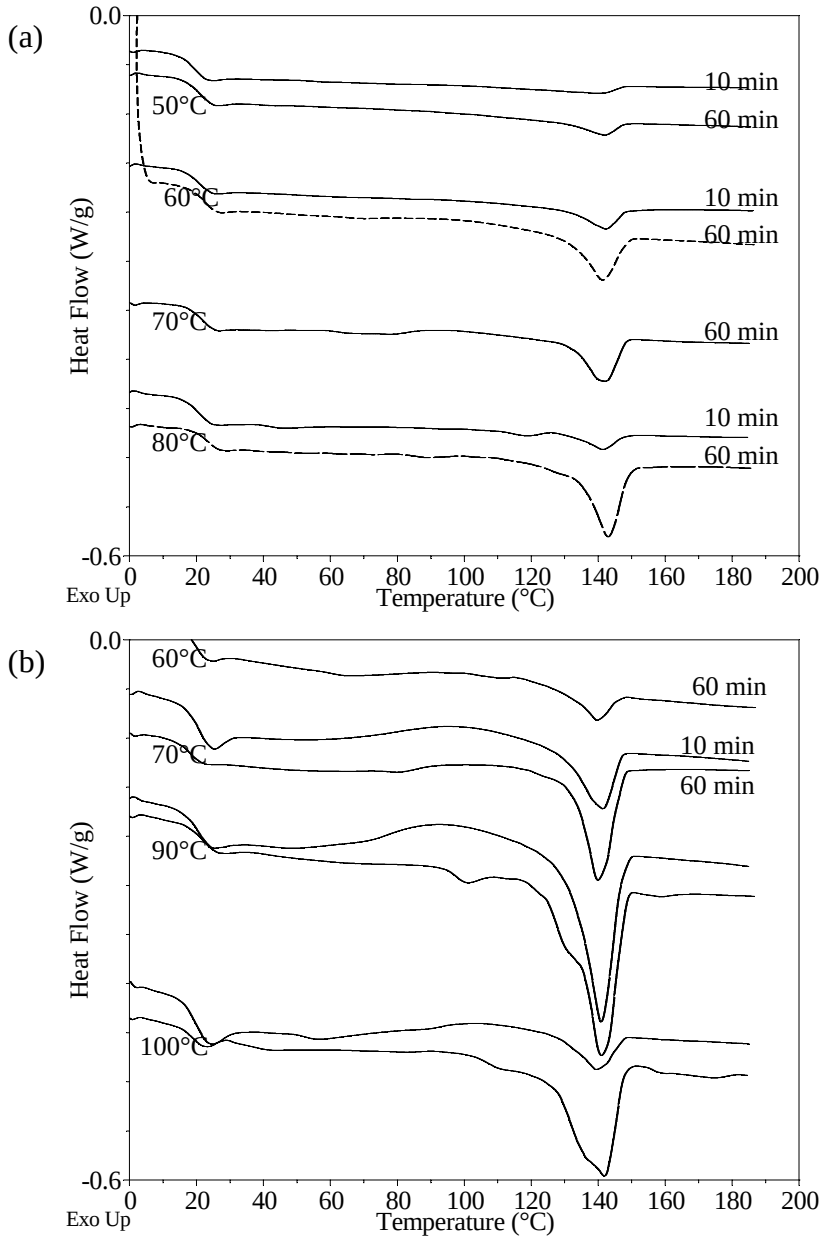

Figure 3.4-2: total heat flow for annealed sample (a) and assembled samples (b).

The comparison between the annealed and the assembled samples provides some clues to analyze the crystallization behavior of PBI.

In the case of samples annealed in the DSC, a small melting peak is present in all the curves, even for the unannealed sample. The presence of this small peak means that the molded-quenched samples have a very low but not null crystallinity. This peak remains roughly identical at each temperature for 10 minutes of annealing and increases between 10 and 60 minutes of annealing.

In the case of assembled samples, the curves look quite different, mainly due to the presence of an exothermic peak in each curve, which corresponds to cold crystallization. The peak of fusion is more pronounced for assembled samples (see for instance the samples annealed or assembled at 70°C for 10 minutes). This difference can be partly explained by the additional cold crystallization in the case of the assembled samples. However, subtracting the cold crystallization heat to the heat of fusion for assembled samples, we still obtained a higher value of the heat of fusion for the assembled samples, which can be quantitatively seen in figure 3.4-4 where the degree of crystallinity is plotted after subtracting the heat of cold crystallization.

Several ideas emerge from these observations. First, very small crystallites have probably been nucleated at the surface during the cooling step in the press leading to this very low degree of crystallinity even for the molded quenched sample. By annealing this sample in the DSC for 10 minutes, the crystallinity does not change within 10 minutes, and no cold crystallization is observed in the last heating ramp. However, for an annealing time of 60 minutes, the overall degree of crystallinity increases. We assume that for the annealed samples, within 10 minutes the crystallinity does not really change, and we thus just observe the melting of the crystallites already present after the molding step. After 60 minutes however, the bulk has started its cold crystallization. In the case of assembled samples, within 10 minutes, the overall crystallinity remains at the same level than for the annealed samples (see Figure 3.4-4), but the cold crystallization in the last heating ramp is enhanced compared to the annealed samples. After 60 minutes of contact, the overall crystallinity of the assembled samples is higher compared to the annealed samples, and the cold crystallization is also enhanced.

We think that in the case of assembled samples, the nucleation process is activated by the presence of the interface and produces a large amount of nuclei during the time of contact. In other words, the balance between nucleation and growth is not the same for the annealed and assembled samples and nucleation is favored in the latter case.

Figure 3.4-3 shows the non-reversing and total heat flows for an annealed sample at 100°C during 40 minutes and for an assembled sample at 100°C for 60 minutes. The curves for the assembled samples are similar to those obtained for annealed samples, even if the times of contact or annealing are not exactly the same. Contrary to figure 3.4-2 (60°C) where cold crystallization occurred for the assembled sample or Figures 3.4-3 and 3.4-4 (70°C and 80°C) where reorganization-recrystallization occurred during melting, the four curves in Figure 3.4-5 show only one endothermic peak. At 100°C the growing process is sufficient enough to produce well defined crystals. This more stable state prevents the sample from cold-crystallizing during the last heating ramp. Hence two melting peaks can be seen on the total heat flow, indicating the presence of a population of smaller crystallites.

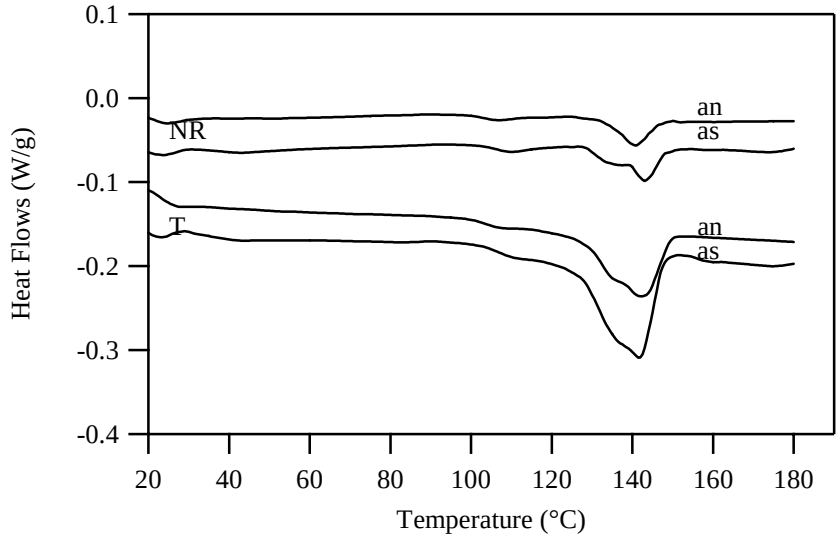

Figure 3.4-3: non-reversing and total heat flows of samples annealed at 100°C for 40 minutes and assembled at 100°C for 60 minutes.

In figure 3.4-4 the calculation of the degree of crystallinity has been performed in each case, applying Equation 3.3-1 (see section 3.3.1), assuming $\Delta H_m^0 = 125 J.g^{-1}$ for the heat of fusion of perfectly crystalline PBI (after Righetti et al. [1])

The unannealed sample has a degree of crystallinity different from zero (1.8%), as can be seen in Figure 3.4-1. However, in the case of the standard procedure, the sample is completely amorphous, whereas the cooling before the last heating ramp was $5°C.min^{-1}$ instead of more than $20°C.min^{-1}$ for the unannealed sample. Hence, we can assume that some nucleation has occurred in the case of the molded-quenched sample, that gives at least a slight amount of crystallinity.

The degree of crystallinity remains very low after an annealing or a contact time of 10 minutes over the complete range of temperatures. After 60 minutes, the degree of crystallinity increases gradually with increasing temperature. Assembled samples have a higher crystallinity, roughly 5% more, than annealed samples. The presence of an

[1] Righetti, M. C. et al, A. Macromolecular Chemistry and Physics, 199: 2063-2070, (1998).

interface must enhance the nucleation step, important in the case of PBI which has slow crystallization kinetics.

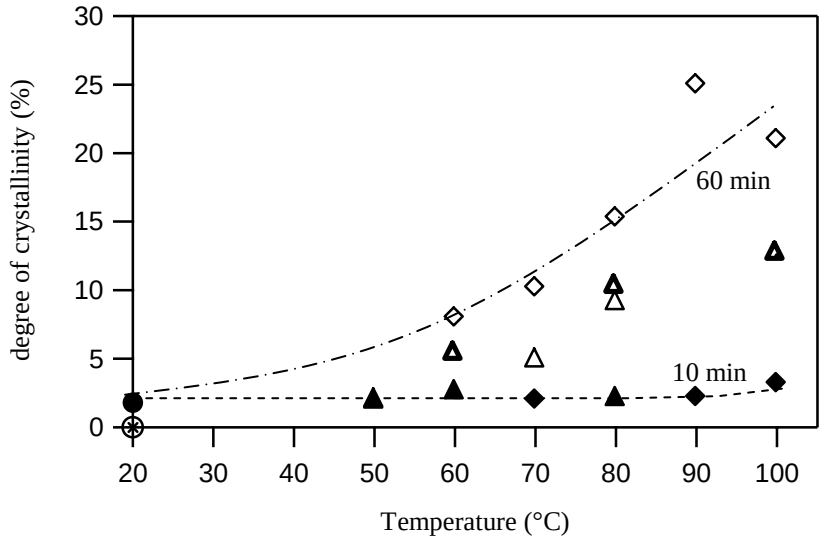

Figure 3.4-4: degree of crystallinity.
samples annealed ▲ or assembled ◆ for 10 minutes
samples annealed △ or assembled ◇ for 60 minutes
samples annealed for 40 minutes ⧋
sample unannealed ● and standard procedure ⊗

We may conclude from the DSC experiments, that :

- Nucleation occurs during the quenching of molded samples, while nothing happens for a granule that undergoes the standard procedure.
- During contact, we have a balance between the nucleation and the growth process, which depends on temperature.
- The degree of crystallinity increases gradually with temperature for a time of contact longer than 10 minutes.

3.4.2 Crystallization kinetics

Thanks to the DSC experiments, the degree of crystallinity of the samples before and after contact is known. As for 45PB[a], we tried to investigate the crystallization kinetics. Contrary to 45PB[a], the heat flow recorded during an isotherm annealing was difficult to interpret. The very slow crystallization kinetics produces a very flat cold crystallization peak which was difficult to see properly.
In Figure 3.4-5 the degree of crystallinity obtained for samples annealed or assembled at 100°C is plotted as a function of time. No maximum seems to be reached, even after 140 minutes. Although very slow, the cold crystallization seems to go on even after 140 minutes at 100°C.

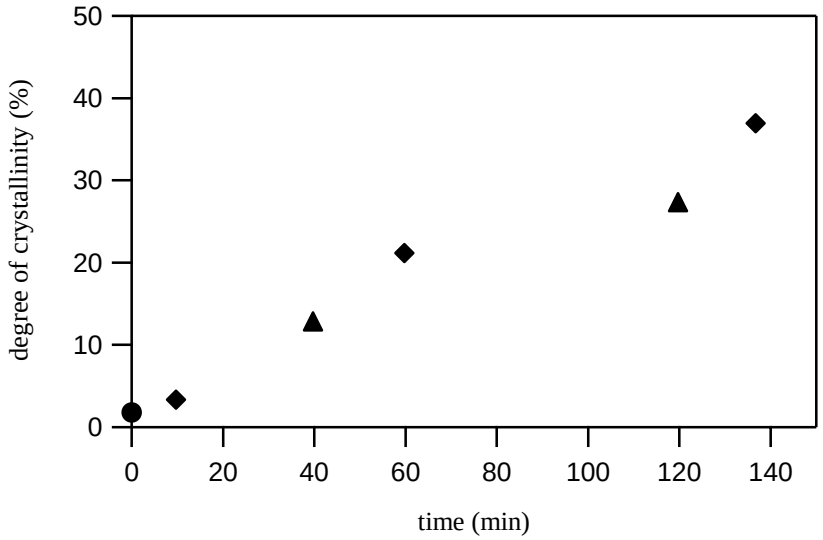

Figure 3.4-5: degree of crystallinity.
samples annealed ▲ or assembled ◆ at 100°C
sample unannealed ●

DMA experiments were carried out on a molded-quenched sample (2 mm thick, cooling from 180°C to 160 at 20°C.min^{-1} then quenched in ice water) as described in section 3.3-2. The results are presented in Figure 3.4-6. Like for 45PB^{a}, a horizontal shift of 7 minutes was applied to the data from the DSC (see section 3.3-2).

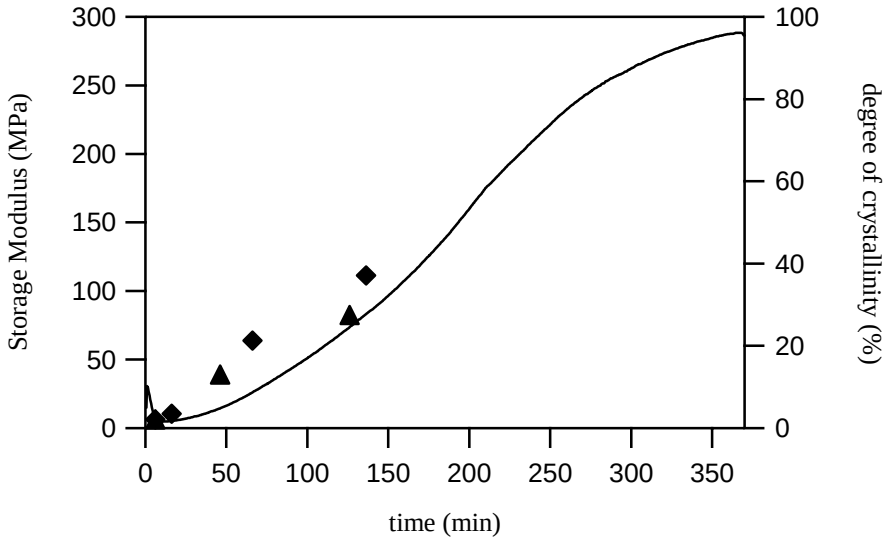

Figure 3.4-6: Storage modulus at 100°C from DMA and degree of crystallinity from DSC.

In figure 3.4-6 the storage modulus reaches a maximum after 350 minutes only. Although the assumption of a linear relationship between the degree of crystallinity and the mechanical behaviour of PBI is indeed wrong, this result underlines the fact that the mechanical properties of PBI are still changing after 140 minutes at 100°C, so does the crystallinity.

3.4.3 Samples observations

The microstructure of the assemblies was studied by optical microscopy. The sample preparation conditions can be found in section 3.2.

We will present some top views of the samples during the DCB test together with side views, obtained by microtoming the sample (post DCB test). The different views are given in Figure 3.4-7.

Image (1) is the side view of a molded quenched sample. It corresponds more or less to the “unannealed” sample in the DSC experiments. In this case, PBI is molded on its PC substrate while for the DSC experiment a 2 mm PBI plate was used. However, for both, the same cooling procedure was used. The sample appears fully amorphous in the bulk and even at the surface, while a slight degree of crystallinity was found in the DSC experiments. In image (2) the top view and the side view (microtomed slice) of a sample assembled at 60°C for 10 minutes are shown. In the top view, the sample is almost transparent, with few whiter spots. In the side view, the bulk appears fully amorphous. At the interface, we see a very thin bright line, which can be a thin crystalline zone. Image (3) shows the assembled sample at 70°C for 10 minutes. The left image appears much whiter than image (2). In the side view, the presence of the bright line is now beyond doubt. Moreover, some white spots are seen close to the PC interface.

Those first two observations are in good agreement with the DSC results which gave a very low, but not null degree of crystallinity.

The sample assembled at 70°C, for 60 minutes, shown in image (4), appears quite crystalline in both the top and side view. Spherulites are clearly seen in the right picture. Still, the bright line at the interface is present. One can notice that most of the spherulites lay near the PC interface.
For contact at 90°C for 10 minutes in image (5), the top view is again more transparent, and similar to the left image (3). As discussed in the previous section for the DSC results, the crystallization of PBI is strongly time dependent. The side view is also similar to the one obtained for a contact at 70°C, with maybe more white spot and not so well defined future spherulites growing. After 60 minutes at the same temperature in image (6), spherulites cover all the surface in the right image and the sample appears almost white in the left image. In image (7) (100°C, 60 minutes), the sperulites are also present. Surprisingly, they do not cover the whole surface, and their shape differs slightly from the right image (6). In the DSC experiment the degree of crystallinity obtained after 60 minutes at 90°C was higher than the one obtained at 100°C. We may think that at 100°C a fusion-recrystallization process has already started.

We may conclude from those observations that a very thin layer of crystallites is present at the surface after molding and quenching, or at least some nuclei, which will develop even for low temperatures of contact (40°C). For short times of contact the growth process will not really develop and the bulk will remain amorphous, but at longer time,

the degree of crystallinity will start to grow with the growth of the spherulites as observed in the micrographs.

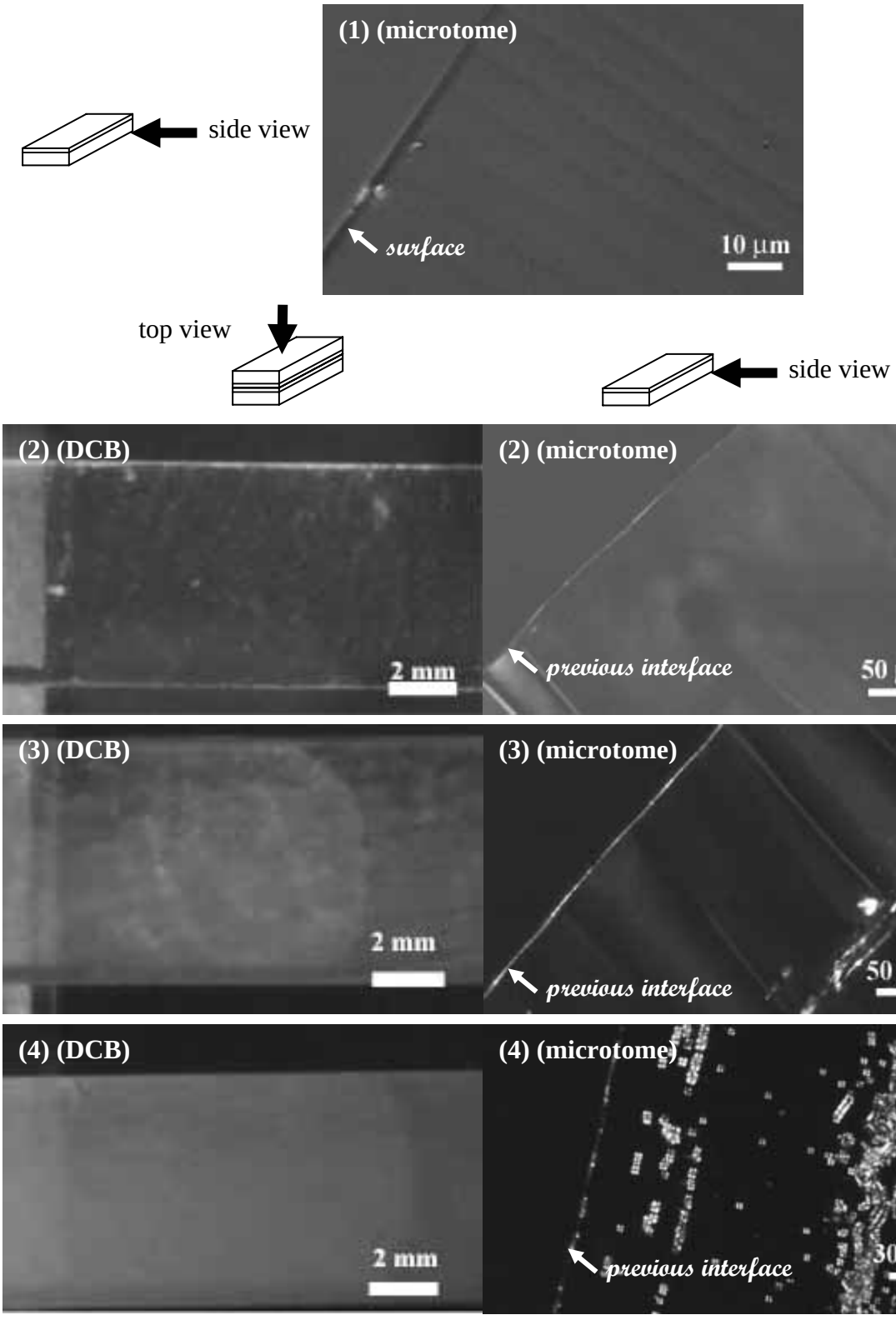

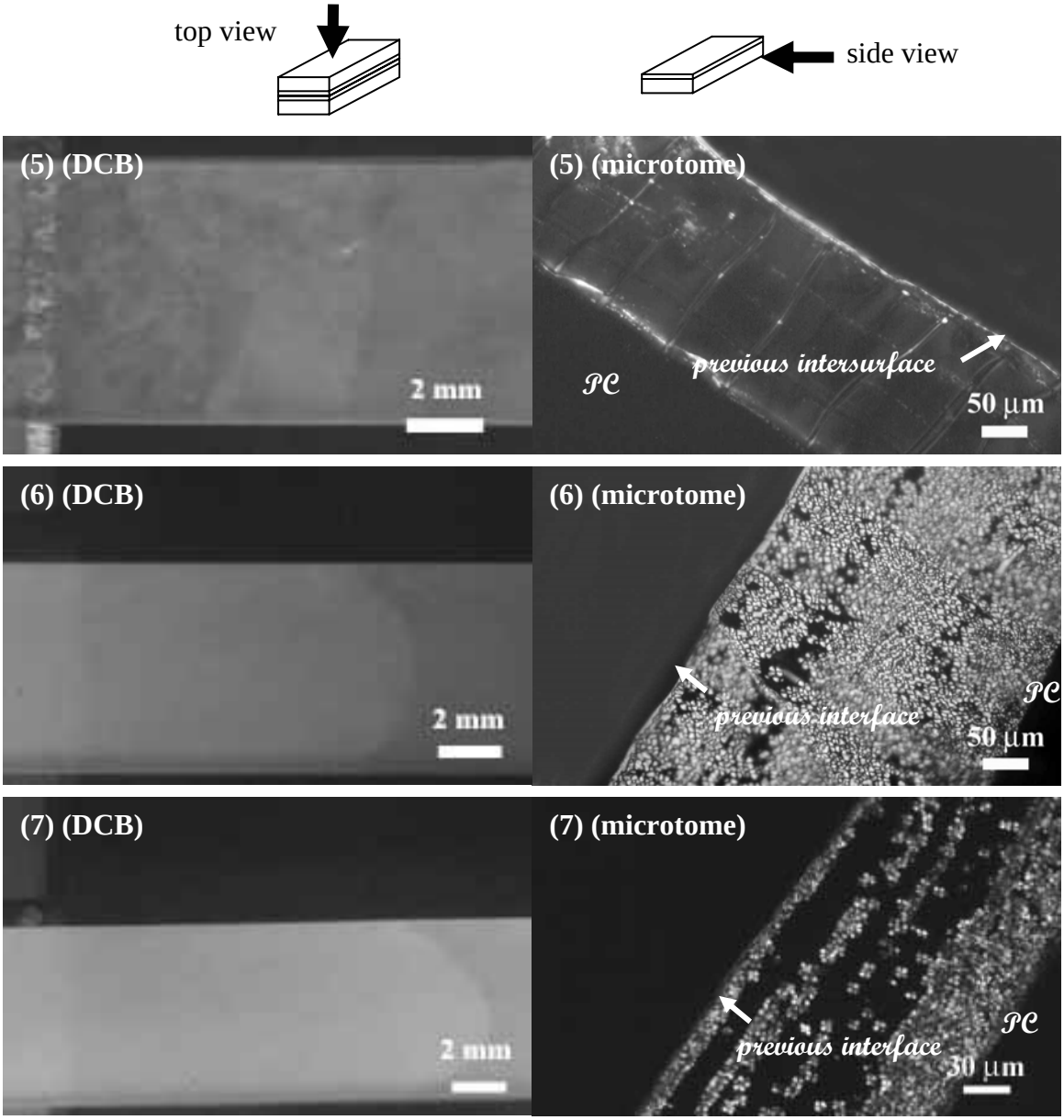

Figure 3.4-7: images from DCB test and optical micrographs of microtomed samples.
1 : molded sample (reference sample) ; 2 : assembled at 60°C for 10 minutes ; 3 : assembled at 70°C for 10 minutes ; 4 : assembled at 70°C for 60 minutes ; 5 : assembled at 90°C for 10 minutes ; 6 : assembled at 90°C for 60 minutes and 7 : assembled at 100°C for 60 minutes.

3.4.4 tensile tests

The mechanical properties of PBI were studied for different annealing times and temperatures.
The specimen preparation can be found in section 2.5 (1 mm thick plate molded at 180°C, cooled to 160°C at 20°C.min^{-1} then quenched in ice water).
The results are given in Figure 3.4-8 (see also section 3.3.4 for more details).
Table 3.4-1 summarizes the main results obtained from Figure 3.4-8.

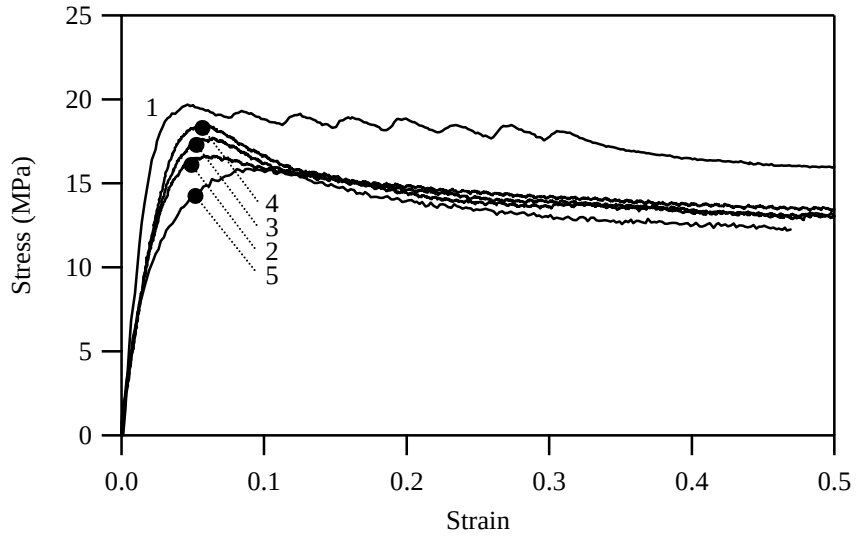

Figure 3.4-8 : stress/strain curves in traction experiments.
1 : annealed at 100°C during 60 minutes
2 : annealed at 100°C during 10 minutes
3 : annealed at 60°C during 60 minutes
4 : annealed at 60°C during 10 minutes
5 : unannealed

Table 3.4-3

T_{an}	t_{an}	σ_y	E
/	/	15.8	340
60	10	18.4	478
60	60	17.6	460
100	10	16.6	452
100	60	19.6	782

Both the yield stress and the Young's modulus increase slightly from the reference sample to the annealed samples.

From figure 3.4-8 the differences between an annealing at 60°C, 10 and 60 minutes and an annealing at 100°C for 10 minutes are not obvious. However the sample annealed at 100°C for 60 minutes has a distinctly higher and more marked yield stress than the other

samples. Moreover, the curve is showing little strain hardening, contrary to the other three annealing treatments, where the plasticity after yield is not so different.

In terms of degree of crystallinity, the differences between the sample annealed at 60°C, 10 minutes, 60°C, 60 minutes and 100°C, 10 minutes were not so important (see Figure 3.4-4). The main change was found for the sample assembled at 100°C for 60 minutes, which has a significantly higher degree of crystallinity.

We may conclude that for PBI, both the degree of crystallinity and the mechanical properties are changing very slowly with the increase of the temperature for a 60 minutes time of contact or annealing. For 10 minutes of contact or annealing, the degree of crystallinity and the mechanical properties remain roughly identical when the temperature increases within the range investigated.

3.4.5 Conclusions on the different results on crystallinity and mechanical behavior

The crystallinity and the mechanical behavior of PBI change relatively slowly with thermal history.

By quenching PBI (with the protocole previously described), we obtained a rather amorphous sample, which can have a very low degree of crystallinity if one trust the DSC results (1.8% of crystallinity). However, the optical microscopy does not reveal any presence of crystallinity.

Even if they are not optically seen, nuclei are probably present at the surface of quenched molded samples. Those nuclei enhance the cold crystallization at the interface of assembled samples, which produce a very thin crystallline layer observed optically.

After annealing or contact for 10 minutes, the degree of crystallinity remains almost constant up to 100°C and the mechanical properties do not change in an appreciable manner.

The degree of crystallinity increases slowly with the temperature of annealing or contact only for 60 minutes of contact or annealing.

To put in a nut shell, by assembling the sample for short time of contact, i.e. 10 minutes, we get a crystalline layer at the interface and an amorphous bulk. By assembling for longer times of contact, i.e. 60 minutes, we still have a crystalline layer but we progressively have a crystalline bulk with an increase in mechanical properties (modulus and yield stress).

3.4.6 Adhesion results

The experimental procedure for all the adhesion experiments can be found in section 3.3-6 (contact between amorphous samples at room temperature, heating to $T_{contact}$, controlled cooling after a time of contact $t_{contact}$).

The time of contact was taken from the moment of contact at room temperature to the beginning of the cooling (see section 2.4).

The effect of the temperature of contact was studied over a 60°C range i.e from 40°C to 100°C for two different times of contact, 10 and 60 minutes.

The DCB tests were carried out at a controlled temperature of 10°C in order to remain below the glass transition temperature.

These conditions are summarised in table 3.3-4. The molding and assembling procedure can be found in chapter 2.

Table 3.4-4: experimental conditions

polymer	T_{mold} (°C)	Cooling molding (°C/min)	t_{ph} (min)	P_c (bars)	t_c (min)	Cooling assembling (°C/min)
PBI	180	Quenched(1)	0	50	10/60	40

(1) the polymer plate was first cooled under the press at 20°C.min^{-1} to 160°C then quenched (see section 2.4)

During the fracture tests, the crack propagation always occurred intermittently in a stick-slip manner exhibiting characteristic G_c values for crack initiation and crack arrest. An example of this "unstable" crack growth is given in Figure 3.4-9 for a sample assembled at 50°C for 10 minutes and a sample assembled at 100°C for 10 minutes. Several pictures of the crack are shown, which correspond to the points 1 to 6 on the graph where the crack length is plotted. The camera took one picture every minute, and the opening displacement was fixed at 0.5mm/min^{-1}.

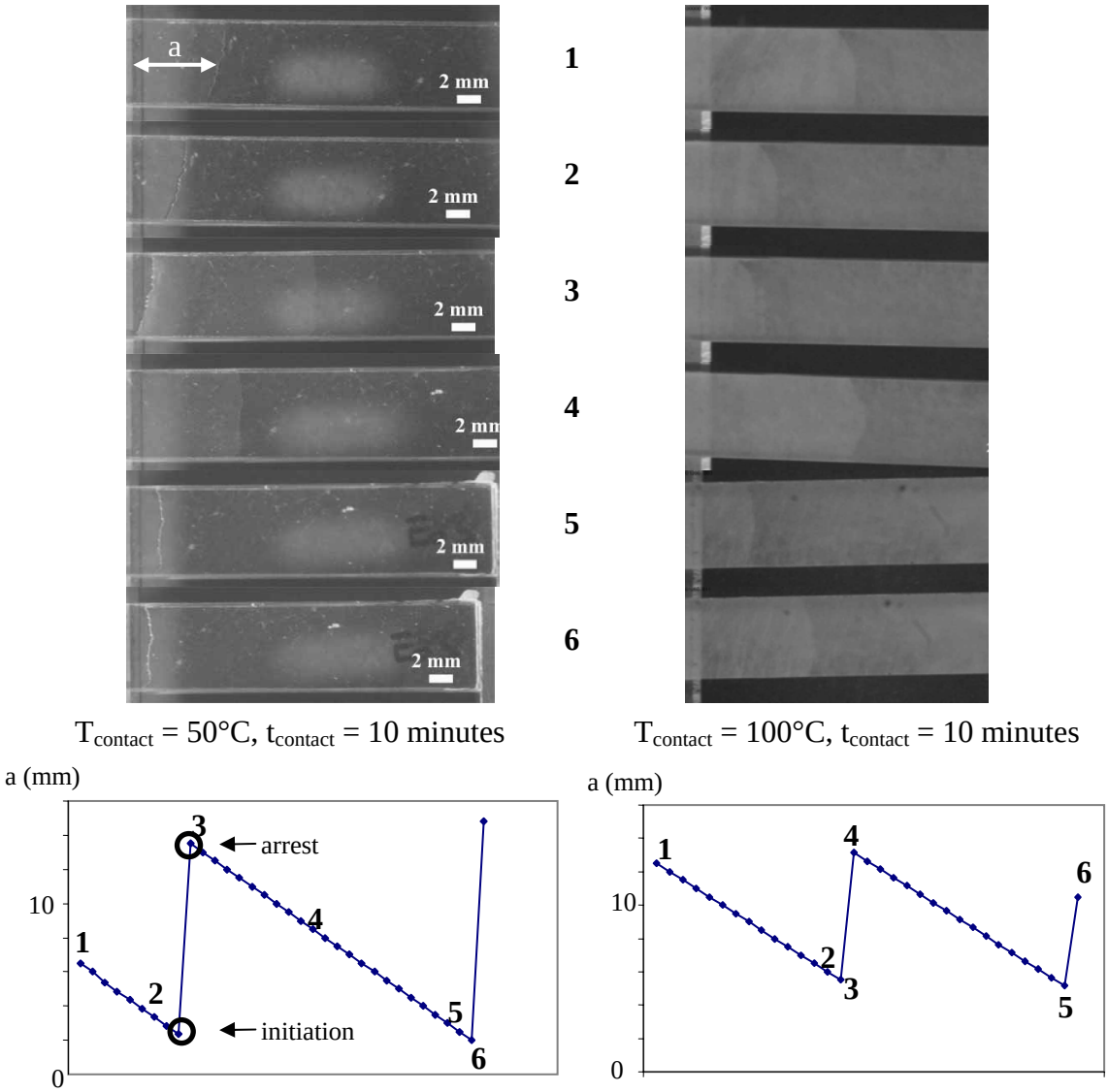

Figure 3.4-9: "unstable" crack growth in the case of a contact at 50°C and 100°C for 10 minutes. Test carried out at 10 °C.

In a way quite similar to what was observed for 45PB[a], the behaviour shown in Figure 3.4-9 is typical of the stick slip behaviour. By following the curve obtained for contact at 50°C, the crack does not move till the initiation point. In picture 3, the crack suddenly moves toward a new position within less than one second.

In the case of a stick-slip behavior, both the value for the crack initiation and the crack arrest are kept for the calculation of the fracture toughness.

In Figure 3.4-10 the G_c values for crack arrest are plotted as a function of the contact temperature for 10 minutes of contact time.

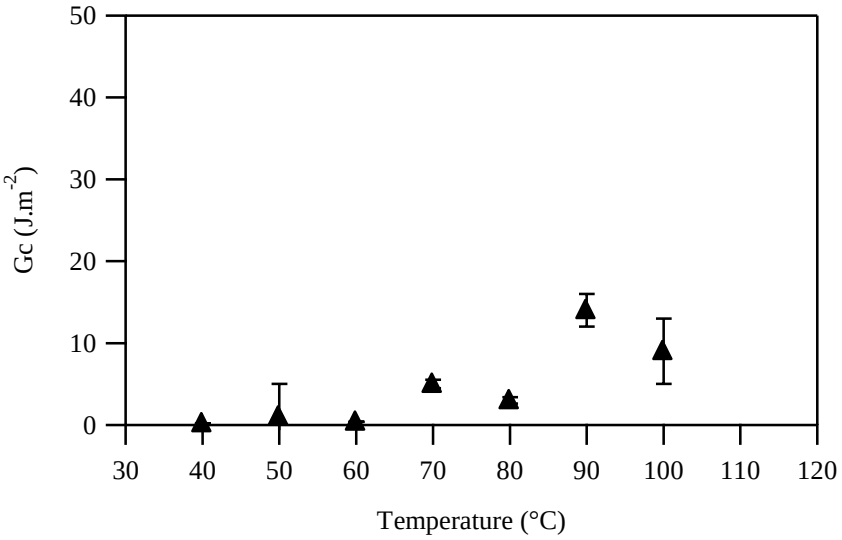

Figure 3.4-10: fracture toughness for crack arrest after 10 minutes contact.

For temperatures of contact between 40°C and 80°C the adhesion remains weak, although these temperatures are above the glass transition temperature (~20°C) and interdiffusion may occur during the time of contact. The thin crystalline layer observed in the micrographs in section 3.4-3 may prevent the chains diffusion across the interface. After 10 minutes of contact, the degree of crystallinity remains low, whatever the temperature, but at the interface, the thin crystalline layer appears brighter in the microscope when the temperature of contact is higher. However, this cold crystallization, located at the interface, has no real impact on the interface reinforcement. We may suppose that the cold crystallisation occurs separately in each part of the assembly, growing from the interface toward the bulk.

In Figure 3.4-11 both the crack arrest and the crack initiation values are represented for 10 minutes of contact.

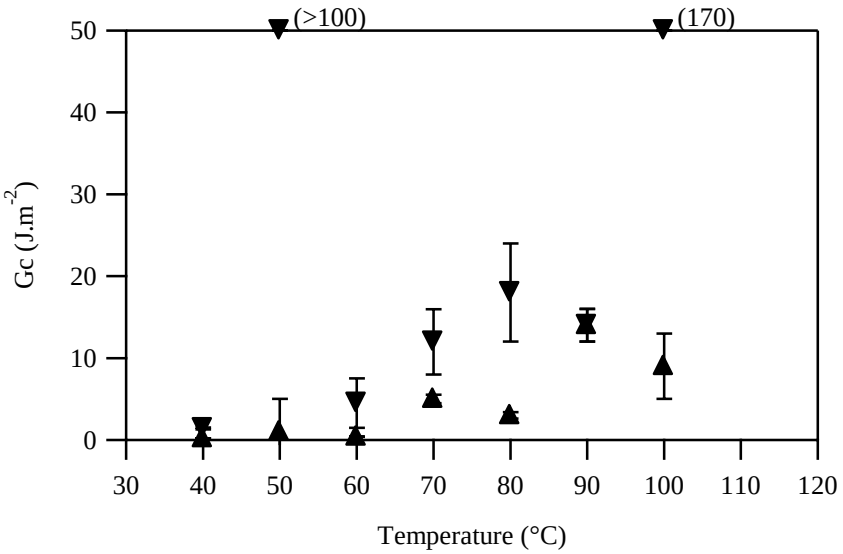

Figure 3.4-11: fracture toughness for the crack arrest (◢) and the crack initiation (▼) after 10 minutes of contact.

The stick-slip propagation does not appear with the same magnitude at each temperature of contact.

Two factors can influence the stick-slip amplitude : the strength of the interface and the mechanical properties of the bulk.

At 40°C and 50°C, the bulk properties must be very close to the properties of the unannealed sample in the tensile test, as the change in crystallinity of the sample starts only at 60°C. Hence, the stick slip is completely different between 40 and 50°C. At 40°C, the strength of the interface must be so weak that the crack has not enough energy to blunt, even with a soft material. At 50°C, the interface is strong enough to produce the blunting of this very soft material, but still the interface is quite weak. Between 60 and 100°C, the curves obtained in the tensile test were similar. We can assume that the change in the mechanical properties with a contact at those temperatures is not so important. Between 60 and 80°C, the strength of the interface is increasing and quite logically, the magnitude of the stick also increases. The behavior at 90°C is not fully understood for the moment. At 100°C, the crack can blunt, and cavitation was also observed ahead of the crack, increasing significantly the energy dissipation. The reason of those cavitations is not fully understood.

In Figure 3.4-12, the fracture toughness for crack arrest, is plotted as a function of the temperature of contact for 10 and 60 minutes of contact time.
At 40 and 50°C the fracture toughness is the same after 10 or 60 minutes of contact. In section 2.2.3 the calculation of the reptation time for PBI from the rheology experiments gave a time of 50 minutes at 50°C. Even with a contact time of 60 minutes, the adhesion is still very weak. At 60°C, 70°C and 80°C, the fracture toughness after 60 minutes of contact time is slightly higher than the fracture toughness after 10 minutes. However, the

adhesion remains weak, and the increase between 10 and 60 minutes of contact time seems not really significant. At 90 and 100°C, the same fracture toughness was obtained after 10 and 60 minutes, meaning that the reinforcement of the interface occurs within the first 10 minutes.

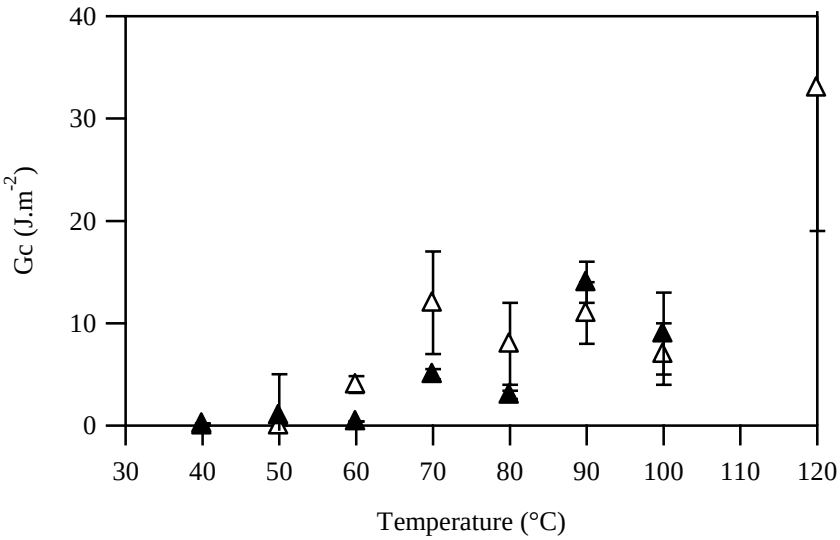

Figure 3.4-12: fracture toughness of PBI
after 10 minutes contact◢ and 60 minutes contact △ (crack arrest)

It can be useful to divide the results in three regions. In region I, at 40 and 50°C, adhesion is very low for 10 and 60 minutes of contact time. These temperatures are probably too low to allow cold crystallization. We will probably get in DSC the same small melting peak obtained in the case of annealed sample at 40 and 50°C in section 3.4.1. This peak was attributed to a crystalline layer formed during the molding process.

In region II, i.e. at 60°C, 70°C and 80°C, cold crystallization occurs with a slow kinetic. The adhesion after 60 minutes of contact is higher because the cold crystallization had more time to take place.

In region III, the contact temperature is probably above the optimum temperature for cold crystallization. The cold crystallization occurred during the heating in contact of the samples, and no further cold crystallization takes place during the isothermal step. Therefore, we get the same adhesion after 10 or 60 minutes of contact.

At 120°C, the fracture toughness increases, but remains relatively low. It is probably the early stage of the onset of the melting process.

In Figure 3.4-13, the fracture toughness for crack arrest and for crack initiation after 60 minutes of contact are plotted as a function of the temperature of contact.

At 40 and 50 minutes, the crack propagates continuously (no stick slip). At 60°C the strength of the interface increases a little bit, while the bulk properties do not change so

much according to the mechanical experiment presented in section 3.4.4 and Figure 3.4-8, leading to an increase of the stick slip.

When the temperature approaches 100°C, the tensile tests show that the mechanical properties change (see Figure 3.4-8). Between a sample annealed at 60°C for 60 minutes and a sample annealed at 100°C for 60 minutes, both the Young's modulus and the yield stress increase in a significant manner. Those changes in the bulk properties make the stick slip decrease.

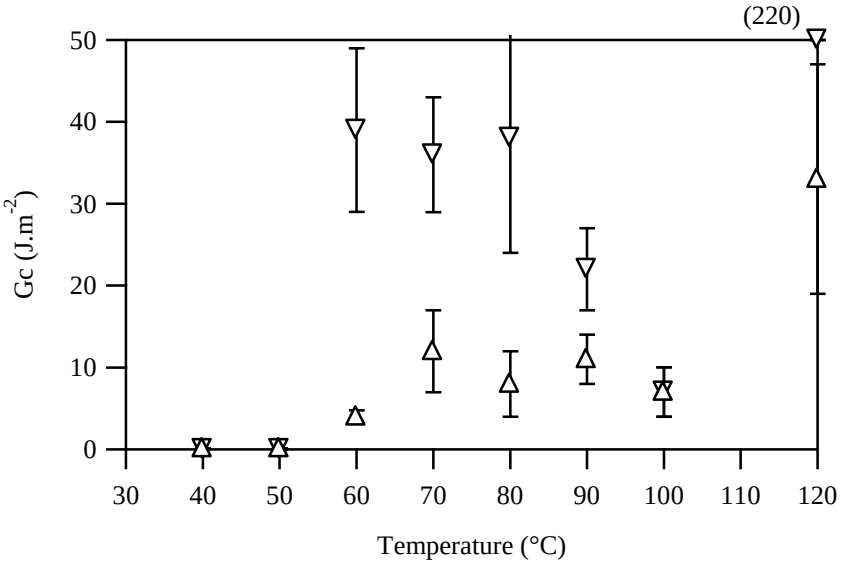

Figure 3.4-13: fracture toughness of PBI after 60 minutes contact : ▽△ (initiation and arrest)

3.4.7 Crack tip observation and TEM

Crack tip observations were made on assemblies welded at different temperatures again using the experimental procedure described in section 2.6 We used both optical and electron microscopy.

Figure 3.4-14 shows the crack tips for different temperatures and times of contact. In image (1), the sample was assembled at 70°C for 10 minutes. The arrow represents the direction of propagation of the crack. The crack tip has a blunted shape. We can notice the huge deformation at the crack tip on the right image.
In figure (2), for a contact at 100°C for 10 minutes, the crack tip appears less deformed. Hence, while preparing the sample for the crack tip observation (see section 3.2.1), it was rather difficult to keep the crack stay in the blunted position. So, in image (2), we probably look to a crack in its arrest position.
Image (3) represents the crack tip in the case of a sample assembled at 90°C for 60 minutes. The crack is quite straight. A transcrystalline zone appears at the interface on both sides of the assembly.

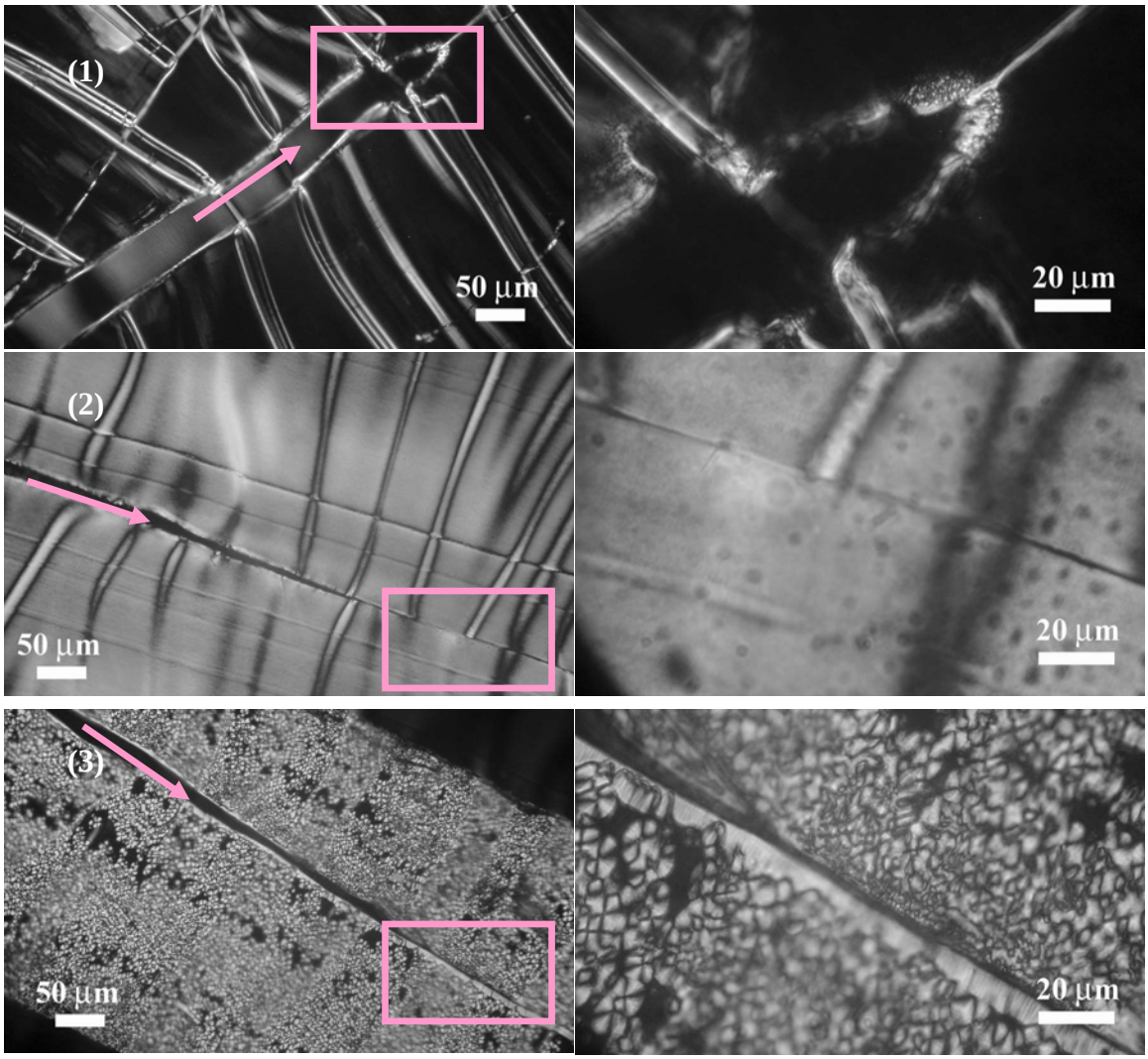

Figure 3.4-14: crack tip view. (1) 70°C, 10 min ; (2) 100°C, 10 min ; (3) 90°C, 60 min

In Figure 3.4-15 several TEM images of the crack tip zone of a sample assembled at 70°C for 10 minutes are presented. The deformed zone at the very tip of the crack (image a) appears crystalline, with the presence of lamellae which seem to be stretched. Ahead of the crack (image c), a transcrystalline zone with oriented lamellae is seen. Image b shows a growing spherulite near the crack tip.

Image c is of great interest as it gives a valuable proof of the development of the cold crystallization from the interface. The bright line seen in the optical observation corresponds to this bilayer of lamellae, which seems to grow from the interface towards the bulk of the sample. We can notice some holes placed at the interface. However, it is hard to say if these holes were there before the preparation of the TEM slice with the ultramicrotome.

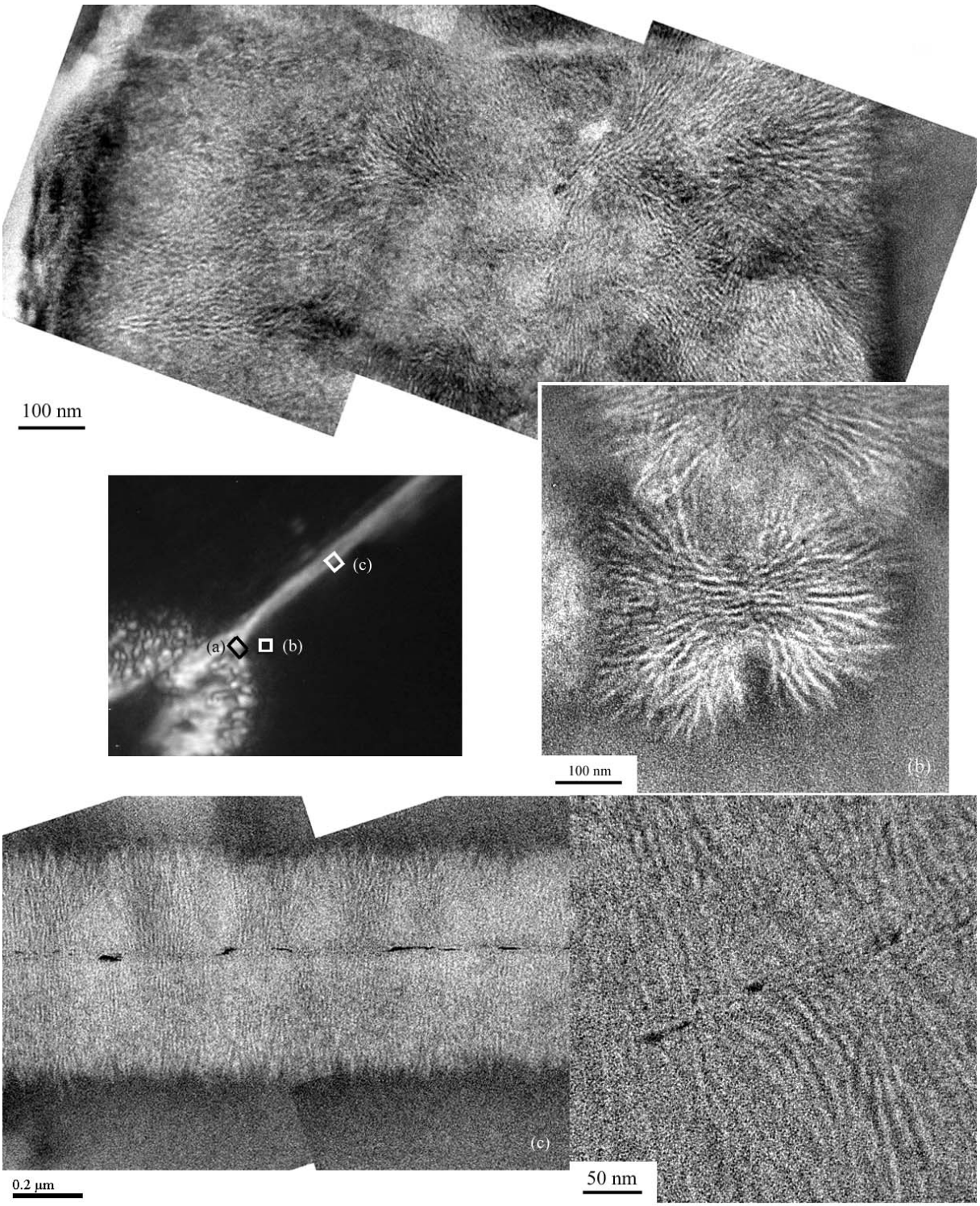

Figure 3.4-15: TEM micrographs (sample assembled at 70°C for 10 min)

3.4.8 Conclusion

PBI has a crystalline structure and crystallization behavior different from those of PBT and the copolymers PBT-PBI. We could not obtain crystalline PBI by cooling it, even very slowly, from melt.

During the adhesion test, all the samples have shown more or less a stick slip behaviour. The fracture toughness calculated for crack initiation corresponds more to the energy stored in the blunted crack and is linked to the bulk properties, while the fracture toughness calculated from the crack arrest values gives a more representative value of the strength of the interface.

The fracture toughness was found extremely weak for temperatures up to 30°C above the glass transition temperature. This weak adhesion was attributed to the presence of a thin crystalline layer, observed optically at the interface of samples assembled at 60°C, which probably hinder the expected interdiffusion (according to the reptation times).
In one of our samples assembled at 70°C for 10 minutes, we managed to see pretty well a transcrystalline zone at the interface constituted by oriented lamellae, which can be a proof of the presence of preexisting nuclei before assembling.

Above a certain temperature of contact (60°C), the fracture toughness increases slightly. The development of the crystalline layer may enhance the adhesion a little. However, the adhesion remains weak (G_c values around 10 $J.m^{-2}$).

Cold crystallization seems to reinforce the interface a little, with a dependence on annealing time between 10 and 60 minutes at 60, 70 and 80°C. Above 80°C, we get the same fracture toughness after 10 or 60 minutes of contact, meaning that the reinforcement occurred within 10 minutes, and probably during the heating stage to the contact temperature.

Chapter 4

Discussion

Table of contents

The results exposed in chapter 3 can be divided in two main sets of experiments. In the first set, contact was made between polymer plates that were cooled slowly and preheated before contact. This thermal treatment resulted in crystallized and equilibrated surfaces before contact. This was the case for experiments on PBT and three copolymers: 15PB, 35PB and 45PB. In the second set of experiments, 45PB and PBI were molded and quenched in order to get amorphous samples. The contact was made at room temperature before a rapid heating to the contact temperature. Then the surface of the sample (and the bulk of the sample itself) is out of equilibrium and cold crystallizes while in contact. The role of the cold crystallization on the structure of the interface and on the mechanical reinforcement of the formed interface was quantified.

In the present section, we will discuss these two sets of experiments separately and try to correlate and rationalize the observed behaviour. This will lead to propose qualitative interpretations of the adhesion mechanisms involved.

4.1 First set : contact between pre-crystallized samples

4.1.1 Overview of the results

The results have been presented in detail by material families in chapter 3. We would like now to discuss the results in a more global way focusing on the comparison between different materials.

As a reminder, in this set of experiments on crystalline samples the polymer plates were molded, slowly cooled and annealed just before contact in order to get the maximum degree of crystallinity for each sample. Both DSC and X-ray confirmed that the maximum possible degree of crystallinity was indeed achieved before contact.

In our experiments on the fracture toughness of interfaces formed between crystallized surfaces, the melting temperature appears to be the most important parameter, since for each polymer, the adhesion was found to be very strong for a contact temperature in the vicinity of T_m, and decreased rather sharply when the contact temperature was reduced. However, the behaviour of each copolymer is specific when the temperature of contact is reduced. In figure 4.1.1 the fracture toughness of each polymer is represented as a function of T_m-T.

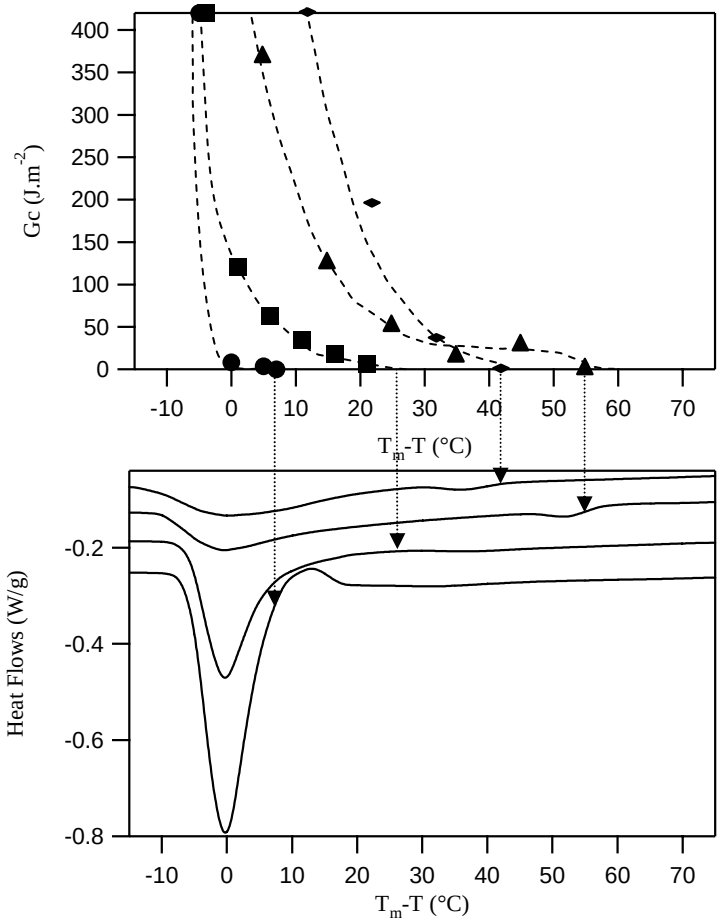

Figure 4.1-1 : fracture toughness as a function of Tm-T for PBT●, 15PB■, 35PB▲ and 45PB◆, and the corresponding DSC curves, recorded at 5°C.min^{-1}

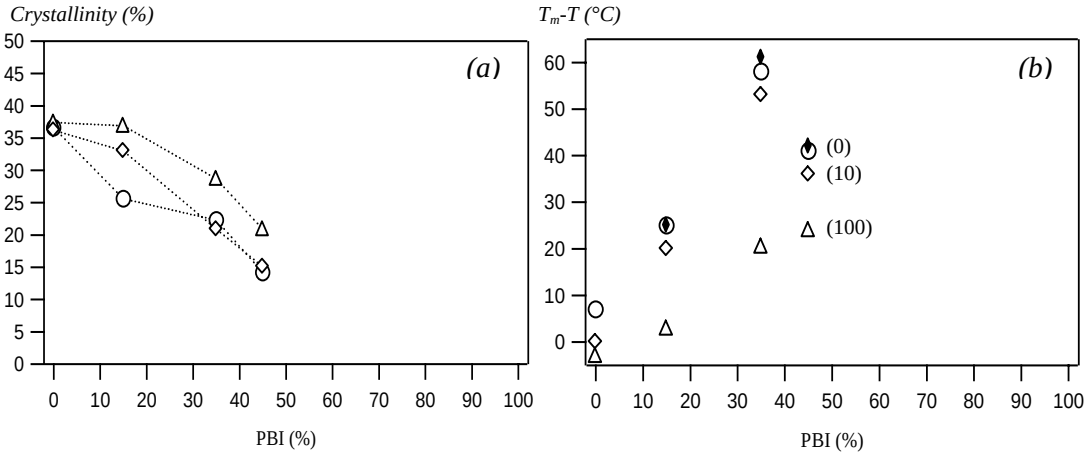

Figure 4.1-2 : (a) degree of crystallinity as a function of PBI content, obtained from X-ray measurements, with the fit functions f_1(◇), f_2(△) and obtained by DSC (○) (b)Onset of fusion from the DSC experiments (◆), temperature ($T-T_m$) of the onset of adhesion○, of a fracture toughness of 10(◇) and 100 J.m^{-2}(△).

When the temperature of contact is in the vicinity of T_m (Slightly above for PBT and slightly below for other samples), the interface is really strong after 10 minutes of contact, and fracture of the sample often occurs in the bulk and not at the interface. This behavior was obtained for all the samples, regardless of the proportion of PBI. This result is not surprising and has been reported in previous studies, as for example that of Smith (strong polypropylene interfaces were obtained within one minute), and that of Xue et al.[1] on ultra high molecular weight PE in which the fracture energy was found comparable to the fracture energy of the bulk material on a time scale shorter than 3 minutes.

Above T_m, the chains can indeed interdiffuse very rapidly (the reptation time obtained for our copolymer at 100°C was of the order of magnitude of 1s, so it will be even shorter at the melting temperature), as soon as the crystallites melt and the chains are free to diffuse. By cooling the samples, the chains can entangle and co-crystallise, on each side of the interface, leading to strong adhesion.

When the temperature is decreased, the fracture toughness decreases but in a different manner from pure PBT to 45PB. A correlation between the melting behavior and the fracture toughness can be established by looking at Figure 4.1-1. At first glance, adhesion decreases over a specific range of temperatures for each copolymer, which is related to the width of the DSC melting peak. The temperature at which the level of adhesion vanishes corresponds well, for each copolymer, to the beginning of the fusion process as detected in the DSC spectra. However, this is no longer true for pure PBT. This peculiar behavior can be explained by the fact that PBT has the particularity to show multiple fusion peaks (see section 2.1.1), and from our TM-DSC experiments, we know that an important reorganisation occurs at the beginning of fusion. This reorganisation is far less pronounced in the case of 15PB and occurs at lower temperatures for 35PB and 45PB which exhibit a cold crystallization behavior.

Figure 4.1-2a shows the maximum degree of crystallinity that could be obtained for each copolymer as a function of PBI content in the copolymer. Figure 4.1-2b on the other hand shows the temperature, at which DSC records the onset of the fusion process and the temperatures where specific values of G_c were obtained (null, 10 $J.m^{-2}$ and 100 $J.m^{-2}$). This figure is plotted as a function of $T_m - T$ to normalize the data for the different copolymers.

One can readily see that the degree of crystallinity decreases continuously from PBT to 45PB, in good agreement with previous studies on these copolymers (Bandiera et al.[2]) (see section 2.1.3), but does not fall to zero even for a nearly fifty-fifty copolymer. It is possible that this still reasonable amount of crystalline phase is due to the slightly blocky nature of the copolymers we have synthesized, but at this stage this remains a speculation.

[1]Xue, Y.-Q., et al. Macromolecules, 31: 3075-3080, (1998).
[2]Bandiera, M., et al. European Polymer Journal, 30(4): 503-508, (1994).

Comparing Figure 4.1.2a and b, it appears that a direct correlation between the increase in the temperature gap between T_m and the temperature of onset of the adhesion is far too simplistic. On the other hand, a very good correlation was found between the onset of the melting process and the onset of adhesion.

What appears clearly in our results is that a minimum degree of melting is needed to achieve some adhesion, even if the degree of crystallinity is quite low, i.e. even if the amorphous part, which is well above its glass transition temperature, is the majority phase.

4.1.2 Discussion on mechanisms

The way the presence of crystallinity influences the healing of an interface between identical semicrystalline polymers, although studied by several authors, remains unclear. The mechanisms now accepted in the case of amorphous polymers show their limitations in the case of semicrystalline polymers. In amorphous polymers, interdiffusion of chains across the interface, creating entanglements on both sides, is the main adhesion promoter. In semicrystalline polymers, there is a complex contribution of the crystallinity, and several mechanisms such has cocrystallization or surface reorganisation of crystallites, can also act to promote or hinder adhesion.

Several ideas emerged from the studies on adhesion of semicrystalline polymers, like the efficiency of cocrystallization for the interface reinforcement (Gent et al.[1]) or the role of epitaxy which can favour co-crystallization and enhance adhesion (Laurens et al.[2]).

Smith et al.[3] showed that for a contact temperature below the melting temperature of the polymer, the fracture toughness of the interface decreased quite sharply with decreasing temperature, since in isothermal conditions, the fracture toughness at 15°C below T_m is only 10 $J.m^{-2}$ (Smith et al.[3]). The same authors showed however that a reasonable adhesion was obtained if at least one side of the assembly was melted before contact. This reasonable adhesion was obtained within 1 minute of contact time by bonding a melted polypropylene (PP) plate with a “cold” PP plate, which was held below the melting temperature of PP before contact, namely at a mean interface temperature below the melting temperature (15°C below). These studies were however limited to PP, a polymer which is highly crystalline and has fast crystallization kinetics.

In the specific case of self adhesion for a contact below the melting temperature, only few studies were carried out (Boiko[4]) and things remain unclear. Some questions are still

[1]Gent, A. N., et al. Journal of Polymer Science Part B-Polymer Physics, 35(4): 615-622, (1997).
[2]Laurens, C., et al. Macromolecules, 37(18): 6814-6822, (2004).
[3]Smith, G. D., et al. Polymer, 42: 6247-6257, (2001).
[4]Boiko, Y. M. Polymer Science Series A, 45(8): 795-799, (2003).

open, like the possibility to achieve a reasonable adhesion below T_m and the role of the amorphous phase and of the cocrystallization in this case.

In our study focused on this problem, the crystallinity at the interface seems to govern the adhesion, since the adhesion was found null at a temperature below the onset of the fusion process regardless of the degree of crystallinity.

In order to understand now the role of the crystallinity at the surface, we should keep in mind that all the samples were preheated before contact, allowing a surface rearrangement prior to contact. Knowing that, we can think of several possible mechanisms for the build-up of adhesion strength.

If we assume that the polymer surface has reached a certain equilibrium after the time of preheating, we may think that the onset of adhesion (T_m-55 for 35PB, T_m-40 for 45PB and T_m-25 for 15PB) is linked to the presence of a certain mobility at the surface, i.e. the fusion of the smallest or more imperfect crystallites would give sufficient mobility to the chains to interdiffuse a little. When the temperature increases, the adhesion also increases and the higher mobility permits a wider penetration of the chains.

Another possible mechanism promoting adhesion is the co crystallization or at least the reorganization of the crystallinity near the interface.

Of course, interdiffusion and reorganization of the crystallites probably occur at the same time, but we can try to figure out which one is dominant. If interdiffusion was involved, for an identical penetration width in the case of self adhesion of 15PB and of 45PB, we should get completely different fracture toughness after cooling for the following reason : the cooling rate, identical for all the experiments, was fast (20°C.min^{-1}) and at such rates we know that 45PB does not crystallize while 15PB does, and for an identical penetration width, the 15PB chains would have a chance to be trapped in a newly formed crystallite (some TEM images have shown lamellae crossing the interface in the case of 15PB assembled at 197°C for 10 min) while the 45PB chains are unlikely to be trapped in a crystallite at such high cooling rates. This should lead to real differences in the measured fracture toughness. Such a behaviour is not observed, and we think that the predominant mechanism is more reorganisation, and at higher temperature, co crystallization, than interdiffusion.

There is indeed a very good correlation between the onset of the fusion process in the DSC curve and the onset of adhesion, which is quite surprising since the DSC gives a bulk and non isothermal information while adhesion results are linked to the surface and obtained in isothermal conditions.

In our samples the time of preheating was varied from PBT to 45PB for experimental reasons. This time was defined as the time to reach a stable temperature close to the contact temperature. This time was then longer for PBT (1h) than for 45PB (10 min). We

understand now that this time has a great influence on the crystallinity. We assume however that even for 45PB, the surface reorganization of the crystallites occurs within 10 minutes, i.e. the equilibrium is reached after 10 minutes. It has been shown for 45PB[a] in an isothermal experiment by DSC (see section 3.3.2), that the sample reached equilibrium within 2-3 minutes. We can consider that the behaviour of 45PB (not quenched) will be similar.

Considering this, we think that the onset of fusion for 15 to 45PB corresponds more to a definitive melting than a melting reorganization. If melting-reorganization had already occurred during preheating, the surface would be already equilibrated at the beginning of contact and the interface would not have been reinforced.

On the contrary, in the case of PBT, we think that we have a fast melting-recrystallization process. Hence, below T_m, there is no adhesion because the unstable crystallites have already recrystallized into more stable ones. This behavior is well known in the case of PBT which has very fast crystallization kinetics, and produces a chaotic crystallization (see section 2.1.1). By heating the sample, the unstable crystallites melt to recrystallize into bigger ones quite rapidly.

Below a fracture toughness of 100 $J.m^{-2}$, we may assume that no cocrystallization, neither entanglement occurred in our sample. When the fracture toughness is higher than 100 $J.m^{-2}$, cocrystallization or entanglements are expected. At the temperature at which the adhesion becomes higher than 100 $J.m^{-2}$, we can notice an influence of the time of contact (see Figure 4.1-3). The two proposed mechanisms, although quite rapid, may take a little while to act on the interface reinforcement.

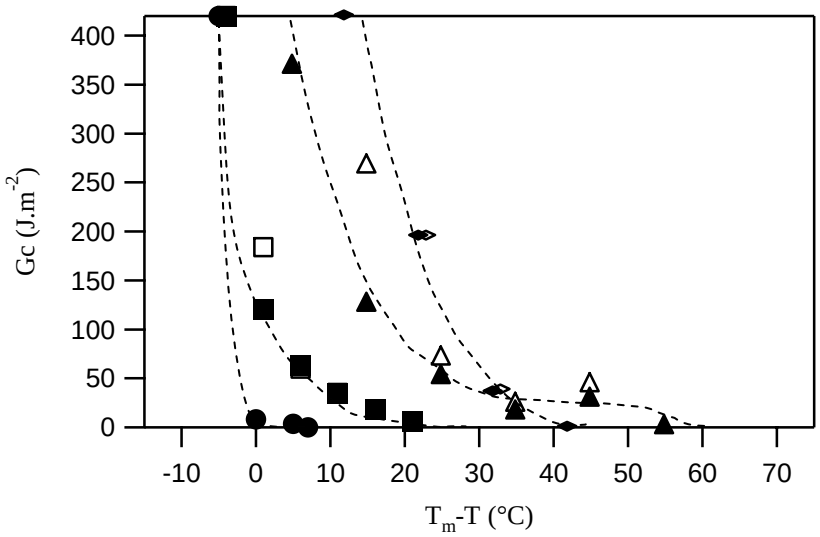

Figure 4.1-3 : fracture toughness as a function of T_m-T for PBT●, 15PB■, 35PB▲ and 45PB◆ for 10 minutes of contact (full symbols) and 30 minutes of contact (open symbols)

The temperature range of the fusion process thus, governs the buildup of adhesion for 15, 35, 45PB. The overall degree of crystallinity of 15PB and 35 PB was found not so important. The differences observed in the range of the fusion process comes from the fact that, because of its larger proportion of PBI, the 35PB crystals are much thinner, the spherulites less well defined (as effectively observed optically). The onset of the fusion process starts indeed at lower temperatures and the fusion process takes place over a much wider range of temperatures. For 45PB, which still crystallizes in the same structure as confirmed by WAXS, the overall degree of crystallinity is much lower, meaning that the most unstable crystals are no longer formed, which can explain that the range of temperatures over which the fusion occurs, is reduced compared to 35PB.

Our results strongly suggests that to obtain at least a weak adhesion, some crystals even the smallest ones, must be melted at the temperature of contact. These results are in contradiction with the results reported by Boiko[1] on another semicrystalline polymer of the group of aromatic polyesters (PET), which showed that, although weaker than an adhesion between amorphous samples, the adhesion between crystalline PET was measurable after contact well below the melting temperature of PET (more than 140°C below the melting temperature). The authors believe that interdiffusion is highly reduced by the presence of crystals but not completely hindered. We are not really convinced by this explanation and we think that in their experiments crystal reorganization could be an alternative explanation for the surface reinforcement, since their temperatures of contact are very close to the temperature of crystallization of PET.

[1]Boiko, Y. M. Polymer Science Series A, 45(8): 795-799, (2003).

Moreover, the shear joint geometry used by Boiko et al. as an adhesion test, will undoubtedly be sensitive to the change in mechanical properties of PET which can cold crystallize, and thus complicate the interpretation of the results.

4.1.3 Conclusions

Regardless of the overall degree of crystallinity, no self-adhesion can be obtained for a contact temperature below that of the onset of the fusion process. Even if the amorphous part is highly mobile (reptation time of less than one tenth of a second) and in large majority (overall degree of crystallinity of 15% in the case of 45PB), the chains of the amorphous part do not cross the interface over a sufficient distance to be able to promote adhesion. This somehow implies that all chains are part of at least one crystallite and hence cannot readily diffuse over distances comparable to their size. Thinking of amorphous polymers this is not so surprising since for a degree of polymerization of 150, typical of our copolymers, the volume fraction occupied by a single chain in the volume delimited by its radius of gyration will be of the order or $N^{-1/2}$ ~ 7-8%. Hence the probability to find free chains for a degree of crystallinity of 15% remains rather high.
On the other hand, there is a good correlation between the onset of the fusion process and the temperature at which adhesion becomes measurable, suggesting that the fusion of the smaller crystallites can free some polymer chains and cause sufficient mobility to reorganize the interface and, upon cooling create some crystallites spanning the interface. Presumably, this first occurs only locally in specific points, precluding then a large increase of the measured G_c, which only occurs when widespread melting takes place at higher T. However if an important reorganization and recrystallization occurs at high temperature (the case of PBT) adhesion should only be high if the polymers are heated in contact.

4.2 Second set : quenched samples of 45PB and PBI

4.2.1 Overview of the results

As discussed in the introduction, in the case of self adhesion between fully amorphous polymers, the fracture toughness of an interface formed above the glass transition temperature increases with contact time to the value found for the bulk material, within a contact time comparable to the reptation time.

In our experiments on quenched samples of 45PB and PBI, obtained in the amorphous state, we expected first a similar behaviour. The adhesion we found was far below the expected values.

We present in Figure 4.2-1 a summary of the adhesion results obtained with 45PB[a] and PBI and reported in Figures 3.3-24 and 3.4-14. We have argued that the crack initiation

value was due to the formation of a new crack in a previously blunted crack tip. This behaviour is closely connected to the bulk properties of the polymers. We argued on the other hand that the crack arrest values were more representative of the interfacial strength and when comparing materials we will therefore focus the discussion on the crack arrest values only. The discussion on the stick-slip crack propagation can be found in section 3.3 and 3.4.

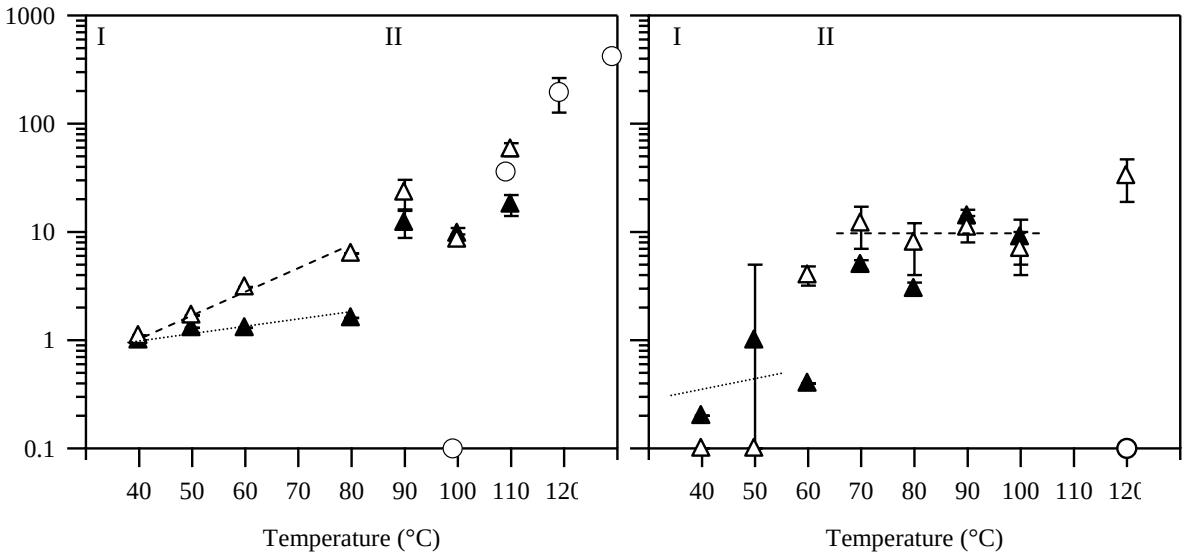

Figure 4.2-1 : fracture toughness (from the crack arrest value) after 10 minutes (full symbol ◢) and 60 minutes (open symbol △) of contact for 45PB[a] and PBI, and for crystallized 45PB and PBI (○) after 10 minutes of contact.

The data of Figure 4.2-1 allow to distinguish 2 regions for adhesion. Region I is characterized by a very weak adhesion for both 45PB and PBI (roughly 1 $J.m^{-2}$ in both cases), while in region II, the fracture toughness reaches more significant values (10 $J.m^{-2}$) and finally reaches relatively high values at temperatures closer to T_m.

From these results, it appears first that the crystallinity acts in a complex way on the adhesion.

For 45PB, we can highlight the fact that for a time of contact of 10 minutes, the bulk crystallinity changes from very low, to the plateau value, between 50 and 60°C. This difference does not affect much the fracture toughness, which reinforces the idea of a different crystallization behavior at or near the interface.

For PBI, after 10 minutes of contact, the bulk degree of crystallinity remains low for all temperatures of contact that we tested. However it increases continuously with temperature for 60 minutes of contact. But here again, the correlation between the bulk degree of crystallinity and the fracture toughness is not acceptable, since the fracture toughness after 60 minutes of contact increases non continuously with temperature.

Actually, G_c goes suddenly from null to a set value, and then remains almost constant with increasing temperature.

Above 60°C, we have probably a reorganization of the crystallinity at the interface as shown in the TEM image of the sample assembled at 70°C for 10 minutes, which exhibits a transcrystalline layer of oriented lamellae. This transcrystalline zone is probably present at each temperature of contact from 70 to 100°C. The slight difference between 10 and 60 minutes observed at 70 and 80°C, is certainly due to the kinetics of formation of such a layer. Above 90°C, the time of formation of the layer may be shorter than 10 minutes and therefore we obtained roughly the same adhesion after 10 or 60 minutes of contact.

For 45PB, the onset of the fusion process was found around 90°C, and the adhesion increases a little at this temperature of contact. However, interdiffusion probably does not occur because the fracture toughness remains low. For such values of G_c, a fracture mechanism involving crazing or the formation of a plastic zone is unlikely.

These results also provide informations on the role played by the amorphous part on the adhesion.

In order to estimate the characteristic times necessary for interdiffusion, we have reported in Figure 4.2-2 the values of the reptation time for 45PB and PBI as a function of T extrapolated from the rheology experiments and the WLF relation, with a reference temperature of 100°C (a shift factor a_T was applied to obtain the reptation times at the different temperatures).

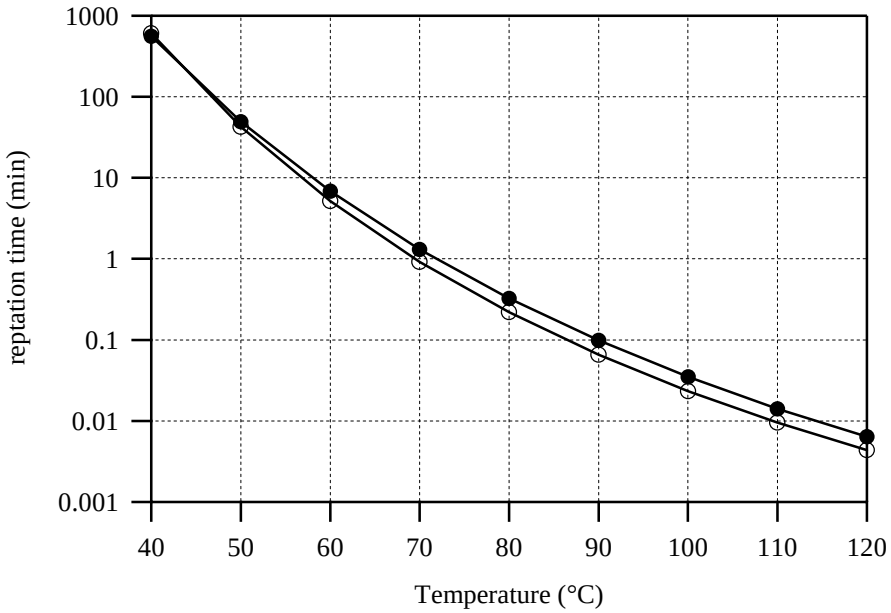

Figure 4.2-2 : reptation time at different temperatures, obtained from the reptation time at 100°C given by the rheology data, and by applying the WLF equation.

It is known as mentioned in the introduction of this section that if two pieces of the same amorphous polymer are put in contact above T_g for a time of contact of the order of magnitude of the reptation time, the fracture toughness of the interface once the assembly is cooled to room temperature, reaches the bulk fracture values. Here at temperatures where the reptation time is of the order of magnitude of the contact time (typically 50°C) the adhesion is still very weak.

In order to confirm these results, additional experiments have been carried out on PBI by varying the time of contact at a constant temperature of contact (40°C). The results are given in Figure 4.2-3. Although the fracture toughness increases a little from 60 minutes of contact to 810 minutes of contact, the adhesion remains very weak. After 2400 minutes of contact, the opacity of the sample has increased very slightly, indicating that probably, even at low temperatures, PBI can cold crystallize. Unfortunately, we had not enough time to carry out optical or TEM observations.

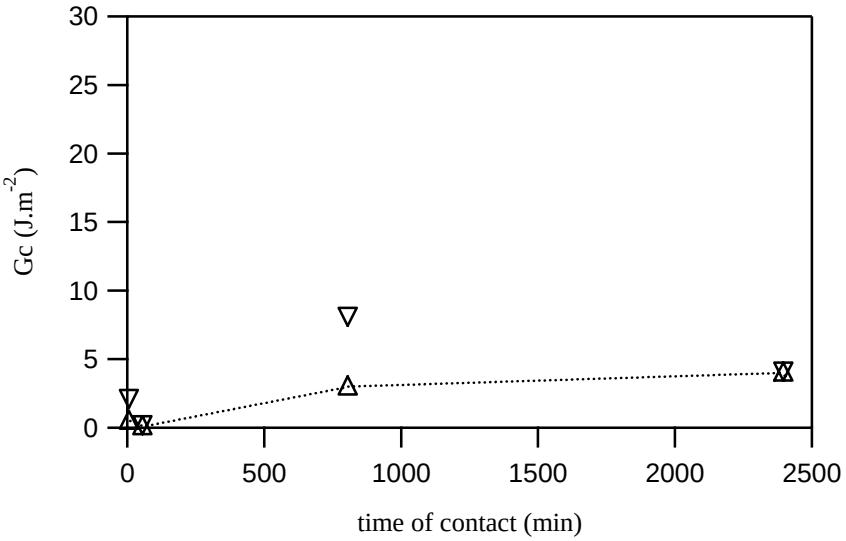

Figure 4.2-3 : fracture toughness for a contact at 40°C as a function of the time of contact.

The reptation time at 40°C is about 9h or 540 min, which is a much shorter time than the longest contact time used in this last study (2400 min). The adhesion remained weak between 810 and 2400 minutes, comforting us in our belief that interdiffusion does not occur, and that the slight increase in fracture toughness is only due to cold crystallization.

The values of G_c obtained for crack initiation deserve further comment. At short times of contact, the bulk polymer is rather soft but the extremely weak adhesion does not really activate the blunting of the crack tip. After 810 minutes of contact, the interfacial strength has increased slightly, probably from cold crystallization at the interface, while the bulk is still completely amorphous, and hence rather soft. In these conditions, the stress transfer across the interface is sufficient to blunt the crack tip. After 2400 minutes of contact, the

bulk has now started to cold crystallize and then its ability to deform easily has been reduced, leading the disappearance of the crack blunting phenomenon.

The different mechanism that can reinforce the interface will be now discussed.

4.2.2 Discussion on the mechanisms

If interdiffusion were the predominant mechanisms in our experiments, the adhesion would increase sharply when the time of contact and the reptation times are of the same order of magnitude. However, the experimental results show a complete decorrelation between the adhesion, which is more or less constant (in the first region) with increasing temperature of contact, and the reptation time which decreases sharply with the increasing temperature. Moreover the experiments carried out at long times of contact unambiguously showed that even for times of contact much longer that the reptation times, no real reinforcement of the interface was observed. We conclude that interdiffusion was hindered somehow, and we strongly believe that the crystalline layer, shown in the optical micrographs of samples annealed at 60°C which is probably already present before contact, is responsible for the low values of fracture toughness which were measured.

It may be convenient to describe the polymer as a bilayer system : one surface layer where crystallites are present, and a bulk layer. In the surface layer, the chains are trapped in the crystallites, and only a small part of the chains can move freely. The free part of the chains will not cross the interface over a sufficient distance to achieve a good anchorage. In the bulk layer, the chains move freely but are stopped by the growing crystalline layer or used for the build up of this layer.

We can reasonably think that cold crystallization is playing a role on the adhesion. Although very weak, the adhesion is indeed not null and may be linked if interdiffusion is hindered, to a reorganization of crystallites at the interface.

In the case of PBI, we can picture this mechanism as represented in Figure 4.2-4 :

Just before the contact is established at room temperature, the compression molded and quenched PBI plate is amorphous in the bulk, but nuclei are present at the interface (1). By raising the pressure of contact to 50 bars at room temperature, intimate contact is achieved (2). Then the temperature of the assembly increases rapidly to the temperature of contact, by thermal conduction from the heating plate of the press. This thermal conduction implies that the temperature increases from the two sides of the assembly in contact with the heating plates (3). We may imagine that in the earliest time of contact, a temperature gradient is present in the polymer, with a maximum temperature at the surface of the assembly in contact with the press and a minimum at the interface, leading

to less mobility of the amorphous part of the polymer near the interface. Hence the lamellae will grow from the nuclei present at the interface toward the bulk of the sample (4) and not across the interface. When the temperature of contact or the time of contact is increased, we may have a certain lateral growth of the lamellae leading to a slight reinforcement of the interface. For longer times of contact, the bulk will start to cold crystallize and spherulites will grow at random in the bulk (5).

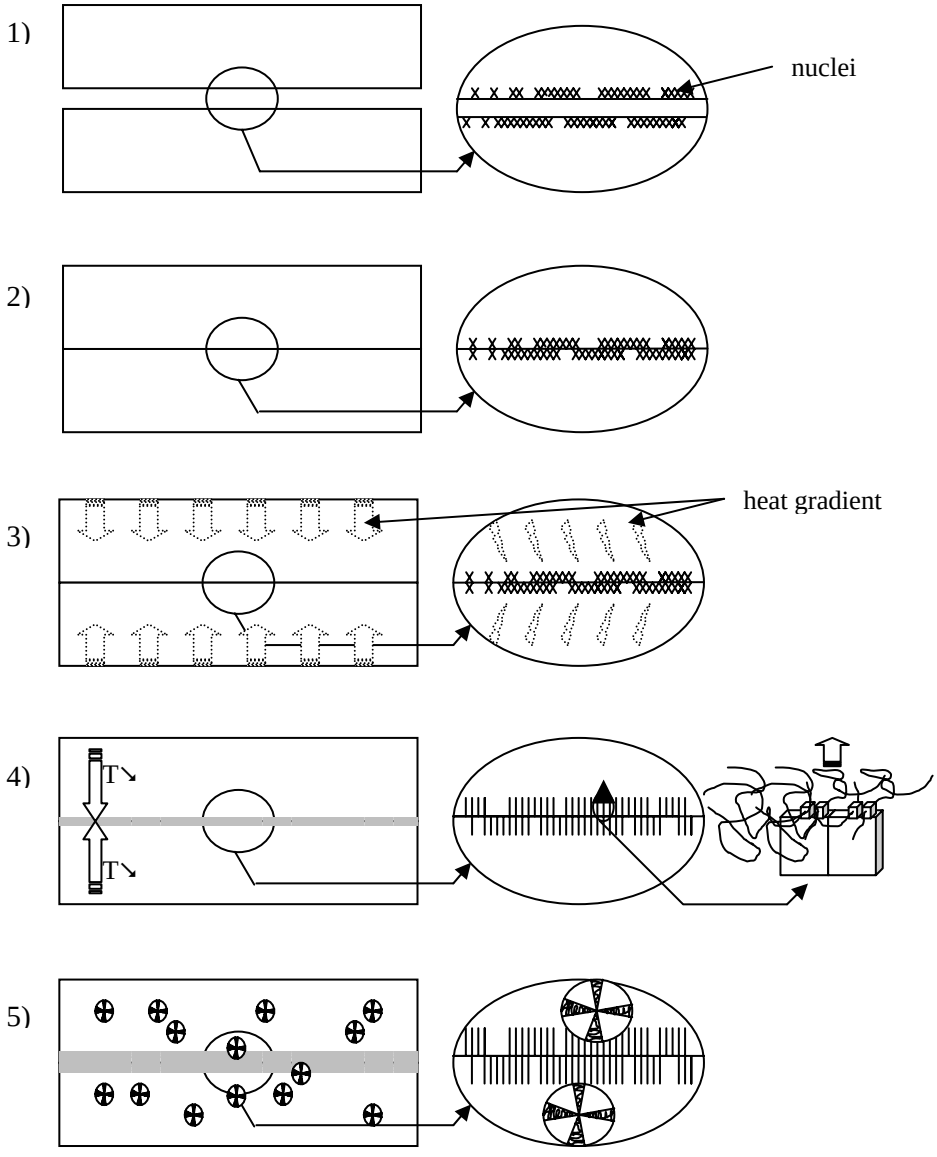

Figure 4.2-4 : schematic representation of a proposed mechanism for PBI

In the case of 45PB, we have probably a similar mechanism, but with a completely different crystallinity. Therefore, the development of the strength of the interface in the case of 45PB[a] is more progressive than in the case of PBI. With 45PB[a], after contact at 40°C for 10 minutes, the interface has probably already reached the step 4 represented in Figure 4.2-4. The steadily increasing fracture toughness with increasing time or temperature is then probably due to a slow densification or reorganisation of the crystallites at the interface.
This slow densification can explain the time dependence observed in region I. A real increase of the fracture toughness will occur in the case of 45PB at temperatures close to the onset of fusion.

4.2.3 Conclusions

Some conclusions can be drawn from these results. First, the fracture toughness of the PBI and 45PB interfaces is especially low at temperatures significantly above T_g (20°C above T_g for the lowest tested temperature). We assume that interdiffusion is hindered by a thin crystalline layer at the interface. From 40°C to 80°C, for both polymers, the fracture toughness increases but remains weak. The formation of a plastic zone at the interface is not likely. Reorganization of crystallites close to the interface and short range interdiffusion are the two possible mechanisms for such reinforcement. Contrary to the studies where co-crystallization enhanced the adhesion to very high values (Gent et al.[1], Xue et al.[2]), in our system, cold crystallization remains a very weak adhesion promoter.

We should notice that even with very short reptation times (few seconds at 70°C) and very low crystallinity, the amorphous part does not really act in the adhesion process.

4.3 Outlook and ideas for future studies

This work can be called an “exploratory” work, since our study remained at a quite qualitative level. However, we tried to extract several ideas from a quite complicated subject, using a complex system, and our analyses, although qualitative, can be the starting point of more quantitative experiments or theoretical improvements.

First, it is quite clear that many parameters act jointly in the crystallization process. Hence the first idea of reducing the overall degree of crystallinity between the different copolymers in order to see the influence of this decrease on adhesion, was indeed naïve, since by changing the overall degree of crystallinity in our samples, a lot of other parameters are also changed. Thus, it is necessary to try to separate the different contributions of the crystallinity on the surface reinforcement. The future of this work

[1]Gent, A. N., et al. Journal of Polymer Science Part B-Polymer Physics, 35(4): 615-622, (1997).
[2]Xue, Y.-Q., et al. Macromolecules, 33: 7084-7087, (2000).

lays in the systematic exploration of the several ideas we raised, by thinking of a specific way of preparing the samples, in order to decorrelate a maximum of crystalline parameters.
Along those lines, we may imagine several types of complementary experiments.

We may think that the melting-recrystallization which occurs in PBT samples, can be used to enhance the adhesion : instead of preheating the sample, contact can be achieved at ambient, and then heated rapidly to the temperature of contact. By doing this, the process of melting-recrystallization will occur when the contact is made and probably act for the surface reinforcement.

In the case of samples obtained in the amorphous state, a special experimental procedure can be imagined to melt the crystalline layer at the surface, by associating a molten sample with an amorphous sample.

We have carried out one experiment with these pre-cited conditions. A PBI plate obtained in the amorphous state, kept at room temperature, was welded with a PBI plate heated above the melting temperature (180°C). We measured the interfacial temperature during contact. The temperature was found more or less constant and equal to 80°C. The results are given in Figure 1.

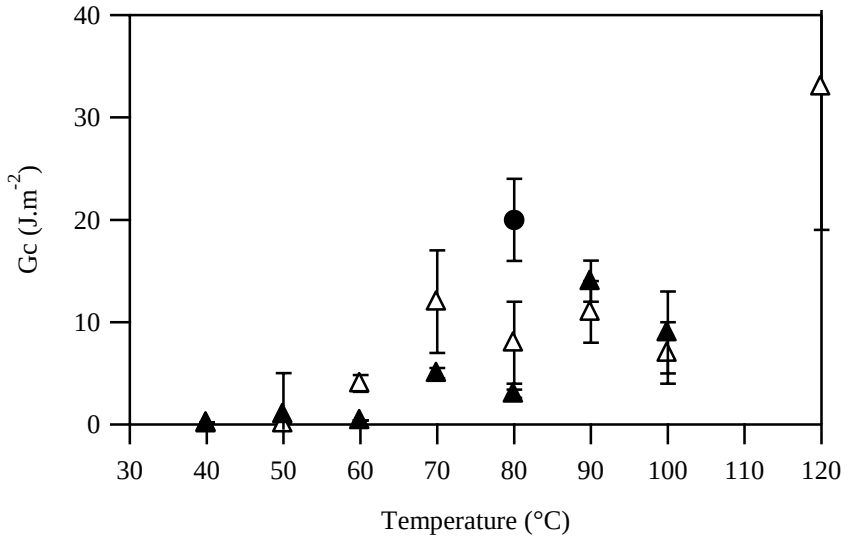

Figure 1 : fracture toughness of PBI for 10 minutes ◢ and 60 minutes of contact △ (crack arrest) and fracture toughness between amorphous and melted sample for 10 minutes of contact ● (crack arrest).

The fracture toughness was found higher in the case of the amorphous/melted assembly. However, the fracture toughness was still relatively weak (20 $J.m^{-2}$).

Our first guess of a rapid melting of the thin crystalline layer at the surface of the amorphous part by the contact with the melting surface, liberating the chains leading to a rapid interdiffusion should be revised. A more extensive study is indeed needed.

Another question emerges from the study of the crystallinity at the surface : which parameters enhance the nucleation of crystalline domains at a polymer surface? Is there a possibility to prevent this surface nucleation?

Ideally, an appropriate experiment to carry out would be a bonding between two semicrystalline polymer, in the amorphous state without any nucleation at the surface. In that case, interdiffusion and cold crystallization should act without disturbing each other.

The presence of nuclei at the surface of compression molded and quenched samples is certainly a common feature of semicrystalline polymers. Thus, to achieve a strong adhesion between semicrystalline polymers, the main objective is probably to get rid of this skin effect.
A possibility might be to get rid of the presence of seeds, by quenching a “free polymer surface”, i.e. try to cool rapidly a free surface from its opposite side.

Instead of heating the polymer from its sides from the heating plate of a press for instance, a heating device can be placed between the two polymer surfaces before contact, in order to melt the crystals at the extreme surface. The contact can be then achieved by quickly removing the heating device. This type of experimental procedure has been used in the work of Lamèthe (Thesis, University of Paris VI, December 2004) on Poly ethyl ester ketone PEEK, and is typically used for fusion bonding.

We may think that in overmolding conditions, the effect of the “crystalline” skin will be dramatic on the adhesion properties. On the other hand, in the case of the injection of a melted polymer on a solid polymer, the melted polymer should be able to melt the very surface of the cold polymer and then lead to a reasonable adhesion. Problems of adhesion may occur in the case where the temperature of the melted polymer is not high enough to melt the very surface of the cold polymer or not high enough to erase the crystalline germs that are known to be still present in a polymer melt which can lead to a rapid surface crystallization.
To achieve a strong adhesion in overmolding conditions, preheating the cold polymer surface just before injecting the polymer melt, by using a heating device placed at the surface of the polymer, might be a solution. Thus at the moment of contact, a certain diffusion should take place before any crystallization process starts.

Conclusion

The initial goal of this thesis was to investigate the possibility of obtaining adhesion between two semi-crystalline polymers put in contact at a temperature above their glass transition temperature but below their melting temperature, i.e. in a range of temperatures where the polymer is macroscopically clearly a solid.

The specific experimental system that we used (a series of random copolymers of poly(butylene terephthalate-co-isophthalate)) allowed us to investigate the effect of a change in degree of crystallization and crystallization rate, in principle from a fully amorphous polymer to a polymer 40% crystalline.

Self-Adhesion was tested by forming interfaces between identical copolymers at various temperatures and during variable contact times, then cooling the sample to room temperature and measuring the fracture toughness of the interface formed in this way.

The main conclusions of our study are the following:

- For all polymers, the fracture toughness of the interface was found to reach the bulk value in the vicinity of the melting temperature, i.e. slightly above in the case of PBT and 15PB and slightly below in the case of 35PB and 45PB.

- For temperatures of contact below the melting temperature, two separate cases must be distinguished : adhesion of pre-crystallized samples and adhesion of quenched samples.

- In the case of **pre-crystallized samples**, when the temperature of contact was decreased from the melting temperature, G_c always decreased significantly to eventually vanish at a temperature which, for all polymers, was well above the glass transition temperature. However this decrease in fracture toughness with increasing (T_m-T) values was found very sharp for PBT, and much less sharp with increasing PBI content in the copolymer.

- The temperature at which the fracture toughness was found null, corresponds well to the onset of the fusion process obtained in a DSC curve of a material prepared in the same conditions as the material used in the adhesion measurements.

- We linked the increase in G_c with increasing temperature beyond the onset of fusion, to the progressive melting of the smallest or unstable crystals, which do not recrystallize immediately after melting. The main mechanism of reinforcement, active after cooling at room temperature seems to be the crystalline reorganization at the interface, for weak values of G_c and co crystallization for higher values of G_c. The interdiffusion as an adhesion

promoting mechanism appears to be active only when an important part of the crystals are melted, i.e. very close or at the melting point.

- In the case of PBT, the first melting peaks, i.e. the melting of the unstable crystals, do not promote the adhesion as recrystallization takes place during the preheating and more stable crystals are formed.

- In the case of **quenched samples of 45PB and PBI**, obtained in the amorphous state, as verified by DSC and WAXS, and put in contact before rising the temperature to the contact temperature, G_c was still, and surprisingly, very low for temperatures of contact well above T_g (up to 60°C above T_g).

- The very thin crystalline layer observed in TEM at 70°C after 10 minutes of contact for PBI, was held responsible of this weak adhesion. Observations in optical microscopy, revealed in both 45PB and PBI samples a very thin bright line, which appears clearly in the case of samples assembled at 60°C during 10 minutes. We assumed that a **certain crystallinity or at least some nuclei were present at the surface of the quenched samples**. These nuclei are the starting point from which the lamellae observed in the TEM experiment have grown.

- Although for a contact temperature of 60°C, the polymer chains of both 45PB and PBI were mobile (confirmed by the calculation of the reptation times at this temperature), a very modest increase in adhesion was observed. Presumably large scale interdiffusion across the interface was prevented or at least greatly hindered by the presence of this crystalline layer at the interface. We observe on the contrary that the mobility of the chains allowed a further growth of this thin crystalline layer localized at the interface, from the nuclei localized at the interface toward the bulk.

- Given the low values of the fracture toughness (below 10 $J.m^{-2}$), neither interdiffusion nor co crystallization were expected to be active below 100°C.

Finally and more generally, we can extract three main conclusions from our work:

The formation of crystalline domains in a polymer is a very effective way to block long range molecular mobility and the crystalline volume fraction must certainly be very low to allow the necessary chain mobility to interdiffuse across an interface below the melting point of the crystals. In a way the crystalline domains act as crosslink points in a rubber.

Furthermore, and unlike the situation of a rubber, surfaces and interfaces act as strong nucleating agents for crystallinity. As a result even a sample macroscopically amorphous in the bulk may have a significant degree of crystallinity at the surface or interface, forming a crystalline skin at the surface. The surface composition will then have a profound effect on the adhesive properties below the melting temperature.

In the case of a contact between quenched semicrystalline polymer samples above T_g, the mobility of the amorphous phase will be used essentially for the growing process of the nuclei if there are present, making impossible any interdiffusion process to take place.

From an industrial point of view, one thing should be kept in mind from this work : the huge influence of the crystallinity at the extreme surface of a semicrystalline polymer when one tries to bond this surface to another surface. In order to obtain a good adhesion between semicrystalline polymers, one must get rid of any crystallinity at the extreme surface of the materials. We believe that co-crystallization is a very efficient way to reinforce the interfaces between semicrystalline polymers, but this mechanism will take place only if a certain interdiffusion occurs before the recrystallization or before cold crystallization in the case of contact between semicrystalline polymers in the amorphous state. In other words, interdiffusion should precede the crystallization in order to have a chance to obtain a strong adhesion between semicrystalline polymers.

References

Alexander, L. E. *X-ray Diffraction Methods in Polymer Science*. (Wiley-Interscience, New York, 1969)

Avrami, M. Journal of Chemical Physics, **7**: 1103, (1939).

Bandiera, M., Munari, A., Manares, P. and Pizzoli, M. *Dilute solution and thermal behaviour of random poly(butylene isophthalate/terephthalate) copolymers*. European Polymer Journal, **30**(4): 503-508, (1994).

Bandiera, M., Munari, A. and Pezzin, G. *Rheological Characterization of random poly(butylene isophthalate:terephthalate) copolymers*. European Polymer Journal, **33**(4): 497-500, (1997).

Behan, P., Bevis, M. and Hull, D. Proceedings of the Royal Society of London, series A: Mathematical and Physical Sciences, **A243**: 525, (1975).

Benkoski, J. J., Flores, P. and Kramer, E. J. *Diblock Copolymer Reinforced Interfaces between Amorphous Polystyrene and Semicrystalline Polyethylene*. Macromolecules, **36**: 3289-3302, (2003).

Benkoski, J.-J., Frederickson, G. H. and Kramer, E. J. *Model for the fracture energy of glassy polymer-polymer interfaces*. Journal of polymer science: Part B: Polymer Physics, **40**(20): 2377-2386, (2002).

Bidaux, J. E., Smith, G. D., Bernet, N., Manson, J. A. E. and Hilborn, J. *Fusion bonding of maleic anhydride grafted polypropylene to polyamide 6 via in situ block copolymer formation at the interface*. Polymer, **37**(7): 1129-1136, (1996).

Bidaux, J. E., Smith, G. D., Manson, J. A. E., Plummer, C. J. G. and Hilborn, J. *Fusion bonding of maleic anhydride grafted polypropylene-polyamide 6 blends to polyamide 6*. Polymer, **39**(24): 5939-5948, (1998).

Boiko, Y. M. *Self-bonding of noncrystallizable and crystallizable amorphous polymers*. Polymer Science Series A, **45**(8): 795-799, (2003).

Boiko, Y. M., Guérin, G., Marikhin, V. A. and Prud'homme, R. E. *Healing of interfaces of amorphous and semi-cristalline poly(ethylene terephthalate) in the vicinity of the glass tansition temperature*. Polymer, **42**: 8695-8702, (2001).

Boucher, E., Folkers, J. P., Creton, C., Hervet, H. and Léger, L. *Enhanced Adhesion between Polypropylene and Polyamide-6: Role of Interfacial Nucleation of the β-Crystalline Form of Polypropylene*. Macromolecules, **30**: 2102-2109, (1997).

Boucher, E., Folkers, J. P., Hervet, H., Leger, L. and Creton, C. *Effects of the formation of copolymer on the interfacial adhesion between semicrystalline polymers*. Macromolecules, **29**(2): 774-782, (1996).

Brochart-Wyart, F. and Pincus, P. *End Segregation Effects on Polymer Interdiffusion*. Comptes Rendus de l'Académie des Sciences de Paris, Série II: 131-138, (1992).

Brown, H. R. *Effect of a Diblock Copolymer on the Adhesion between Incompatible Polymers*. Macromolecules, **22**: 2859-2860, (1989).

Brown, H. R. *Mixed-mode effect on the toughness of polymer interfaces*. Journal of Materials Science, **25**: 2791-2794, (1990).

Brown, H. R. *A Molecular Interpretation of the Toughness of Glassy Polymers*. Macromolecules, **24**: 2752-2756, (1991).

Brown, H. R. *Relation between the width of an interface between two polymers and its toughness*. Macromolecules, **34**: 3720-3724, (2001).

Brown, H. R., Deline, V. R. and Green, P. F. *Evidence for cleavage of polymer chains by crack propagation*. Nature, **341**: 221-222, (1989).

Champetier, G. and Monnerie, L. *Introduction à la chimie macromoléculaire.* (Masson, Paris, 1969)

Char, K., Brown, H. R. and Deline, V. R. *Effects of a Diblock Copolymer on Adhesion between Immiscible Polymers. 2. PS-PMMA Copolymer between PPO and PMMA.* Macromolecules, **26**: 4164-4171, (1993).

Cheng, S. Z. D., Pan, R. and Wunderlich, B. *Thermal-Analysis of Poly(Butylene Terephthalate) for Heat-Capacity, Rigid-Amorphous Content, and Transition Behavior*. Makromolekulare Chemie-Macromolecular Chemistry and Physics, **189**(10): 2443-2458, (1988).

Cho, K., Brown, H. R. and Miller, D. C. *Effect of a block copolymer on the adhesion between incompatible polymers. I. Symmetric tests*. Journal of Polymer Science: Part B: Polymer Physics, **28**: 1699-1718, (1990).

Cho, K. and Li, F. *Reinforcement of amorphous and semicrystalline polymer interfaces via in-situ reactive compatibilization*. Macromolecules, **31**: 7495-7505, (1998).

Creton, C., Brown, H. R. and Deline, V. R. *Influence of chain entanglement on the failure modes in block copolymer toughened interfaces*. Macromolecules, **27**: 1774-1780, (1994).

Creton, C., Kramer, E. J., Hui, C. Y. and Brown, H. R. Adhesion and fracture of interfaces between immiscible polymers: From the molecular to the continuum scale. Advance in Polymer Science : Molecular Simulation Fracture Gel Theory. **156:** 53-136, (2002)

Creton, C., Kramer, E. J., Hui, C. Y. and Brown, H. R. *Failure mechanisms of polymer interfaces reinforced with block copolymers*. Macromolecules, **25**: 3075-3088, (1992).

Dangseeyun, N., Srimoaon, P., Supaphol, P. and Nithitanakul, M. *Isothermal melt-crystallization and melting behavior for three linear aromatic polyesters*. Thermochimica Acta, **409**: 63-77, (2004).

de Gennes, P. G. Journal of Chemical Physics, **55**: 572-579, (1971).

de Gennes, P. G. *Scaling Concepts in Polymer Physics*. (Cornell University Press, London, 1979)

de Gennes, P. G. *Compatible Polymer Systems - Special Properties for Mutual Diffusion and for Adhesion*. Comptes Rendus De L Academie Des Sciences Serie Ii, **292**(23): 1505-1507, (1981).

de Gennes, P. G. *Entangled Polymers*. Physics Today, **36**(6): 33-&, (1983).

Desborough, I. J. and Hall, I. H. *Comparison of Published Crystalline-Structures of Poly(Tetramethylene Terephthalate)*. Polymer, **18**(8): 825-830, (1977).

Doi, M. and Edwards, S. J. Journal of the Chemical Society; Faraday Transactions, **74**: 1789-1801, 1802-1818, 1818-1832, (1978).

Dugdale, D. S. Journal of Mechanics and Physics of Solids, **8**: 100, (1960).

Ferry, J. D. *Viscoelastic properties of polymers*. (John Wiley, New York, 1970)

Finelli, L., Lotti, N. and Munari, A. *Crystallization kinetics and melting behavior of poly(butylene isophthalate/terephthalate) random copolyesters*. European Polymer Journal, **37**: 2039-2046, (2001).

Flory, P. J. Journal of Chemical Physics, **17**: 303, (1949).

Flory, P. J. *Principles of Polymer Chemistry*. (Cornell University Press: Ithaca, New York, 1953)

Gedde, U. W. *Polymer Physics*. (Kluwer Academic Publisher, 1995)

Gent, A. N., Kim, E. G. and Ye, P. *Autohesion of crosslinked polyethylene*. Journal of Polymer Science Part B-Polymer Physics, **35**(4): 615-622, (1997).

Gervat, L. *Structure, propriétés mécaniques et renforcement au choc du Poly(terephthalate de butylene glycol)*. (Université de Paris VI, Paris, 2001)

Gledhill, R. A., Kinloch, A. J., Yamini, S. and Young, R. J. *Relationship between Mechanical-Properties of and Crack Propogation in Epoxy-Resin Adhesives*. Polymer, **19**(5): 574-582, (1978).

Griffith, A. A. Philosophical Transactions of the Royal Society of London, series A: Mathematical and Physical Sciences, **A221**: 163, (1920).

Haubruge, H. G., Jonas, A. M. and Legras, R. *Staining of poly(ethylene terephthalate) by ruthenium tetroxide*. Polymer, **44**: 3229-3234, (2003).

Helfand, E. and Tagami, Y. *Theory of Interface between Immiscible Polymers*. Journal of Chemical Physics, **57**(4): 1812-&, (1972).

Hobbs, S. Y. and Pratt, C. F. *Multiple Melting in Poly(Butylene-Terephthalate)*. Polymer, **16**(6): 462-464, (1975).

Hoffman, J. D., Davis, G. T. and Lauritzen, J. I. *Treatise on Solid State Chemistry*New York, 1976)

Hoffman, J. D. and Weeks, J. J. *Melting Process and Equilibrium Melting Temperature of Polychlorotrifluoroethylene*. Journal of Research of the National Bureau of Standards Section a-Physics and Chemistry, **66**(JAN-F): 13-&, (1962).

Hui, C. Y., Ruina, A., Creton, C. and Kramer, E. J. *Micromechanics of crack growth into a craze in a polymer glass*. Macromolecules, **25**: 3948-3955, (1992).

Huo, P. P. and Cebe, P. *Melting-Point Depression in Poly(Butylene Terephthalate)/Polyarylate Blends*. Macromolecules, **26**(12): 3127-3130, (1993).

Huo, P. P., Cebe, P. and Capel, M. *Real-Time X-Ray-Scattering Study of Thermal-Expansion of Poly(Butylene Terephthalate)*. Journal of Polymer Science Part B-Polymer Physics, **30**(13): 1459-1468, (1992).

Illers, K. *Heat of fusion and specific volume of PET and PBT*. Colloid and Polymer Science, **258**(2): 117-124, (1980).

Illers, K. H. *Heat of Fusion and Specific Volume of Poly(Ethylene-Terephthalate) and Poly(Butylene Terephthalate)*. Colloid and Polymer Science, **258**(2): 117-124, (1980).

Irwin, G. R. Journal of Applied Mechanics, **29**: 651-654, (1962).

Jadhav, J. *Encyclopedia of polymer science and engineering*. (Wiley, New York, 1988)

Janik, H., Walch, E. and Gaymans, R. J. *Ruthenium tetroxide staining of polybutylene terephthalate (PBT) and polyisobutylene-b-PBT segmented block copolymers*. Polymer, **33**(16): 3522-3524, (1992).

Jud, K., Kausch, H. H. and Williams, J. G. *Fracture Mechanics Studies of Crack Healing and Welding of Polymers*. Journal of Materials Science, **16**: 204-210, (1981).

Kalb, F. *Adhésion, microstructure et microdéformations à l'interface de polymères semi-cristallins*. (Université Paris VI, Paris, 1998)

Kalb, F., Leger, L., Creton, C., Plummer, C. J. G., Marcus, P. and Magalhaes, A. *Molecular control of crack tip plasticity mechanisms at a PP-EPDM/PA6 interface*. Macromolecules, **34**(8): 2702-2709, (2001).

Kanninen, M. F. *An augmented Double Cantilever Beam Model for Studying Crack Propagation and Arrest*. International Journal of Fracture, **9**: 83-92, (1973).

Kelly, A. *Stong solids*. (Charendon Press, Oxford, 1966)

Kim, H. J., Lee, K. J. and Seo, Y. *Enhancement of interfacial adhesion between polypropylene and nylon 6: Effect of surface functionalization by low-energy ion-beam irradiation*. Macromolecules, **35**(4): 1267-1275, (2002).

Kinloch, A. J. and Williams, J. G. *Crack blunting mechanisms in polymers*. Journal of Materials Science, **15**: 987-996, (1980).

Kovacs, A. J. *La Contraction Isotherme Du Volume Des Polymeres Amorphes*. Journal of Polymer Science, **30**(121): 131-147, (1958).

Kramer, E. J. *Microscopic and Molecular Fundamentals of Crazing*. Advances in Polymer Science, **52-3**: 1-56, (1983).

Kramer, E. J. and Berger, L. L. *Fundamental Processes of Craze Growth and Fracture*. Advances in Polymer Science, **91/92**: 1-68, (1990).

Kunz, K. and Stamm, M. *Initial Stages of Interdiffusion of PMMA across an Interface*. Macromolecules, **29**: 2548-2554, (1996).

Landau, L. and Lifchitz, E. *Théorie de l'élasticité*. (Mir, Moscou, 1967)

Laurens, C., Creton, C. and Léger, L. *Adhesion Promotion Mechanisms at Isotactic Polypropylene/Polyamide 6 Interfaces: Role of the Copolymer Architecture*. Macromolecules, **37**(18): 6814-6822, (2004).

Laurens, C., Ober, R., Creton, C. and Léger, L. *Crystalline Orientation and Adhesion at Polypropylene/Polyamide 6 Interfaces Compatibilized with Syndiotactic Polypropylene-Polyamide 6 Diblock Copolymers*. Macromolecules, **37**(18): 6806-6813, (2004).

Li, J. X. and Cheung, W. L. *RuO_4 Staining and Lamellar Structure of α– and β–PP*. Journal of Applied Polymer Science, **72**: 1529-1538, (1999).

Li, J. X., Ness, J. N. and Cheung, W. L. *Lamellar Structure of POM Spherulites Imaged by a Two-Stage RuO_4 Staining Technique*. Journal of Applied Polymer Science, **59**: 1733-1740, (1996).

Liu, J. and Geil, P. H. *Electron diffraction and computer modeling studies of the crystal structure of poly(butylene terephthalate) alpha-form single crystals*. Journal of macromolecular Science - Physics, **B36**(2): 263-280, (1997).

Lo, C. T., Laabs, F. C. and Narasimhan, B. *Interfacial adhesion mechanisms in incompatible semicrystalline polymer systems*. Journal of Polymer Science Part B-Polymer Physics, **42**(14): 2667-2679, (2004).

Lo, C. T., Seifert, S., Thiyagarajan, P. and Narasimhan, B. *Phase behavior of semicrystalline polymer blends*. Polymer, **45**(11): 3671-3679, (2004).

Magill, J. H. *Morphogenesis of Solid Polymers*. (Academic Press, New York, 1977)

Marrs, W., Peters, R. H. and Still, R. H. *Copolyester Studies .2. Melting and Crystallization Behavior of Tetramethylene Terephthalate-Tetramethylene Sebacate Copolymers*. Journal of Applied Polymer Science, **23**(4): 1077-1093, (1979).

McCrum, N. G., Reed, B. E. and William, G. *Anelastic and dielectric effets in polymeric solids*. (John Wiley, London, 1967)

Mencik, Z. *Crystal-Structure of Poly(Tetramethylene Terephthalate)*. Journal of Polymer Science Part B-Polymer Physics, **13**(11): 2173-2181, (1975).

Miller, P., Buckley, D. J. and Kramer, E. J. *Microstructure and origin of cross-tie fibrils in crazes*. Journal of Materials Science, **26**: 4445-4454, (1991).

Misra, A. and Garg, S. N. *Morphology and Properties of Poly(Butylene Terephthalate)*. Journal of Polymer Science Part C-Polymer Letters, **20**(2): 121-125, (1982).

Montezinos, D., Wells, B. G. and Burns, J. L. *The Use of Ruthenium in Hypochlorite as a Stain for Polymeric Materials*. Journal of Polymer Science, Polymer Letters Edition, **23**: 421-425, (1985).

Murthy, N. S. and Minor, H. *General procedure for evaluating amorphous scattering and crystallinity from X-ray diffraction scans of semicrystalline polymers*. Polymer, **31**: 996-1002, (1990).

Nichols, M. E. and Robertson, R. E. *The Multiple Melting Endotherms from Poly (Butylene Terephthalate)*. Journal of Polymer Science Part B-Polymer Physics, **30**(7): 755-768, (1992).

Odian, G. *Principles of Polymerization*. (Wiley, New York, 1981)

Peszkin, P. N., Schultz, J. M. and Lin, J. S. *Kinetics of Fiber Heat-Treatment .3. Poly(Butylene Terephthalate) Fibers*. Journal of Polymer Science Part B-Polymer Physics, **24**(12): 2617-2630, (1986).

Phillips, R. A., McKenna, J. M. and Cooper, S. L. *Glass-Transition and Melting Behavior of Poly(Ether-Ester) Multiblock Copolymers with Poly(Tetramethylene Isophthalate) Hard Segments*. Journal of Polymer Science Part B-Polymer Physics, **32**(5): 791-802, (1994).

Plummer, C. J. G. and Kausch, H. H. *Micronecking in thin films of isotactic polypopylene*. Macromolecular Chemistry and Physics, **197**(6): 2047-2063, (1996).

Plummer, C. J. G., Kausch, H. H., Creton, C., Kalb, F. and Léger, L. *Structure and Microdeformation of (iPP/iPP-g-MA)-PA6 Reaction Bonded Interfaces*. Macromolecules, **31**(18): 6164-6176, (1998).

Pompe, G., Haussler, L. and Winter, W. *Investigations of the equilibrium melting temperature in PET and PC/PBT blends*. Journal of Polymer Science Part B-Polymer Physics, **34**(2): 211-219, (1996).

Prager, S. and Tirrell, M. *The Healing Process at Polymer-Polymer Interfaces*. Journal of Chemical Physics, **75**(10): 5194-5198, (1981).

Pratt, C. F. and Hobbs, S. Y. *Comparative Study of Crystallization Rates by Dsc and Depolarization Microscopy*. Polymer, **17**(1): 12-16, (1976).

Rempp, P. and Merrill, E. W. *Polymer Synthesis*. (Hüthig & Wepf Verlag Basel, New York, 1991)

Righetti, M. C. and Munari, A. *Influence of branching on melting behavior and isothermal crystallization of poly(butylene terephthalate)*. Macromolecular Chemistry and Physics, **198**: 363-378, (1997).

Righetti, M. C., Pizzoli, M., Lotti, N. and Munari, A. *Crystallization kinetics and melting behavior of poly(butylene adipade), poly(butylene isophthalate) and their copolymers*. Macromolecular Chemistry and Physics, **199**: 2063-2070, (1998).

Runt, J., Miley, D. M., Zhang, X., Gallagher, K. P., McFeaters, K. and Fishburn, J. *Crystallization of Poly(Butylene Terephthalate) and Its Blends with Polyarylate*. Macromolecules, **25**(7): 1929-1934, (1992).

Russell, T. P., Deline, V. R., Dozier, W. D., Felcher, G. P., Agrawal, G., Wool, R. P. and Mays, J. W. *Direct Observation of Reptation at Polymer Interfaces*. Nature, **365**: 235-237, (1993).

Schawe, J. E. K. *A comparison of different evaluation methods in modulated temperature DSC*. Thermochimica Acta, **260**: 1-16, (1995).

Schnell, R., Stamm, M. and Creton, C. *Direct Correlation between Interfacial Width and Adhesion in Glassy Polymers*. Macromolecules, **31**: 2284-2292, (1998).

Schnell, R., Stamm, M. and Creton, C. *Mechanical Properties of Homopolymer Interfaces: Transition from Simple Pullout to Crazing with Increasing Interfacial Width*. Macromolecules, **32**(10): 3420-3425, (1999).

Schweizer, K. S. Journal of Chemical Physics, **91**: 5822, (1989).

Sha, Y., Hui, C. Y., Ruina, A. and Kramer, E. J. *Detailed simulation of craze fibril failure at a crack tip in a glassy polymer*. Acta Materialia, **45**(9): 3555-3563, (1997).

Smith, G. D., Plummer, C. J. G., Bourban, P. E. and Manson, J. A. E. *Non-isothermal fusion bonding of polypropylene*. Polymer, **42**: 6247-6257, (2001).

Sperling, L. H. *Introduction to physical polymer science*. (Wiley-interscience, New York, 1992)

Stambaugh, B., Koenig, J. L. and Lando, J. B. *X-Ray-Investigation of the Structure of Poly(Tetramethylene Terephthalate)*. Journal of Polymer Science Part B-Polymer Physics, **17**(6): 1053-1062, (1979).

Stamm, M., Hüttenbach, S., Reiter, G. and Springer, T. *Initial Stages of Polymer Interdiffusion Studied by Neutron Reflectometry*. Europhysics Letters, **14**(5): 451-456, (1991).

Stein, R. S. and Misra, A. *Morphological-Studies on Polybutylene Terephthalate*. Journal of Polymer Science Part B-Polymer Physics, **18**(2): 327-342, (1980).

Strobl, G. *The Physics of Polymers*. (Springer-Verlag, Berlin, 1996)

Tadokoro, H. *Structure of Crystalline Polymers*. (Wiley-Interscience, New York, 1979)

Tashiro, K., Nakai, Y., Kobayashi, M. and Tadokoro, H. *Solid-State Transition of Poly(Butylene Terephthalate) Induced by Mechanical Deformation*. Macromolecules, **13**(1): 137-145, (1980).

Voyutskii, S. S. *The diffusion theory of adhesion*. Rubber Chemistry and Technology: 748-756,

Voyutskii, S. S. and Vakula, V. L. *The role of diffusion phenomena in Polymer to polymer adhesion*. Journal of Applied Polymer Science, **7**: 475-491, (1963).

Ward, I. M. *Mechanical Properties of Solid Polymers*. (Wiley, Chichester, 1983)

Warren, B. E. *X-Ray Diffraction*. (Dover, New York, 1969)

Washiyama, J., Creton, C. and Kramer, E. J. *TEM fracture studies of polymer interfaces*. Macromolecules, **25**: 4751-4758, (1992).

Washiyama, J., Creton, C., Kramer, E. J., Xiao, F. and Hui, C. Y. *Optimum toughening of homopolymer interfaces with block copolymers*. Macromolecules, **26**: 6011-6020, (1993).

Washiyama, J., Kramer, E. J., Creton, C. and Hui, C. Y. *Chain pullout fracture of polymer interfaces*. Macromolecules, **27**: 2019-2024, (1994).

Westergaard, H. M. Journal of Applied Mechanics, **A June**: 46, (1939).

Williams, J. G. *Fracture Mechanics of Polymers*. (Ellis Horwood Limited, New York, 1984)

Wu, S. H. *Control of Intrinsic Brittleness and Toughness of Polymers and Blends by Chemical-Structure - a Review*. Polymer International, **29**(3): 229-247, (1992).

Wunderlich, B. *Macromolecular Physics*. (Academic Press, Orlando, 1973)

Xiao, F., Hui, C.-Y., Washiyama, J. and Kramer, E. J. *Phase angle effects on fracture toughness of polymer interfaces reinforced with block copolymers*. Macromolecules, **27**: 4382-4390, (1994).

Xu, D. B., Hui, C. Y., Kramer, E. J. and Creton, C. *A micromechanical model of crack growth along polymer interfaces*. Mechanics of Materials, **11**: 257-268, (1991).

Xue, Y.-Q., Tervoort, T. A. and Lemstra, P. J. *Welding Behavior of Semicrystalline Polymers. 1. The effect of Nonequilibrium Chain Conformations on Autoadhesion of UHMWPE*. Macromolecules, **31**: 3075-3080, (1998).

Xue, Y.-Q., Tervoort, T. A., Rastogi, S. and Lemstra, P. J. *Welding Behavior of Semicrystalline Polymers. 2. Effect of Cocrystallisation on Autoadhesion*. Macromolecules, **33**: 7084-7087, (2000).

Yasuniwa, M., Tsubakihara, S., Ohoshita, K. and Tokudome, S. *X-Ray studies on the Double Melting Behavior of Poly(butylene terephthalate)*. Journal ofPolymer Science: Part B, **39**: 2005-2015, (2001).

Yokouchi, M., Sakakibara, Y., Chatani, Y., Tadokoro, H., Tanaka, T. and Yoda, K. *Structures of Two Crystalline Forms of Poly(butylene terephthalate) and Reversible Transition between Them by Mechanical Deformation*. Macromolecules, **9**(2): 266-273, (1976).

Young, R. J. and Lovell, P. A. *Introduction to polymers*. (Chapman & Hall, London, 1991)

Yuan, B. L. and Wool, R. P. *Strength Development at Incompatible Semicrystalline Polymer Interfaces*. Polymer Engineering and Science, **30**(22): 1454-1464, (1990).

Zhao, W., Zhao, X., Rafailovich, M. H. and Sokolov, J. *Segregation of Chain Ends to Polymer Melt Surfaces and Interfaces*. Macromolecules, **26**: 561-562, (1993).

Extended abstract in French

Introduction

L'adhésion est un vaste sujet qui concerne la force de couplage qui peut exister entre n'importe quelle paire de matériaux. Dans cette étude, nous avons considéré le cas d'un couplage entre matériaux polymère et plus précisément entre polymères semi-cristallins. L'adhésion entre polymères semi-cristallins a été largement étudiée depuis une quinzaine d'années du fait des nombreuses applications industrielles concernant l'association de deux ou plusieurs polymères semi-cristallins. Malgré tout, de nombreuses questions restent à ce jour encore sans réponse.

Dans le but d'obtenir une meilleure compréhension du rôle que joue la cristallinité sur l'adhésion, nous avons étudié le cas simple de l'auto-adhésion (adhésion d'un composé sur lui-même) entre polymères semi-cristallins de taux de cristallinité variable. L'adhésion a été mesurée par un test de fracture des interfaces formées à des températures comprises entre leur température de fusion T_f et leur température de transition vitreuse T_g, dans le but de définir le rôle de la cristallinité sur l'adhésion et sur les mécanismes de fracture.

Les mécanismes permettant le renforcement des interfaces entre polymères amorphes sont aujourd'hui relativement bien connus, mais leur transposition simple au cas des interfaces entre polymères semi-cristallins ne permet pas d'expliquer certains comportements mis en évidence dans les études sur les assemblages entre polymères semi-cristallins. En effet, les quelques études menées jusqu'à présent mettent en lumière le rôle essentiel que joue la cristallinité sur l'adhésion, sans pour autant parvenir à expliquer par quels mécanismes précis la cristallinité joue sur le renforcement des interfaces. Certains mécanismes comme la co-cristallisation de chaînes provenant de part et d'autre de l'interface, ou l'organisation des cristallites à l'interface tel la croissance epitaxiale de cristallites à l'interface, sont reconnus comme ayant une influence sur l'adhésion. Cependant, ces mécanismes ont été observés la plus part du temps pour des températures de contact supérieures à la température de fusion des polymères étudiés ou au moins supérieures à la température de fusion d'un des polymères dans le cas d'assemblages asymétriques. Dans ces conditions, au moment du contact, les chaînes du fondu peuvent se mouvoir librement et les mécanismes d'interdiffusion puis de co-cristallisation lors du refroidissement de l'assemblage sont susceptibles de se produire. Malgré tout, les paramètres qui influencent les mécanismes de co-cristallisation et d'interdiffusion aux interfaces entre polymères semi-cristallins sont encore mal connus. Il convient définir ces paramètres qui pourraient influencer les mécanismes de co-cristallisation et d'étudier plus en détail l'évolution de l'adhésion lorsque la température de contact est abaissée sous la température de fusion.

Dans l'étude présente, nous avons essayé de répondre à certaines de ces questions, mais également de mieux comprendre l'influence que pouvait avoir la phase amorphe dans le cas d'un contact effectué en dessous de T_f, mais au dessus de T_g. Pour cela, nous avons

utilisé une série de copolymères statistiques de polybutylène(téréphthalate-co-isophthalate), pouvant être préparés avec différents taux de cristallinité en fonction de l'histoire thermique et de la composition (proportion de PBI par rapport au PBT), que nous avons mis en contact à différentes températures comprises entre T_g et T_f. Après une caractérisation fine de la cristallinité des différents copolymères, l'adhésion a été mesurée à température ambiante par un test de fracture : le test de clivage en coin.

Partie expérimentale et caractérisations

Synthèse

Des copolymères de *poly(butylène téréphtalate-co-isophthalate)* ont été synthétisés par polycondensation ainsi qu'un homopolymère, le *polybutylène d'isophthalate (PBI)*. Le *polybutylene de téréphthalate (PBT)* est un produit industriel. L'association du *PBT* et du *PBI* a permis d'avoir accès à une large gamme de taux de cristallinité, de températures de fusion ainsi qu'à différents comportements de cristallisation ou de fusion (fusion multiple, fusion-recristallisation…). Nous avons utilisé pour cette étude deux homopolymères : le *PBT* et le *PBI*, ainsi que trois copolymères définis par la proportion relative en masse de *PBI* : le *15PB* (15%PBI et 85%PBT), le *35PB* et le *45PB*.

Caractérisations

Une caractérisation a été menée sur les différents polymères et copolymères, afin d'obtenir les différents paramètres nécessaires à l'interprétation des résultats d'adhésion. Tout d'abord une caractérisation au niveau moléculaire a été menée : par dosage des bouts de chaîne, nous avons obtenu une masse molaire moyenne en nombre M_n de 20 kg.mol^{-1} pour le *PBT*, de 21 à 24 kg.mol^{-1} pour les 3 copolymères et enfin de 30 kg.mol^{-1} pour le *PBI*. Des masses moyennes entre points d'enchevêtrement, M_e, d'environ 4 kg.mol^{-1}, et des temps de reptation, τ_{rept}, d'environ 2 s, pour une température de référence de 100°C, ont été obtenus par une étude en rhéologie à partir du fondu pour *35PB*, *45PB* et *PBI*. Du fait de leur cristallisation rapide, cette méthode n'a pu être utilisée pour déterminer M_e et τ_{rept} dans le cas du *PBT* et du *15PB*. Le temps de reptation a été considéré identique à celui obtenu pour le *35PB*, *45PB* et *PBI* et la valeur de M_e pour le *PBT* et le *15PB* a été prise à partir de données de la littérature : 1.6 kg.mol^{-1}. L'étude RMN du carbone mené sur les copolymères a permis de montrer que les copolymères comprenaient une certaine proportion de blocs courts et n'étaient donc par purement statistiques.

Les différents polymères ont également été caractérisés par des techniques d'analyse thermique différentielles modulée (TM-DSC), d'analyse mécanique dynamique (DMA) et de diffraction de rayons X aux grands angles (WAXS).

La DSC modulée a permis de caractériser le comportement des différents polymères et copolymères en cristallisation et fusion anisotherme. Une procédure expérimentale identique a été appliquée à tous les polymères : lors de cette procédure dite « standard », les différents granulés de polymères ont été recuits à 260°C, bien au dessus de leur température de fusion, dans le but d'effacer l'histoire thermique, puis refroidis de manière contrôlée (5°C.min^{-1}) jusqu'à -50°C, largement en dessous de la température de transition vitreuse, et chauffés enfin de manière également contrôlée (5°C.min^{-1}) jusqu'au dessus de leur température de fusion. Deux familles de comportement ont pu être mises en évidence. D'un côté le *PBT* et le *15PB,* qui de part leur cristallisation relativement rapide, cristallisent pendant le refroidissement contrôlé et qui ne montrent pas de cristallisation froide lors de la chauffe. De l'autre côté, le *35PB,* le *45PB* et le *PBI* qui cristallisent plus lentement, ce qui se traduit par une absence de pic de cristallisation lors du refroidissement à cette vitesse. La présence d'un pic de cristallisation froide lors de la chauffe a été observée pour le *35PB* et le *45PB.* Toutefois, nous avons constaté que le *35PB* cristallisait tout de même partiellement durant le refroidissement d'après le calcul du taux de cristallinité après le refroidissement et avant la chauffe. Pour le *PBI* aucun pic de cristallisation froide ne pu être observé dans les conditions standard, probablement du fait de la cinétique trop lente de cristallisation froide du *PBI.*

Les spectres rayons X aux grands angles ont montré que la structure cristalline des copolymères était pratiquement identique à celle du PBT, le PBI quant à lui cristallisant dans une structure différente. Le taux de cristallinité a pu être calculé à partir des spectres rayons X en effectuant le rapport entre les pics cristallins et la bosse amorphe. Les taux de cristallinité obtenus par cette méthode étaient semblables à ceux obtenus par DSC. Une diminution progressive du taux de cristallinité a été observée du *PBT* au *45PB.*

Les propriétés mécaniques des différents polymères et copolymères ont été étudiées en DMA. Une première série d'expériences a été menée sur le *PBT*, le *15PB* et le *35PB* refroidis lentement après avoir été moulés à haute température. La courbe de *G'* en fonction de la température suivait un comportement classique de polymères semi-cristallins, avec une diminution du module à la T_g suivie d'une chute de ce module à la température de fusion. Dans une deuxième série, le *35PB*, le *45PB* et le *PBI* ont été trempés après avoir été moulés. La cristallisation froide a pu être observée mécaniquement par l'augmentation brutale du module *G'* pour des températures supérieures à la température de transition vitreuse.

Résultats et interprétations

D'après ces caractérisations, nous avons effectué deux séries d'expériences. Dans une première série d'expériences l'adhésion a été mesurée à l'ambiante sur des assemblages formés après contact entre plaques pré-cristallisées. Les différents polymères (*PBT*, *15PB*, *35PB*, *45PB*) ont été moulés dans des conditions identiques, à une température 20°C supérieure à la température de fusion de chaque polymère, puis refroidis de manière contrôlée et lente (2.5°C.min^{-1}) jusqu'à température ambiante. Un montage spécialement

conçu pour ces travaux a permis de préchauffer les plaques à la température de contact avant d'effectuer le contact. Ce temps de préchauffage permet à la surface d'atteindre une température proche de la température de contact (température contrôlée par un thermocouple de surface) avant le contact et d'atteindre un état d'équilibre vis à vis d'une éventuelle cristallisation ou fusion. Des analyses thermiques furent menées en parallèle sur des plaques moulées dans les conditions précitées et recuites dans le cas du *35PB* et *45PB* à des températures et des temps de recuit simulant l'étape de préchauffage avant assemblage.

Pour les quatre polymères, nous avons obtenu une adhésion forte pour des températures de contact proches de la T_f. En abaissant la température de contact, le taux critique de restitution d'énergie, G_c diminue plus ou moins rapidement selon le polymère, jusqu'à devenir nul à une température inférieure à T_f mais bien supérieure à la température de transition vitreuse des différents polymères. Pour le *PBT*, la diminution de G_c lorsque la température de contact est progressivement abaissée sous T_f est extrêmement rapide, G_c passant d'une valeur élevé à quelques $J.m^{-2}$ pour une diminution de la température de contact de 5°C. La diminution de G_c avec $T_{contact}$ est beaucoup plus progressive pour le *15PB* et surtout pour les *35PB* et *45PB*. La température au dessus de laquelle une certaine adhésion apparaît correspond à la température du début du pic de fusion du matériau ayant subi le même traitement thermique que celui subi lors des expériences d'adhésion. L'apparition de l'adhésion correspond donc à la fusion des premiers cristallites. Cependant, aux vu des valeurs faibles de G_c obtenues à de telles températures de contact, les mécanismes de cette adhésion ne sont liés ni à des phénomènes d'interdiffusion à longue distance ni à une co-cristallisation, mécanismes qui conduiraient à des valeurs de G_c bien supérieures à celles obtenues. L'adhésion est plus vraisemblablement liée à une réorganisation de la cristallinité à l'interface. Cette organisation a sans doute lieu à proximité immédiate de l'interface, les observations en microscopie optique n'ayant pour ces faibles énergies d'adhésion révélé aucun changement dans la zone transcristalline de l'interface, apparemment identique à la zone transcristalline observée à la surface des plaques. Des observations en TEM sur le *15PB* ont toutefois montré que des lamelles pouvaient traverser l'interface. Dans le cas du *PBT*, un processus de fusion recristallisation rapide pendant l'étape de préchauffage vient sans doute empêcher toute future organisation lors du contact. À des températures de contact proches de la température de fusion, la diffusion et la co-cristallisation sont cette fois des mécanismes plausibles, aux vu des fortes valeurs de G_c obtenues.

Pour conclure sur cette première série d'expériences, quelque soit la proportion de la phase amorphe, c'est à dire quelque soit le taux de cristallinité, l'adhésion est nulle à des températures de contact inférieures à la température de fusion des premiers cristallites, c'est à dire que la phase amorphe même mobile (car bien au dessus de sa température de transition vitreuse) ne participe pas au renforcement de l'interface en présence de cristallites. Pour des températures de contact situées entre la température de fusion des premiers cristallites et la température du pic de fusion, l'adhésion augmente progressivement de valeurs relativement faibles (renforcement provenant

vraisemblablement d'un mécanisme réorganisation cristalline), jusqu'à des valeurs fortes pour $T_{contact}$ proche de T_f où des mécanismes d'interdiffusion à longue distance ou de co-cristallisation peuvent enfin avoir lieu.

Dans une deuxième série d'expériences, le *45PB* et le *PBI* obtenus à l'état amorphe par une trempe après avoir été moulés au dessus de la température de fusion, sont mis en contact à température ambiante avant d'être rapidement chauffés jusqu'à la température de contact. Le but de ce type d'expérience est de mettre en contact des polymères amorphes et de regarder l'influence de l'interdiffusion et de la cristallisation froide sur l'énergie d'adhésion. Nous avons tout d'abord noté dans la grande majorité des expériences de clivage en coin une propagation instable de la fissure. Deux valeurs de G_c ont été calculées pour ce type de propagation, l'une au moment de l'amorçage de la fissure et l'autre au moment de son arrêt. La différence entre les valeurs d'amorçage et d'arrêt varie selon la température et le temps de contact. Ce comportement a pu être expliqué par les changements des propriétés en volume des polymères suivant la température et le temps de contact entraînant une plus ou moins grande cristallisation en volume. Nous avons choisi de nous concentrer sur l'interprétation des valeurs de G_c obtenues pour l'arrêt de la fissure, valeurs qui nous ont semblé plus caractéristiques de la résistance à la fracture de l'interface elle même. Les valeurs d'énergie d'adhésion trouvées dans ce cas sont très faibles pour *45PB* et *PBI*. Dans le cas du *45PB*, pour des températures de contact allant de 20°C à 60°C au dessus de la T_g, l'adhérence augmente lentement avec la température de contact, mais reste extrêmement faible (quelques $J.m^{-2}$). L'adhérence augmente légèrement avec le temps de contact entre 10 et 60 minutes. Pour le *PBI*, l'adhérence est également très faible jusqu'à T_g+40°C. Ces faibles énergies d'adhérence montrent clairement l'absence d'une interdiffusion à longue distance, pourtant attendue à de telles températures dans le cas de polymères amorphes. La fine couche cristalline observée à l'interface pour un contact à 60°C pendant 10 minutes en microscopie optique et également observée en TEM sur un échantillon mis en contact 10 minutes à 70°C, semble être à l'origine de cette absence d'interdiffusion à longue distance. Les chaînes situées à proximité de l'interface sont probablement piégées dans des cristallites, ce qui diminue fortement leur possibilité de diffusion sur des distances comparables à leur rayon de giration.

Les mécanismes de renforcement de l'interface peuvent être interprétés comme suit. Pour le *45PB*, la densification et la réorganisation progressive des cristallites à l'interface entraînent une augmentation progressive de l'adhésion. Au dessus d'une certaine température, la fusion des premiers cristallites se produit, conduisant à une augmentation plus significative de l'adhésion. Pour le *PBI*, en dessous d'une certaine température, 60°C, le développement de germes de cristallites à l'interface ne se produit pas et l'adhésion reste faible et constante. Au dessus de 60°C, les germes commencent à se développer à l'interface et G_c passe de quelques J à 10 $J.m^{-2}$. Pour le *PBI*, Il faut atteindre une température d'au moins 120°C pour obtenir une réelle augmentation de l'énergie d'adhésion.

Conclusions

Nous pouvons retenir de cette étude les quelques points suivants.

- Pour tous les polymères, G_c atteint de très fortes valeurs pour des températures de contact proches de T_f.

- Dans le cas de surfaces mises en contact après équilibre, c'est à dire après un temps de préchauffage permettant au processus de cristallisation ou de fusion de se stabiliser, l'adhésion ne devient mesurable qu'au dessus de la température de fusion des premiers cristallites, si cette fusion n'est pas suivie d'une recristallisation immédiate.

- Quelque soit le taux de cristallinité du polymère, la phase amorphe ne semble jouer aucun rôle dans l'adhésion au dessous de cette température, qui est cependant bien supérieure à la température de transition vitreuse.

- Dans le cas du *45PB* et *PBI* obtenus à l'état amorphe et mis en contact à l'ambiante avant d'être rapidement chauffés à la température de contact, les énergies d'adhésion obtenues sont extrêmement faibles. Les mécanismes attendus dans de telles conditions de températures pour des polymères amorphes ne se produisent pas.

- La fine couche cristalline observée dans certains échantillons en microscopie optique et électronique, empêche probablement l'interdiffusion sur des longues distances. Le renforcement observé, progressif dans le cas de *45PB* et discontinu dans le cas du *PBI*, est sans doute dû à une densification et une réorganisation des cristallites à l'interface.

Cette étude a mis en exergue le rôle déterminant joué par la surface, de part son effet nucléant, sur la formation d'un assemblage entre deux polymères semi-cristallins. Nous avons observé la formation d'une couche cristalline en surface même lors de refroidissement relativement rapide de polymères peu cristallins. Dans la gamme de température étudiée (entre T_g et T_f) les mécanismes de renforcement des interfaces ont été trouvés différents de ceux observés pour des polymères amorphes et la partie amorphe n'a pas semblé jouer de rôle important dans le renforcement des interfaces.

We studied the self adhesion of semicrystalline polymers with variable degrees of crystallinity by performing fracture studies of interfaces formed between their glass transition temperature, T_g, and their melting temperature, T_m, in order to elucidate the role of crystallinity. We used a series of copolymers of polybutylene(terephthalate-co-isophthalate). For pre-crystallized samples, when the temperature of contact ($T_{contact}$) was decreased below T_m, the fracture toughness, G_c decreased with $T_{contact}$ to vanish at a temperature corresponding to the onset of the fusion process. For quenched samples obtained in the amorphous state and put in contact before rising the temperature to $T_{contact}$, G_c was very low for temperatures of contact well above T_g. The very thin crystalline layer observed in TEM was held responsible of this weak adhesion. The essential role played by surfaces and interfaces in nucleating crystallinity was shown to be an important factor affecting self-adhesion below T_m.

Keywords :
Adhesion, Reinforcement, Semi-crystalline polymers, Polybutylene(terephthalate-co-isophthalate), Crystallinity at interfaces, Self-adhesion

---

Nous avons étudié l'auto-adhésion de polymères semi-cristallins de taux de cristallinité variable, par un test de fracture des interfaces formées entre leur température de fusion, T_f, et leur température de transition vitreuse, T_g, dans le but de définir le rôle de la cristallinité sur l'adhésion. Nous avons utilisé des copolymères de polybutylène(téréphthalate-co-isophthalate). Pour les polymères pré-cristallisés, l'énergie de fracture, G_c, diminue fortement avec la température de contact (pour $T_{contact}<T_f$), pour devenir nulle à T correspondant au début de la fusion. Pour les polymères obtenus à l'état amorphe après trempe, mis en contact avant d'être chauffés à $T_{contact}$, G_c reste faible pour des températures de contact supérieures à T_g. La fine couche cristalline observée en TEM est probablement responsable de la faiblesse de l'adhésion. Le rôle essentiel joué par les surfaces et les interfaces dans la nucléation de la cristallinité est un facteur important pour l'auto-adhésion sous T_m.

Mots clés :
Adhésion, Renforcement, Polymères semi-cristallins, Polybutylene(terephthalate-co-isophthalate), Cristallinité aux interfaces, Auto-adhésion